



**UNIVERSITY OF LEEDS**

# **Osteochondral tissue engineering using biphasic silk re-enforced 3D printed scaffolds**

**Thomas Michael Braxton**

Submitted in accordance with the requirements for the degree of

Doctor of Philosophy

The University of Leeds

**March 2023**

# **Intellectual Property and Publication Statements**

The candidate confirms that the work submitted is his own and that appropriate credit has been given where reference has been made to the work of others.

This copy has been supplied on the understanding that it is copyright material and that no quotation from the thesis may be published without proper acknowledgement.

# Acknowledgements

As a great man once said "Do. Or do not. There is no try."

## Abstract

Osteochondral tissue damage is a serious concern, with even small levels of cartilage damage increasing an individual's risk of suffering from joint discomfort or pain, with some instances even leading to osteoarthritis. Cartilage damage is often seen as a result of traumatic injury from sports or work. Currently, one of the most common treatments for osteoarthritis is joint replacement; however, this is not an optimal treatment because the replacements and procedure itself are highly invasive and the joint replacement has a limited lifespan. Therefore, especially with younger and more active patients, an earlier intervention is needed to repair the initial cartilage damage and its underlying subchondral bone. 3D printing is an exciting scaffold development method for tissue regeneration, especially within personalised medicine. However, many 3D printing techniques rely on creating a lattice structure, which often demonstrates poor cell bridging between filaments due to its large pore size, reducing regenerative capacity as cells are unable to efficiently remodel the scaffold. To tackle this issue a novel biphasic silk reinforced 3D printed scaffold was developed. This biphasic scaffold consisted of a 3D printed poly(ethylene glycol)-terephthalate-poly(butylene-terephthalate) (PEGT/PBT) lattice, infilled with a cast and freeze dried porous silk scaffold (derived from *Bombyx mori* silk fibroin), which continued on to a seamless silk top layer. Compression testing showed that scaffolds had a compressive modulus, ultimate compressive strength and fatigue resistance that would allow for their theoretical survival during implantation and joint articulation without stress-shielding mechanosensitive cells. Fluorescent microscopy showed biphasic scaffolds could support human bone marrow stromal cell (hBMSC) attachment and spreading after 24 hours of seeding. Scaffolds were able to successfully support cell growth for three weeks under chondrogenic conditions, and six weeks under osteogenic conditions. Histological analysis also demonstrated scaffolds allowed for osteogenic or chondrogenic differentiation of seeded hBMSCs. Histological analysis revealed, however, that scaffolds failed to create osteochondral like tissue *in vitro* within osteochondral culture conditions. By combining two different and unique materials, this biphasic scaffold possesses the mechanical and structural advantages of PEGT/PBT with the biocompatibility and cell supporting characteristics of silk, with none of the individual materials' disadvantages. However, future experimentation is needed to improve the osteochondral conductivity of the biphasic scaffold.

## Abbreviations

ANOVA - Analysis of variance  
ACI - Autologous chondrocyte implantation  
ACL - Anterior cruciate ligament  
AM - Additive manufacturing  
ATR - Attenuated total reflectance  
 $\alpha$ -MEM – Alpha minimum essential medium  
AT-MSC - Adipose tissue derived mesenchymal stem cell  
 $\beta$ -TCP – beta tricalcium phosphate  
bFGF-Basic fibroblast growth factor  
 $^{\circ}\text{C}$  - Degrees Celsius  
cm - Centimetre  
 $\text{CO}_2$  - Carbon dioxide  
CFMDA - 5-chloromethylfluorescein diacetate  
DAPI - 4',6-Diamidino-2-phenylindole  
DMSO - Dimethyl sulfoxide  
ds DNA – Double stranded deoxyribonucleic acid  
DNA - Deoxyribonucleic acid  
DPX - Dibutylphthalate polystyrene xylene  
DAB - 3,3'-Diaminobenzidine  
 $\text{dH}_2\text{O}$  - Distilled water  
BM-MSC - Bone marrow-derived mesenchymal stem cell  
ECM - Extracellular matrix  
EtOH - Ethanol  
EthD- - Ethidium homodimer-1  
EDX - Energy dispersive X-ray analysis  
EDS - Energy dispersive X-ray analysis  
FBS - Foetal bovine serum  
FTIR - Fourier-transform infrared spectroscopy  
GAG - Glycosaminoglycan  
GPa - Gigapascal  
HA – Hyaluronic acid  
 $\text{H}_2\text{O}$  – Water  
hBMSCs - Human bone marrow stromal cells

HBSS - Hanks' Balanced Salt Solution  
H&E - Haematoxylin and eosin  
Hz - Hertz  
ITS - Insulin-transferrin-selenium  
IHC - Immunohistochemistry  
ICRS - International Cartilage Repair Society  
ISO - International Organization for Standardization  
J – Joules  
KPa - Kilopascals  
LDH - Lactate dehydrogenase  
M - molarity  
Mol - mole  
mm - millimetre  
mg - milligrams  
ml - Millilitres  
mj - Millijoules  
MLCS - Multilayered cell sheet  
MSCs - Mesenchymal stem cells  
MRI – Magnetic resonance imaging  
MMP - Matrix metalloproteinase  
MPa - Megapascal  
Min - Minutes  
N - Newtons  
nm - Nanometres  
ng - Nanograms  
NAD<sup>+</sup> - Nicotinamide adenine dinucleotide  
NADH - Nicotinamide adenine dinucleotide hydrogen  
NBF - Neutral buffered formalin  
NREC - National Office for Research Ethics Committees  
OCD - Osteochondral defects  
OCL - Osteochondral lesion  
RPM - Revolutions per minute  
RNA - Ribonucleic acid  
P/S - Penicillin-streptomycin

PEGT/PBT- Poly(ethylene glycol)-terephthalate-poly(butylene terephthalate) block copolymers

PLA - Poly(lactic acid)

PGA - Poly(glycolic acid)

PEG - Poly(ethylene glycol)

PPF - Poly(propylene fumarate)

PDO - Poly(dioxanone)

PCL - Poly( $\epsilon$ -caprolactone)

PLGA - Polylactic-co-glycolic acid

pH - Potential hydrogen

QQ-plot - Quantile-quantile plot

SEM - Scanning electron microscope

Spss - Statistical Product and Service Solutions

PBS - 1 × phosphate-buffered saline solution

TGF - Transforming growth factor

RGD - Arginine-glycine-aspartic

Wt% - percentage by weight

$\mu\text{g}$  - Micrograms

$\mu\text{l}$  - Microlitres

$\mu\text{m}$  - Micrometre

3D - Three dimensional

2D - Two dimensional

## Table of Contents

Chapter 1 Literature review .....	17
1.1 Anatomy, physiology and pathology of articular cartilage.....	18
1.1.1 The current issues with articular cartilage degeneration .....	18
1.1.2 Molecular and zonal components of articular cartilage related to structural function .....	19
1.1.2.1 Anatomical zones of articular cartilage .....	19
1.1.2.2 Molecular components of articular cartilage .....	21
1.1.3 Cartilage damage .....	26
1.1.3.1 Causes of cartilage damage .....	26
1.1.3.2 Mechanisms of cartilage damage and subsequent degradation.....	27
1.1.3.3 Characterisation and grading of cartilage defects .....	29
1.1.3.4 Long term impact of cartilaginous defects to the patient .....	32
1.2 The current treatment strategies for cartilaginous lesions .....	33
1.2.1 Microfracture or micro-drilling .....	34
1.2.2 Osteochondral autografts (also known as mosaicplasty) .....	35
1.2.3 Osteochondral allografts.....	36
1.2.4 Autologous chondrocyte implantation .....	37
1.3 Tissue engineering approaches.....	38
1.3.1 Cell sources for cell-based therapies for cartilage regeneration .....	39
1.3.2 Growth factors involved and used for osteochondral regeneration .....	40
1.4 Scaffolds for an osteochondral tissue engineering approach .....	43
1.4.1 Cell material interactions .....	44
1.4.2 Surface topography.....	47
1.5 Requirements of a scaffold to be used in tissue regeneration .....	48
1.5.1 General requirements of a scaffold to be used in regeneration .....	48
1.5.2 Requirements of scaffolds used for cartilage regeneration .....	49
1.5.3 Requirements of a scaffold to be used for bone regeneration .....	49

1.6 Types of Biomaterials for osteochondral tissues engineering .....	50
1.6.1 Natural polymers.....	50
1.6.1.1 Silk fibroin from the <i>Bombyx mori</i> .....	50
1.6.2 Synthetic polymers.....	53
1.6.2.1 PEGT/PBT Thermoplastic .....	53
1.6.3 Ceramics and glasses.....	54
1.6.4 Metallic scaffolds .....	55
1.6.5 Scaffold surface chemistry modification.....	55
1.6.6 A combined approach .....	56
1.6.7 Smart materials and instructive surfaces.....	56
1.7 Scaffold physical morphology .....	58
1.7.1 Hydrogels .....	58
1.7.2 Porous/sponge scaffolds .....	59
1.7.3 Electrospun scaffolds .....	59
1.7.4 3D printing.....	59
1.8 Multiphasic scaffolds .....	60
1.8.1 Scaffold free cartilage implanted on a bone scaffold .....	61
1.8.2 Assembled bilayered scaffold .....	61
1.8.3 Integrated biphasic scaffold .....	62
1.9 Summary .....	62
1.10 Aims and objectives .....	64
1.10.1 Requirements for an osteochondral scaffold .....	64
Chapter 2 Materials and methods.....	65
2.1 Scaffold preparation .....	66
2.2 Characterisation of the chemical, physical, and mechanical properties of biphasic 3D printed silk reinforced scaffolds .....	67
2.2.1 Light visualisation.....	67
2.2.2 Scanning electron microscope (SEM).....	67
2.2.3 Energy Dispersive X-Ray Analysis (EDX) .....	68
2.2.4 Fourier Transform Infrared Spectroscopy analysis .....	69

2.2.5 Swelling capacity testing .....	70
2.2.6 <i>In vitro</i> scaffold degradation testing.....	70
2.2.7 Porosity testing .....	71
2.2.8 Mechanical characterisation .....	72
2.2.8.1 Uniaxial compression testing .....	72
2.2.8.2 Fatigue testing.....	73
2.3 Osteochondral tissue engineering <i>in vitro</i> using human bone marrow stromal cells and biphasic 3D printed silk reinforced scaffolds .....	74
2.3.1 Cell culture .....	74
2.3.1.1 hBMSC isolation .....	74
2.3.1.2 Culturing of cells .....	75
2.3.1.3 Passaging cells.....	75
2.3.1.4 Cell counting .....	75
2.3.1.5 Cell freezing and cryopreservation .....	76
2.3.1.6 <i>In vitro</i> expansion of hBMSCs .....	76
2.3.1.7 Live cell fluorescent labelling.....	77
2.3.1.8 Static seeding of hBMSCs on scaffolds.....	77
2.3.1.9 Dynamic seeding of hBMSCs on scaffolds .....	78
2.3.1.10 Osteogenic induction culture.....	79
2.3.1.11 Chondrogenic induction culture .....	79
2.3.2 Sterility testing .....	80
2.3.3 Contact cytotoxicity assay.....	80
2.3.4 Indirect cytotoxicity assay .....	81
2.3.5 Scaffold FBS surface modification.....	82
2.3.6 Cell migration .....	82
2.3.7 AlamarBlue™ assay for analysis of cell metabolic activity.....	83
2.3.8 LDH assay for analysis of cell death percentage/ rate.....	84
2.3.9 Seeding and culturing of hBMSCs on scaffolds under chondrogenic conditions.....	85
2.3.10 Seeding and culturing of hBMSCs on scaffolds under osteogenic conditions .....	85
2.3.11 Seeding and culturing of hBMSCs on scaffolds under osteochondral conditions .....	85
2.3.12 Histology.....	86
2.3.12.1 Paraffin embedding and sectioning .....	86
2.3.12.2 Haematoxylin and eosin (H&E) staining .....	86

2.3.12.3 Picrosirius red/Alcian blue staining.....	87
2.3.12.4 Safranin-O staining for proteoglycans .....	87
2.3.12.5 Von Kossa staining for mineral nodule formation .....	88
2.3.12.6 Immunohistochemistry .....	88
2.4 Statistical analysis .....	89
<b>Chapter 3 Characterisation of the chemical, physical, and mechanical properties of biphasic 3D printed silk reinforced scaffolds.....</b>	<b>90</b>
3.1 Results .....	91
3.1.1 Scaffold morphology and porosity.....	92
3.1.2 Elemental distribution within the scaffolds.....	95
3.1.3 Scaffold protein crystallinity .....	97
3.1.4 Scaffold porosity .....	99
3.1.5 Scaffold swelling potential .....	100
3.1.6 Scaffold degradability.....	103
3.1.7 Characterisation of scaffold mechanical properties .....	105
3.1.7.1 Uniaxial compression test.....	105
3.1.7.2 Fatigue behaviour .....	108
3.1.7.3 Hysteresis behaviour.....	112
3.2 Discussion.....	115
3.2.1 Scaffold pore size and porosity .....	115
3.2.2 Mechanical properties .....	118
3.2.3 Swelling and degradation.....	121
3.2.4 Summary .....	123
<b>Chapter 4 Osteochondral tissue engineering <i>in vitro</i> using human bone marrow stromal cells and biphasic 3D printed silk reinforced scaffolds.....</b>	<b>125</b>
4.1 Results .....	126
4.1.1 Scaffold sterility.....	126
4.1.2 Scaffold cytotoxicity .....	128
4.1.2.1 Contact cytotoxicity .....	128
4.1.2.2 Indirect cytotoxicity .....	129
4.1.3 Scaffold seeding optimisation.....	131
4.1.4 The effect of surface modification on the attachment and growth of hBMSCs on biphasic scaffolds .....	132

4.1.5 Dynamic versus static seeding .....	133
4.1.6 Cell migration and morphological shape .....	136
4.1.7 Cell metabolic activity and cell death rate.....	138
4.1.8 Scaffold seeding technique .....	140
4.1.9 Culturing of hBMSCs on scaffolds under chondrogenic conditions.....	143
4.1.9.1 Evaluation of cell migration and morphology via H and E staining under Chondrogenic conditions .....	143
4.1.9.2 Long term viability in chondrogenic conditions of cells on scaffolds .....	145
4.1.9.3 Collagen and GAG deposition by hBMSCs within scaffolds under chondrogenic conditions. ....	147
4.1.9.4 Collagen Type I and II deposition by hBMSCs within scaffolds under chondrogenic conditions. ....	148
4.1.9.5 Proteoglycan deposition by hBMSCs within scaffolds under chondrogenic conditions.....	151
4.1.10 Culturing of hBMSCs on scaffolds under osteogenic conditions.....	152
4.1.10.1 Evaluation of cell migration and morphology via H&E staining under osteogenic conditions.....	152
4.1.10.2 Long term viability of cells on scaffolds under osteogenic conditions.....	154
4.1.10.3 Collagen and GAG of hBMSCs within deposition within scaffolds under osteogenic conditions. ....	156
4.1.10.4 Collagen Type I and II deposition of hBMSCs within scaffolds under osteogenic conditions. ....	157
4.1.10.5 Mineral nodule deposition of hBMSCs within scaffolds under osteogenic conditions. ....	159
4.1.11 Culturing of hBMSCs on scaffolds under osteochondral conditions.....	160
4.1.11.1 Evaluation of cell migration and morphology via H&E staining within osteochondral conditions.....	160
4.1.11.2 Collagen and GAG deposition within scaffolds under osteochondral conditions. ....	162
4.1.11.3 Collagen Type I and II deposition of hBMSCs within scaffolds under osteochondral conditions.....	164
4.1.11.4 Proteoglycan deposition of hBMSCs within scaffolds under osteochondral conditions. ....	167
4.1.11.5 Mineral nodule deposition of hBMSCs within scaffolds under osteochondral conditions.....	169
4.1 Discussion.....	171

4.1.1 Scaffold sterilisation .....	171
4.1.2 Cytotoxicity .....	172
4.1.3 Cell adhesion .....	174
4.1.4 Cell seeding strategies.....	176
4.1.5 Long-term <i>in vitro</i> term cell culture .....	177
4.1.6 Scaffold capability for cartilage regeneration <i>in vitro</i> .....	179
4.1.7 Scaffold capability for subchondral bone regeneration <i>in vitro</i> .....	181
4.1.8 Scaffold capability for osteochondral tissue regeneration <i>in vitro</i> .....	183
4.1.9 Summary .....	188
<b>Chapter 5 General discussion .....</b>	<b>189</b>
5.1.1 Project overview .....	190
5.1.2 Pore size and its impact on cellular differentiation .....	191
5.1.3 Biocompatibility .....	192
5.1.4 Rehydration and cell penetration .....	193
5.1.5 Mechanical properties and handling .....	194
5.1.6 Osteochondral culture .....	196
5.1.7 Study limitations .....	197
<b>Chapter 6 Conclusions and Future Work .....</b>	<b>198</b>
6.1.1 Conclusion .....	199
6.1.2 Future work.....	199
<b>References .....</b>	<b>203</b>
<b>Appendix 1 .....</b>	<b>232</b>

## LIST OF FIGURES

Figure 1 Diagram demonstrating the structural layers that make up articular cartilage. ....	21
Figure 2 Diagram demonstrating the structure of a proteoglycan aggregate. ....	24
Figure 3 Transmission electron microscopy of an articular chondrocyte .....	26
Figure 4 ICRS Cartilage Injury Evaluation.....	31
Figure 5 Mechanisms of the formation of osteoarthritis within the human knee .....	33
Figure 6 Endoscopic images of microfracture of a chondral defect .....	35
Figure 7 Mosaicplasty of the human knee.....	36
Figure 8 ACI treatment of the patella.....	38
Figure 9 The differences between 3D culture and 2D monolayer culture on cell behaviour .....	45
Figure 10 Cell locomotion along a substrate .....	47
Figure 11 Chemical structure of silk fibroin from Bombyx mori .....	51
Figure 12 Chemical structure of PEGT/PBT segmented block copolymers .....	54
Figure 13 How surface modification, water and other biomolecules can affect cell adhesion and tissue regeneration .....	56
Figure 14 A generalised stress strain curve for materials under compression .....	73
Figure 15 In-house constructed dynamic seeder .....	79
Figure 16 Representative Stereomicroscope image representing the structural similarities and differences between created scaffold types .....	91
Figure 17 Representative Compiled SEM images demonstrating complete structure and morphology of scaffolds .....	93
Figure 18 Scaffold pore size distribution .....	94
Figure 19 EDX analysis for elemental distribution within scaffolds .....	96
Figure 20 Relative elemental distribution found within the scaffold types as determined by EDX.....	97
Figure 21 The relative distribution of the protein's secondary structure.....	98
Figure 22 Scaffold porosity.....	100
Figure 23 Scaffold swelling .....	101
Figure 24 negative pressure rehydration for scaffold rehydration .....	103
Figure 25 In vitro degradation of scaffolds.....	104
Figure 26 Representative stress-strain curves for the scaffolds under uniaxial compression testing .....	106
Figure 27 Scaffold compressive modulus .....	107
Figure 28 Scaffold ultimate compressive strength.....	108
Figure 29 Resultant strain from fatigue testing of scaffolds .....	110
Figure 30 Scaffold height reduction due to fatigue testing .....	111
Figure 31 . Representative Scaffold hysteresis loops under fatigue testing .....	113
Figure 32 Scaffolds absorbed energy during fatigue testing .....	114
Figure 33 Scaffold sterility testing .....	127
Figure 34 Scaffold contact cytotoxicity .....	128
Figure 35 Indirect cytotoxicity.....	130
Figure 36 Indirect cell growth retardation.....	131
Figure 37 Impact of FBS scaffold preincubation on cell adhesion .....	133
Figure 38 . A comparison of cell distribution after dynamic or static seeding.....	135
Figure 39 Cell cytoskeleton scaffold interaction.....	137
Figure 40 Cell metabolic activity on scaffolds as determined by alamarBlue.....	139
Figure 41 Released LDH activity .....	140

Figure 42, valuation of impact of scaffold orientation during static seeding .....	142
Figure 43 H&E staining of biphasic and silk control scaffolds under chondrogenic conditions .....	144
Figure 44 Live cell staining of hBMSCs on biphasic and silk control scaffolds under chondrogenic conditions .....	146
Figure 45 Picrosirius red/Alcian blue staining of biphasic and silk control scaffolds under chondrogenic conditions .....	148
Figure 46 ICH staining for Type I and Type II collagen of biphasic and silk control scaffolds under chondrogenic conditions .....	150
Figure 47 Safranin-O staining of biphasic and silk control scaffolds under chondrogenic conditions .....	151
Figure 48 H&E staining of biphasic and silk control scaffolds under osteogenic conditions .....	153
Figure 49 live cell staining of hBMSCs on biphasic and silk control scaffolds under osteogenic conditions.....	155
Figure 50 Picrosirius red/Alcian blue staining staining of biphasic and silk control scaffolds under osteogenic conditions.....	156
Figure 51 IHC staining of Type I and Type II collagen of biphasic and silk control scaffolds under osteogenic conditions.....	158
Figure 52 Von Kossa staining of biphasic and silk control scaffolds under osteogenic conditions.....	159
Figure 53 H&E staining of biphasic and silk control scaffolds under osteochondral conditions .....	161
Figure 54 Picrosirius red/Alcian blue staining of biphasic and silk control scaffolds under osteochondral conditions .....	163
Figure 55 IHC staining for Type I collagen of biphasic and silk control scaffolds under osteochondral conditions.....	165
Figure 56 IHC staining for type II collagen of biphasic and silk control scaffolds under osteochondral conditions.....	166
Figure 57 Safranin-O staining of biphasic and silk control scaffolds under osteochondral conditions .....	168
Figure 58 Von Kossa staining of biphasic and silk control scaffolds under osteochondral conditions .....	170
Figure 59 Microfluidic culture device for osteochondral tissue on a chip model .....	186
Figure 60 (appendix) trilineage differentiation assay of isolated hBMSC from routine hip arthroplasty .....	233
Figure 61 (appendix) Raw FTIR data utilised to determine protein secondary structure.....	234

## LIST OF TABLES

Table 1 Types of collagens within articular cartilage, their morphological location and function .....	23
Table 2 Parameters to consider when designing an osteochondral scaffold. ....	64
Table 3 Age and gender distribution of cells isolated from explants from total hip arthroplasty.....	75
Table 4 Reactivity grades for contact cytotoxicity testing .....	81
Table 5 . Primary antibody information utilised during IHC .....	89

# Chapter 1 Literature review

This section presents the relevant literature to the thesis. Firstly, the review focuses on natural articular cartilage, its role within the human body, and how cartilage damage occurs. Following this, a review of current surgical techniques and their pitfalls is undertaken, followed by a more in-depth examination into how tissue engineering is currently tackling the issue of cartilage damage and how what we know now can shape treatments of the future.

# 1.1 Anatomy, physiology and pathology of articular cartilage

## 1.1.1 The current issues with articular cartilage degeneration

Cartilage tissue damage is a serious concern, with even small levels of damage increasing an individual's risk of suffering from osteoarthritis (Madry, Luyten and Facchini, 2012). It has been estimated that over eight million people in the UK suffer from osteoarthritis, costing the economy 36 million lost workdays (£3.2 billion). Currently, one of the most common treatments for osteoarthritis is joint replacement; however, this is not an optimal treatment because the replacements and procedure itself are highly invasive and the joint replacement only has a limited lifespan (Jacobs *et al.*, 2006; Hunziker *et al.*, 2014; Gademan *et al.*, 2016). Therefore, especially with younger and more active patients, an earlier intervention is needed to attempt to regenerate the articular cartilage tissue in the initial stages of damage (osteochondral defect), preventing its future degradation into the considerably more debilitating condition of osteoarthritis. There are several current early interventions in clinical use to treat osteochondral tissue damage but these all have serious drawbacks, with many of them failing to completely regenerate cartilage or its underlying subchondral bone (Li *et al.*, 2017; Martín *et al.*, 2019). Due to the current treatments being unable to demonstrate adequate and complete regeneration of cartilage and its underlying subchondral bone, there is a need for the development of an effective, new early intervention.

## **1.1.2 Molecular and zonal components of articular cartilage related to structural function**

Articular cartilage is an extremely specialised variant of cartilage which lines the end of bones in synovial or diarthrodial joints (Madry, Luyten and Facchini, 2012; Chang, K and Martin, 2020). Articular cartilage presents a unique structure, it is a multi-phasic composite material that is also aneural, avascular and devoid of lymphatics (Loeser, 2010). The primary function of articular cartilage is to provide a smooth, lubricated surface with a low coefficient of friction to allow for effortless articulation of the joint (Responde, Natoli and Athanasiou, 2007; Gomoll and Minas, 2014). Articular cartilage also functions to distribute load within a joint to the underlying subchondral bone. Due to its unique structure and function, once articular cartilage is damaged it has an extremely poor intrinsic healing capacity, and therefore, articular cartilage damage becomes a fundamental cause of musculoskeletal disorders in clinical orthopaedics (Jiang and Tuan, 2015).

### **1.1.2.1 Anatomical zones of articular cartilage**

The thickness of human articular cartilage varies between 2 to 4 mm and is split into four distinct zones (Figure 1), each zone possesses a unique structure and ECM composition which is ideally suited to its role (Sophia Fox, Bedi and Rodeo, 2009). This ECM is deposited and maintained by a sparse population of cells referred to as chondrocytes.

The superficial zone: this is the thinnest of all four zones and forms the articulating surface of the cartilage (Bhosale and Richardson, 2008; Sophia Fox, Bedi and Rodeo, 2009; Becerra *et al.*, 2010). The collagen fibrils are orientated parallel to the articulating surface and mainly consist of Type II and IX Collagen. This orientation allows the surface layer to resist the shear and tensile forces experienced during articulation. This zone also contains a relatively high number

of chondrocytes which have a flat morphology. This zone has a low proteoglycan content (Huber, Trattnig and Lintner, 2000).

The transitional zone: the superficial zone is immediately followed by the transitional zone. This zone functionally bridges the gap between the superficial zone and the deep zone and is the initial zone that resists compression during loading (Zheng Ming, Kirk Thomas and Wu Jian, 2008; Chen *et al.*, 2013). Here, collagen fibrils are thicker and arranged obliquely, and this layer contains proteoglycans. The transitional zone has very few chondrocytes sparsely spread throughout.

The deep zone: this contributes the most to articular cartilage's ability to resist compressive loading (Williams, Klisch and Sah, 2008). The collagen fibrils are even thicker in this zone and arranged perpendicular to the articulating surface. This zone also contains the highest concentration of proteoglycans. Its perpendicularly arranged collagen fibrils also extend into the lower calcified zone, helping to anchor the articular cartilage to the subchondral bone and calcified zone. Chondrocytes in this zone are of columnar morphology and appear to line up with the collagen fibrils.

The calcified zone of articular cartilage forms the transition zone from cartilage to the underlying subchondral bone. This zone allows for the transition in mechanical properties between cartilage and bone as well as playing a key role of anchoring the cartilage into the subchondral bone (Mansfield and Peter Winlove, 2012). The calcified zone is separated from the other zones of articular cartilage by the tidemark. The tidemark acts as a barrier, preventing the migration of cells and signalling molecules between the subchondral bone and articular cartilage (Madry, van Dijk and Mueller-Gerbl, 2010). It also prevents vascular invasion of the cartilage from the subchondral bone.

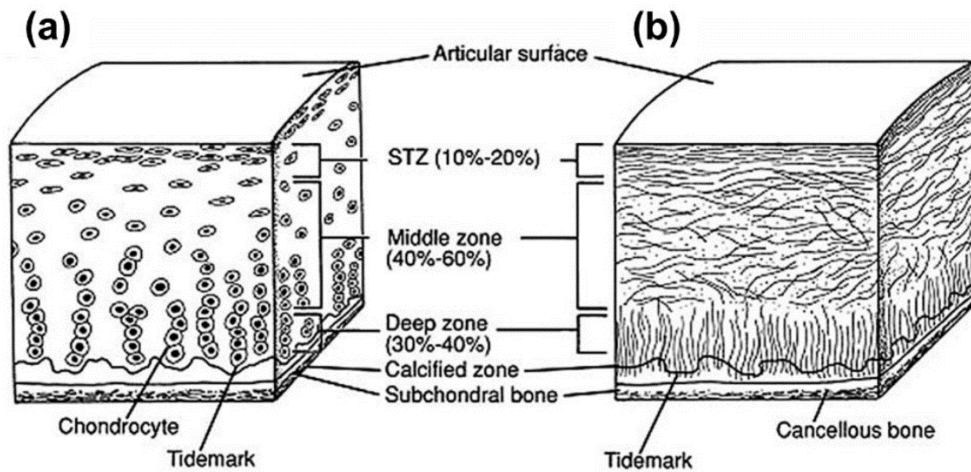


**Figure 1 Diagram demonstrating the structural layers that make up articular cartilage.** Chondrocyte morphology and location is represented in (a), and collagen structure and direction are represented in (b). Reprinted from B Buckwalter, J. A., Mow, V. C. and Ratcliffe, A. (1994) 'Restoration of Injured or Degenerated Articular Cartilage', *J Am Acad Orthop Surg*, 2(4), pp. 192-201. With permission of the American Academy of Orthopaedic Surgeons.

### 1.1.2.2 Molecular components of articular cartilage

The principal components of articular cartilage ECM are water, collagen, proteoglycans, and a number of noncollagenous proteins (Sophia Fox, Bedi and Rodeo, 2009). The ECM of articular cartilage is extremely stable in nature, and it has been suggested that collagen within the ECM of articular cartilage has a half-life of several decades and proteoglycans several years (Madry, Luyten and Facchini, 2012). Despite this, under certain conditions, this once extremely stable ECM can quickly be degraded.

Water is by far the most abundant component of articular cartilage, contributing up to 80% of wet weight (Maroudas *et al.*, 1991). The distribution of water throughout articular cartilage is not even, there is a higher proportion of water seen closer to the articulating surface. Approximately 30% of the water found within articular cartilage is closely associated with collagen fibrils, and in conjunction with other proteins it is able to form a gel-like structure (Buckwalter, Mow and Ratcliffe, 1994). The majority of the remaining water is located within pores of the ECM. Under loading conditions, the water found within articular

cartilage appears to be able to move, which allows for the distribution of the compressive load (Torzilli *et al.*, 1983; Becerra *et al.*, 2010). Under loading it has also been seen that water is released from the articulating surface, potentially acting as a joint lubricant. This has the added role of helping to circulate nutrients from the synovial fluid to the cartilage ECM as a joint loads and unloads.

Synovial fluid is derived from the blood plasma, as well as protein molecules produced by the cells surrounding the joint, such as the synovium, and is mostly made up of hyaluronan (Bennike *et al.*, 2014). The principal role of synovial fluid is to reduce friction of articular cartilage of synovial joints during movement (Tamer, 2014). As well as this, synovial fluid acts as a nutrient source, where through passive diffusion nutrients can be provided to the surrounding articular cartilage.

Collagen is the most abundant structural molecule found within articular cartilage, and of this, 90% to 95% is Type II collagen (Sophia Fox, Bedi and Rodeo, 2009). The Type II collagen forms a microfibrillar framework which is intertwined with proteoglycan aggregates. The Type II collagen functions to give articular cartilage its resistance to tensile forces and shear forces. Table 1 illustrates the roles of all the variants of collagen found within articular cartilage.

**Table 1 Types of collagens within articular cartilage, their morphological location and function**  
(Wu, Woods and Eyre, 1992; Pfaff *et al.*, 1993; Luckman, Rees and Kwan, 2003; Xu *et al.*, 2008; Alcaide-Ruggiero *et al.*, 2021)

Collagen type	Morphological location	Function
<b>II</b>	Principal component of the microfibrillar framework	Tensile and shear resistance
<b>VI</b>	Pericellular matrix	Mediates cell–matrix interactions and intermolecular interactions
<b>IX</b>	Cross-linked to surface of the microfibrillar framework	Reinforcement of Type II collagen by crosslinked of the microfibrillar framework
<b>X</b>	Closely related to the hypertrophy cells in calcified cartilage layer	Maintenance of cartilage stiffness, metabolic regulation of chondrocytes, facilitation of calcification
<b>XI</b>	Within, or on, the microfibrillar framework	Regulation of cartilage formation by functioning as a nucleation site for the microfibrillar framework

Proteoglycans are heavily glycosolated protein monomers (Yanagishita, 1993; Roughley and Lee, 1994; Knudson and Knudson, 2001). The structure of proteoglycans consists of a central core protein with one or more linear glycosaminoglycan chains attached through a covalent bond. These chains can often consist of more than 100 monosaccharide chains. These monosaccharide chains extend out of the monosaccharide core, remaining separated due to repulsion of the negative charges on their sulphate and carboxylate groups. These negatively charged side chains also help proteoglycans to undertake their main function of maintaining the electrolyte and fluid balance within articular cartilage (Buckwalter and Mankin, 1998). These negatively charged components result in repulsion of other negatively charged molecules and the attraction of positively charged molecules, thus the concentration of inorganic ions is increased within the matrix. This high concentration of ions functions to increase the osmolarity, creating a Donnan effect (Günther *et al.*, 1997). This attraction of water to the proteoglycans is what gives articular cartilage its compressive strength and its ability to resist extreme compressive loads.

Aggrecan is the most abundant proteoglycan variant found within articular cartilage (Roughley and Lee, 1994; Roughley and Mort, 2014; Ruiz Martínez *et al.*, 2020). It consists of its core protein surrounded by more than 100 chondroitin sulphate and keratan sulphate chains. Aggrecan does not exist in isolation and rather forms a proteoglycan aggregate within the ECM. This proteoglycan aggregate consists of a central HA molecule attached to multiple noncovalently bonded aggrecans and these bonds are then stabilised by a link protein (Figure 2).

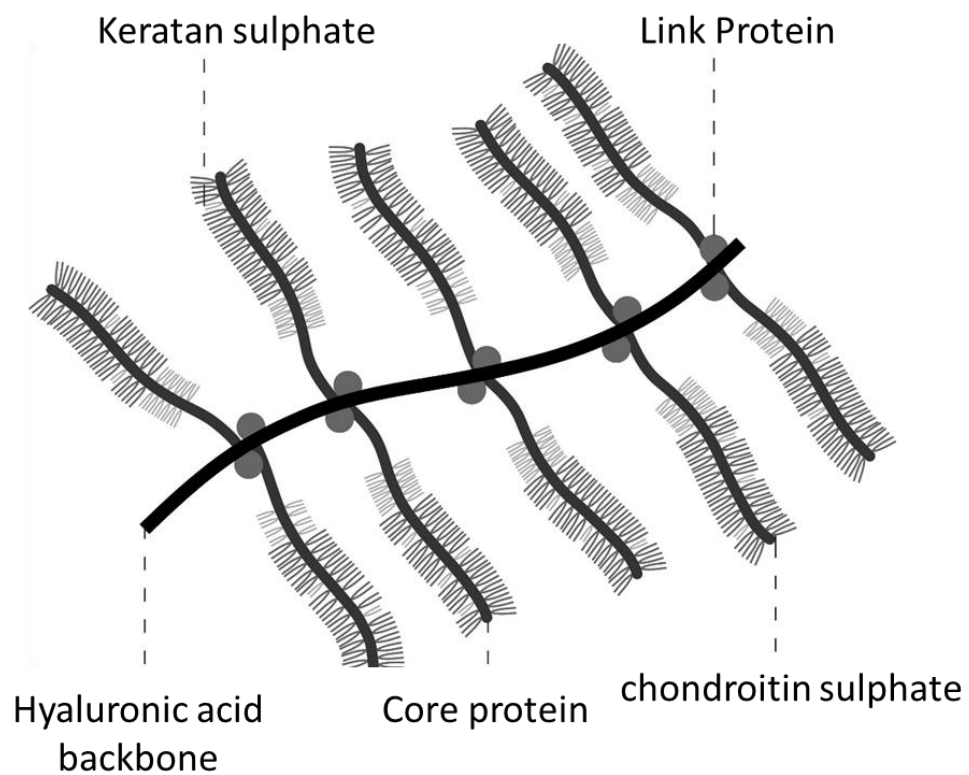


**Figure 2 Diagram demonstrating the structure of a proteoglycan aggregate.**

Proteoglycan aggregate consisting of a central hyaluronic acid backbone connected to noncovalently bonded aggrecan molecules, which are stabilised by a link protein. Modified from Ruiz Martínez, M. A., Peralta Galisteo, S., Castán, H. and Morales Hernández, M. E. (2020) 'Role of proteoglycans on skin ageing: a review', *International Journal of Cosmetic Science*, 42(6), pp. 529-535. With permission from *International Journal of Cosmetic Science*

The resident cell type of articular cartilage is the chondrocyte. Chondrocytes are a highly specialised cell type that are uniquely equipped for development, maintenance, and repair of ECM (Archer and Francis-West, 2003). Due to the avascular nature of articular cartilage, all the nutrient and metabolite exchange occurs at the surface of the articular cartilage coming from the synovial fluid. Due to this, chondrocyte metabolism is geared towards anaerobic respiration via glycolysis with the chondrocyte possessing relatively few mitochondria. The percentage of available oxygen varies between 10% at the superficial zone to <1% in the deep zone (Akkiraju and Nohe, 2015). Even with this lack of abundant oxygen chondrocytes still appear to be relatively synthetically active.

Each chondrocyte produces its own microenvironment in its immediate vicinity and is solely responsible for the turnover of the ECM within this microenvironment (Figure 3) (Sophia Fox, Bedi and Rodeo, 2009; Mobasheri *et al.*, 2014). Due to the extremely dense nature of the ECM that is produced in articular cartilage, it has been suggested that the chondrocytes become trapped within the microenvironment and are unable to migrate throughout the ECM. However, other studies have put the case forward that chondrocytes may be able to migrate through the ECM through the use of proteolytic enzymes (Morales, 2007).

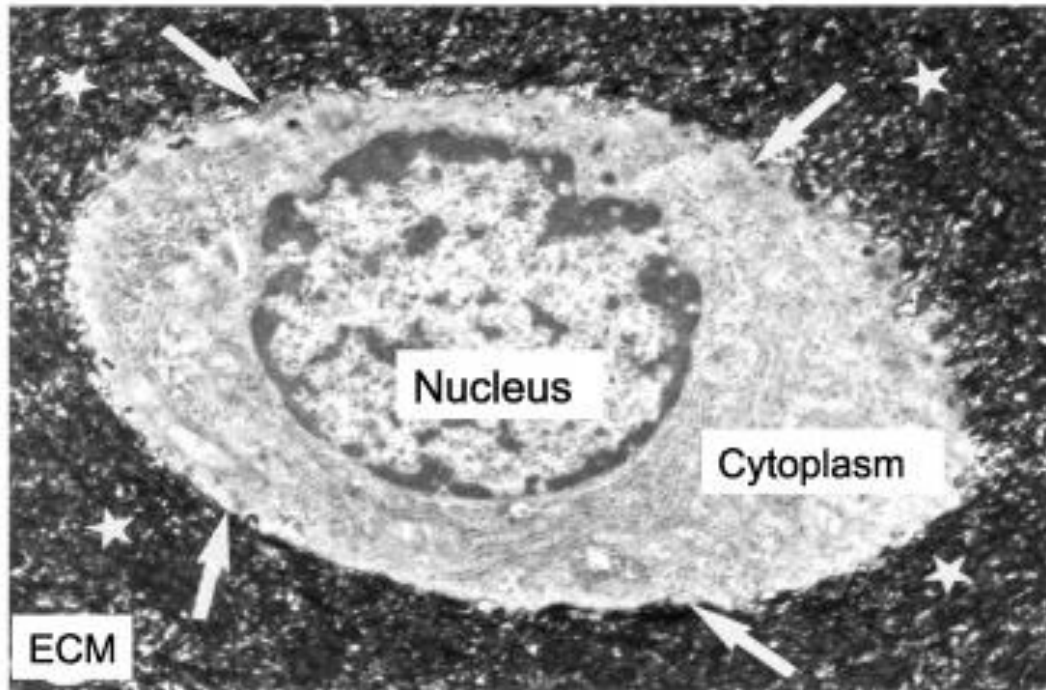


**Figure 3 Transmission electron microscopy of an articular chondrocyte**

Articular chondrocyte showing rounded morphology and isolated nature within the cartilage ECM. Reprinted from Mobasheri, A., Kalamegam, G., Musumeci, G. and Batt, M. E. (2014) 'Chondrocyte and mesenchymal stem cell-based therapies for cartilage repair in osteoarthritis and related orthopaedic conditions', *Maturitas*, 78(3), pp. 188-198. With permissions from Maturitas.

### 1.1.3 Cartilage damage

#### 1.1.3.1 Causes of cartilage damage

Upon analysis of the literature, the joints that have been shown to most frequently suffer from cartilage-based damage are those most associated with weight-bearing such as the knee and ankle (Rubin, 1998; Bohndorf, 1996; Sanders and Crim, 2001), with elbow and shoulder injuries being more frequent in throwing athletes and gymnasts. Injuries to small joints such as in the hands are extremely rare. There are also a number of inflammatory disorders such as rheumatoid arthritis that can lead to cartilage damage (Rannou *et al.*, 2006).

The exact cause of articular cartilage damage is still poorly understood with many cases being idiopathic in nature; however traumatic injury to the cartilage appears

to be one of the known causes, especially in young active patients. The traumatic injury often consists of an impacting, avulsing, or shearing force that is rapidly applied to the articular cartilage, causing damage (Pape *et al.*, 2010). It has also been proposed that some of the idiopathic cases may actually be due to repeated relatively low intensity traumas to the cartilage leading to its degradation. This is somewhat supported by the suggestion that 55 to 60% of patients showing cartilage damage are involved in some kind of sporting athletic activity (Krishnan and Grodzinsky, 2018). Other causes such as point loading have been suggested, this could be potentially due to loss of ligamentous support due to trauma or rupture of said ligaments, leading to point loading of the articular cartilage (Gartsman and Taverna, 1997; Fleming *et al.*, 2005). Obesity has also been suggested as another cause of joint overloading (King, March and Anandacoomarasamy, 2013).

### **1.1.3.2 Mechanisms of cartilage damage and subsequent degradation**

In its simplest form, damage to articular cartilage can be classified as either partial-thickness, known as chondral defects/lesions, or full-thickness, known as osteochondral defects/lesions. The way in which these defects are formed varies depending on the causative factors. Acute traumatic injuries often lead to the formation of OCD, this is due to the high amount of energy involved in the injury pushing both the articular cartilage and subchondral bone past its mechanical failing point (Buckwalter *et al.*, 2003). In OCD, the cartilage and underlying subchondral bone are damaged via impacting, leading to fracturing of both and the potential dislocation of loose bodies consisting of osteochondral tissue (Pape *et al.*, 2010). Following this kind of acute traumatic injury, the fracturing of the subchondral bone and marrow allows for a limited healing response which is induced as blood from the marrow is able to form a fibrin clot within the defect; this also brings chondroprogenitor cells (Altman *et al.*, 1992; Shapiro, Koide and

Glimcher, 1993; Jackson *et al.*, 2001) which, in turn, begin to fill the defect with new tissue. However, this new tissue is non-enduring, rarely lasting longer than a few months (Jackson *et al.*, 2001; Dell'accio and Vincent, 2010). If any tissue lasts longer than this it is functionally incompetent and is a poor replacement for the native uninjured tissue (Metsäranta *et al.*, 1996; McMahon, O'Brien and Prendergast, 2008; Anderson *et al.*, 2011).

In the absence of an obvious traumatic event, the cause of articular cartilage damage is more poorly understood. In some cases, there is a potential that the cause of articular cartilage degradation and defects is due to a source of misloading of the cartilage, leading to it being loaded beyond normal physiological levels (Jeffrey, Thomson and Aspden, 1997; Loening *et al.*, 2000). This kind of cartilage damage appears to be unable to be caused by normal physiological loading, rather, repetitive loading that is greater than physiologically normal (Chu, 2001). As previously mentioned, this misloading can come from a variety of sources such as loss of ligamentous support and obesity. The way in which this misloading induces cartilage degradation is poorly understood but seems to lead to increased matrix degradation and damage to chondrocytes (Thompson *et al.*, 1991).

This ECM loss appears to initially affect proteoglycans, leading to an increase in the degradation as well as a loss of their ability to properly aggregate (Grenier, Bhargava and Torzilli, 2014). As long as the increased degradation of proteoglycans is at a low enough level that chondrocytes are able to up regulate synthesis to maintain homeostasis, joint degradation is arrested (Krishnan and Grodzinsky, 2018). However, once the depletion of proteoglycans and extracellular matrix components is such that the chondrocytes are unable to regenerate at a sufficiently fast rate, cartilage degradation continues to increase inexorably with time. It is still unclear at what point this transfer is seen and where the tipping point that causes irreversible cartilage damage lies. When this point is reached the cartilage appears to dramatically lose stiffness, and greater

loads are transferred to other molecules such as collagen which are unable to mechanically support the tissue; this leads to their degradation as well as fibrillar disorganization (Hayes, Brower and John, 2001). The loss of the ECM support causes large loads to pass directly onto the chondrocytes leading to their death and apoptosis, ensuring an inability for cartilage regeneration. As well as chondrocyte destruction, greater forces are transferred to the subchondral bone, therefore reducing its compliance, which in turn increases loading on the articular cartilage, further leading to even more damage (Tetteh, Bajaj and Ghodadra, 2012). Once homeostasis is lost within the articular cartilage, chondrocytes appear to be unable to proliferate and migrate to the degradation site to regenerate new cartilage, which allows the defects to continue to increase in size to OCD. In addition, the defects appear to expand in width over time as well as in depth, potentially due to the higher stress seen at the edge of the defect leading to edge loading and cartilage destruction (Gratz *et al.*, 2009). It has also been shown that individuals suffering with chondral defects and OCD have a significantly increased risk of suffering from osteoarthritis later on in life, further demonstrating the potential progressive degrading nature of cartilage damage (Messner and Maletius, 1996).

### **1.1.3.3 Characterisation and grading of cartilage defects**

There are a number of grading systems that aim to characterise the level of damage seen in articular cartilage, probably the best known of which was developed by Outerbridge (Outerbridge, 1961). In the Outerbridge classification system, cartilage defects are classified as Grade 0 (normal cartilage), Grade I (softening or swelling), Grade II (partial thickness defect), Grade III (full thickness defect) and Grade IV (osteochondral defect) (Deng, Chang and Wu, 2019). The Outerbridge system is easy to understand and use, but can often lack specificity in description of the defect and some studies have shown that the system has poor repeatability and reproducibility among orthopaedic surgeons. The overall

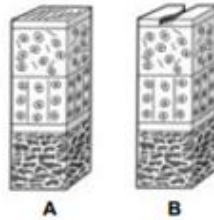
interobserver reliability ranges from somewhat moderate ( $\kappa = 0.52$ ) to extremely weak ( $\kappa = 0.28$ ), where absolute agreement is  $\kappa = 1.00$  (Cameron, Briggs and Steadman, 2003; Amenabar *et al.*, 2015). In addition to this, the Outerbridge system is dramatically held back by the difficulties of using it in conjunction with MRI imaging. Due to the limitations of the Outerbridge system, the International Cartilage Repair Society (ICRS) grading system is seeing a rise in prevalence. This system allows for arthroscopic or MRI grading. The ICRS grading system uses four grades, with some containing subcategories (Figure 4) (Brittberg and Winalski, 2003; Hoemann *et al.*, 2011). Normal cartilage demonstrating no defects or abnormalities is graded as 0. If the cartilage demonstrates surface softening or fibrillation this is characterised as a 1a with a 1b classification being given if small fissures or lacerations are seen. Defects which show obvious loss in the overlying cartilage but are no deeper than 50% of the cartilage's thickness are then classified as a Type 2 defect. In general, Type 3 defects are those that extend >50% of the cartilage thickness, and Type 3 is further split into three subtypes. Type 3a are defects that extend through more than 50% of the cartilage's depth but do not enter the calcified zone of cartilage. Type 3b are extended through the calcified zone but do not interrupt subchondral bone. Type 3c shows light defects in the subchondral bone. Type 4 defects extend the entire articular cartilage surface and also demonstrate severe damage and loss to the underlying subchondral bone.

**ICRS Grade 0 - Normal**



**ICRS Grade 1 – Nearly Normal**

Superficial lesions. Soft indentation (A) and/or superficial fissures and cracks (B)



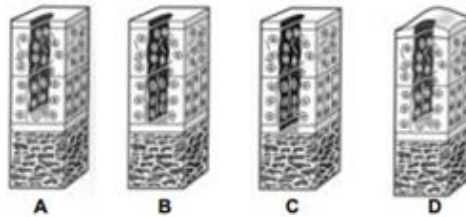
**ICRS Grade 2 – Abnormal**

Lesions extending down to <50% of cartilage depth



**ICRS Grade 3 – Severely Abnormal**

Cartilage defects extending down >50% of cartilage depth (A) as well as down to calcified layer (B) and down to but not through the subchondral bone (C). Blisters are included in this Grade (D)



**ICRS Grade 4 – Severely Abnormal**

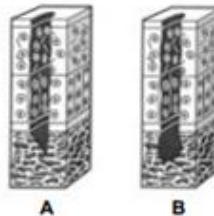


**Figure 4 ICRS Cartilage Injury Evaluation**

Visual demonstration of the appearance of each grading of cartilage damage. Reprinted from the ICRS Cartilage Injury Evaluation Package [www.cartilage.org], with permission from the International Cartilage Repair Society.

### **1.1.3.4 Long term impact of cartilaginous defects to the patient**

Acute traumatic injury to articular cartilage can rapidly show symptoms that present as pain in the joint when it is loaded, along with potential corresponding swelling (Gorbachova *et al.*, 2018). The joint may also have a dull aching sensation and patients may experience unlocking or clicking in the affected joint. On the other hand, damage arising from repetitive small trauma often presents asymptotically due to the aneural nature of cartilage (Krishnan and Grodzinsky, 2018; Tuerlings *et al.*, 2022). However, due to the low regenerative capacity of cartilage to heal as described above, the cartilage damage will progress over time to a full OCD, and the resulting symptoms are extremely similar to the symptoms seen during acute trauma. This kind of cartilage damage appears in some cases to progress to post-traumatic osteoarthritis, although it is unclear within the literature what the exact risk factors are. This subtype of osteoarthritis has been approximated to arise in around 50% of patients with a traumatic joint injury as described previously (Anderson *et al.*, 2011; Jang, Lee and Ju, 2021) (Figure 5). Post-traumatic osteoarthritis has been estimated to account for 12% of all osteoarthritis cases, but this estimate is hard to verify due to the large lag time that can potentially be present between the trauma and the formation of osteoarthritis (Brown *et al.*, 2006). It is important to note that once OCDs progress to osteoarthritis, the only widespread clinically available treatment is pain management or joint replacement (Hunziker *et al.*, 2014). Therefore, it is essential to intervene early at the OCD stage before disease progression occurs. It is also important to note that further treatments discussed within this literature review focus on treating OCD and not osteoarthritis.

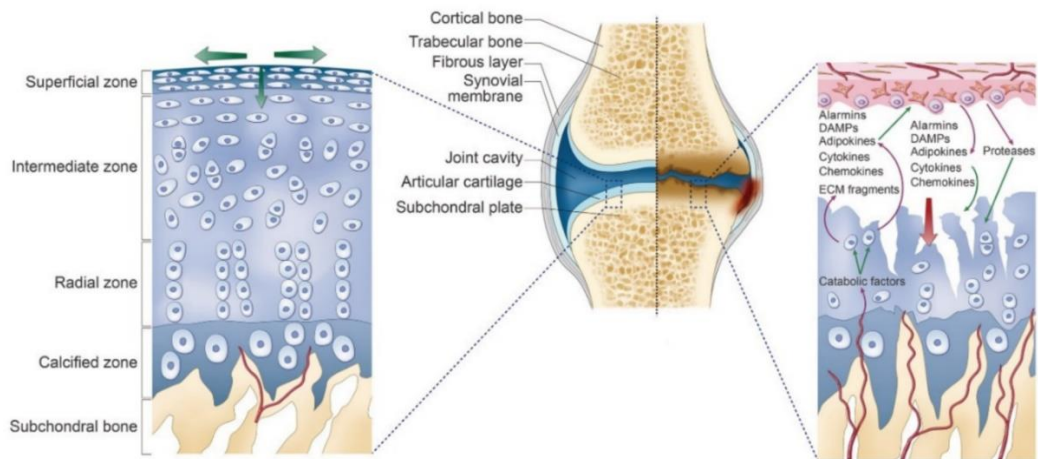


**Figure 5 Mechanisms of the formation of osteoarthritis within the human knee**

Left, healthy articular cartilage in its avascular state, with a continuous, uninterrupted structure. Right, osteoarthritic cartilage with vascular and bony invasion and breakdown of the continuous cartilage layer, and the presence of inflammatory and signalling molecules such as cytokines, chemokines, alarmins. Reprinted from Jang, S., Lee, K. and Ju, J. H. (2021) 'Recent Updates of Diagnosis, Pathophysiology, and Treatment on Osteoarthritis of the Knee', *International Journal of Molecular Sciences*, 22(5), pp. 2619. With open access article permissions

## 1.2 The current treatment strategies for cartilaginous lesions

There is currently no ideal drug-based or biological-based therapy for treating OCD, the only treatment options currently available are surgically based (Schindler, 2011; Hunziker *et al.*, 2014; Chimutengwende-Gordon, Donaldson and Bentley, 2020). However, the main current surgical interventions for OCD still do not provide satisfactory outcomes, each having serious flaws as discussed below. Furthermore to this, these surgical interventions are only appropriate for the treatment of OCD, and when the disease progresses to osteoarthritis the only appropriate surgical intervention is joint replacement (Hunziker *et al.*, 2014).

### 1.2.1 Microfracture or micro-drilling

This treatment modality relies on induction of an endogenous healing response, which is done through drilling of the subchondral bone at the area of the defect (Figure 6). This is undertaken through the use of a high-speed drill with a diameter of 1 to 2 mm with holes spread 3 to 5 mm apart (Steadman *et al.*, 1997; Camp, Stuart and Krych, 2013; Trofa *et al.*, 2022). This induces a healing response by causing surgically induced bleeding and subsequent clot formation as well as opening up the OCD to the vascular and perivascular spaces under the subchondral bone, the bony tissue itself, adipose tissue and the synovium. By opening up the subchondral defect to the underlying bone, growth factors as well as bone marrow derived stem cells are able to enter the defect to encourage endogenous healing responses. This microfracture treatment relies on a patient's own cells to encourage endogenous healing response, and thus is often more effective for younger patients who have a greater cellular activity and therefore are more likely to have a more active healing response (Asik *et al.*, 2008). However, on review of clinical investigations it is, clear that the cartilage formed is often fibrous rather than hyaline cartilage. This fibrous cartilage is able for a short time to reduce symptoms and restore some joint modality, but often will break down over time and will no longer be functional. Furthermore, due to the treatment relying on the individual's own endogenous healing response, it has high levels of variability and does not provide a consistent healing response between patients (Furukawa *et al.*, 1980; Jackson *et al.*, 2001; Chen *et al.*, 2009).



**Figure 6 Endoscopic images of microfracture of a chondral defect**

(a) Shows the original defect, (b) shows a debrided defect and (c) shows the defect following microfracture. Reprinted from Camp, C. L., Stuart, M. J. and Krych, A. J. (2013) 'Current Concepts of Articular Cartilage Restoration Techniques in the Knee', *Sports Health*, 6(3), pp. 265-273. With permission from the Journal of Sports Health.

### **1.2.2 Osteochondral autografts (also known as mosaicplasty)**

This treatment involves taking small cylindrical osteochondral plugs (4 to 10 mm in diameter, 15 to 20 mm in depth) (Figure 7) from less weight-bearing areas of the joint or another joint from the same individual (Hangody *et al.*, 2008; Patil and Tapasvi, 2015). These plugs are then transplanted into the OCD in a mosaic pattern to fill the defect. This technique has seen some promising outcomes in cartilage regeneration. However, upon review of the treatment, a serious problem still remains concerning donor site morbidity that can cause further damage to an already diseased joint (Hangody *et al.*, 2001; Koh *et al.*, 2004; Baumbach *et al.*, 2008).

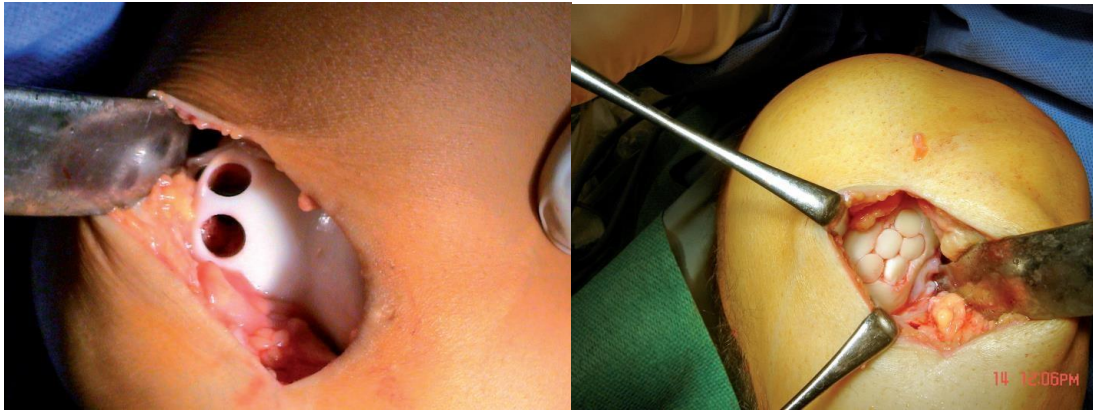


**Figure 7 Mosaicplasty of the human knee**

Mosaicplasty undertaken in a human knee by using five pieces of 6.5mm graft. Reprinted from Hangody, L., Vásárhelyi, G., Hangody, L. R., Sükösd, Z., Tibay, G., Bartha, L. and Bodó, G. (2008) 'Autologous osteochondral grafting--technique and long-term results', *Injury*, 39 Suppl 1, pp. S32-9. With permission from Injury International Journal of the Care of the Injured.

### 1.2.3 Osteochondral allografts

This treatment involves transplantation of cadaveric tissue into a damaged lesion. Rather than inducing a healing response, allograft transplantation aims to directly replace the lost or damaged cartilage (Hunziker *et al.*, 2014; Trofa *et al.*, 2022) and thus conveys the benefits of no donor site morbidity and the ability to fill relatively large size defects. However, it has been suggested that the use of cadaveric tissue poses the risk of immune rejection, though a number of studies have found little immunological reaction to the use of cadaveric tissue with no need for the use of immunosuppressants (Phipatanakul *et al.*, 2004). One downfall of this treatment is that there is a dramatic shortage of fresh donor material, as well as the ever-looming risk of disease transmission (Chahal *et al.*, 2013). The risk of disease transmission was particularly highlighted when individuals receiving an ACL reconstruction from allograft tissue suffered sepsis of the knee (Kainer *et al.*, 2004).

## 1.2.4 Autologous chondrocyte implantation

This treatment involves the harvesting of an individual's own chondrocytes through arthroscopic biopsy of a less weight-bearing area of the joint (Brittberg *et al.*, 1994). These chondrocytes are then enzymatically extracted from the cartilaginous tissue and then expanded in culture, allowing for the generation of >10 million cells from the hundred thousand obtained from the biopsy. These chondrocytes are then reimplanted into the OCD under a periosteal flap (Figure 8). Although the biopsy site is small, it has been shown that there can be morbidity and a heightened risk of the formation of arthritis in the biopsy area (Bhosale and Richardson, 2008; Jones *et al.*, 2008). Moreover, due to requirement of the two surgical procedures and tissue culture, this treatment is extremely expensive and long-term patient planning is required. Although the ACI-technique is highly popular, however, its ability to outperform other simpler and cheaper interventions such as microfracture has yet to be established. Knutsen *et al.*, 2007 showed after five years post intervention, no significant difference was seen between ACI and microfracture in clinical outcomes and radiographic results. It was suggested by Hunziker *et al.*, 2014 that the reason for the lack of significant difference between these interventions is that, both treatments' mechanisms of healing are basically the same. When the ACI technique is performed the walls and floor of the defect are debrided and "neatened", this then induces local bleeding and a spontaneous repair response from the bone-marrow spaces as seen with in microfracture.

In more recent years, the ACI approach has been Improved to create the new technique of matrix-associated autologous chondrocyte implantation (MACI). Within MACI, autologous chondrocytes are implanted within a matrix which then functions as a scaffold to help tissue regeneration. The use of a matrix removes the requirement for the periosteal flap as the chondrocytes are no longer suspended within fluid (Jones *et al.*, 2008). However, although this approach has shown excellent promise, a lack of sufficient data still exists to confidently prove

its superiority over other interventions (Hunziker *et al.*, 2014; Colombini *et al.*, 2023).

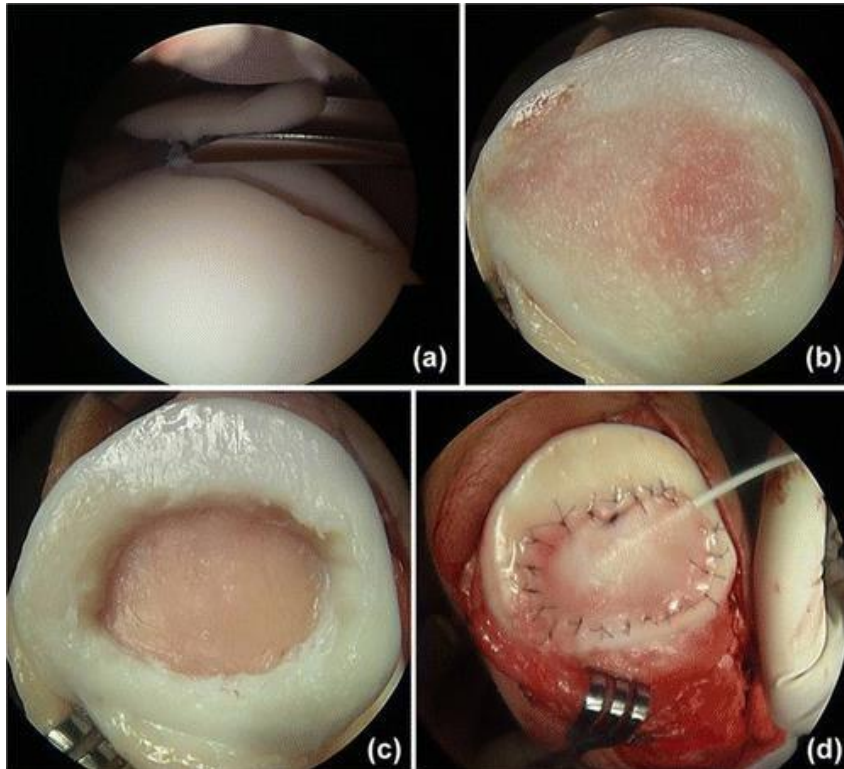


**Figure 8 ACI treatment of the patella**

Osteochondral defect of the patella treated with ACI. (a) The biopsy site for chondrocyte harvesting located in the superolateral trochlea. (b) Identification of the lesioned area. (c) debrided area. (d) Cells were injected under a flap. Reprinted from Camp, C. L., Stuart, M. J. and Krych, A. J. (2013) 'Current Concepts of Articular Cartilage Restoration Techniques in the Knee', *Sports Health*, 6(3), pp. 265-273. With permission from the Journal of Sports Health.

### 1.3 Tissue engineering approaches

Due to the lack of a satisfactory surgical intervention, there is a chronic need for a more effective intervention that does not contain the serious drawbacks of the current treatment methods. A new intervention must produce cartilage which is physiologically identical to natural cartilage as well as enduring. A tissue engineering approach may be required. As an emerging field of research, tissue engineering aims to develop functional tissue replacements by the combination of experimental biological and engineering approaches and represents a particularly

attractive approach for the treatment of musculoskeletal diseases (Armiento *et al.*, 2018).

### **1.3.1 Cell sources for cell-based therapies for cartilage regeneration**

Utilisation of an individual's own cells seems to play a key role in many tissue engineering approaches for cartilage regeneration (Tuan, Boland and Tuli, 2003). One of the most commonly used cell types for cartilage regeneration is the primary chondrocyte, with a proven clinical track record of relative success (Pelttari *et al.*, 2006). However, primary chondrocytes have a number of disadvantages, given the fact that donor site morbidity is seen from the harvesting process, potentially damaging further an already diseased joint (Benz *et al.*, 2002). Primary chondrocytes also have a very limited lifespan in culture, with the risk of de-differentiation being ever present; this makes them difficult to expand to usable levels. Expansion *in vitro* also often sees a conversion from their spherical morphology to a flattened, fibroblast-like phenotype. Therefore, the utilisation of stem cells may be a better approach. Stem cells possess a wide availability within different adult tissues, including on but not limited to bone marrow (BM-MS) and adipose tissue (AT-MS). Adult stem cells also show a large capacity and tolerance to *in vitro* expansion (Zuk *et al.*, 2001; Lee *et al.*, 2004; Acharya *et al.*, 2012; Chen *et al.*, 2012; Lee *et al.*, 2023). To utilise MSs within cartilage regeneration, MSs are required to differentiate to chondrocytes. The chondrogenic differentiation process relies on a multitude of factors, including a variety of growth factors and other parameters such as cell density, cell adhesion and three-dimensional environments. To induce chondrogenesis, high-density cultures in the presence of a multitude of specific growth factors and supplements are required (Cassiede *et al.*, 1996; Johnstone *et al.*, 1998; Barry *et al.*, 2001; Sekiya, Colter and Prockop, 2001; Tuan, Boland and Tuli, 2003). However, the utilisation of MSs to create chondrocytes does not come without disadvantages

(Sekiya *et al.*, 2002; Winter *et al.*, 2003; Pelttari *et al.*, 2006). It has been shown that MSC derived chondrocytes present the risk of phenotypic instability with premature hypertrophy compared to primary chondrocytes, with the up regulation of Type X collagen and matrix metalloproteinase 13 (MMP-13), as well as undesirable calcification of cultures.

With the push towards using stem cells to generate chondrocytes for cartilage regeneration, the issue remains of maintaining and ensuring these chondrocytes are directed towards the defect and remain in place after implantation (Hunziker *et al.*, 2014). It has been shown within ACI that use of a direct cell suspension during injection into the defect demonstrates extremely low cell retention (Nixon *et al.*, 2011).

Other methods have been developed to help improve cell retention by using a periosteal flap, but they still exhibit donor site morbidity (Kajitani *et al.*, 2004; Barié *et al.*, 2020). Therefore, if these differentiated chondrocytes are to be used for cartilage regeneration, a strategy to encapsulate and maintain these chondrocytes in the site of the defect is required. This could take the form of a 3D scaffold expanding on the work seen within MACI.

### **1.3.2 Growth factors involved and used for osteochondral regeneration**

Utilisation of growth factors and signalling molecules as part of a combined tissue engineering approach plays a key role in osteochondral tissue engineering as these signalling molecules can induce cellular differentiation, as well as direct tissue specific extracellular matrix deposition (Seo *et al.*, 2014). There are a variety of methods of deploying these growth factors to direct and assist osteochondral regeneration, varying from their presence within cell culture media to their incorporation into biological scaffolds. A large and varied number of

growth factors/cytokines are in current use for cartilage tissue regeneration including TGF- $\beta$ 1, insulin-like growth factor-1 (IGF-1) and fibroblast growth factor-2 (FGF-2) (Mano and Reis, 2007; Santo *et al.*, 2012; Niu *et al.*, 2023). There is also a correspondingly wide variety of factors/cytokines for bone regeneration including BMPs, IGF-1/2 and FGFs (Salgado, Coutinho and Reis, 2004).

Traditional chondrogenic media consists of TGF- $\beta$ , Insulin-Transferrin-Selenium (ITS), Dexamethasone and Ascorbic acid (vitamin C). Of these growth factors, TGF- $\beta$ 1, 2, and 3 are probably the most ubiquitously utilised and most well-known growth factors within cartilage regeneration (Solchaga, Penick and Welter, 2011). These growth factors have been demonstrated to induce expression of Sox-9 (a key transcription factor in chondrogenic differentiation and maintenance) as well as induce cartilaginous ECM production in MSCs (Oh *et al.*, 2014). ITS is a supplement used in chondrogenic culture systems to support the formation of cartilage (Solchaga, Penick and Welter, 2011). ITS in general is associated with improving cell survival and maintenance of metabolic activities in differentiated chondrocytes (Kisiday *et al.*, 2005; Enochson, Brittberg and Lindahl, 2012). Insulin is the main active component of ITS and promotes extracellular matrix production in chondrocytes via direct or indirect activation of the IGF-1 receptor (Mueller *et al.*, 2013; Kellner *et al.*, 2001). Dexamethasone promotes chondrogenesis by directly regulating the expression of cartilage ECM genes as well as synergistically enhancing TGF- $\beta$  mediated upregulation of their expression (Derfoul *et al.*, 2006; Tangtrongsup and Kisiday, 2015). Ascorbic acid is required as a cofactor for enzymes that hydroxylate proline and lysine in pro-collagen, allowing collagen to form its proper helical structure, leading to up regulation in collagen deposition (Temu *et al.*, 2010; Asnaghi *et al.*, 2018; Theruvath *et al.*, 2021).

In addition to traditional chondrogenic media, other factors have been utilised for cartilage regeneration. IGF-1 is another signalling molecule extensively used within cartilage regeneration, with it being a major anabolic factor seen within cartilage (Schmidt, Chen and Lynch, 2006; Re'em *et al.*, 2012; Wen *et al.*, 2021).

Anabolic effects induced by IGF-1 originate from its ability to induce an increased synthesis of proteoglycans and collagens while simultaneously inhibiting the transcription of degradative enzymes such as MMPs (Hui, Rowan and Cawston, 2001; Davies *et al.*, 2008; Tahimic, Wang and Bikle, 2013). IGF-1 also been shown to synergistically interact with other signalling molecules such as TGF- $\beta$  to induce further cartilage regeneration (Longobardi *et al.*, 2006; Davies *et al.*, 2008).

Traditional osteogenic media consists of Dexamethasone and Ascorbic acid (vitamin C). Dexamethasone has been shown to activate the Wnt/ $\beta$ -catenin and BMP signalling pathway, leading to the activation of RUNX2, which induces osteogenesis (Hamidouche *et al.*, 2008; Shafaei and Kalarestaghi, 2020). RUNX2 is a critical factor in differentiation and maturation of osteoblasts and therefore plays a fundamental role in bone formation and growth (Kawane *et al.*, 2018; Xin, Zhao and Wang, 2022). Whereas ascorbic acid plays the same role as in traditional chondrogenic media, leading to up regulation of collagen deposition (Jaiswal *et al.*, 1997; Robey, 2011; Langenbach and Handschel, 2013). In addition to traditional osteogenic media, other factors have been utilised for subchondral bone regeneration, the potential utilisation of BMP-2 has been extensively investigated for its potential to increase scaffold's osteogenic capacity. BMP-2 functions to improve the scaffold's osteogenic capacity by inducing osteoblast differentiation, as well as stimulating ECM deposition and mineralisation (Li *et al.*, 2006). In particular, BMP leads to the increase in expression of Type I collagen, osteopontin, osteocalcin, bone sialoprotein, and alkaline phosphatase (ALP) (Geiger, Li and Friess, 2003; Plantz and Hsu, 2020).

## 1.4 Scaffolds for an osteochondral tissue engineering approach

Another element which is being extensively explored as an engineering approach for cartilage regeneration is the utilisation of scaffolds. Using a scaffold-based approach for cartilage regeneration conveys a number of benefits, firstly that the scaffold is able to replace the lost bulk morphology of both cartilage and underlying subchondral bone (Frenkel and Di Cesare, 2004). As well as this, it provides a three-dimensional environment which can encourage cell proliferation and reintegration of the scaffold with native cartilage (Ge *et al.*, 2012; Fahmy *et al.*, 2017).

It is important that any scaffold is able to regenerate both the cartilage and underlying subchondral bone, and failure to do this is the downfall of many cartilage regenerating tissue engineering techniques (Hunziker *et al.*, 2014). Without this underlying subchondral bone, any overlying cartilage regeneration technique has an extreme risk of subsidence and therefore failure. It is important to create resilient subchondral bone that is able to resist and distribute articular cartilage loading.

The designing of scaffolds for osteochondral regeneration presents a unique difficulty in the fact that the design requires a scaffold to conform to the different tissue types of bone and cartilage (Frenkel and Di Cesare, 2004). The absolute minimum function of a tissue engineering scaffold is to provide a 3D environment which encourages the embedding of native cells to degrade the scaffold and replace the scaffold with new synthesised natural tissue.

The new tissue will hopefully replace the old scaffold, taking on the scaffold's original shape and dimensions. The design criteria for a scaffold include that it must first and foremost be biocompatible, in that the scaffold itself should not have any adverse inflammatory or immune response due to degradation products

(Babensee *et al.*, 1998). A large number of factors exist that affect scaffold biocompatibility, ranging from the chemical make-up of the scaffold, its structure and morphological features, the way the scaffold has been processed and the sterilisation techniques used (Lu *et al.*, 2001). Residual chemicals such as solvents used in the creation of the scaffold can also lead to bioincompatibility if residue is left within the scaffold.

In addition, the scaffold must have enough porosity to allow ingrowth of host cells (and/or preloading with appropriate cell types) but also have adequate mechanical stability to allow for its survival during handling and implantation, as well as loading during normal joint articulation (Risbud and Sittinger, 2002; Frenkel and Di Cesare, 2004). However, a caveat is that the scaffold cannot have so great mechanical properties, in particular stiffness, to cause shielding of the mechanosensitive cartilage-forming cells during loading which would lead to its failure to integrate (Huey, Hu and Athanasiou, 2012).

### **1.4.1 Cell material interactions**

A major downfall of what look like excellent tissue engineering scaffolds, in terms of physical and mechanical properties, is the scaffold's ability to interact with cells. It is well established that cells act differently in a 3D environment compared to a 2D monolayer (Baker and Chen, 2012) (Figure 9). Cells cultured in a two-dimensional environment grow in a flat monolayer and can spread freely in the X and Y planes, with an absolute restriction to the Z plane. This leads to cells cultured under these conditions to have a forced apical–basal polarity. These culture conditions may be relevant to some cell types, like epithelial cells, but for many others this presents a physiological irrelevant environment. A more physiologically relevant environment is one consisting of a three-dimensional structure, often mimicking ECM, where embedded cells form a stellate morphology, only forming regions of polarization during cell locomotion (Mseka,

Bamburg and Cramer, 2007). This variation in cell morphology between 2D and 3D has been shown to directly impact cell characteristics, dramatically improving the tissue regenerative capacity of cells (Weaver *et al.*, 2002; McBeath *et al.*, 2004; Meyers, Craig and Odde, 2006). Therefore, when designing a three-dimensional scaffold for tissue regeneration, several nuanced factors need to be taken into account which may not be seen by culturing cells in 2D. First and foremost, the scaffold material must be non-toxic both to cells in contact with the scaffold and cells that may be in contact with degradation products of the scaffold. After this, cells must be able to adhere, colonise, proliferate and differentiate on the scaffold surface, eventually over time converting the scaffold itself into native tissue.

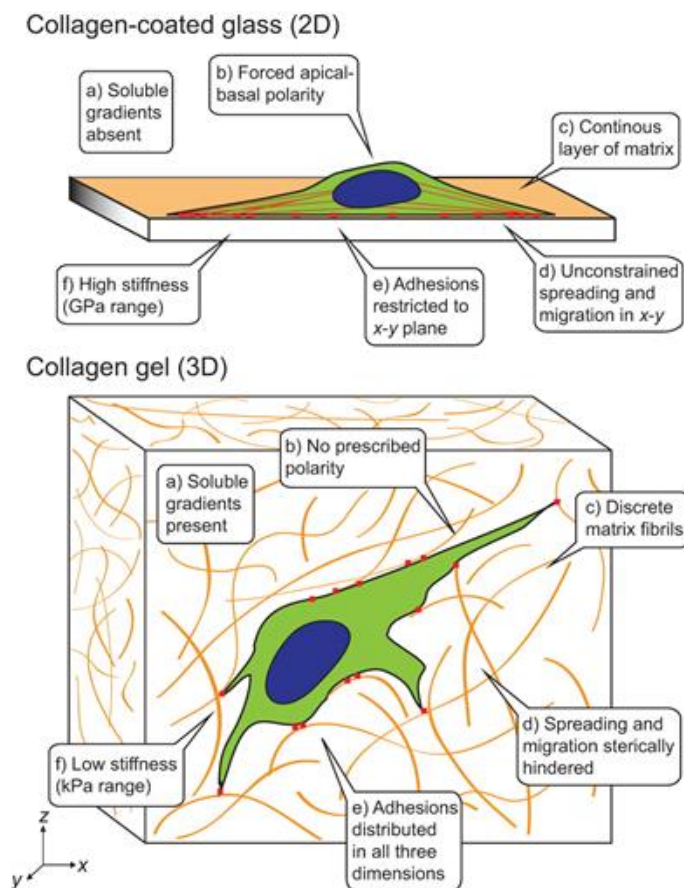


**Figure 9 The differences between 3D culture and 2D monolayer culture on cell behaviour**  
 For many cell types, two-dimensional monolayer culture presents a physiologically irrelevant environment, and thus detrimentally affects cell behaviour in regards to potential tissue regeneration. Reprinted from Baker, B. M. and Chen, C. S. (2012) 'Deconstructing the third dimension – how 3D culture microenvironments alter cellular cues', *Journal of Cell Science*, 125(13), pp. 3015-3024. With permissions *Journal of Cell Science*.

For cells to be able to adhere to the scaffold's surface, cell adhesions must be able to be formed between the cell and the scaffold's surface; these cell adhesions consist of large transmembrane multi-protein complexes (Sun, Guo and Fässler, 2016; Jansen, Atherton and Ballestrem, 2017; Revach, Grosheva and Geiger, 2020). These complexes function to form a mechanical coupling between the cell's internal cytoskeleton in the extracellular microenvironment and allow for cell locomotion along a scaffold's surface, as well as allowing for cells to penetrate through the scaffold's material structure (Pelham and Wang, 1997) (Figure 10). Thus, it is important for a scaffold's surface to contain motifs that allow for the binding of a family of adhesion proteins known as integrins, allowing for cell attachment and locomotion upon the scaffold surface (Revach, Grosheva and Geiger, 2020).

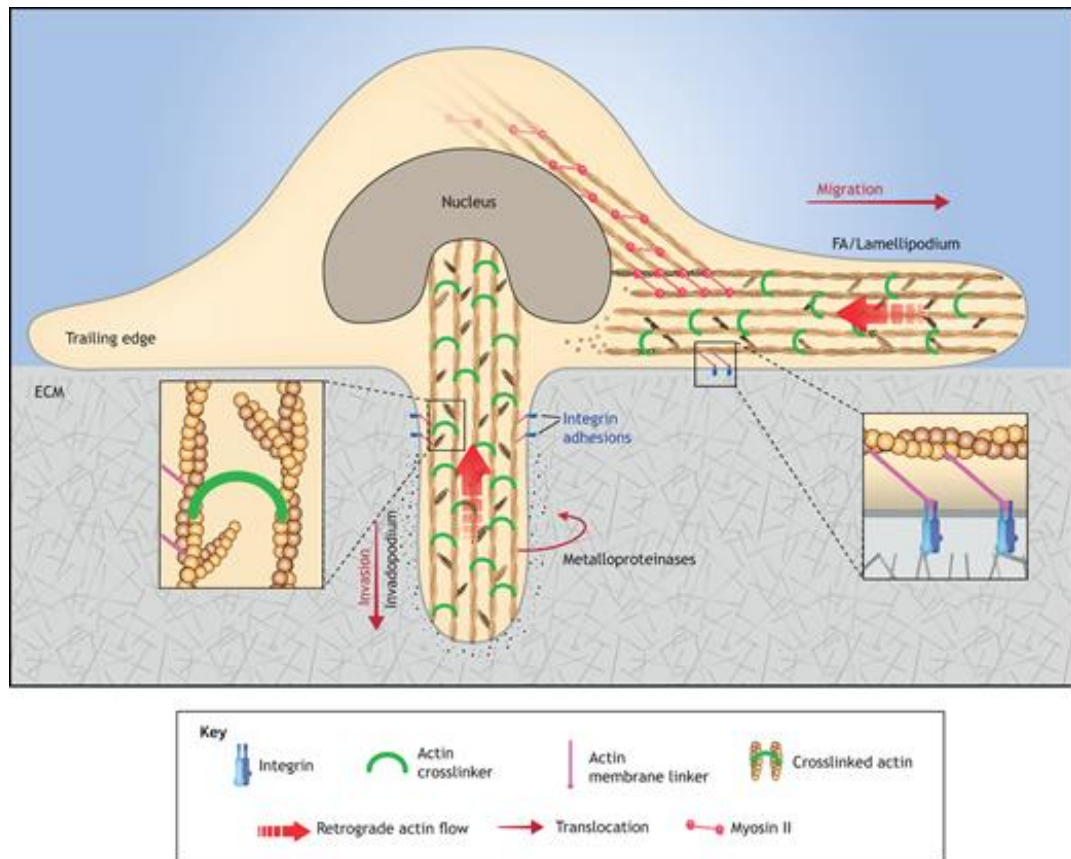


**Figure 10 Cell locomotion along a substrate**

Cell locomotion along a scaffold's surface via the utilisation of integrins and cytoskeleton, as well as cellular penetration into the scaffold's surface. Reprinted from Revach, O.-Y., Grosheva, I. and Geiger, B. (2020) 'Biomechanical regulation of focal adhesion and invadopodia formation', *Journal of Cell Science*, 133(20), pp. jcs244848. With permissions from the *Journal of Cell Science*.

## 1.4.2 Surface topography

Scaffold surface topography can play a key role in guiding and influencing cell fate determination. Surface topography can affect cell behaviour through numerous pathways, impacting cell adhesion, alignment, morphology, proliferation, and cell differentiation (Hatano *et al.*, 1999; Muzzarelli *et al.*, 2016). A key component of surface topography is surface roughness, with rougher surfaces showing an increased surface area compared to smooth surfaces. It has been demonstrated that rougher scaffold surfaces show increased protein adsorption, as well as increased cell surface interactions leading to increased level of cell adhesion and increased degradation rate (Pérez *et al.*, 2013; Perez and Mestres, 2016; Zhang *et al.*, 2018a; Majhy, Priyadarshini and Sen, 2021). Furthermore, rougher surfaces

have been shown to increase the potential for osteogenic differentiation and bone like extracellular matrix deposition. Hatano et al., 1999 showed that primary rat osteoblasts demonstrated significantly elevated osteocalcin expression and ALP activity on the rough surface (0.81  $\mu\text{m}$ ) in comparison with the smooth one. It still remains to be elucidated whether surface roughness is able to impact chondrogenesis. The few studies that have investigated this have found that surface stiffness had a far greater impact than roughness on a scaffold's ability to support chondrogenesis (Wu *et al.*, 2016; Zhang, Yu and Zhao, 2016).

## **1.5 Requirements of a scaffold to be used in tissue regeneration**

### **1.5.1 General requirements of a scaffold to be used in regeneration**

The general requirements of a scaffold to be used in regeneration include firstly biocompatibility, meaning it should be non-toxic and should not elicit an immune response or cause adverse reactions when in contact with living tissues or cells (O'Brien, 2011). It should also possess an interconnected porosity that allows for the ingrowth and infiltration of cells, as well as the free movement of nutrients and oxygen (Li *et al.*, 2023). The scaffold must also possess adequate mechanical properties that allow it to survive manipulation, as well as post-implantation loading. It is important for the scaffold to possess biodegradability, allowing for the gradual degradation of the scaffold over time and its replacement with newly regenerated tissue (Rezwan *et al.*, 2006). Scaffold sterility is also an essential characteristic, ensuring the scaffold is free from microbial contamination (Dai *et al.*, 2016). Finally, the scaffold must be scalable and cost-effective, enabling its mass production to meet clinical demand.

## 1.5.2 Requirements of scaffolds used for cartilage regeneration

The requirements of the scaffold for cartilage regeneration are the same as those seen within the general requirements. However, there are also additional factors to consider when creating cartilage scaffolds (Hutmacher, 2000). The scaffold must be able to help direct chondrogenesis and promote new cartilage formation. In addition to this, the scaffold must not support the formation of blood vessels, neurons, and lymphatics (Wasyłeczko, Sikorska and Chwojnowski, 2020). The scaffold should preferably have a pore diameter in the range of 90-120  $\mu\text{m}$  and surface stiffness in the range of 10-50 kPa (Kuboki, Jin and Takita, 2001; Kong *et al.*, 2005; Engler *et al.*, 2006; Rowlands, George and Cooper-White, 2008; Kim *et al.*, 2010; Shih *et al.*, 2011; Witkowska-Zimny *et al.*, 2013; Yang *et al.*, 2017b; Datko Williams *et al.*, 2018; Sun *et al.*, 2018; Yang *et al.*, 2020; Gavazzo *et al.*, 2021).

## 1.5.3 Requirements of a scaffold to be used for bone regeneration

The scaffold requirements for bone regeneration align with the general requirements, but there are additional factors to consider specifically for bone scaffolds. The scaffold needs to actively guide osteogenic differentiation and facilitate the formation of new bone tissue. It should also support mineralization of the newly formed ECM (Filippi *et al.*, 2020). Furthermore, the scaffold should allow for vascular invasion to facilitate neovascularization and support the development of a blood supply (Hutmacher, 2000). Ideally, the scaffold should have a pore diameter around 300  $\mu\text{m}$ , a surface stiffness ranging from 40-100 kPa, and possess a rough surface topography (Kong *et al.*, 2005; Engler *et al.*, 2006; Rowlands, George and Cooper-White, 2008; Shih *et al.*, 2011; Witkowska-Zimny *et al.*, 2013; Pérez *et al.*, 2013; Yang *et al.*, 2017b; Datko Williams *et al.*, 2018; Sun *et al.*, 2018; Zhang *et al.*, 2018a; Yang *et al.*, 2020; Gavazzo *et al.*, 2021).

## **1.6 Types of Biomaterials for osteochondral tissues engineering**

Typically, four types of biomaterials are used in scaffolds for osteochondral regeneration: ceramics, metals, synthetic polymers and natural polymers, each with unique advantages and disadvantages (O'Brien, 2011).

### **1.6.1 Natural polymers**

Natural biomaterials can be derived from plants or animal sources (Bernhard and Vunjak-Novakovic, 2016), with numerous options in current use and research. Some examples of natural biomaterials are agarose, alginate, chitosan, collagen, fibrin, and silk. Due to the natural biomaterials' sources, they have the notable advantage of having innate cell adhesion and proliferation behaviours providing a physiologically natural environment for cells (Panseri *et al.*, 2012). In addition, natural materials are biodegradable and biocompatible, often mimicking natural ECM. However, natural biomaterials often show notable disadvantages such as immunogenicity, batch variation, the risk of animal disease transmission, they are often mechanically weak if not properly modified, and pose the risk of being rapidly degraded (Lee and Shin, 2007; Nocera *et al.*, 2018).

#### **1.6.1.1 Silk fibroin from the *Bombyx mori***

Silk is a natural protein-based material that is produced by a variety of members of the Class Arachnida and Order Lepidoptera (Craig, 1997; Altman *et al.*, 2003; Choi *et al.*, 2018). These organisms use silk in the creation of a structural framework such as in web or cocoon formation. Due to silk's pre-existing extensive use within the textile industry, it was estimated that in 2002, there were approximately 400,000 tons of dry silkworm cocoons available worldwide per

annum. Silk is already used within a variety of biomedical applications (Zhang, 2002). The reason for its extensive use is that silk fulfils many of the requirements for successful biomaterials as previously discussed; it possesses biodegradability, biocompatibility, a minimal inflammatory response post implantation, as well as long-term compatibility, and allows for cell adhesion to its surface (Thurber, Omenetto and Kaplan, 2015; Teramoto, Shirakawa and Tamada, 2020; Rnjak-Kovacina *et al.*, 2015a; Rnjak-Kovacina *et al.*, 2015b).

The silk created by the domesticated silkworm *Bombyx mori* consists of two main components: silk fibroin and sericins (Zhou *et al.*, 2000). Silk fibroin fibres have a diameter of approximately 10–25 µm and consist of two proteins, a heavy chain approximately 390 kDa in size and a light chain approximately 26 kDa in size (Tanaka, Mori and Mizuno, 1993; Tanaka *et al.*, 1999). These proteins exist in a one-to-one ratio linked by a single disulphide bond between the Cys-c20 of the heavy chain and Cys-172 of the light chain (Inoue *et al.*, 2000) (Figure 11). A 25 kDa glycoprotein, named P25, is also non-covalently linked to the silk fibroin (Tanaka, Inoue and Mizuno, 1999). This protein structure is coated with family proteins refer to as sericins which are hydrophilic in nature and are 20–310 kDa in size (Zhou *et al.*, 2000; Cao and Wang, 2009).

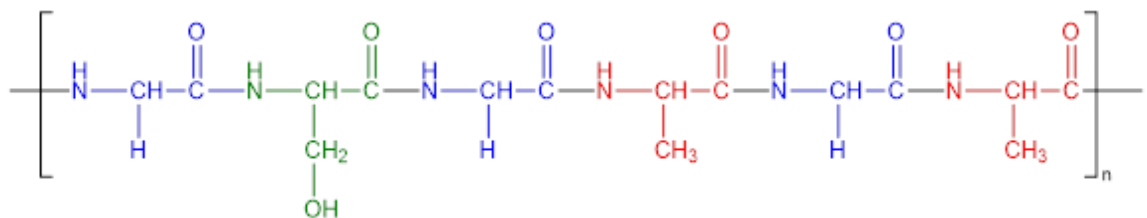


**Figure 11 Chemical structure of silk fibroin from *Bombyx mori***

Blue represents the amino acid glycine, green represents the amino acid serine, and Red represents the amino acid arginine. Image was compiled in chemDraw 22.0.

Silk fibroins require purification to create the aqueous silk fibroin solution that serves as a base material for silk fibroin tissue engineering. This involves removal of sericin which accounts for 25-30% of the silk cocoon's mass (Zhang, 2002). This process is typically undertaken by boiling silk cocoons in an alkaline solution of sodium carbonate, which removes the undesirable glue-like sericin protein. This is followed by solubilisation in aqueous lithium bromide solvent and purification via dialysis. This process renders an aqueous solution of relatively pure silk fibroin.

The reasoning for the removal of sericin is that numerous studies have demonstrated that this small protein is able to induce immunological response when implanted inside the body (Aramwit *et al.*, 2009; Teuschl, van Griensven and Redl, 2013; Li *et al.*, 2015b; Zhang *et al.*, 2021; Ode Boni *et al.*, 2022). In some applications such as wound care this immunological response may have beneficial effects, as the immunological reaction causes cells to be drawn to the site of the wound, helping to encourage healing and lowering the likelihood of infection (MacLeod and Mansbridge, 2015). However, in applications such as osteochondral scaffolds, this immunological response is non-desirable as it increases the likelihood of scaffold failure and the probability of fibrocartilage formation rather than hyaline (Jia *et al.*, 2021; Li *et al.*, 2022).

To convert the silk fibroin solution into a usable biological scaffold for use within tissue engineering, the silk fibroin solution can be subjected to freezing which leads to the formation of ice crystals within the solution (Wray *et al.*, 2012; Saha *et al.*, 2013; Gu *et al.*, 2022). Following this, via sublimation within a freeze-drier, the ice crystals are removed, leaving a porous scaffold behind. This process utilises no harmful solvents as it fundamentally relies on the properties of water alone. This process also has advantages over the utilisation of porogens such as sodium chloride in the fact that it provides greater control over scaffold crystallinity as well as degradation properties (Hu *et al.*, 2011).

## 1.6.2 Synthetic polymers

Synthetic biomaterials are derived within the laboratory from monomers which are polymerised creating such materials as poly(lactic acid) (PLA), poly(glycolic acid) (PGA), Poly(ethylene glycol) (PEG) and their co-polymers Polylactic-co-glycolic acid (PLGA), poly(propylene fumarate) (PPF), poly(dioxanone) (PDO) and poly( $\epsilon$ -caprolactone) (PCL) (Mano and Reis, 2007; Trofa *et al.*, 2022). Synthetic materials present a notable advantage over natural biomaterials due to their synthetic nature: their mechanical properties and rate of degradation can be easily modified, meaning that the mechanical properties of the material can be better aligned with that of natural cartilage and the degradation rate matched with the rate of new cartilage production (Capito and Spector, 2003). They also have the benefit of easy reproducibility with smaller batch variation (Oh *et al.*, 2003; Sheikh *et al.*, 2016). However, unlike natural materials, synthetic materials often lack cell adhesion motifs and are often hydrophobic preventing cell attachment and proliferation on their surface (Sarasam, Krishnaswamy and Madihally, 2006). Furthermore, these scaffolds face degradation *in vivo* via a hydrolysis reaction, and although this does not directly produce by-products that are immunoactive, it has the potential to reduce local pH, possibly stimulating an immunological response (Getgood *et al.*, 2009).

### 1.6.2.1 PEGT/PBT Thermoplastic

PEGT/PBT is a series of segmented block copolymers (often sold under the tradename Polyactive™); the properties of this thermoplastic, as with all block copolymers, are a result of its constituent segments blending both their mechanical and physical properties (Fakirov and Gogeva, 1990b; Fakirov and Gogeva, 1990a) (Figure 12). The relatively soft and hydrophilic nature of the PEGT segments contribute elastomeric properties as well as hydrophilicity, whereas the hard hydrophobic PBT segments contribute rigidity and improved mechanical

strength. By varying the weight ratios of the two segments (PEGT and PBT) and the segments' molecular weights, an entire family of polymers can easily be obtained with wide ranging physicochemical, biological and mechanical properties (Papadaki *et al.*, 2001). This gives rise to the possibility of utilising different blends of PEGT/PBT depending on the scaffold's requirements. Various studies have been undertaken to demonstrate the biocompatibility, as well as the biodegradability of this polymer blend (van Dorp *et al.*, 1999; Ring *et al.*, 2007; Lamme *et al.*, 2008). It has been used within a large number of applications such as cartilage, bone, and skin regeneration and within clinical trials for the creation of artificial tympanic membrane (Grote, 1990), as well as bioactive coatings on load-bearing dental and hip implants (Meijer *et al.*, 1995; Sakkars *et al.*, 2000).

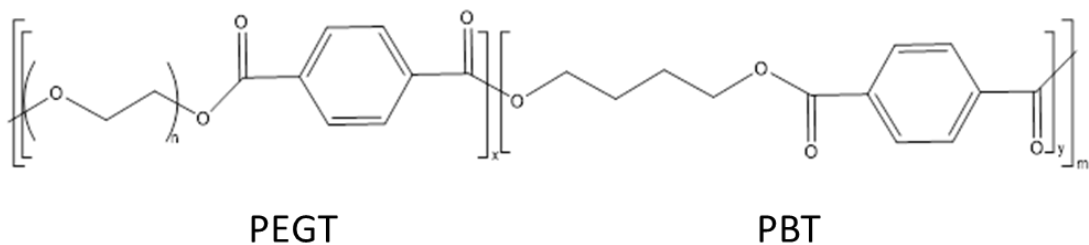


**Figure 12 Chemical structure of PEGT/PBT segmented block copolymers**  
Image was compiled in chemDraw 22.0.

### 1.6.3 Ceramics and glasses

Ceramics, such as hydroxyapatite and other calcium phosphate-based ceramics, as well as bioactive glasses such as Bioglass<sup>®</sup>, have been widely explored within bone regeneration; thus, potentially making them suitable for subchondral bone regeneration (Rezwan *et al.*, 2006; Jones, Lee and Hench, 2006; Trofa *et al.*, 2022). Bioglasses and ceramic scaffolds have been shown to encourage and enhance biomineralization of the scaffold, allowing for the formation of a bone-like apatite layer on the scaffold surface. This layer encourages osteointegration with the host tissue. This scaffold type has also been shown to be osteoconductive and osteoinductive (Xynos *et al.*, 2000; Mastrogiacomo *et al.*, 2005). Ceramics and

bioglasses can also have their degradation rates modified by changing their porosity, allowing them to be tailored so that their degradation kinetics are the most appropriate to the tissue. The notable disadvantage of ceramics and bioglass is that although they demonstrate excellent stiffness, they are extremely brittle and show very little ability to plastically deform and therefore are unable to absorb large amounts of energy during high stress loading (Nooeaid *et al.*, 2012). Furthermore, increases in porosity to adjust degradation rate can further impair the mechanical properties.

### **1.6.4 Metallic scaffolds**

Metallic materials have been extensively used within orthopaedic implants, with the main materials used being titanium, titanium alloys, stainless steels, and cobalt-chromium alloy (Barui *et al.*, 2017; Zhang *et al.*, 2019). Their relative success in bone implants makes them potentially useful as a replacement for lost subchondral bone. The main benefits of using metallic scaffolds are their excellent mechanical properties and fatigue resistance, however they have the notable disadvantage of being bio-inert, and due to their lack of degradation functionality they act to replace bone rather than encourage its healing (Guo *et al.*, 2013). It is also possible for the production and accumulation of wear particles over time as well as scaffold corrosion (Bal *et al.*, 2010).

### **1.6.5 Scaffold surface chemistry modification**

Scaffolds can also undergo surface modification to improve cell adhesion; this can be the adhesion of water or biological molecules like those naturally found within body fluid, or the active addition of molecules such as Arg–Gly–Asp (RGD), which is derived from fibronectin (Hersel, Dahmen and Kessler, 2003; Tallawi *et al.*, 2015) (Figure 13). Surface modification can also improve cell proliferation through the addition of growth factors, such as bFGF (Huang *et al.*, 2021). Other growth

factors can also be used for surface modification. For example, the addition of factors that can affect cell differentiation, such as TGF-  $\beta$  (Saha *et al.*, 2013; Yang *et al.*, 2017a). In addition, in situ genetic modification of cell populations can be undertaken via the adherence of plasmids or viral vectors (Wilkinson *et al.*, 2021).

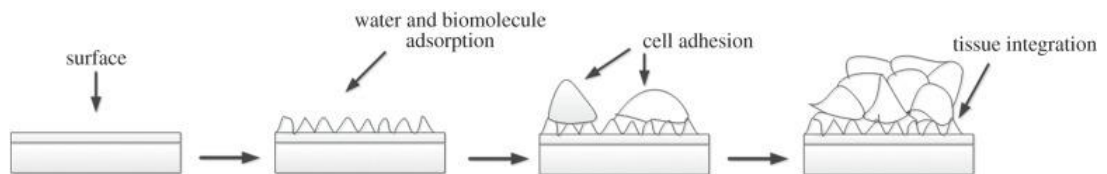


**Figure 13 How surface modification, water and other biomolecules can affect cell adhesion and tissue regeneration**

Reprinted from Tallawi, M., Rosellini, E., Barbani, N., Cascone, M. G., Rai, R., Saint-Pierre, G. and Boccaccini, A. R. (2015) 'Strategies for the chemical and biological functionalization of scaffolds for cardiac tissue engineering: a review', *Journal of The Royal Society Interface*, 12(108), pp. 20150254. With permissions from *Journal of The Royal Society Interface*.

## 1.6.6 A combined approach

Typically speaking, naturally derived polymers like silk have superior biological features but inferior mechanical properties when compared to their synthetic polymer counterparts (Cengiz *et al.*, 2017; Cengiz *et al.*, 2019). Synthetic polymers present improved mechanical properties and greatly increase the reproducibility and controllable degradation rate. Therefore, by combining a natural, biologically friendly environment with the resilience and reproducibility of a synthetic polymer, both materials should theoretically be able to act synergistically to reduce the other's drawbacks.

## 1.6.7 Smart materials and instructive surfaces

Smart materials are materials that can respond to environmental changes or external triggers in a controlled and predictable manner. These materials can

change a variety of properties such as stiffness, conductivity, and shape (Pérez *et al.*, 2013; Khan and Tanaka, 2018). Materials can also be induced to release bioactive factors or function as a drug delivery system (Ruskowitz and Deforest, 2018). All of these potential changes can be induced as a response to specific stimuli like temperature, pH, light, magnetic, or electrical signals (Zhao *et al.*, 2011; Khan and Tanaka, 2018). Examples of smart materials include shape memory polymers, hydrogels with reversible swelling behaviours, and electroactive materials (Wong, Langer and Ingber, 1994; Miyata, Asami and Uragami, 1999; Cicotte *et al.*, 2017; Buffington *et al.*, 2019). Instructive biomaterials are designed to actively guide and influence cellular behaviour during tissue regeneration (Lutolf and Hubbell, 2005). These materials are able to provide biological cues to cells and the surrounding tissue through a variety of instructions, leading to the promotion of tissue growth or the initiation of healing processes. Instructive biomaterials function by having innate active molecules within their structure or containing growth factors or signaling molecules (Li *et al.*, 2006; Longobardi *et al.*, 2006; Abdul Halim, Hussein and Kandar, 2021). The presence of these factors can affect cell behavior. The material's mechanical properties and topography can also provide inductive and instructive characteristics to the biomaterial (Ji and Guvendiren, 2019; Majhy, Priyadarshini and Sen, 2021; Gavazzo *et al.*, 2021). The potential of Smart Instructive Biomaterials was highlighted by Zhao *et al.*, 2011, who was able to show the ability of the biomaterial Poly(2-acrylamido-2-methyl-propane sulfonic acid-co-N-butylmethacrylate) to release a number of drugs from the scaffold when the scaffold was induced with a magnetic field. Furthermore, Re'em *et al.* 2012 was able to demonstrate that an instructive surface consisting of affinity-bound TGF-beta to RGD-modified alginate scaffolds was able to direct hBMSCs down the chondrogenic lineage. On the other hand, Bernardo *et al.* 2022 was able to utilize a hydroxyapatite-based scaffold to increase osteogenesis of mouse BMSCs seeded on their scaffolds.

Unlike Smart Instructive Biomaterials, inert materials are chemically stable and exhibit minimal reactivity with their environment (Barone, Raquez and Dubois, 2011). Inert materials do not actively respond to external stimuli or changes in their environment. They maintain their properties and behaviour without significant alterations or adaptations.

## 1.7 Scaffold physical morphology

A scaffold's biological and mechanical properties are not only determined by material selection, but also their structure.

### 1.7.1 Hydrogels

Hydrogels (highly hydrated polymer networks) are typical scaffold structures and have been widely investigated for cartilage tissue engineering (Izadifar, Chen and Kulyk, 2012; Benmassaoud *et al.*, 2020). Utilising hydrogels has been shown to have a number of benefits, such as uniform cell distribution with the ability to encapsulate cells, *in-situ* gelation that allows conformation to the defect morphology, and the ability to mimic cartilage ECM due to high water content. However, several disadvantages have also been cited with utilisation of hydrogels, reducing their potential use within cartilage regeneration. The main issue with hydrogels is that their mechanical properties often make them difficult to handle and prone to failure *in vitro*, as well as having poor fatigue resistance (Mintz and Cooper, 2014; Formica *et al.*, 2016; Sun *et al.*, 2016; Sánchez-Téllez, Téllez-Jurado and Rodríguez-Lorenzo, 2017). There is the potential for toxicity due to the cross-linking agents used, as well as potential unstable gelation and degradation kinetics (Yun, Lee and Kim, 2013; Sandker *et al.*, 2013; Mansour *et al.*, 2014; Fukui *et al.*, 2014; Lin *et al.*, 2014; Formica *et al.*, 2016). There is also a potential difficulty for migration and incorporation of native cells due to the hydrogel's structure.

## 1.7.2 Porous/sponge scaffolds

Solid scaffolds can be formed into foam or sponge like structures that mimic native ECM architecture, allowing cells to interact effectively with their environment (Wang *et al.*, 2011; Li and Sun, 2022). The porous nature of these scaffolds also gives the physical surface onto which the cells can lay their own ECM (Ma and Zhang, 2001). Due to their architecture, they are potentially more suitable for use within cartilage regeneration than hydrogels, as they have more desirable mechanical properties and a greater fatigue resistance whilst maintaining comparable biocompatibility and cellular behaviour.

## 1.7.3 Electrospun scaffolds

Electrospinning is a viable technique for generating ultrathin fibres via electrical forces (Xue *et al.*, 2019). Due to the fibrous nature of electrospun scaffolds, they are able to resist both tensile and compressive forces (Niemczyk-Soczynska *et al.*, 2021). This scaffold type also shows a high volume to surface area ratio, allowing excellent cell ingrowth potential. However, electrospun scaffolds show the notable disadvantage of limited control of pore structure with pore diameter being fundamentally controlled by fibre diameter; smaller diameter fibres lead to smaller pores and vice versa (Dahlin, Kasper and Mikos, 2011).

## 1.7.4 3D printing

Additive manufacturing through 3D printing has emerged as an extremely versatile manufacturing process in the field of osteochondral engineering due to its ability to be a cost-effective way to produce complex structures with extremely precise control over bulk geometry (Zhang *et al.*, 2019; Chen *et al.*, 2023a). Advancements in 3D printing, such as within stereolithography, fused deposition modelling, and laser sintering, along with the development of new inks and

filaments, show the fundamental way in which 3D scaffold design for engineering tissue has been accelerated forwards (Do *et al.*, 2015; Castro, O'Brien and Zhang, 2015). 3D printing allows for convenient, fast, and individualized scaffold creation and shortens the production period. Achieving balance in the printing process between the scaffold's load-bearing ability and its success at cellular viability is imperative; new, up-and-coming hybridisation between synthetic polymers and natural materials may help to find this balance. This novel combination of materials may be able to combine both the desirable mechanical properties and repeatability of synthetic materials and the bioactivity and biodegradability of natural materials. However, especially within lattice printed scaffolds, there appears to be an issue with cellular migration across the large pores with cells being unable to bridge the gaps between filaments, leading to retardation of cellular migration (Hu and Athanasiou, 2006; Ji and Guvendiren, 2019; Buenzli *et al.*, 2020).

## 1.8 Multiphasic scaffolds

So far, the discussed scaffolds have been monophasic in nature, but as previously mentioned osteochondral defects span two clearly distinct tissue groups of cartilage and bone. Growing two unique tissue types on a single scaffold appears to be an extremely difficult task (Niederauer *et al.*, 2000; Martin *et al.*, 2007; O'Shea and Miao, 2008). A better strategy may be the employment of a bilayered scaffold with distinct regions which represent the cartilage and bone phases. To achieve these tissue specific biological environments, each region would have varied structural, mechanical and biomechanical properties, allowing each region to more closely mimic the tissue it is aiming to regenerate, hopefully leading to improved outcomes. Throughout the literature there appear to be three different approaches to achieving this bilayered strategy.

### **1.8.1 Scaffold free cartilage implanted on a bone scaffold**

This approach to creating a bilayered scaffold does not utilise two distinct scaffolds and instead relies on chondrocytes which have been expanded *in vivo* to create cartilaginous tissue to be seeded onto a bone scaffold (O'Shea and Miao, 2008). One of the advantages of this approach is that it eliminates the need for an additional scaffold to support the cartilage construct, which can reduce the risk of implant rejection, inflammation, and other complications. This strategy has been used with varying levels of success. Some early studies demonstrated poor regenerative capacity of cartilaginous tissue *in vitro* (Niederauer *et al.*, 2000).

### **1.8.2 Assembled bilayered scaffold**

This method of bilayered scaffold creation involves two distinct individual scaffolds that have been independently shown to have the regenerative abilities of their corresponding tissue type, i.e. one scaffold for cartilage regeneration and one scaffold for bone regeneration. These two scaffolds are then combined post-synthesis either before or during surgical implantation (Gao *et al.*, 2001; Schaefer *et al.*, 2002; O'Shea and Miao, 2008; Fu *et al.*, 2022). It is widely cited in the literature that scaffolds that rely on two separate combined scaffolds have issues related to poor mechanical stability between the layers, potentially leading to mechanical failure, as well as poor biological integration post *in vivo* implantation between these layers (Mano and Reis, 2007; O'Shea and Miao, 2008). However, a number of studies have reported contradictory information to this assertion demonstrating no detrimental impact between layers when using connecting measures, fibrin glue, sutures, and even press fitting. Rather than the above, the failing of this strategy appears to be a failure of the scaffold to regenerate articular cartilage, rather than a failure of scaffold connectivity (Gao *et al.*, 2001; Schaefer *et al.*, 2002).

### **1.8.3 Integrated biphasic scaffold**

This variant of biphasic scaffolds utilises a single scaffold which is completely integrated but has distinct regions that contain different and unique properties best suited to their corresponding tissue. This allows for the complete structural integration between the cartilage phase and the bone phase requiring no additional attachment (O'Shea and Miao, 2008; Mukundan, Nirmal and Nair, 2022).

## **1.9 Summary**

The clinical need for osteochondral defect repair arises from the desire to restore the structure and function of the affected joint. Left untreated, osteochondral defects can worsen over time, leading to a much more debilitating condition of osteoarthritis. Therefore, there is a clinical need for an effective early intervention which is able to regenerate osteochondral tissue, preventing further degeneration into osteoarthritis. There is a clear potential for an integrated multiphasic scaffold which mimics osteochondral structure and supports the regeneration of both the cartilage phase and the subchondral bone phase. However, the current available scaffold systems do not meet such unique requirements. For example: hydrogels fail due to their weak mechanical properties and fatigue resistance; 3D scaffolds fail to represent both cartilage and its underlying subchondral bone, leading to failure of regeneration; and multiphasic scaffolds fail to achieve the correct blend of regenerating both the underlying bone and overlying cartilage, leading to the failure of one of the components and thus the scaffold as a whole. Over the last few years, 3D printing has been rapidly applied in the field of tissue engineering, and this has allowed for a new influx of potential biological scaffolds for tissue regeneration; this is because 3D printing has excellent control over bulk morphology and mechanical properties of the structure. However, 3D printed scaffolds alone have some issues- due to their lattice structure these scaffolds often struggle with cell migration between filaments. Therefore, a silk infilled

scaffold may be able to blend the 3D printed scaffold's mechanical properties and the silk's excellent biocompatibility and cell adhesion behaviour. Therefore, the combination of 3D printed scaffolds with silk infill could be an excellent unique way to tackle cartilage regeneration.

## 1.10 Aims and objectives

The aim of this project was to regenerate osteochondral tissue *in vitro* utilising novel biphasic 3D printed silk reinforced scaffolds.

Objectives

- Characterisation of the chemical, physical, and mechanical properties of the biphasic 3D printed silk reinforced scaffolds.
- Osteochondral tissue engineering *in vitro* using human bone marrow stromal cells and biphasic 3D printed silk reinforced scaffolds.

### 1.10.1 Requirements for an osteochondral scaffold

Osteochondral scaffolds present a unique challenge in the fact there is a requirement to generate two different and very distinct tissue types in the form of cartilage and bone, as well as having many of the standard properties found for other scaffold-based tissue regeneration strategies (Table 2). Therefore, there is a requirement for an osteochondral scaffold to have two distinct regions within one scaffold focusing on cartilage and bone regeneration.

**Table 2 Parameters to consider when designing an osteochondral scaffold.**

<b>Mechanical and physical properties</b>	<b>Biological properties</b>
Resistance to compression	Biocompatibility
Resistance to fatigue	Supports cell adhesion
Appropriate porosity	Support of cell proliferation
Ease of manufacturing	Support of cell differentiation
	Degradability
	Defect filling ability
	Sterility

# Chapter 2 Materials and methods

This chapter covers all the materials and methods utilised to create this thesis. It is split into two distinct sections; 2.1 which deals with the chemical, physical, and mechanical properties of the scaffolds and 2.2 which deals with cell culture and adding cells to the scaffolds. These sections relate directly to the two distinct results chapters that follow.

## 2.1 Scaffold preparation

The 3D printed scaffolds were designed and manufactured in collaboration with the University of Otago, New Zealand, after extensive discussions regarding optimal fabrication techniques with Prof Woodfield, Dr Lim and Dr Yang. Poly(ethylene glycol)-terephthalate-poly(butylene terephthalate) block copolymers (Polyactive 300PEGT55PBT45, PolyVation, The Netherlands) with a PEG molecular weight (MW) of  $300 \text{ g mol}^{-1}$  and a PEGT/PBT weight percent (wt%) ratio of 55:45) were used for printing the 3D PEGT:PBT scaffold ( $15 \times 15 \times 2 \text{ mm}^3$ ) with a 0.75 mm pore size at a printing temperature of  $180^\circ\text{C}$ . To increase pore size, 3D printed scaffold filaments were printed in a double stack. After extensive discussions regarding optimal fabrication techniques with Dr Yang and with collaborators Dr Joukhdar and Dr Rnjak-Kovacina at The University of New South Wales, Australia, silk fibroin was extracted from *Bombyx mori* cocoons. To do this, initially, silk cocoons were degummed (to remove sericins) by placing cocoons into a boiling sodium carbonate solution (0.02 M) (Sigma-Aldrich, 497-19-8) for 30 minutes. The pure silk fibroin was then solubilized in a lithium bromide solution (9.3 M) (Sigma-Aldrich, 7550-35-8) at  $60^\circ\text{C}$  for 4 hours at a 20% wt/v of silk to lithium bromide. Lithium bromide was then removed from the solution via dialysis using D-Tube Dialyzers (3500 MWCO, Millipore) in deionized water for 3 days. To determine silk solution concentration, a known volume (1ml) was dried and the mass of the remaining solids was taken. This protocol resulted in a 6–8% wt/v silk solution. Silk solutions were stored at  $4^\circ\text{C}$ . A 5% silk solution was then cast into 3D printed lattices or alone into 12 well plates (1.5ml of silk solution into each well). To improve pore filling by the silk solution over the 3D printed scaffolds, scaffolds were placed in a desiccator for 5 minutes. Following this, samples were frozen overnight at  $-20^\circ\text{C}$  followed by lyophilisation in a freeze-dryer. Dried constructs were then removed from the plate and placed in aluminium foil and autoclaved at  $121^\circ\text{C}$  for 20 minutes to sterilise the constructs and induce beta-sheet formation. The silk component of biphasic scaffolds was attached to the 3D printed component via interlocking of the silk component within the 3D printed

component after freeze-drying. Nonreinforced scaffolds were also created the same way but without the 3D printed lattice. Just before use, scaffolds were cut to 5mm x 5mm constructs and rehydrated overnight by rocking in PBS at room temperature. This was followed by placing them within a desiccator under negative pressure for five minutes whilst being submerged within PBS (unless stated otherwise).

## **2.2 Characterisation of the chemical, physical, and mechanical properties of biphasic 3D printed silk reinforced scaffolds**

### **2.2.1 Light visualisation**

To confirm bulk scaffold morphology, as well as successful creation of scaffolds, a stereomicroscope (Leica M205 C) connected with a Google Pixel 3A camera was utilised to visually inspect the scaffolds and photograph their cross-sectional structure (n=3).

### **2.2.2 Scanning electron microscope (SEM)**

A scanning electron microscope produces images of a sample by scanning the surface of the sample with electrons that are accelerated and focused through a series of lenses. By detecting the backscattered and secondary electrons, SEM images can be created.

The morphology of the 3D printed silk reinforced scaffolds was investigated through the utilisation of a scanning electron microscope (SEM) (Hitachi S3400N variable pressure SEM) at various magnifications with an electron acceleration

voltage of 10.0-20.0 Kv. Prior to imaging, samples were sputter coated with gold (to prevent sample charging).

SEM images of complete scaffolds (n=4) were taken at a magnification of 40x. Each photo was made up of six photos taken across the scaffold surface and combined in Adobe lightroom (3.2.1).

Pore size was determined for the 3D printed control scaffolds, silk control scaffolds, and the biphasic scaffolds (both the cartilage and the bone phase) by taking SEM images at 100x magnification at three zones in three separate scaffolds (n=3). Average pore diameter was calculated by manually measuring the diameter of a minimum of 40 pores per image in 3 scaffolds using Image J. software (version 1.41).

### **2.2.3 Energy Dispersive X-Ray Analysis (EDX)**

The accelerated electrons from the SEM can be utilised with energy-dispersive X-ray (EDX, also referred to as EDS). Once atoms in the sample are exposed to the electron beam within the SEM, unique x-rays are released that correspond to the atom's atomic number. This allows for elemental detection within samples. This can be conducted over a large or narrow area and allows the determination of relative atomic abundance within a sample as quantitative elemental distribution.

Energy dispersive x-ray analysis was performed with a dual Bruker XFlash detector attached to a Hitachi S3400N variable pressure SEM. Analysis was undertaken with Quantax analysis software. Accelerating voltage was set to 10 kV for all EDX measurements. Quantifications were undertaken at 3 distinct locations within 4 scaffolds for each scaffold (3D printed control scaffolds, silk control scaffolds, and the biphasic scaffolds (both the cartilage and the bone phase)) and the average was taken. Quantax analysis software utilises a peak-to-background ZAF

evaluation (P/B-ZAF) algorithm to quantify presence of various elements found within the sample. Bremsstrahlung background was automatically calculated. A Bayes deconvolution was used for line overlap separation and quantitative elemental distribution was determined.

## **2.2.4 Fourier Transform Infrared Spectroscopy analysis**

Fourier Transform Infrared (FTIR) spectroscopy is a common technique used to understand the molecular bonding within a sample by utilising the infrared absorption spectrum of samples. This is conducted by subjecting the sample to infrared radiation, which causes a corresponding change in the dipole moments of some molecular bonds, leading them to move from the ground to an excited state. This change causes a vibrational energy gap which can be interpreted, leading to the formation of corresponding peaks to different molecular bonds and structures on an infrared absorption spectrum.

A Vertex 70 FTIR spectrophotometer was used to analyse molecular vibration of the scaffolds. The FTIR spectrophotometer was used in attenuated total reflection mode (ATR). A KBr beam splitter and a mid-infrared light source was utilised. Each sample of the silk control scaffolds (n=4) and biphasic scaffolds (both bone phase (n=4) and cartilage phase (n=4)) were scanned 150 times in the 500 – 3500  $\text{cm}^{-1}$  range at a spectral resolution of 4  $\text{cm}^{-1}$ .

To determine the silk component of the scaffold protein's secondary structure, spectroscopic deconvolution was undertaken in Origin (Version 12) in the Amide I region (1600–1800  $\text{cm}^{-1}$ ) of the FTIR spectrum. Deconvolution peaks in the range of 1,648–1,657  $\text{cm}^{-1}$  were associated with  $\alpha$ -Helixes, peaks in the range of 1,623–1,641  $\text{cm}^{-1}$  and 1,674–1,695  $\text{cm}^{-1}$  were associated with  $\beta$ -Sheets and peaks in the range of 1,642–1,657  $\text{cm}^{-1}$  were associated with random coils (Jackson and Mantsch, 1995). The comparative area under each peak gave the relative

percentage makeup of the protein's secondary structure within the scaffolds. Peak devolution and area determination was undertaken in Origin (Version 12).

## 2.2.5 Swelling capacity testing

The swelling capacity of the scaffolds was assessed using PBS (Corning 21-040-CV). Silk control scaffolds (n=4), 3D printed control scaffolds (n=4), and biphasic scaffolds (n=4) were pre-weighed, followed by rehydration in PBS at 37°C; every one hour, scaffolds were removed and excess liquid was removed using filter paper and weight was recorded. The scaffolds were then returned to PBS. Percentage increase in mass was calculated by comparing the scaffolds' dry and hydrated mass. After 18 hours, scaffolds were placed within a desiccator whilst submerged in PBS and left under negative pressure for five minutes before being weighed and compared to mass before negative pressure rehydration.

$$\text{Swelling \%} = \frac{(W_w - W_d)}{W_d} \times 100$$

Where  $W_w$  and  $W_d$  are wet and dry weights of the samples, respectively.

## 2.2.6 *In vitro* scaffold degradation testing

The scaffolds were subjected to an accelerated *in vitro* degradation model in the presence of protease XIV (Li, Ogiso and Minoura, 2003; Rnjak-Kovacina *et al.*, 2015b; Baptista *et al.*, 2020). *In vitro* degradation is useful to elucidate the potential degradation rate of different scaffolds based on their properties.

The initial mass of the dry scaffolds was recorded (3D printed (n=4), silk control scaffolds (n=4), and biphasic scaffolds (n=4)). The scaffolds were then placed in pre-weighed 1.5 mL Eppendorf tubes. 1 mL of 2 U/mL protease XIV solution in PBS (Sigma-Aldrich P5147-1G) was added to each tube and incubated at 37°C. The protease XIV was removed every 2 days. Scaffolds were then washed with deionized water and dried overnight at 60°C. Dry mass was recorded and

remaining mass percentage was calculated, and then fresh protease XIV solution was added.

$$\Delta Wd (\%) = \frac{(W_o - Wd1)}{Wd1} \times 100$$

Where  $W_o$  refers the initial sample weight and  $Wd1$  the sample weight at after incubation in protease XIV.

## 2.2.7 Porosity testing

Scaffold porosity was calculated as per the Archimedes method (Ho and Hutmacher, 2006). This technique for deriving porosity is based on a principle of Archimedes: *“A body wholly or partly immersed in a fluid is buoyed up by a force equal to the weight of the fluid displaced”* (de Terris et al., 2019). Using this principle, porosity can be determined via knowing the wet mass of the scaffold, the dry mass of the scaffold, and the submerged mass of the scaffold.

Silk control scaffolds (n=4), biphasic scaffolds (n=4) and 3D printed scaffolds (n=4) were pre-weighed, followed by rehydration in ethanol under negative pressure for five minutes. The scaffolds were then removed, and excess liquid was removed using filter paper and weight was recorded. The scaffolds were then re-submerged in ethanol and the submerged weight was measured. Scaffold porosity was then calculated.

$$Porosity = \frac{M_{Wet} - M_{Dry}}{M_{Wet} - M_{Sub}} \times 100$$

Where  $W_{Dry}$  is the dry weight of scaffolds,  $W_{Wet}$  is the weight of the scaffold after hydration in ethanol, and  $W_{Sub}$  is the weight of the scaffolds submerged in ethanol.

## 2.2.8 Mechanical characterisation

### 2.2.8.1 Uniaxial compression testing

Uniaxial compression testing is a methodology for confirming the short-term strength of a material under a consistent compressive load rate until its failure point (Figure 14). By plotting the stress-strain information, the material's ultimate compressive strength and compressive modulus can be determined.

Load to failure uniaxial compression testing was undertaken in wet unconfined conditions to determine the structural integrity of the biphasic scaffolds (n=4), 3D printed control scaffolds (n=4), and the silk control scaffolds (n=6). Prior to mechanical testing, all scaffolds were rehydrated in PBS for 24 hours and negatively pressure rehydrated to confirm full rehydration. Uniaxial compression testing was utilised to confirm ultimate compressive strength and Young's modulus. Biphasic scaffolds and 3D printed control scaffolds were tested with a 500 N load cell at a strain rate of 0.1 mm min<sup>-1</sup> (Instron 3365). The silk control scaffolds were tested on 1000 G load cell at a strain rate of 0.1 mm min<sup>-1</sup> (Bose ElectroForce® 3200 Series III Test Instrument). Load displacement data obtained from mechanical testing rigs was converted into stress and strain utilising the equations:

$$\sigma = \frac{A}{F}$$

Where  $\sigma$  is the stress, A is the area of the material and F is the applied force.

$$\varepsilon = \frac{\Delta L}{L}$$

Where  $\varepsilon$  is the material strain,  $\Delta L$  is the change in material length and L is the original length.

From this, ultimate compressive strength was obtained. This was measured as the highest stress seen within the scaffold before failure. Strain at failure was taken as

the strain of the scaffold when the scaffold failed. The compressive modulus was determined as the gradient of the elastic region of the scaffold.

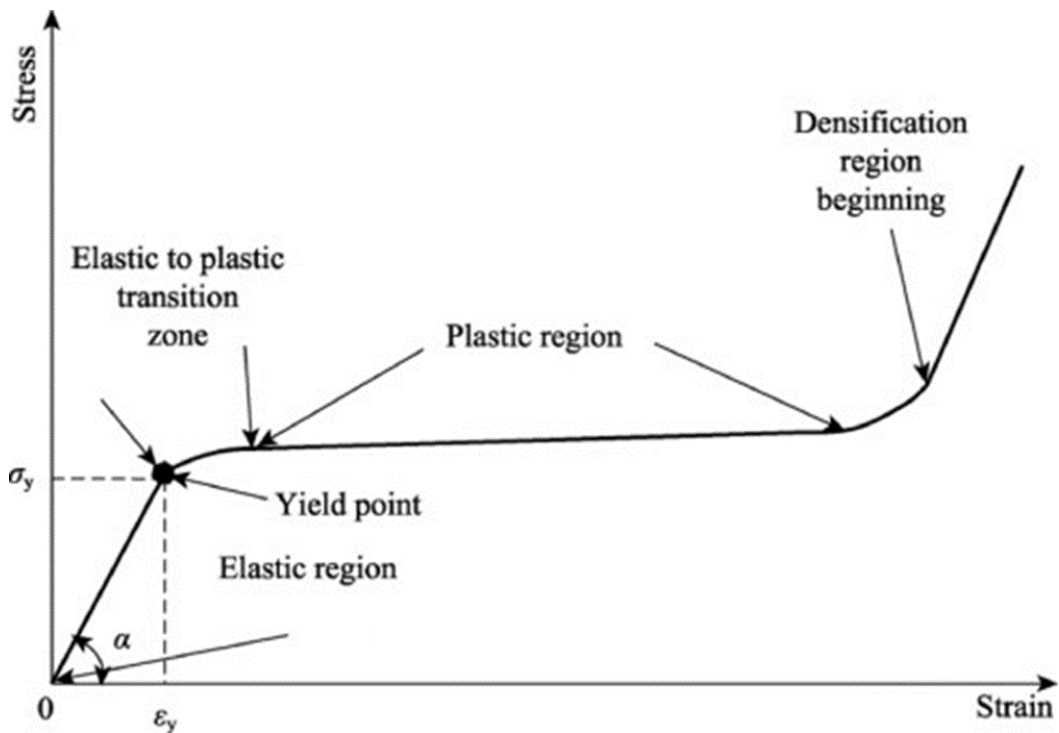


**Figure 14 A generalised stress strain curve for materials under compression**

Key regions of the curve are highlighted. Reprinted from Huang, C., Gong, M., Chui, Y. and Chan, F. (2020) 'Mechanical behaviour of wood compressed in radial direction-part I. New method of determining the yield stress of wood on the stress-strain curve', *Journal of Bioresources and Bioproducts*, 5(3), pp. 186-195. With open access article permissions.

## 2.2.8.2 Fatigue testing

Fatigue testing was utilised to determine the long-term resistance to mechanical loading. Silk control scaffolds (n=4), 3D printed scaffolds (n=4) and biphasic scaffolds (n=3) were subjected to a load of 8 N at 100,000 cycles with a 1 Hz sinusoidal wave pattern on a Bose ElectroForce® 3200 Series III Test Instrument with a 1000 g load cell. The maximum induced strain, as well as the complete hysteresis loop data was recorded every 100 cycles, and the height of the scaffolds after testing was determined and the percent reduction in height was calculated. The absorbed energy for the hysteresis loop data was determined as per the area within the hysteresis curve calculated on Origin Pro (version 10).

## **2.3 Osteochondral tissue engineering *in vitro* using human bone marrow stromal cells and biphasic 3D printed silk reinforced scaffolds**

### **2.3.1 Cell culture**

#### **2.3.1.1 hBMSC isolation**

hBMSCs were isolated from human femoral heads extracted as part of routine hip arthroplasty surgery with ethical approval obtained from the NREC Yorkshire and Humberside National Research Ethics Committee (numbers 18/YH/0166) (Table 3). Isolating hBMSCs from the marrow consisted of agitation of the femoral head in HBSS (Sigma Aldrich H9394). This HBSS was replaced with fresh solution until the solution ran clear. The solution containing the extracted hBMSCs was then centrifuged at 1100 RPM for 5 minutes. Pellets were then resuspended in basal media, filtered with a 70µm cell strainer (Corning 352350) and then counted in the presence of an equal volume of 0.1% acetic acid (Sigma Aldrich A6283). Cells were then seeded to a density of 250,000 cells per square centimetre. Cells were then left for seven days to allow for cell adhesion, after which non-adhered cells were washed away with two PBS washes. The adhered cells were then cultivated in basal media, consisting of  $\alpha$ -MEM (Corning 15-012-CV), containing 10% (v/v) FBS (Sigma-Aldrich, F75240), P/S (100 units/ml, 100 µg/ml)(Sigma Aldrich P0781) and 1 ng/ml recombinant human basic fibroblastic growth factor (bFGF) (Peprotech 100-18B). The medium was changed every 3-4 days. Cells were passaged when approaching 80% confluence. Cells of up to passage 3 were used for experiments. All of the isolated hBMSCs were confirmed for their trilineage differentiation capacity as shown in Appendix 1.

**Table 3 Age and gender distribution of cells isolated from explants from total hip arthroplasty.**

<b>Donor sex</b>	<b>Donor age</b>
<b>F</b>	83 years
<b>F</b>	78 years
<b>F</b>	78 years
<b>M</b>	72 years

### **2.3.1.2 Culturing of cells**

All experimental work involving or requiring aseptic technique was undertaken within a class II laminar flow hood. All experiments that used cells were incubated at 37°C with 5% CO<sub>2</sub> and 100% humidity within a tissue culture incubator.

### **2.3.1.3 Passaging cells**

Passaging of cells was undertaken via aspiration of culture media followed by washing with PBS twice, followed by incubation with trypsin (Sigma-Aldrich, T4049) at 37°C for 5 to 10 minutes. The culture dish was agitated to ensure complete cell detachment. Cell suspension was neutralised by utilisation of equal parts of basal media followed by centrifugation at 1200 RPM for five minutes to allow for cells to pellet. Cells were then counted and seeded at the appropriate density based on experimental requirements.

### **2.3.1.4 Cell counting**

To determine cell number, 45 µl of cell suspension was taken and added to 5 µl trypan blue solution (Sigma-Aldrich, T8154). 10µl of this solution was added to a haemocytometer and counted under a light microscope. The total number of viable cells were counted within four quadrants and the average determined. This was then utilised to determine the total number of cells by multiplying the

average determined from the haemocytometer, the trypan blue dilution factor, the cell suspension volume and by multiplying by 10,000.

Cell concentration = average cell count x trypan blue dilution factor x total volume of cell suspension x 10,000.

### **2.3.1.5 Cell freezing and cryopreservation**

For long-term storage, cells were frozen at  $1 \times 10^6$  cells/ml in cryoprotectant freezing medium which consisted of 40% FBS (v/v) (Sigma-Aldrich, F75240), 50% cell culture media (v/v) and 10% dimethyl sulfoxide (DMSO) (v/v) (Sigma Aldrich, D2650). 1 ml of cell suspension was added to each cryovial and frozen down in a Mr. Frosty™ freezing container (Thermo Scientific, 5100-0001) in a -80°C freezer overnight followed by placing in liquid nitrogen storage.

### **2.3.1.6 *In vitro* expansion of hBMSCs**

All hBMSCs were expanded in basal expansion medium consisting of a-MEM (Corning 15-012-CV), containing 10% (v/v) FBS (Sigma-Aldrich, F75240), P/S (100 units/ml, 100 µg/ml) (Sigma Aldrich P0781) and 1 ng/ml recombinant human basic fibroblastic growth factor (bFGF) (Peprotech 100-18B). bFGF was included in cell culture media to accelerate BMSC proliferation for expansion purposes, to allow experiments to be conducted in a timely manner. It has been previously demonstrated that the presence of bFGF has no negative impacts on the differentiation or capacity of BMSCs (Hori *et al.*, 2004; Wang *et al.*, 2018). The medium was changed every 3-4 days. All cells were passaged at approaching 80% confluence until passage 3 where they were experimentally used.

### **2.3.1.7 Live cell fluorescent labelling**

CellTracker™ Green CFMDA (5-chloromethylfluorescein diacetate) dye (ThermoFisher Scientific, C7025) was used to label live cells. CFMDA is a molecule that can freely pass through cell membranes. This is converted into a cell impermeable product which presents fluorescence. Cells were stained by mixing 10 µl of DMSO (Sigma Aldrich, D2650) into 50 µg CFMDA which was diluted further in 15 ml serum-free basal medium to create a 7 µM solution of CFMDA. This solution was then added to either cells or scaffolds containing cells and incubated for 45 minutes. This was followed by two washes in PBS and imaging was undertaken on a fluorescence Leica DMI6000 B inverted microscope or a confocal laser scanning microscope (CLSM, Leica-TCS-SP8).

A second cell viability tracker (CellTracker™ red CMTPX dye) was utilised when simultaneous cell labelling was required allowing for the identification of unique cell populations within the same scaffold (as seen in section 4.1.8). This can help to assess cell penetration and migration from one phase to the other within the scaffold. CellTracker™ red CMTPX dye (ThermoFisher Scientific, C34552) was also used to label live cells. CMTPX is a molecule that can freely pass through cell membranes. This is converted into a cell impermeable product which presents fluorescence. Cells were stained by mixing 10 µl of DMSO to 50 µg CMTPX which was diluted further in 6 ml serum-free basal medium to create a 12 µM solution of CMTPX. This solution was then added to the cells and incubated for 45 minutes. This was followed by two washes in PBS and imaging was undertaken on a confocal laser scanning microscope (CLSM, Leica-TCS-SP8).

### **2.3.1.8 Static seeding of hBMSCs on scaffolds**

Cells were statically seeded onto scaffolds. This was undertaken by submerging scaffolds in a 1.5mL cell suspension containing the required number of cells per scaffold for 12 hours in a standard cell incubator before being moved to a 24 well

plate or 24 well low attachment plate. All seeding of scaffolds was undertaken statically unless stated otherwise.

### **2.3.1.9 Dynamic seeding of hBMSCs on scaffolds**

To achieve dynamic seeding of cells onto scaffolds an in-house dynamic seeding device was used (Figure 15). Briefly, a 1.5 mL cell suspension was placed in a 1.5 mL sterile Eppendorf with a hole drilled into the lid. The rehydrated scaffolds were pre-treated with basal media containing 10% FBS. Scaffolds were then placed into the Eppendorfs (one scaffold per Eppendorf) with a hole drilled in the top. The Eppendorf was then covered with a layer of Opsite (Smith & Nephew, Cat. No: 4630) adherent, which is a polyurethane film that is gas permeable but liquid impermeable and normally used within wound care. This film cover enables gas exchange whilst keeping the contents of the tube sterile. These Eppendorfs were then placed into the in-house dynamic seeder (rotation rate of 10 RPM). The dynamic seeder was kept in a standard incubator for the duration of seeding (48 hours).



**Figure 15 In-house constructed dynamic seeder**

Black arrow indicates the part of the dynamic seeder which rotates providing drive to the dynamic seeder, causing it to rotate at approximately 10 RPM. An example empty Eppendorf is also loaded to indicate sample location during the dynamic seeding.

### **2.3.1.10 Osteogenic induction culture**

To induce osteogenic differentiation, basal media was supplemented with 50  $\mu\text{M}$  L-ascorbate 2-phosphate sesquimagnesium salt hydrate (Sigma-Aldrich, A8960), 100 nM dexamethasone (Sigma-Aldrich, D4902). The medium was changed every 2-3 days.

### **2.3.1.11 Chondrogenic induction culture**

To induce chondrogenic differentiation,  $\alpha$ -MEM (Corning 15-012-CV) was supplemented with 1% P/S (10,000 units/mL penicillin, 10 mg/mL streptomycin) (Sigma Aldrich P0781), 10% FBS, 1% ITS (Gibco, 41400-045), 50  $\mu\text{g}/\text{ml}$  ascorbate 2-phosphate (Sigma-Aldrich, A8960), 0.1  $\mu\text{M}$  dexamethasone (Sigma-Aldrich, D4902), and 10 ng/ml TGF $\beta$ 1 (Peprotech 100-21). The medium was changed every 2-3 days.

### **2.3.2 Sterility testing**

For sterility testing, thioglycollate medium containing resazurin was made up utilising the manufacturer's instructions. In brief, 29.75 g thioglycollate medium powder (Millipore, 90404) was dissolved in 1 L of distilled water. This was then heated to 90°C to dissolve the powder, and solutions were visualised to check for a colour change from blue to purple. Following this, the media was decanted into glass bottles before autoclaving at 121°C for 15 minutes. The media was then allowed to cool to room temperature before scaffolds were placed into the media under aseptic conditions (n=4). Positive controls were created via opening tubes to the air and leaving on the bench side at room temperature for 10 minutes. The broth was then visually inspected for turbidity and photographed on a Google Pixel 3a camera at days 0, 3, 7, 14.

### **2.3.3 Contact cytotoxicity assay**

Contact cytotoxicity was carried out as per ISO10993-5:2009(E) part 5: Tests for *in vitro* cytotoxicity. Scaffolds were placed within six well plates (n=4) and secured to the bottom via steri-strips (Medisave, R1540C). Scaffolds were washed twice in PBS, followed by the adding of basal media containing  $5 \times 10^4$  cells per well. Plates were then cultured at 37°C in 5% (v/v) CO<sub>2</sub> in an incubator for 96 hours. Following 96 hours of culture, the scaffolds were washed twice in PBS, followed by fixation in neutral buffered formalin for 15 minutes. Cells were then stained using Giemsa solution (Sigma-Aldrich GS500) for five minutes. Plates were then air dried and examined and imaged on a Leica DM16000 B inverted microscope for cell morphology, confluency, attachment, and detachment. Wells were also graded as per Table 4.

**Table 4 Reactivity grades for contact cytotoxicity testing**

Grade Reactivity	Description of reactivity zone
0	None; No detectable zone around or under specimen
1	Slight; Some malformed or degenerated cells under specimen
2	Mild; Zone limited to area under specimen
3	Moderate; Zone extending specimen size up to 1,0 cm
4	Severe; Zone extending farther than 1,0 cm beyond specimen

### **2.3.4 Indirect cytotoxicity assay**

To determine any potential for indirect cytotoxicity, ISO standard: ISO10993-5:2009(E) and ISO standard: ISO10993-12:2007 were followed. Briefly, scaffolds (n=3) were placed into 6 well plates containing 5 ml of  $\alpha$ -MEM culture media (Corning 15-012-CV), containing 10% (v/v) FBS (Sigma-Aldrich, F75240), P/S (100 units/ml, 100  $\mu$ g/ml) (Sigma Aldrich P0781) and incubated at 37°C in 5% (v/v) CO<sub>2</sub> for 72 hours, 1 week, 2 weeks, 3 weeks, 4 weeks, and 8 weeks. At each time point, media was collected and frozen at -80°C in cryovials until required.

Following the collection of all six aliquots, hBMSCs were seeded into 96-well plates, with a cell density of 10,000 cells/well. Cytotoxicity testing and proliferation testing was carried out with 1000 cells/well. The 96 well plates were then incubated at 37°C in 5% CO<sub>2</sub> for 24 h in basal media, before exchanging for 100  $\mu$ L of the thawed collected media containing scaffold eluates. Cytotoxicity testing was then undertaken for 48 hours (n=4 per group), and cell proliferation testing six days (n=4 per group). The negative and positive controls consisted of  $\alpha$ -MEM media with 10% DMSO (Sigma Aldrich, D2650) and  $\alpha$ -MEM media, respectively.

Following this, XTT assays were undertaken as per manufactures instructions (Sigma-Aldrich 11465015001). In brief, media was replaced within the wells with XTT assay solution and incubated for 4 h at 37 °C in 5% CO<sub>2</sub>. Following this, 100 µL was aliquoted into new 96 well plates and read on a Thermo Scientific Varioskan Flash plate reader at 450 nm and 650 nm (reference wavelengths). The values at 650 nm were deducted from 450 nm to obtain the final optical density (OD). The test well ODs were normalised to the positive control ODs to measure cell viability for cell proliferation testing.

### **2.3.5 Scaffold FBS surface modification**

All scaffolds were preincubated at 4°C overnight in basal media and, depending on the experiment undertaken, with either 0% FBS, 10% FBS or 20% FBS.

### **2.3.6 Cell migration**

Phalloidin is a bicyclic peptide derived from the *Amanita phalloides* mushroom and can selectively label F-actin, whilst Alexa Fluor 488 provides a fluorescent chromophore for imaging. F-actin is a key component of the cellular cytoskeleton and plays a fundamental role in cellular migration and cell shape. DAPI blue-fluorescent DNA stain demonstrates a 20-fold increase in fluorescence upon binding to dsDNA and is utilised as a nucleus counter stain.

Cell adhesion was investigated with Alexa Fluor® 488 phalloidin to look at F-actin positioning. Staining was undertaken on scaffolds that were seeded with 50,000 hBMSCs for 2 days (n=4 per group). After 2 days, scaffolds were washed with PBS three times before being fixed in 10% NBF for 15 mins then permeabilised with 0.1% Triton-X for 20 mins. Following this, scaffolds were stained with Alexa Fluor® 488 phalloidin stain (ThermoFisher Scientific, A12379), at a 1 in 10 dilution for 2 hours at room temperature and with DAPI (Sigma Aldrich, D9542) at a

concentration of 1 µg/ml dilution for 20 minutes. Samples were then visualised under a confocal microscope.

### **2.3.7 AlamarBlue™ assay for analysis of cell metabolic activity**

AlamarBlue is a product containing a molecule called resazurin, which is a cell permeable non-toxic weakly fluorescent dye. AlamarBlue can be utilised to quantitatively assess cell metabolic activity and can function as an analogue of cell growth and proliferation. Resazurin undergoes a colorimetric change as part of an oxidation-reduction reaction within living cells forming a reduced product called resorufin, which is pink and highly fluorescent; the intensity of the fluorescence is directly proportional to the number of living cells and metabolic activity.

To measure the change in cell metabolic activity over time, scaffolds were seeded statically as previously described with 100,000 hBMSCs per scaffold. Scaffolds were split into three groups- biphasic scaffolds (cartilage phase), biphasic scaffolds (bone phase), and silk control scaffolds (n=4 per group). After seeding, the scaffolds were placed in low adhesion culture dishes and cultured for 1, 4, 8, 12, and 16 days. At each time point, scaffolds were removed and placed in 48 well plates containing a 10% alamarBlue (BIO-RAD BUF012A) media solution. These were then incubated for three hours before the alamarBlue solution was read on a Thermo Scientific Varioskan Flash plate fluorescent plate reader at an excitation wavelength of 560 nm, and an emissions wavelength of 590 nm. Scaffolds were then washed in PBS before being returned to the original plates with fresh media where they continued to be cultured until the next time point.

### **2.3.8 LDH assay for analysis of cell death percentage/ rate**

LDH is a cytosolic enzyme found within a variety of mammalian cells, including hBMSCs. Damage to the plasma membrane of cells leads to the release of LDH from the cytosol into the surrounding cell culture medium. Thus, by measuring the relative amounts of LDH in the surrounding medium, an analogue of cell cytotoxicity can be obtained. Quantification of the LDH is undertaken by a coupled enzymatic reaction where the LDH catalyses the conversion of lactate to pyruvate via NAD<sup>+</sup> reduction to NADH. NADH is then further used to reduce a tetrazolium salt to a red formazan product, from which absorbance can then be measured. The amount of formed red formazan product is directly proportional to LDH levels found within the cell culture medium.

To measure the change in cell LDH release activity over time, scaffolds were seeded statically as previously described with 100,000 hBMSCs per scaffold. Scaffolds were split into three groups- biphasic scaffolds (cartilage phase), biphasic scaffolds (bone phase), and silk control scaffolds (n=4 per group). After seeding, the scaffolds were placed in low adhesion culture dishes and cultured for 2, 4, 8, 12, and 16 days. An LDH release toxicity assay was conducted utilising a CytoTox 96<sup>®</sup> Non-Radioactive Cytotoxicity Assay kit (Promega G1780) and experimentation was undertaken as per manufacturer's instructions. In brief, 50 µL of cell media was transferred from the culture dish containing scaffolds to a 96 well plate. Following this, 50 µL of CytoTox 96<sup>®</sup> reagent was then added to the aliquots and incubated whilst protected from light for 30 minutes at room temperature. Following this, 50 µL solution was then added and plates were read for absorbance at 490 nm.

### **2.3.9 Seeding and culturing of hBMSCs on scaffolds under chondrogenic conditions**

Scaffolds were rehydrated as previously described, and then seeded with 500,000 cells on the cartilage phase or top of the silk scaffolds. These were then cultured for three weeks in chondrogenic media before being utilised for experimentation.

### **2.3.10 Seeding and culturing of hBMSCs on scaffolds under osteogenic conditions**

Scaffolds were rehydrated as previously described, and then seeded with 500,000 cells on the bone phase or underside of the silk scaffolds. These were then cultured for six weeks in osteogenic media before being utilised for experimentation.

### **2.3.11 Seeding and culturing of hBMSCs on scaffolds under osteochondral conditions**

Scaffolds were rehydrated as previously described, and then seeded with 500,000 cells on the bone phase or underside of the silk scaffolds. These were then cultured for six weeks in osteogenic media, followed by seeding of the cartilage phase of biphasic scaffolds or the top of silk scaffolds with either pre-cultured hBMSCs (hBMSCs that were placed in chondrogenic media for two weeks prior to seeding) or non-pre-cultured hBMSCs. The seeding density was 500,000 cells per scaffold. These were then cultured for an additional three weeks in chondrogenic media.

## **2.3.12 Histology**

### **2.3.12.1 Paraffin embedding and sectioning**

All samples, prior to embedding, were fixed overnight in 10% NBF prior to tissue processing with a VIP Tissue Processor (Sakura). During processing, samples passed through four graded alcohol changes followed by xylene and paraffin wax. Following processing, samples were placed in a paraffin wax cassette. Samples were then sectioned at a thickness of 6µm and mounted on Superfrost™ Plus Microscope Slides (Fisherbrand) via floating on a 40°C water bath. Slides were then dried in a 37°C incubator. Prior to histological analysis, samples were dewaxed in a 100% xylene solution followed by rehydration to water through graded alcohol.

### **2.3.12.2 Haematoxylin and eosin (H&E) staining**

Haematoxylin is a positively charged molecule which, when used in histological staining is able to bond with DNA and RNA to form a red stain and is utilised to identify cell nuclei. This stain is then 'blued' in slightly basic water. Eosin is a molecule which is able to electrostatically bind the positive amino acid residues staining them pink and is used to identify cytoplasm.

Slides were initially rehydrated through graded alcohol were then stained in Harris's Haematoxylin for three minutes, followed by washing under running tap water until the water ran clear. Samples were then placed in Scott's tap water for one minute. Slides were then counter stained in eosin for three minutes, followed by washing under running tap water until the water ran clear. Samples were then dehydrated in graded EtOH, followed by three 100% xylene washes for five minutes. Samples were then mounted in DPX (distyrene, plasticizer and xylene, Agar Scientific, R1340) and observed under an Olympus BX50 microscope.

### **2.3.12.3 Picrosirius red/Alcian blue staining**

Alcian blue is a copper-containing stain. The stain consists of a copper-containing phthalocyanine ring linked to four isothiuronium groups. The dye molecules are able to bind to carboxyl and sulphur groups staining them a bright blue and are commonly used to stain polysaccharides such as glycosaminoglycans in cartilages and other body structures. Picrosirius red is a strong, linear anionic dye, consisting of six sulfonate groups that are able to associate along cationic collagen fibres, staining them red.

Slides were initially rehydrated through graded alcohol and were then stained with Alcian blue solution for 10 minutes (1% w/v in 3% acetic acid, TCS Biosciences, HS116-500). The slides were then washed under running water for one minute, followed by incubation in 1% phosphomolybdic acid (Polysciences, Inc, 24901A) for 20 minutes. The slides were then washed under running tap water for one minute and counter stained with picrosirius red (Polysciences, Inc, 24901B) for 60 minutes, followed by another wash under running tap water until the water ran clear. Samples were then dehydrated in graded EtOH, followed by three 100% xylene washes for five minutes. Samples were then mounted in DPX (distyrene, plasticizer and xylene, Agar Scientific, R1340) and observed under an Olympus BX50 microscope.

### **2.3.12.4 Safranin-O staining for proteoglycans**

Safranin-O is a positively charged basic cationic dye that binds to the negatively charged sulfate and carboxyl groups of the GAG chains in proteoglycans with a high affinity, forming a reddish pink complex (Wall and Board, 2014).

Slides were initially rehydrated through graded alcohol and were then stained with a 0.02% Fast Green solution for 1 minute. Following this, slides were dipped in 0.1% acetic acid solution for 30 seconds, and then in 1% safranin-O solution for

30 minutes. Samples were then dehydrated in graded EtOH, followed by three 100% xylene washes for five minutes. Samples were then mounted in DPX (distyrene, plasticizer and xylene, Agar Scientific, R1340) and observed under an Olympus BX50 microscope.

### **2.3.12.5 Von Kossa staining for mineral nodule formation**

Von Kossa staining was utilised to detect calcium deposits. This stain functions via the transfer of calcium salts to silver salts. This functions by the substitution of phosphate bound calcium ions with silver ions, followed by exposure to bright light which leads to a photochemical degradation of the silver, causing it to become visible.

Slides were initially rehydrated through graded alcohol and were then stained with Von Kossa stain with a Staining Kit (Atom Scientific, RRSK39-100) as per the manufacturer's instructions. In brief, slides were incubated in 10% (w/v) aqueous silver nitrate solution at room temperature under a 50 W lamp for 45 minutes. This was followed by three washes in dH<sub>2</sub>O before incubation with 5% sodium thiosulfate for 5 minutes. Samples were then counterstained with Giemsa solution for five minutes. Samples were then dehydrated in graded EtOH, followed by three washes with 100% xylene. Samples were then mounted in DPX (distyrene, plasticizer and xylene, Agar Scientific, R1340) and observed under an Olympus BX50 microscope.

### **2.3.12.6 Immunohistochemistry**

Immunohistochemistry (IHC) is a technique used in to detect specific proteins or antigens in tissues with extremely high specificity. It involves the use of antibodies that bind specifically to the target antigen and are then visualized by a detection system.

Immunohistochemical analysis was undertaken in order to qualitatively evaluate and localize the Type I and Type II collagen within the scaffolds. Slides were initially rehydrated through graded alcohol, followed by a 20-minute incubation at room temperature in proteinase K (Agilent, S302030-2). After this, samples were incubated at room temperature for 20 minutes in Dual Endogeneous Enzyme Block (Agilent, S200389-2) and then 30 minutes in a 2% milk solution (Panreac Applichem, A0830). Primary antibody (Table 5) was then added and incubated at 4° overnight. After the overnight incubation, slides were incubated in the presence of secondary antibody (DAKO Anti-mouse HRP (Agilent, K400311-2). Samples were then developed by utilising Liquid DAB (3,3'-Diaminobenzidine) (Agilent K346811-2) for 10 minutes. Samples were then dehydrated in graded EtOH, followed by three washes with 100% xylene. Samples were then mounted in DPX (distyrene, plasticizer and xylene, Agar Scientific, R1340) and observed under an Olympus BX50 microscope.

**Table 5 . Primary antibody information utilised during IHC**

<b>Antibody target</b>	<b>Manufacturer</b>	<b>Catalogue number</b>	<b>Antibody concentration</b>
<b>Collagen Type I</b>	Abcam	ab6308	1/150
<b>Collagen Type II</b>	Merck	CP18	1/500

## 2.4 Statistical analysis

Statistical analysis was run using SPSS (26). Data were tested for normality using a Shapiro-Wilk test and QQ plots, all data were found to be normally distributed. A two-tailed T-Test and ANOVA with Bonferroni post-hoc tests were performed.

# **Chapter 3 Characterisation of the chemical, physical, and mechanical properties of biphasic 3D printed silk reinforced scaffolds**

This chapter is the first results chapter and is designed to cover the chemical, physical and mechanical properties of the created biphasic scaffolds in comparison to silk control scaffolds and 3D printed control scaffolds.

### 3.1 Results

A novel biphasic scaffold, consisting of a 3D printed lattice infilled with silk was successfully fabricated in collaboration with the University of Otago, New Zealand and the University of New South Wales, Australia. Scaffold design arose as part of an in-depth discussion process, combining expertise from the three institutions of the University of Leeds, University of Otago and the University of New South Wales. This successful fabrication was identified by initial visual examination (Figure 16) and through further investigation with SEM microscopy (Figure 17).

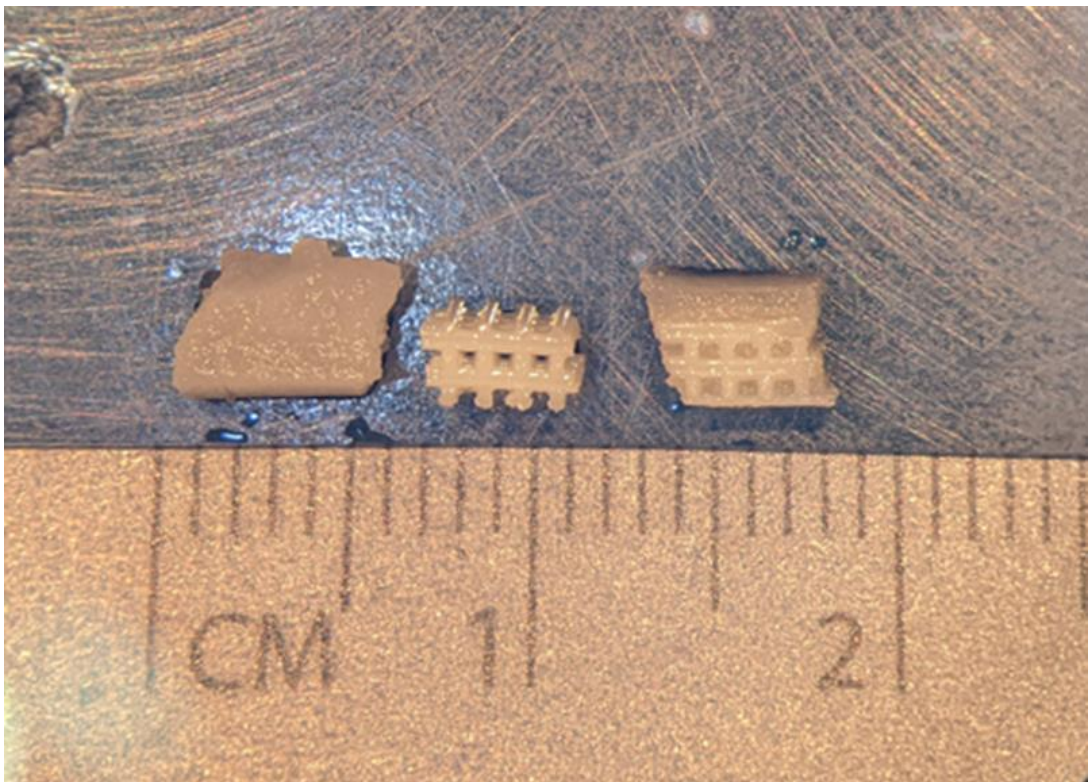


**Figure 16 Representative Stereomicroscope image representing the structural similarities and differences between created scaffold types**

Silk scaffolds are represented on the left of the image, 3D printed scaffolds are represented in the centre of the image, and biphasic scaffolds are represented on the right-hand side of the image (n=4). Images obtained with a stereomicroscope (Leica M205 C) with a connected Google Pixel 3A camera.

### 3.1.1 Scaffold morphology and porosity

To understand scaffold morphology, SEM analysis was undertaken on the biphasic scaffolds, which showed two distinct regions. The cartilage phase showed a thin sheet-like network of lamellae with interconnected porosity (Figure 18A), which seamlessly continued into the bone phase with no obvious change in silk morphology, with it successfully casting around the 3D printed lattice. The silk component of the biphasic scaffold showed no obvious morphological differences to the silk control scaffolds (Figure 18C). The 3D printed component of the bone phase of the biphasic scaffold showed no obvious difference to that seen within the 3D printed control scaffolds (Figure 18D), with there being no visible impacts of silk infilling and freeze-drying on the 3D printed component of the bone phase. By utilising the SEM images, pore size distribution could be valuated to better understand the scaffolds' potential to accept cell infiltration as well as the potential for osteochondral differentiation of seeded cells. Both biphasic scaffolds and silk control scaffolds showed a wide distribution of pore sizes ranging from 15  $\mu\text{m}$  to 370  $\mu\text{m}$  (Figure 18A-C). No significant difference ( $p>0.05$ ) was seen in mean pore size of the cartilage phase ( $117 \pm 15 \mu\text{m}$ ), bone phase ( $124 \pm 24 \mu\text{m}$ ), and silk control scaffolds ( $103 \pm 13 \mu\text{m}$ ). All scaffolds showed significantly smaller pore sizes than the 3D printed scaffolds ( $768 \pm 28 \mu\text{m}$ ) (Figure 18 D,H) ( $p<0.05$ ).

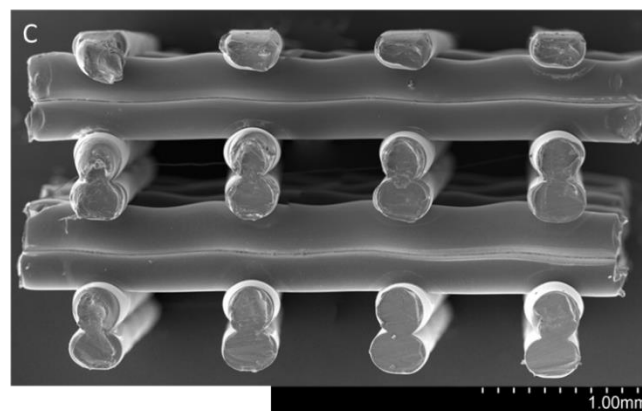
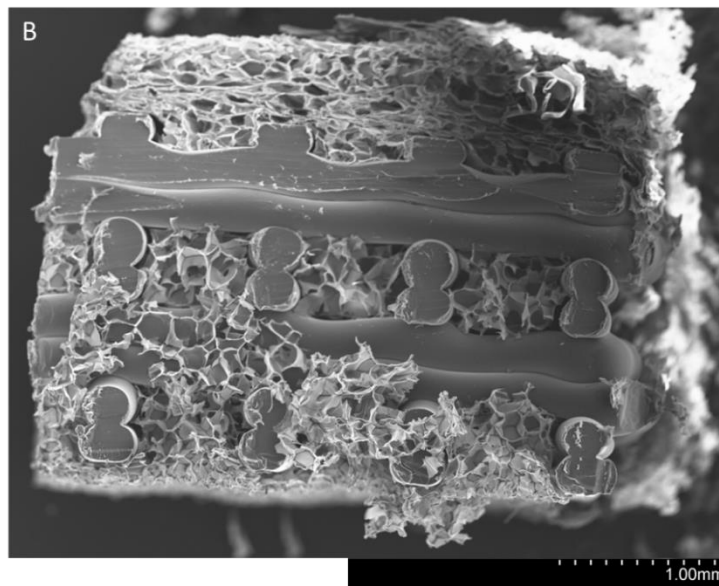
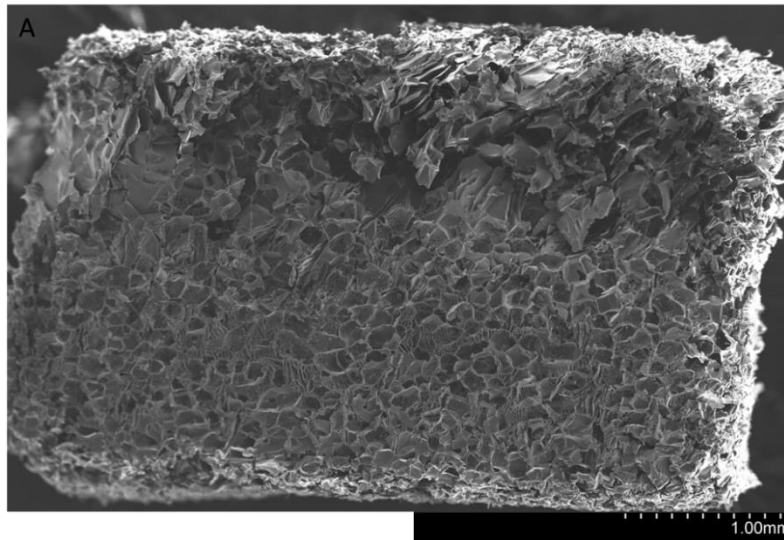


**Figure 17 Representative Compiled SEM images demonstrating complete structure and morphology of scaffolds**

(A) Silk scaffolds (B) biphasic scaffolds (C) 3D printed scaffolds. Images were obtained with a Hitachi S3400N variable pressure SEM at a magnification of 40x. Each photo was made up of six photos taken across the scaffold surface and combined in Adobe lightroom (3.2.1).

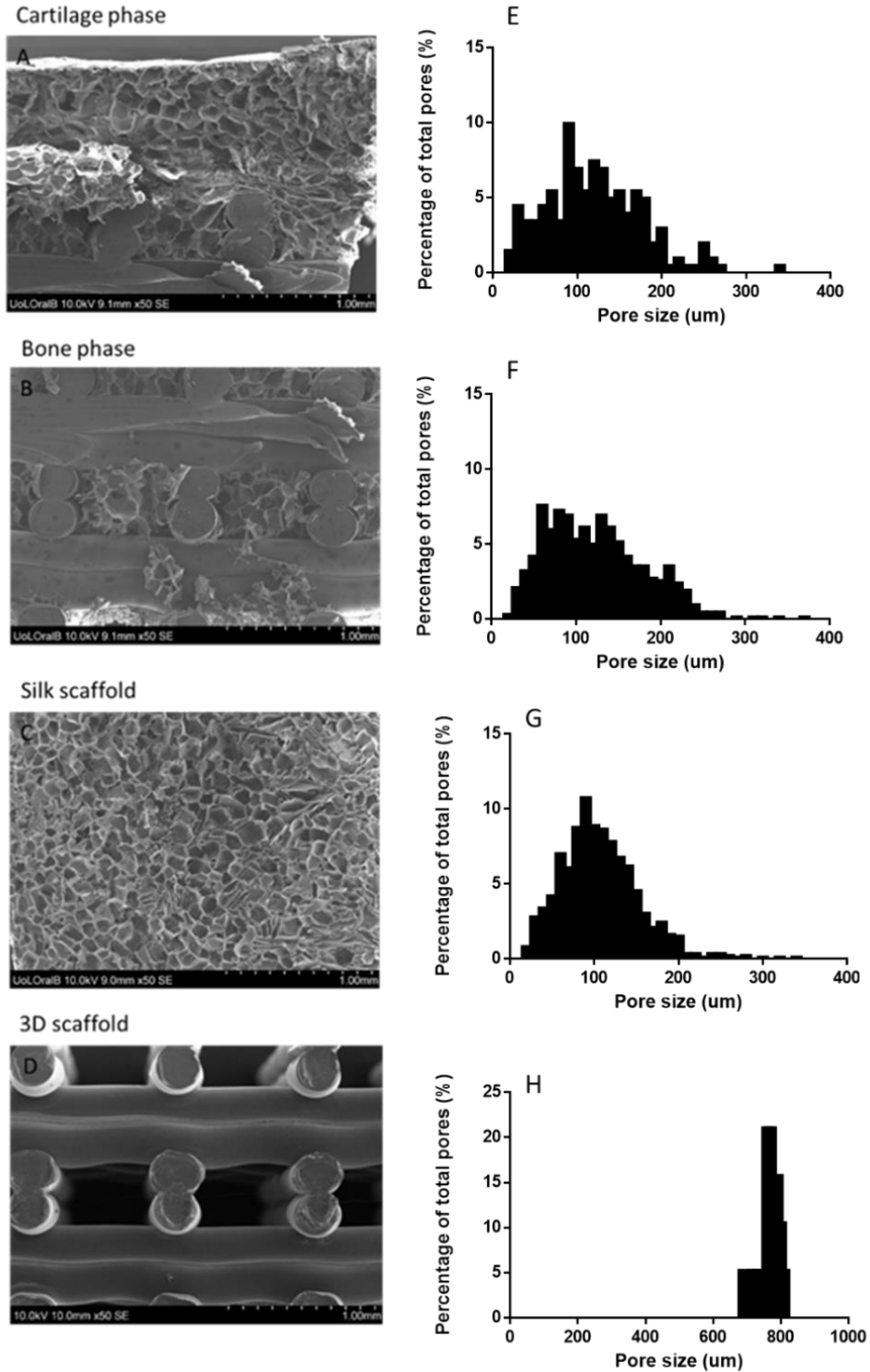


**Figure 18 Scaffold pore size distribution**

Representative SEM images of scaffolds showing pore morphology at 50 times magnification, A-D. Cartilage phase of biphasic scaffolds (A), bone phase of biphasic scaffolds (B), silk scaffolds (C), 3D printed scaffolds (D). Pore size distribution obtained from the three technical repeats over three scaffolds measuring a minimum of 40 pores per image. E-H. Cartilage phase of biphasic scaffolds (E), bone phase of biphasic scaffolds (F), silk scaffolds (G), 3D printed scaffolds (H). There was no statistically significant difference between the average pore size in silk scaffolds, the cartilage phase of biphasic scaffolds and the bone phase of biphasic scaffolds ( $p > 0.05$ ). However, 3D printed scaffolds did show significantly larger average pore size than all other scaffold types ( $p < 0.05$ ).

### 3.1.2 Elemental distribution within the scaffolds

EDX analysis was undertaken to better understand the elemental distribution within the scaffolds, as well as the presence or absence of any elemental contamination introduced during fabrication. This investigation indicated that the only elements found within the 3D printed scaffolds, biphasic scaffolds, and silk control scaffolds were carbon, oxygen and nitrogen, as well as gold (Figure 19 A-D). The presence of gold was associated with the sputter coating process required to visualise biological materials within the SEM due to its electrical conductivity. No other unexpected elements were seen. This indicates that no elemental contaminants were introduced into the scaffold during fabrication, such as lithium, bromide or calcium which are used during the silk purification process. Further investigation into the normalised weight distribution of carbon, nitrogen and oxygen (Figure 20) between scaffolds showed that the silk control scaffolds have a distribution of  $45.67 \pm 1.40\%$  carbon,  $21.67 \pm 0.31\%$  nitrogen and  $32.65 \pm 1.26\%$  oxygen; this was non-significantly different ( $p > 0.05$ ) to the cartilage phase of the biphasic scaffolds, which have the distribution of  $45.15 \pm 1.39\%$  carbon, nitrogen  $20.35 \pm 0.83\%$  and  $34.50 \pm 0.95\%$  oxygen. These two scaffolds were compared to the bone phase of the biphasic scaffolds, which showed a significant increase ( $p < 0.05$ ) in carbon  $51.06 \pm 1.89\%$ , a significant decrease ( $p < 0.05$ ) in nitrogen  $15.24 \pm 1.13\%$ , and no significant change ( $p > 0.05$ ) in oxygen content  $33.69 \pm 0.77\%$ . On the other hand, the 3D printed scaffolds showed significantly higher ( $p < 0.001$ ) carbon levels  $65.51 \pm 0.31\%$ , as well as significantly lower ( $p < 0.001$ ) nitrogen  $1.49 \pm 0.10\%$ , with no significantly different ( $p > 0.05$ ) oxygen levels  $33.00 \pm 0.21\%$ .

Elemental distribution of nitrogen, oxygen and carbon were at the expected levels based on the molecular ratios in their molecular structure, with the silk scaffolds and the cartilage phase of the biphasic scaffolds showing the highest nitrogen content due to their protein-based nature. The bone phase of the biphasic scaffold showed the second highest nitrogen content, with the nitrogen content

being reduced compared to the cartilage phase and silk scaffolds due to its mix of protein and synthetic polymer. The 3D printed scaffolds showed negligible levels of nitrogen due to their synthetic polymer nature.

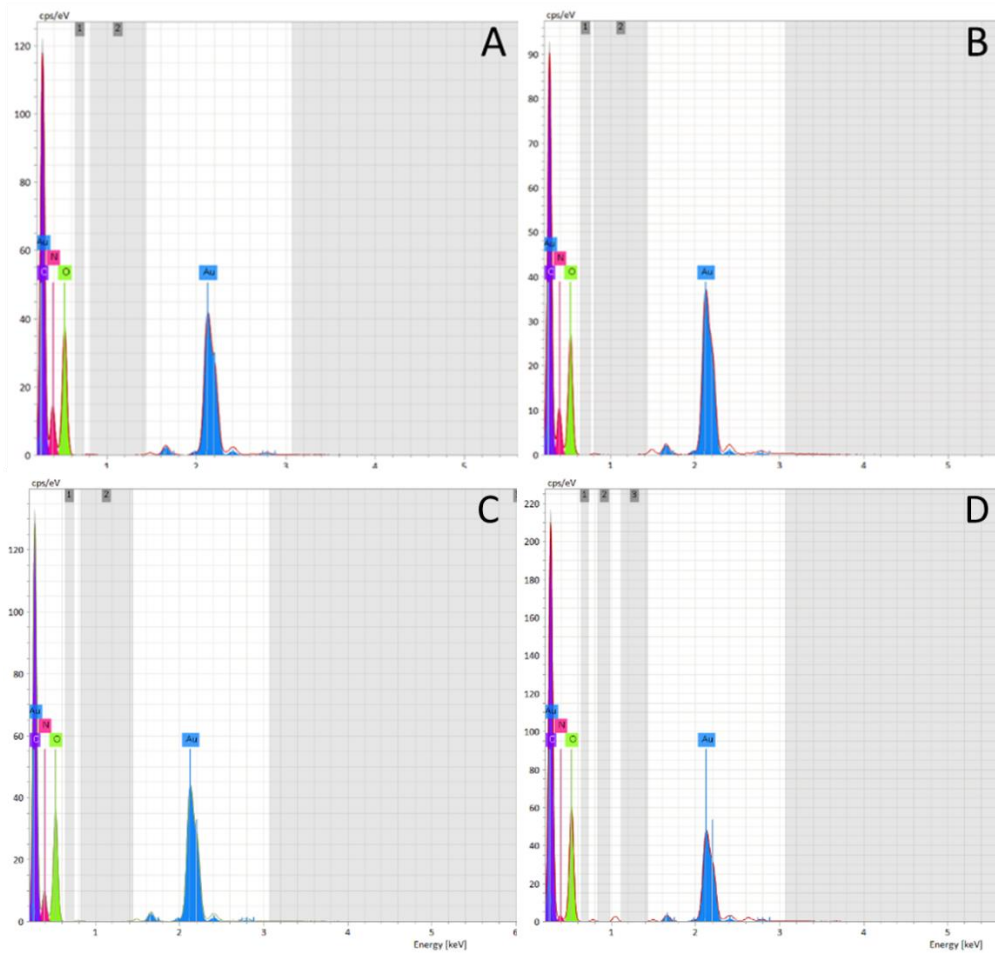


**Figure 19 EDX analysis for elemental distribution within scaffolds**

(A) silk control, (B) cartilage phase of the biphasic scaffolds, (C) bone phase of the biphasic scaffolds, (D) 3D printed scaffolds. (Purple) carbon, (pink) nitrogen, (green) oxygen, (blue) gold.

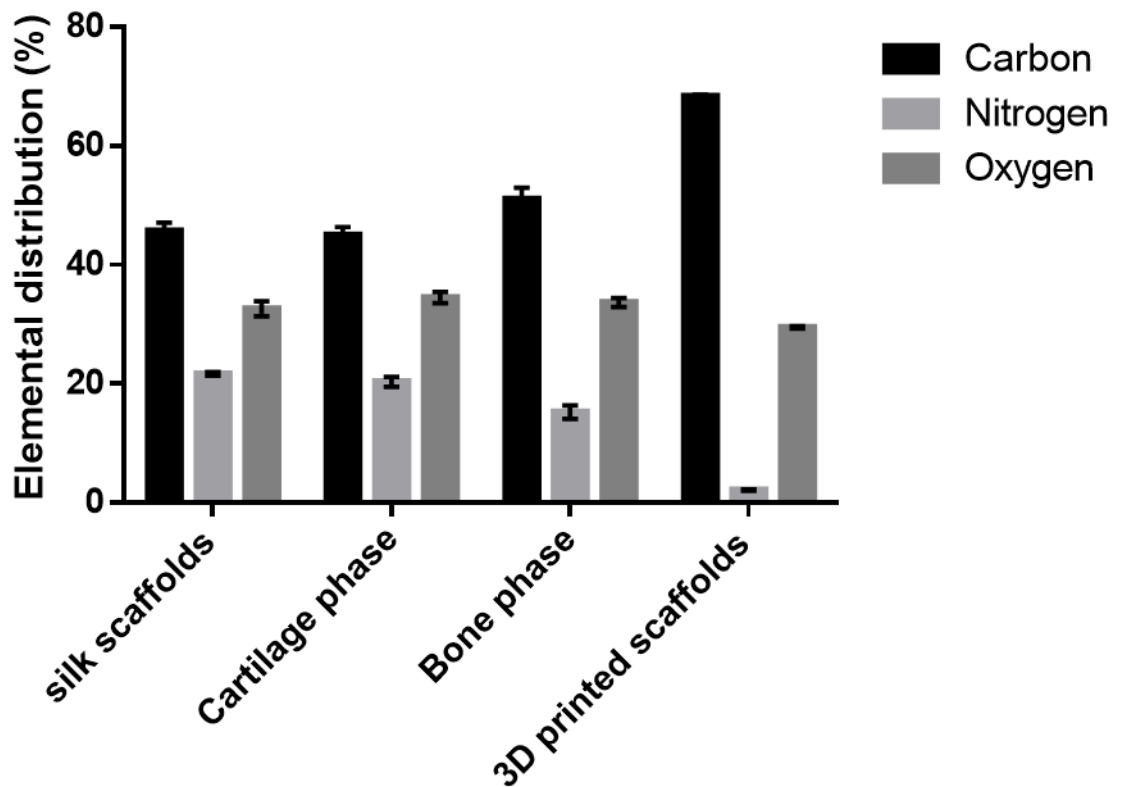


**Figure 20 Relative elemental distribution found within the scaffold types as determined by EDX** Black - carbon, light grey-nitrogen and dark grey-oxygen. Elemental distribution was determined in 3 distinct locations within 4 scaffolds for each scaffold. The distribution of all elements in silk scaffolds and the cartilage phase of biphasic scaffolds are non-significantly different ( $p > 0.05$ ). These two scaffolds were compared to the bone phase of the biphasic scaffolds, which showed a significant increase ( $p < 0.05$ ) in carbon, a significant decrease ( $p < 0.05$ ) in nitrogen, and no significant change ( $p > 0.05$ ) in oxygen content. On the other hand, the 3D printed scaffolds showed significantly higher ( $p < 0.001$ ) carbon levels as well as significantly lower ( $p < 0.001$ ) nitrogen levels, with non-significantly different ( $p > 0.05$ ) oxygen levels. Data represent mean  $\pm$  SD.

### 3.1.3 Scaffold protein crystallinity

The secondary structure of the protein component of the scaffolds (beta sheets, random coils and alpha helices) (Figure 21) plays a fundamental role in the protein's degradability and mechanical properties. To investigate protein crystallinity, FTIR was undertaken. This showed that the beta sheet content of the silk scaffolds was  $48.2 \pm 3.6\%$ , the cartilage phase of the biphasic scaffolds was  $50.1 \pm 0.9\%$ , and the bone phase of the biphasic scaffolds was  $51.0 \pm 3.5\%$ . The beta sheet content at both zones of the biphasic scaffolds and silk control

scaffolds showed no significant difference compared to each other ( $p>0.05$ ), inferring that casting process of the silk over the 3D printed components had no impact on the silk protein's ability to form beta sheets. Further to this, there was also no significant difference ( $p>0.05$ ) in the proportion of random coils in the cartilage phase, which showed a percentage of  $39.2 \pm 1.0\%$ , the bone phase which showed a percentage of  $37.8 \pm 6.7\%$ , and the silk control scaffold which showed a percentage of  $39.0 \pm 4.8\%$ . There was also no significant difference ( $p>0.05$ ) in alpha helix proportion between the cartilage phase ( $10.6 \pm 0.5\%$ ), the bone phase ( $11.2 \pm 5.5\%$ ), and silk scaffolds ( $12.8 \pm 2.1\%$ ). Raw FTIR data is shown in appendix 1 (Figure 61)

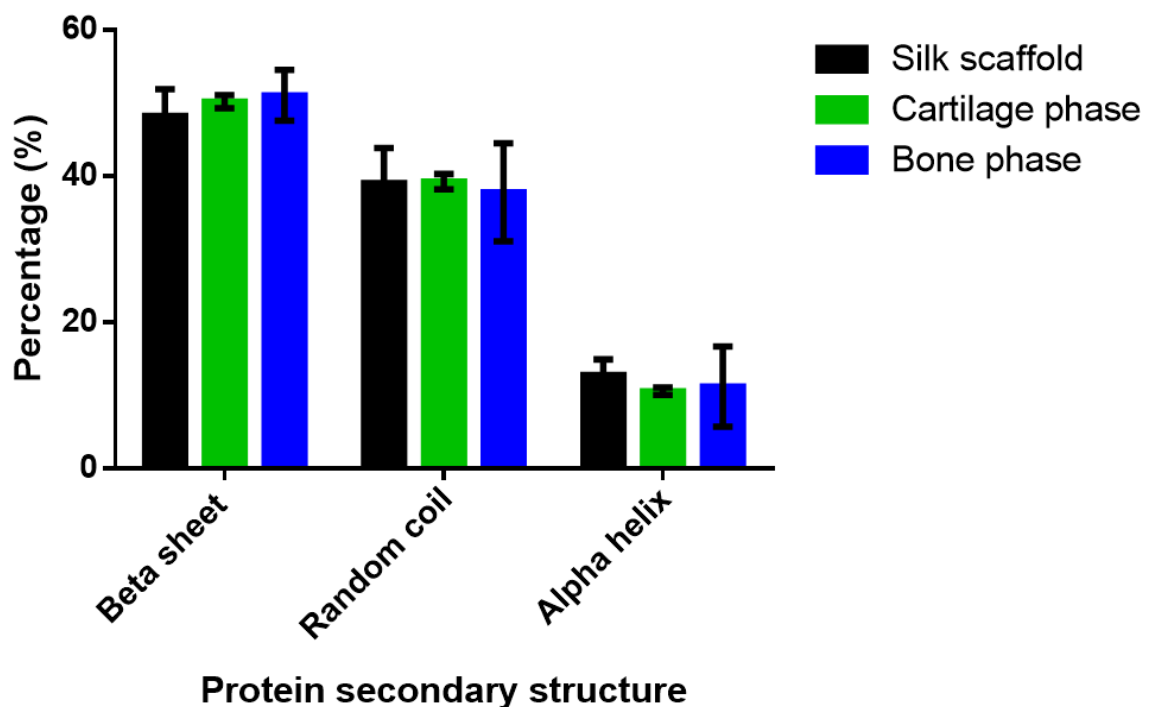


**Figure 21 The relative distribution of the protein's secondary structure**

Protein secondary structure- beta sheets, random coils and alpha helices- found within the scaffolds as determined by FTIR. Black- silk control scaffold, green- the cartilage phase of the biphasic scaffolds, blue- the bone phase of the biphasic scaffolds ( $n=4$  per scaffold). No statistically significant difference was seen between any scaffold and its protein secondary structure ( $P>0.05$ ). Data represent mean  $\pm$  SD.

### 3.1.4 Scaffold porosity

Scaffold porosity was evaluated using the Archimedes method (Figure 22).

Scaffold porosity plays a key role in determining the available surface area for cell growth and colonisation, and cell–biomaterial interactions. Scaffold porosity is also an indicator for the scaffold’s permeability for oxygen, nutrients and waste exchange. Both the silk control scaffolds and cartilage phase of the biphasic scaffolds showed porosities greater than 70%, whereas the 3D printed scaffolds and the bone phase of the biphasic scaffolds showed porosities lower than 70%. Silk control scaffolds and the cartilage phase of the biphasic scaffolds showed the two highest porosities, with  $90.03 \pm 1.8\%$  and  $90.93 \pm 2.7\%$  respectively, which were non-significantly different ( $p>0.05$ ); whereas, the 3D printed scaffolds and the bone phase of the biphasic scaffolds showed significantly lower ( $p<0.01$ ) porosities of  $56.99 \pm 0.4\%$  and  $61.01 \pm 1.63$  respectively. There was no significant difference ( $p>0.05$ ) between the porosity of the 3D printed scaffolds and the bone phase of the biphasic scaffolds.

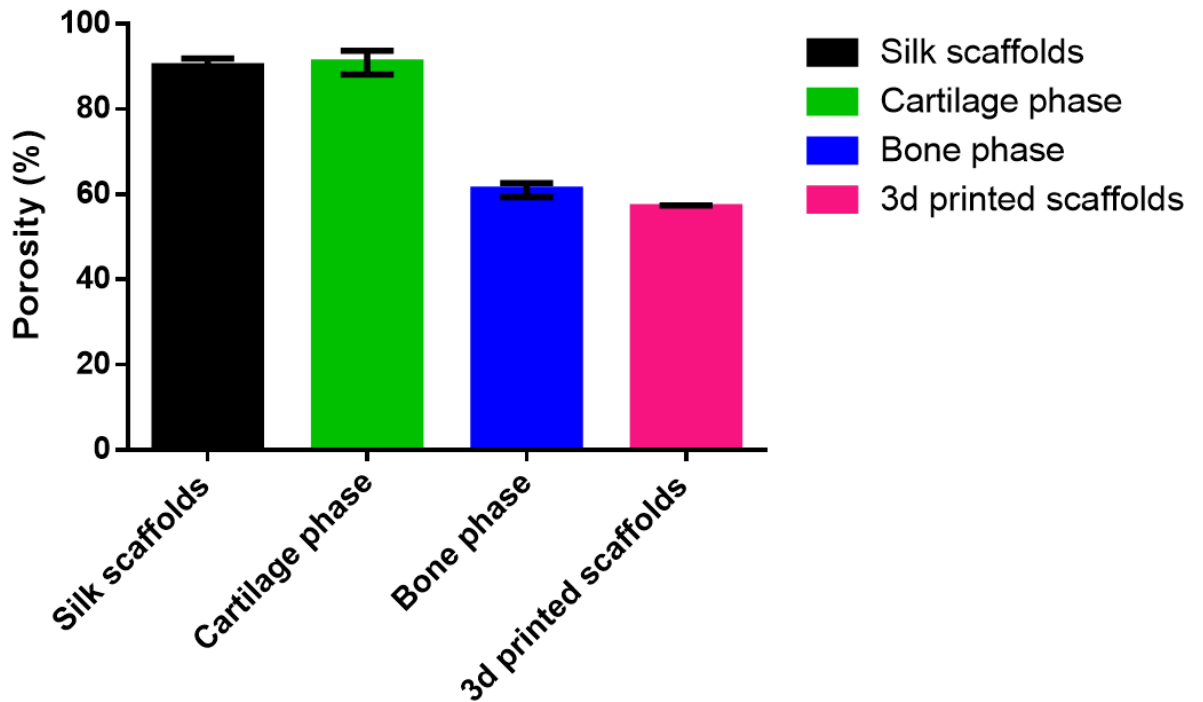


**Figure 22 Scaffold porosity**

Percentage porosity of scaffolds as determined by the Archimedes method. Black- silk control scaffold, green- the cartilage phase of the biphasic scaffolds, blue- the bone phase of the biphasic scaffolds, pink- 3D printed scaffolds (n=4 per group). Silk scaffolds and the cartilage phase of the biphasic scaffolds showed the 2 highest porosities which were non-significantly different ( $p > 0.05$ ); whereas 3D printed scaffolds and the bone phase of the biphasic scaffolds showed significantly lower ( $p < 0.01$ ) porosity. There was no significant difference ( $p > 0.05$ ) between the porosity of the 3D printed scaffolds and the bone phase of the biphasic scaffolds. Data represent mean  $\pm$  SD.

### 3.1.5 Scaffold swelling potential

The behaviour of scaffolds in the presence of fluid and their ability to rehydrate from a dried state was investigated. Scaffold swelling ability is an important index to understand as it is directly related to pore size, interconnectivity and scaffold volume. Furthermore, it is essential to understand whether scaffolds are able to fully hydrate from a dried state, that is the complete removal of gas from all interconnected pores and its replacement with fluid, as any remaining gas can lead to the retardation of cell migration. Both the biphasic scaffolds and the silk control scaffolds saw an initial rapid increase in mass after one hour of incubation in PBS at 37°C, with the biphasic scaffolds seeing an increase of  $172 \pm 19\%$ , the silk

control scaffolds seeing an increase of  $1075 \pm 103\%$ , and the 3D printed scaffolds seeing very little increase of  $12 \pm 4.7\%$  (Figure 23). All percentage of mass changes after the first hour were significantly different ( $p < 0.0001$ ). Following the initial increase within the first hour, all three scaffolds saw no significantly different further changes in mass in the subsequent 18 hours ( $p > 0.05$ ). All changes in mass were significantly different between groups all time points ( $p < 0.001$ ). The significantly greater increase in mass within the silk control scaffolds compared to the biphasic scaffolds was assigned to the non-swelling properties of the 3D printed component of the biphasic scaffold, which also contributed to a noticeably greater starting mass.

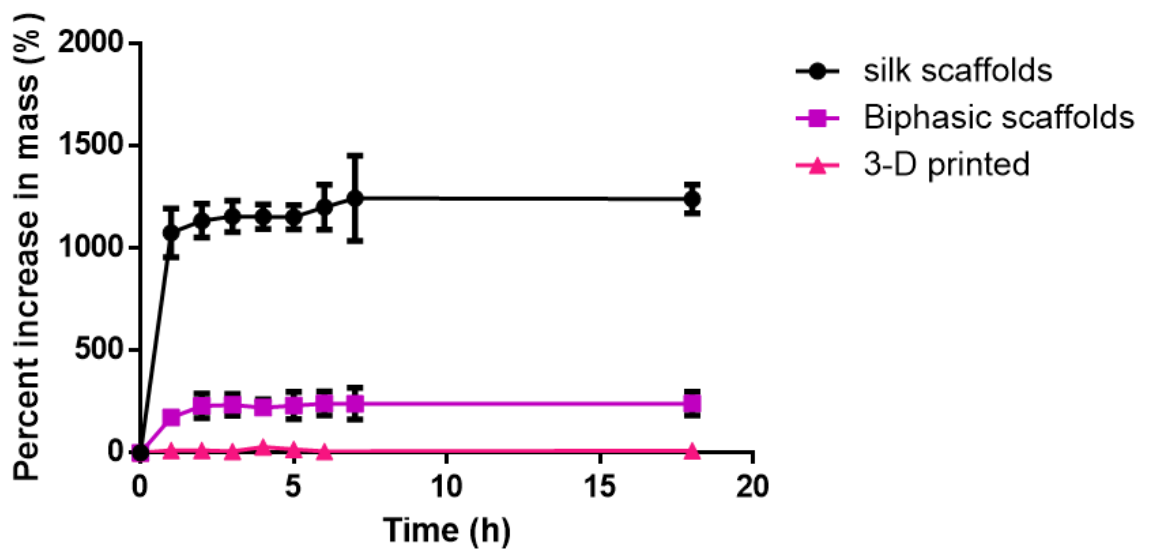


**Figure 23 Scaffold swelling**

Swelling potential of scaffolds over an 18-hour time period. Black- silk, purple- biphasic scaffold, pink- 3D printed scaffold (n=4 per group). All percentage of mass changes after the first hour were significantly different ( $p < 0.0001$ ). Following the initial increase within the first hour, all three scaffolds saw no significantly different further changes in mass in the subsequent 18 hours ( $p > 0.05$ ). All changes in mass were significantly different between groups all time points ( $p < 0.001$ ). Data represent mean  $\pm$  SD.

To confirm whether the scaffolds were fully rehydrated after 18 hours of PBS incubation, a negative pressure step was added to extract any present air bubbles. By placing the scaffolds within a desiccator whilst they were submerged in PBS, it was hoped that the low-pressure environment within the desiccator would draw out any air bubbles trapped within the scaffold and replace them with the PBS in which the scaffolds were placed. To compare scaffold rehydration after 18 hours with rehydration after 18 hours plus desiccation, scaffolds were incubated in PBS at 37°C for 18 hours and weighed. Scaffolds were further desiccated, and their masses were re-weighed. Both the silk control scaffolds, and the biphasic scaffolds saw significant increases in mass, whereas the 3D printed scaffolds saw no increase in mass (Figure 24). Silk control scaffolds increased from the 18-hour level of  $1241 \pm 61\%$  to the post desiccation level of  $1611 \pm 106\%$  ( $p < 0.01$ ), and the biphasic scaffolds increased from an 18-hour level of  $240 \pm 47\%$  to a post desiccation level of  $299 \pm 62\%$  ( $p < 0.01$ ). However, the 3D printed scaffolds saw no change between the 18-hour level of  $11 \pm 1.4$  and the post desiccation level of  $11 \pm 2.6$  ( $p > 0.05$ ). This indicates that passive diffusion of fluid into the biphasic and silk scaffolds was not satisfactory to fully rehydrate the scaffolds, and desiccation is required for complete scaffold rehydration. This was further visually confirmed by the scaffolds transitioning from floating when placed within liquid to sinking.

Is italicised

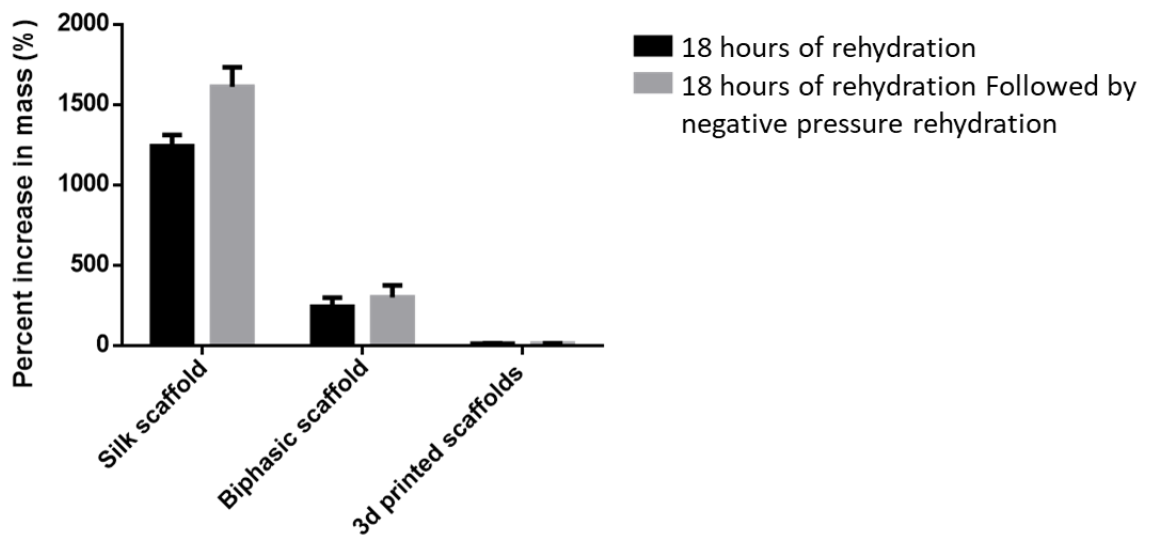


**Figure 24 negative pressure rehydration for scaffold rehydration**

Comparison of scaffold rehydration after 18 hours of rehydration in PBS with rocking (black) or 18 hours of rehydration plus negative pressure rehydration within a desiccator for five minutes submerged in PBS (grey) (n=4 per group). Silk scaffolds and biphasic scaffolds showed a significant increase in percentage mass increase ( $p < 0.01$ ), whereas the 3D printed scaffolds saw no significant change ( $p > 0.05$ ). Data represent mean  $\pm$  SD.

### 3.1.6 Scaffold degradability

It's important to understand the rate and ability of the scaffold to undergo degradation over time. Ideally, the scaffold will initially provide mechanical and biological support to guide and assist the regeneration of native tissue, followed by complete degradation and reabsorption of the scaffold and replacement with native tissue (Bachtiar *et al.*, 2016). To understand the degradation potential of biphasic scaffolds and silk control scaffolds, the scaffolds were subjected to an accelerated *in vitro* degradation model in the presence of protease XIV. *In vitro* degradation is useful to elucidate the potential degradation rate of different scaffolds based on their properties. Initially, silk scaffolds, biphasic scaffolds and 3D printed scaffolds showed similar degradation rates, with after two days there being no significant difference ( $p > 0.05$ ) in mass decrease, with the biphasic scaffolds having  $98.8 \pm 1.1\%$  of original mass remaining, silk scaffolds having  $94.5 \pm 4.2\%$  remaining and 3D printed scaffolds having  $99.3 \pm 1.1\%$  remaining (Figure

25). However, in all the following days, the silk scaffolds had a more significant decrease in mass than the biphasic scaffolds and 3D printed scaffolds. After 20 days, all scaffolds showed a significant difference in mass. The biphasic scaffolds had  $85.4 \pm 2.6\%$  of original mass compared to the silk scaffolds'  $5.3 \pm 4.6\%$  and the 3D printed scaffolds'  $98.8 \pm 0.6\%$ . Visual inspection of the biphasic scaffolds after eight days showed very little degradation to the 3D printed component compared to the silk, inferring protease XIV had mostly broken down the silk component of the biphasic scaffold, rather than the 3D printed component.

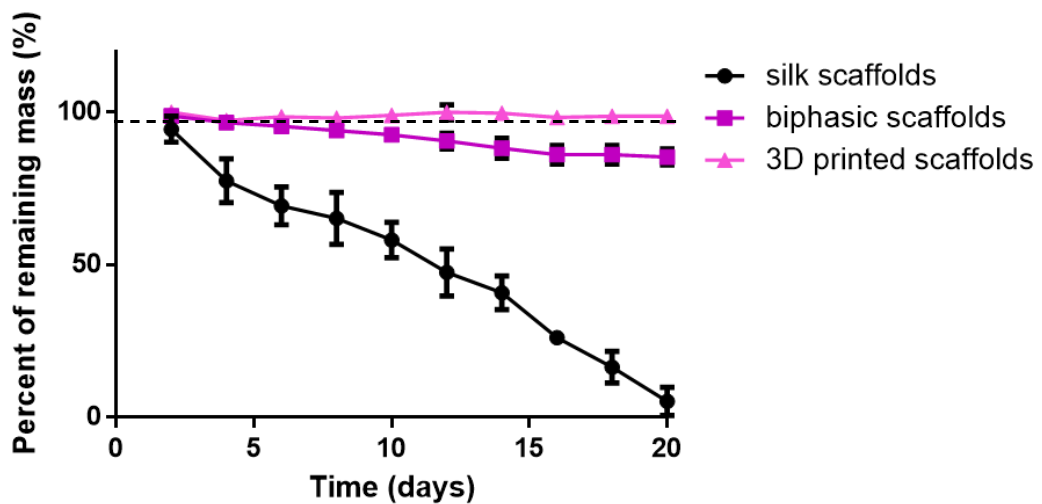


**Figure 25 *In vitro* degradation of scaffolds**

*In vitro* degradation of scaffolds submerged in protease solution over 20 days. Black circle- silk control scaffolds, purple square- biphasic scaffolds, pink triangle- 3D printed scaffold (n=4 per group). Initially, silk scaffolds, biphasic scaffolds and 3D printed scaffolds showed similar degradation rates, with after two days there being no significant difference ( $p>0.05$ ) in mass decrease. However, in all the following days, the silk scaffolds had a more significant decrease in mass than the biphasic scaffolds and 3D printed scaffolds. After 20 days, all scaffolds showed a significant difference in mass. Dotted line represents the point below which the scaffold mass loss due to silk degradation. Line positioning is determined by mass of 3D printed scaffolds. Data represent mean  $\pm$  SD.

## 3.1.7 Characterisation of scaffold mechanical properties

### 3.1.7.1 Uniaxial compression test

One of the main forces that osteochondral scaffolds will endure post implantation and during manipulation is compression. Therefore, it is essential to understand how the scaffolds interact and behave under compression (Francis *et al.*, 2018). To investigate this, initially, basic uniaxial compression testing was undertaken to understand the mechanical properties of both silk scaffolds alone (n=6), the biphasic scaffolds (n=4) and the 3D printed scaffolds (n=4). A typical compressive stress-strain curve is shown in Figure 26. As shown by the stress strain curve, the 3D printed lattice appears to provide rigidity and a greater load resistance. The compressive modulus was significantly greater ( $p < 0.001$ ) in the bone phase of the biphasic scaffold group ( $12.56 \pm 1.94$  MPa) compared to the silk scaffolds ( $0.113 \pm 0.028$  MPa) (Figure 27). However, there was no significant difference ( $P > 0.05$ ) between the silk scaffold and the cartilage phase of the biphasic scaffold ( $0.152 \pm 0.010$  MPa). There was also no significant difference ( $P > 0.05$ ) between the bone phase of the biphasic scaffold and the 3D printed scaffold ( $14.60 \pm 0.53$  MPa).

The incorporation of the silk layer appears to have no detrimental effects to the biphasic scaffold's ultimate compressive strength, demonstrated by there being no significant difference ( $P > 0.05$ ) between the 3D printed scaffold's ultimate compressive strength of  $1.88 \pm 0.087$  MPa and the biphasic scaffold's ultimate compressive strength of  $1.56 \pm 0.337$  MPa (Figure 28). The presence of the silk top layer on the biphasic scaffold was also able to significantly increase the strain at failure from the 3D printed scaffold's  $25.7 \pm 4.5$  % to the biphasic scaffold's  $42.1 \pm 7.3$  % ( $p < 0.001$ ). The biphasic scaffold retrieved at the end of compression testing consisted of a flattened silk scaffold which remained well-integrated to the 3D printed scaffold. There was no sign of delamination between phases. The

presence of silk appeared to increase the resilience of the scaffold dramatically, extending the toe region as seen in Figure 26.

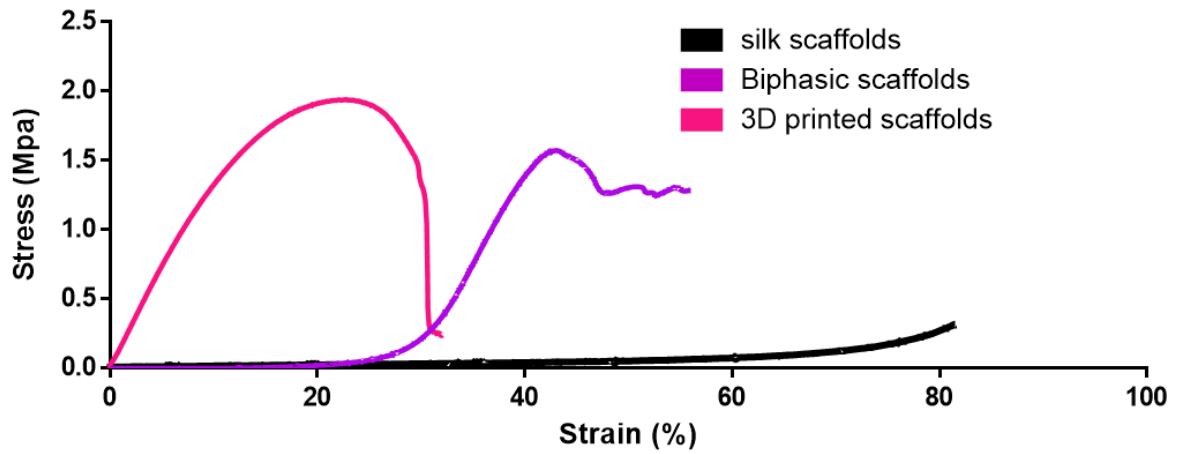


**Figure 26 Representative stress-strain curves for the scaffolds under uniaxial compression testing**  
Black- silk control scaffolds, purple- biphasic scaffolds, pink- 3D printed scaffolds.

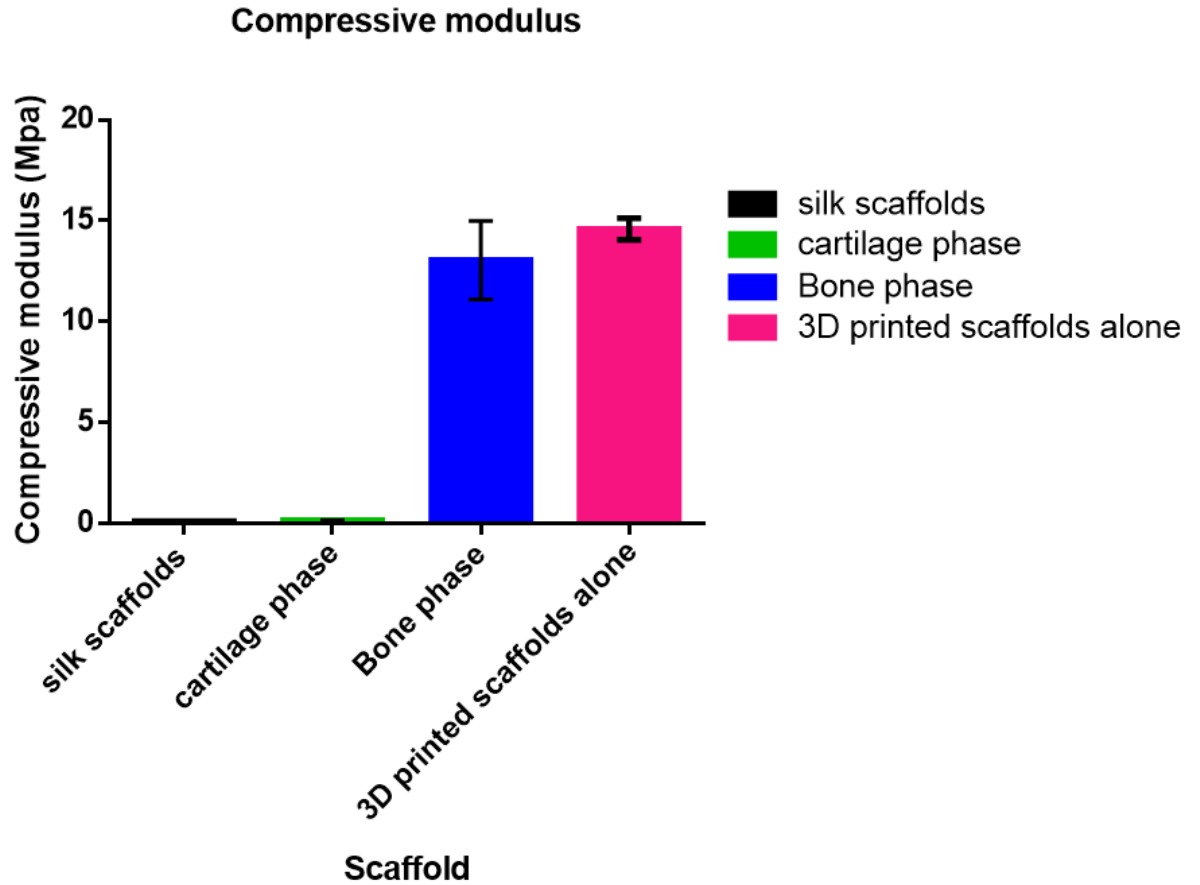


**Figure 27 Scaffold compressive modulus**

Scaffold compressive modulus under uniaxial compression testing as determined via stress-strain curves. Black- silk control scaffolds (n=6), green- cartilage phase of the biphasic scaffolds(n=4), blue- bone phase of the biphasic scaffolds(n=4), pink- 3D printed scaffolds (n=4). Silk scaffolds and the cartilage phase of the biphasic scaffolds showed the 2 lowest compressive modulus which were non-significantly different ( $p>0.05$ ); whereas 3D printed scaffolds and the bone phase of the biphasic scaffolds showed significantly higher ( $p<0.001$ ) compressive modulus. There was no significant difference ( $p>0.05$ ) between the compressive modulus of the 3D printed scaffolds and the bone phase of the biphasic scaffolds. Data represent mean  $\pm$  SD.

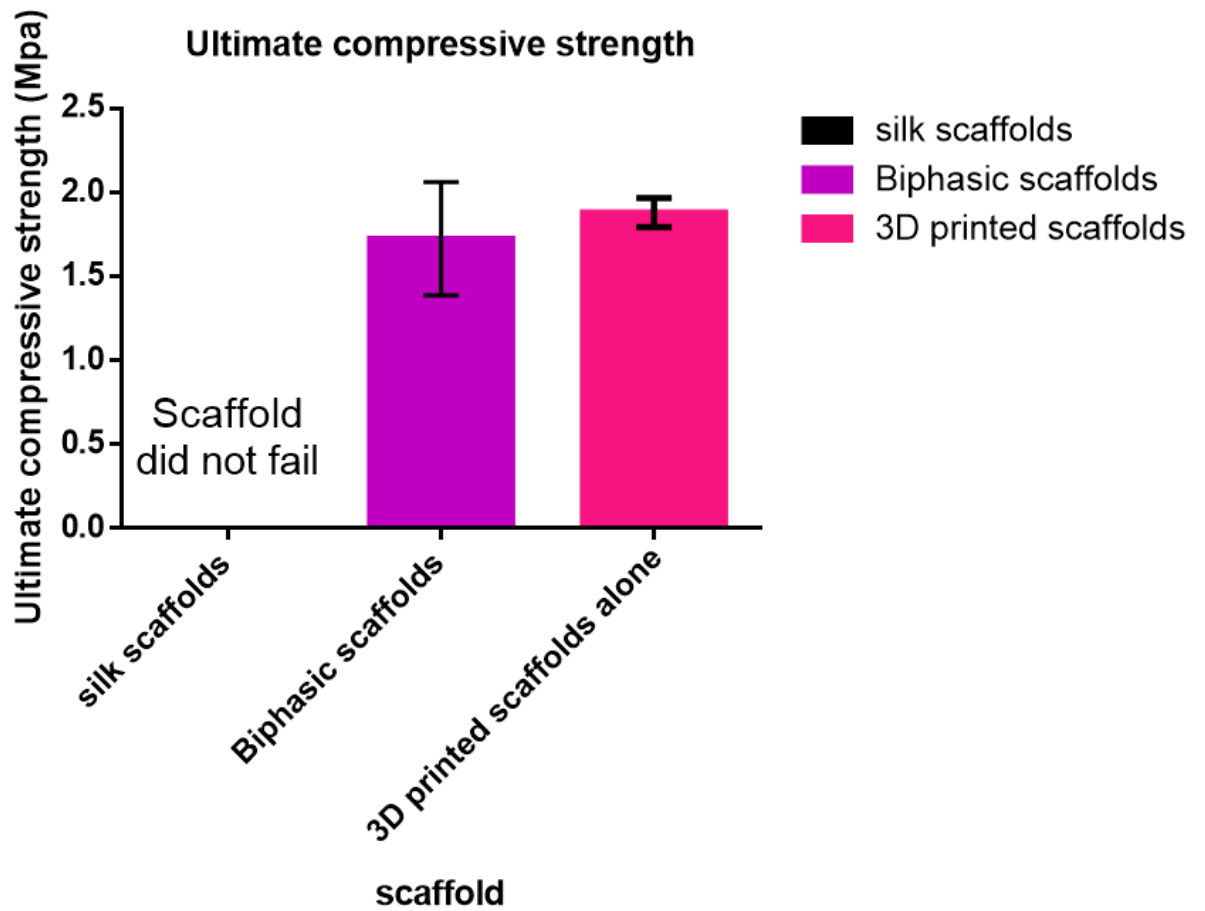


**Figure 28 Scaffold ultimate compressive strength**

Ultimate compressive strength under uniaxial compression testing as determined via stress-strain curves. Black- silk control scaffolds (n=6), purple- biphasic scaffolds (n=4), pink- 3D printed scaffolds (n=4). No statistically significant difference was seen in ultimate compressive strength between biphasic scaffolds and 3D printed control scaffolds ( $p > 0.05$ ). Data represent mean  $\pm$  SD.

### 3.1.7.2 Fatigue behaviour

Rather than implanted scaffolds experiencing overload forces, it is much more likely that they will experience low intensity repeated fatigue loading during normal articulation. To understand the scaffold's behaviour in relation to long-term repeated loading, fatigue testing was undertaken over 100,000 cycles.

During fatigue testing, both the silk control scaffolds and biphasic scaffolds saw a dramatic increase in resultant strain after the first 100 cycles, followed by a plateau with very little further change (Figure 29). This contrasts with the 3D printed scaffolds, which saw a slight decrease in resultant strain. Silk control

scaffolds showed a significant increase ( $p < 0.05$ ) from resultant strain at cycle one ( $83.08 \pm 1.92\%$ ) to cycle 100 ( $85.13 \pm 1.60\%$ ), and the biphasic scaffolds also showed a significant increase ( $p < 0.05$ ) between the resultant strain at cycle 1 ( $-35.88 \pm 0.69\%$ ) to cycle 100 ( $36.55 \pm 0.64\%$ ). This is in comparison to the non-significant change ( $p > 0.05$ ) between the resultant strain at cycle 1 ( $5.81 \pm 0.58\%$ ) to cycle 100 ( $5.99 \pm 0.60\%$ ) seen in the 3D printed scaffolds. However, the decrease seen within the silk control scaffolds of  $2.05 \pm 0.34\%$  was significantly greater ( $p < 0.05$ ) than the decrease seen within the biphasic scaffolds ( $0.67 \pm 0.11\%$ ). This indicates that the majority of lasting fatigue damage happens in the initial first 100 cycles and very little further damage is seen following this, with biphasic scaffolds having a greater fatigue resistance than silk control scaffolds, but still not as high a fatigue resistance as the 3D printed scaffolds.

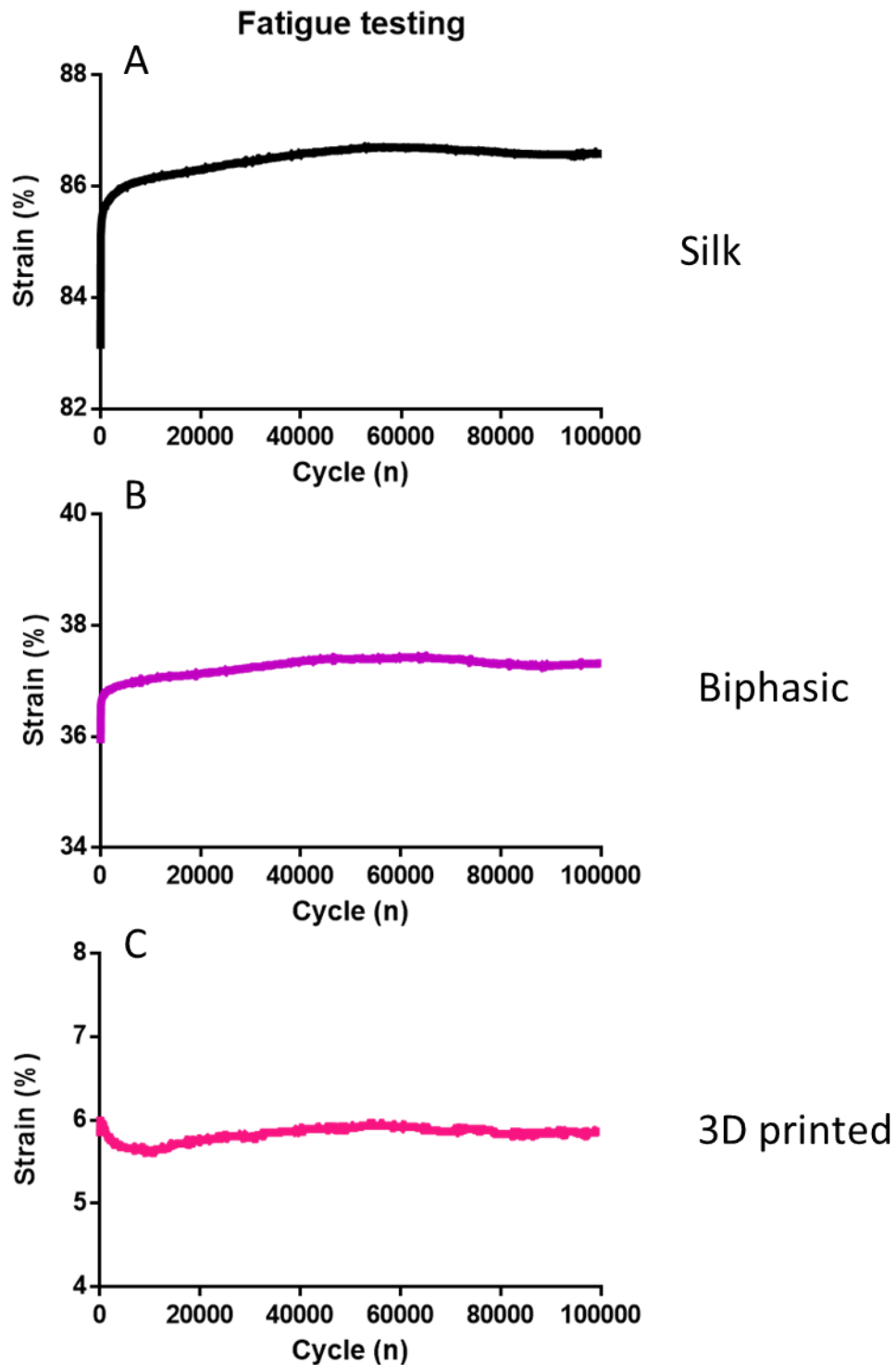


**Figure 29 Resultant strain from fatigue testing of scaffolds**

Fatigue testing showing resultant strain every 100 cycles after applied force of 8N over 100,000 cycles. A – silk, B – biphasic, C – 3D printed (n=4 per group). Silk control scaffolds showed a significant increase ( $p < 0.05$ ) from resultant strain at cycle one to cycle 100. Biphasic scaffolds also showed a significant increase ( $p < 0.05$ ) between the resultant strain at cycle 1 to cycle 100 after cycle 100 no further significant ( $p > 0.05$ ) changes were seen for both scaffolds. This is in comparison to the non-significant change ( $p > 0.05$ ) between the resultant strain at cycle 1 to cycle 100 seen in the 3D printed scaffolds. The decrease seen within the silk control scaffolds at cycle 100 was significantly greater ( $p < 0.05$ ) than the decrease seen within the biphasic scaffolds

Following 100,000 cycles, samples were evaluated for change in overall height as a measure of permanent damage to the scaffolds (Figure 30). All Scaffolds showed significantly different heights after fatigue testing ( $p < 0.001$ ). Silk control scaffolds showed a reduction of  $33.9 \pm 1.5\%$ , whereas the biphasic scaffolds only saw a reduction of  $18.5 \pm 2.5\%$ , and the 3D printed scaffold alone saw a reduction of  $2.4 \pm 0.5\%$ .

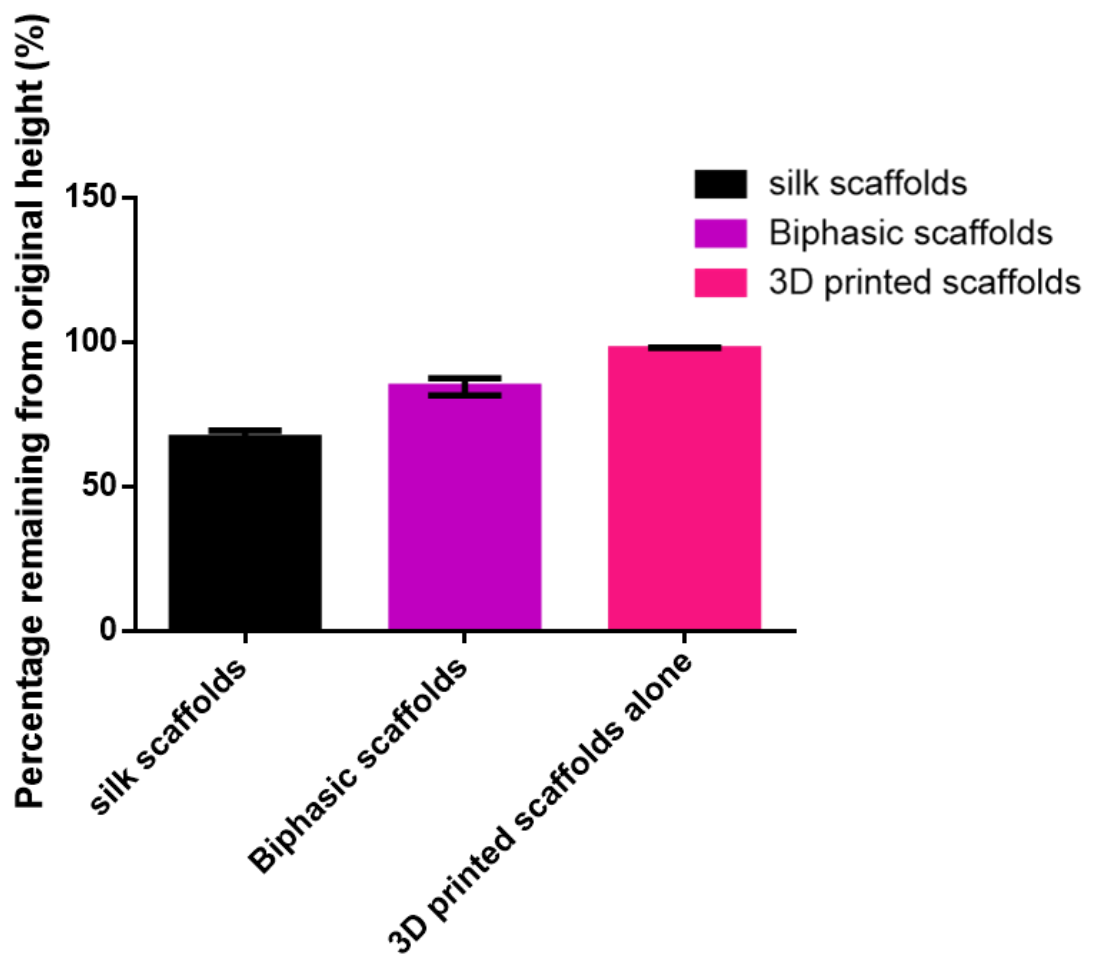


**Figure 30 Scaffold height reduction due to fatigue testing**

Percentage remaining of height of scaffolds after 100,000 cycles of fatigue testing at a load of 8N. Black- silk control scaffolds, purple- biphasic scaffolds, pink- 3D printed scaffolds. All Scaffolds showed significantly different heights after fatigue testing ( $p < 0.001$ ). Data represent mean  $\pm$  SD.

### 3.1.7.3 Hysteresis behaviour

All scaffold types showed significantly different ( $p < 0.01$ ) absorbed energy at each cycle count between each other (Figure 31 and Figure 32). Both biphasic and silk scaffolds showed significant decreases ( $p < 0.05$ ) in absorbed energy over increasing cycle count until the 10,000<sup>th</sup> cycle, after which no further significant decreases ( $p > 0.05$ ) were seen. Silk scaffolds went from an absorbed energy of  $0.936 \pm 0.148$  mJ at cycle 1 to an absorbed energy of  $0.396 \pm 0.016$  mJ at cycle 1000, and biphasic scaffolds went from an absorbed energy of  $0.393 \pm 0.096$  mJ at cycle 1 to an absorbed energy of  $0.125 \pm 0.0216$  mJ at cycle 1000. 3D printed scaffolds showed no significant ( $p > 0.05$ ) change between any cycle count with the cycle 1 absorbed energy being  $0.027 \pm 0.003$  mJ, cycle 1000 absorbed energy being  $0.0198 \pm 0.002$  mJ, cycle 10,000 absorbed energy being  $0.0179 \pm 0.001$  mJ and cycle 100,000 absorbed energy being  $0.0165 \pm 0.0005$  mJ.

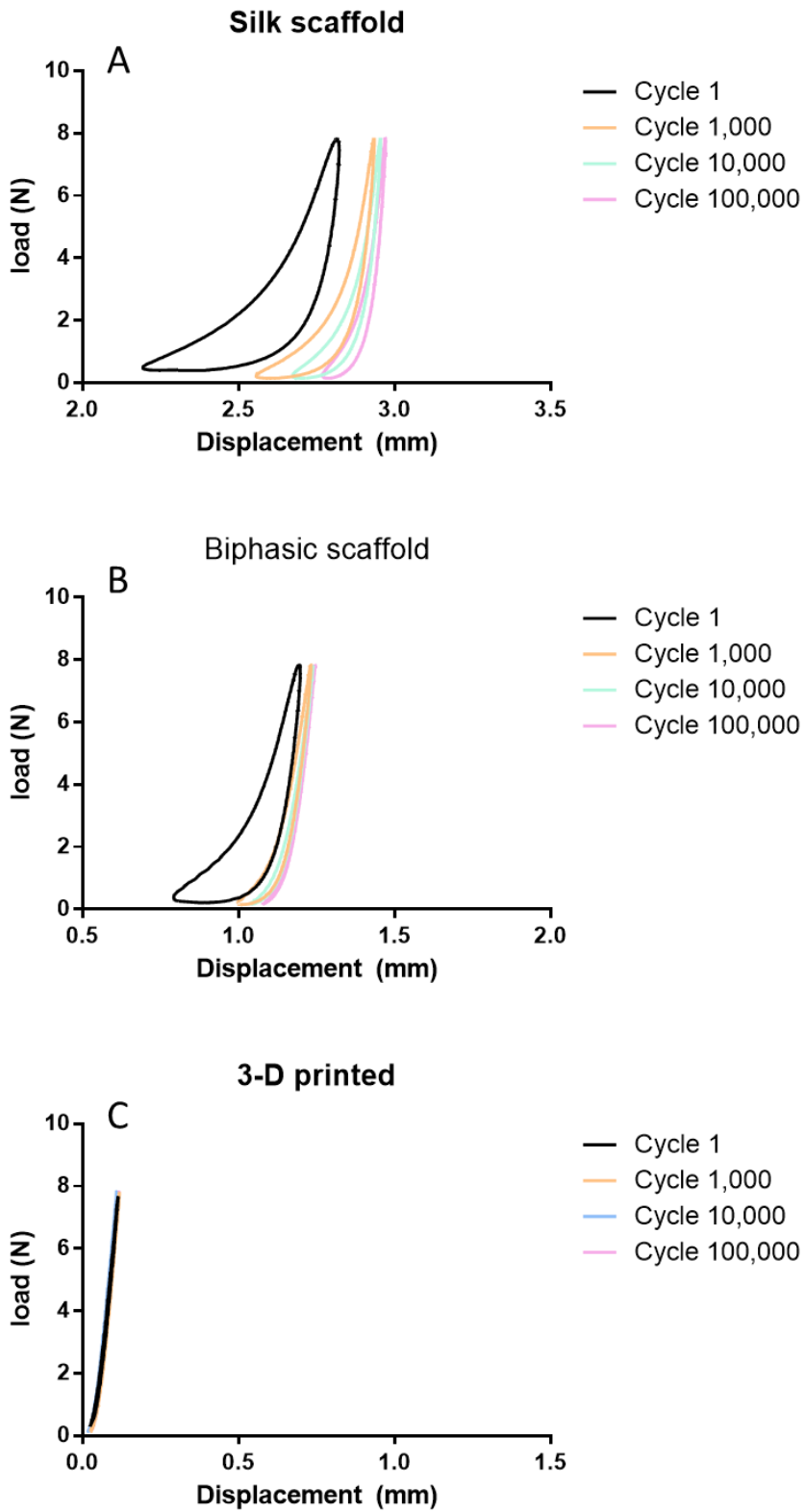


**Figure 31 . Representative Scaffold hysteresis loops under fatigue testing**  
 Scaffold hysteresis loops showing scaffold behaviour during loading and unloading at cycle one (black), 1000 (orange) 10,000 (blue) and 100,000 (pink). A-silk control scaffolds, B-biphasic scaffolds, C- 3D printed scaffolds.

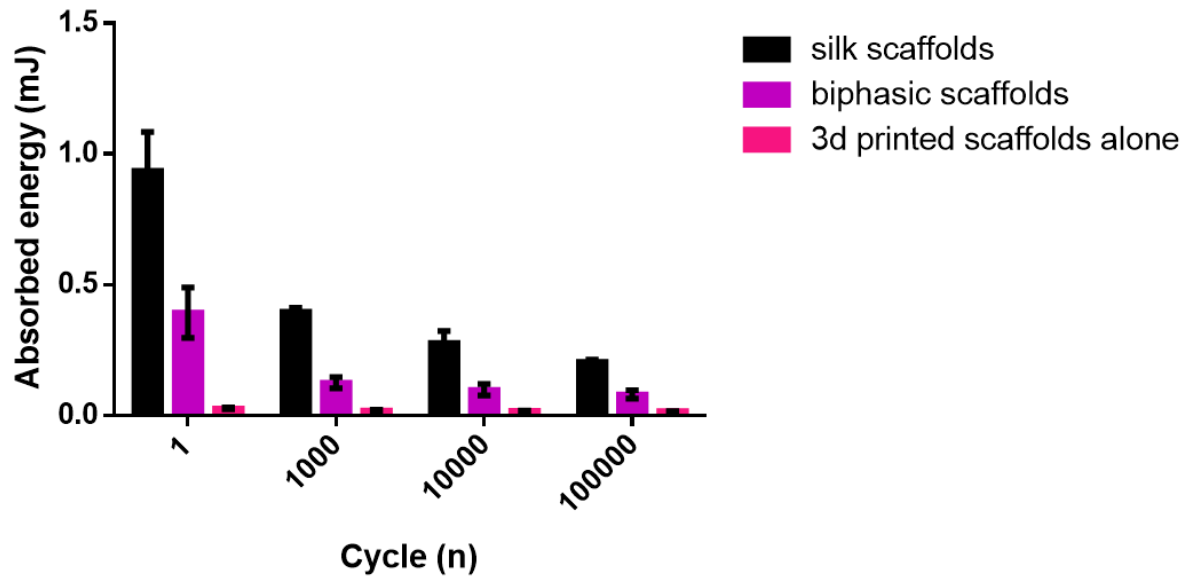


**Figure 32 Scaffolds absorbed energy during fatigue testing**

Absorbed energy during hysteresis loading as determined by the area within the hysteresis loop over one cycle, 1000 cycles, 10,000 cycles and 100,000 cycles. Black- silk control scaffolds, purple- biphasic scaffolds, pink- 3D printed scaffolds (n=4 per group). All scaffold types showed significantly different ( $p < 0.01$ ) absorbed energy at each cycle count between each other. Both biphasic and silk scaffolds showed significant decreases ( $p < 0.05$ ) in absorbed energy over increasing cycle count until the 10,000th cycle, after which no further significant decreases ( $p > 0.05$ ) were seen. 3D printed scaffolds showed no significant ( $p > 0.05$ ) change between any cycle count. Data represent mean  $\pm$  SD.

## 3.2 Discussion

Due to the extremely hierarchal and complex architecture of osteochondral tissue, grafts which represent both cartilage and bone phase may be required for proper and satisfactory osteochondral regeneration (Lopa and Madry, 2014). However, the existence of two unique tissue types means that osteochondral regeneration is particularly challenging. This thesis chapter tackled this challenge by using two pre-existing biomaterials and deploying them in a unique way; this was done via the creation of a bone phase consisting of a 3D printed Poly(ethylene glycol)-terephthalate-poly(butylene terephthalate) scaffold in which silk was utilised as an infill material which was continuously blended to a silk only cartilage phase. The use of silk within both phases allows for seamless integration between the cartilage phase and the bone phase, improving regenerative capacity due to interphase integration between the two tissue types. The choice to take a nonconventional manufacturing approach in the form of additive manufacturing via 3D printing conveys a number of benefits (Yan *et al.*, 2015; Sosio *et al.*, 2015; Du *et al.*, 2017), such as easy upscaling for mass production, greater control over bulk morphology, and the potential for future use in personalised medicine.

### 3.2.1 Scaffold pore size and porosity

Scaffold porosity and pore size is integral to the scaffold's function, as these two factors would dramatically affect cell adhesion, proliferation, and differentiation, as well as affecting transport of nutrients and waste products. The avascular nature of cartilage means that nutrient and waste exchange occurs between cartilage tissue and synovial fluid, either via passive diffusion or during joint articulation (Sophia Fox, Bedi and Rodeo, 2009; Liu, Shah and Luo, 2021). Porosity and pore size also play a fundamental role in angiogenesis and revascularisation *in vivo* (Karageorgiou and Kaplan, 2005; Wang and Yeung, 2017). When designing a scaffold with an optimal pore size for osteochondral tissue regeneration, a

difficulty is often seen in that both subchondral bone and cartilage scaffolds have differing optimal pore sizes (Lin *et al.*, 2019). Studies have previously demonstrated that for optimal cartilage regeneration a pore size of approximately 90  $\mu\text{m}$  to 120  $\mu\text{m}$  is desirable as this helps to direct and encourage chondrogenesis (Kuboki, Jin and Takita, 2001; Kim *et al.*, 2010). It has been previously shown that optimal scaffold pore size for subchondral bone regeneration is a larger size than that seen for chondrogenesis (approximately 300  $\mu\text{m}$ ), as this pore size seems to favour direct osteogenesis whilst also allowing for vascularisation, providing a relatively high oxygenation within the scaffold. Smaller pores still allow for osteogenic differentiation, however, via osteochondral ossification (Tsuruga *et al.*, 1997; Kuboki, Jin and Takita, 2001; Götz *et al.*, 2004; Karageorgiou and Kaplan, 2005). Osteochondral ossification is a process of bone formation in which cartilage tissue is converted into bone by extracellular matrix remodelling and mineralisation. The difficulty in this variability in optimal pore sizes is that the requirements of the manufacturing process of the seamless silk scaffold require a single pore range which has to be consistent between both the cartilage and bone phase. This is because, during fabrication, the temperature in which the silk is initially frozen for lyophilisation controls this parameter. The created pore size of the biphasic scaffold within this study is affected by the initial freezing temperature prior to lyophilisation. It has been previously shown that the lower the freezing temperature, the smaller the pore size created (Luo *et al.*, 2015). This is because lower freezing temperatures show an increased cooling rate, and thus an increase in the pore nucleation driving force- the resulting structures contain a higher number of smaller pores.

The average pore size seen within the cartilage phase ( $117 \pm 15 \mu\text{m}$ ) and the bone phase ( $124 \pm 24 \mu\text{m}$ ) of this biphasic scaffold sit within the optimal range for chondrogenesis, inferring that the scaffold has excellent chondrogenic potential whilst still allowing for osteogenesis. However, this has the potential disadvantage of not being the optimal size for vascularisation of the scaffold *in vivo*, with the pores being approximately 200  $\mu\text{m}$  smaller than the optimal size, although this

may not be a major concern due to the degradability of the silk component of the biphasic scaffold.

Within this study, the cartilage phase of the biphasic scaffold showed a comparable porosity to the silk control scaffolds, with a porosity of  $90.93 \pm 2.7\%$ . The literature indicates that a porosity of greater than 70% is suitable for tissue regeneration (Karageorgiou and Kaplan, 2005; Cheng *et al.*, 2018; Lutzweiler, Ndreu Halili and Engin Vrana, 2020; Abbasi *et al.*, 2020), as a porosity of this amount theoretically allows for cell infiltration into the scaffold surface, as well as adequate permeability for oxygen, nutrients and waste exchange. However, the bone phase of the biphasic scaffolds showed a less than 70% porosity of  $61.01 \pm 1.63\%$ ; this is comparable to the 3D printed scaffolds. The reasoning for the reduced porosity was assigned to the non-porous nature of the 3D printed component of the bone phase. Although the porosity of the bone phase is less than the indicated 70%, this fails to take into account the nuances of the scaffold design, as the silk component of the bone phase is most likely to have a comparable porosity to a silk control scaffold. Thus, although the bone phase of the biphasic scaffold as a whole has less than 70% porosity, the regional variability of the scaffold should mean that there should still be adequate cell infiltration as well as nutrition, oxygen, and waste exchange via the silk component of the bone phase.

Some tissue engineering approaches using osteochondral scaffolds select to create a tidemark mimicking feature between the cartilage and bone phase (Niu *et al.*, 2023). An artificial tidemark included within multiphasic scaffolds often consists of a thin region with no or negligible porosity and is designed to separate the bone and cartilage phase within the scaffold. The introduction of an impermeable membrane to split these two tissue types, helping to both better mimic native tissue and prevent bony invasion and blood vessel invasion of the cartilage, therefore hopefully improving regenerative outcomes (Yildirim *et al.*, 2023). Although some studies have shown success with incorporating tidemarks into

their scaffold design, it has also been shown that the incorporation of a tidemark can create a region within the scaffold which is mechanically weak and is at risk of causing stress localisation during loading, leading to a point of failure (Dormer, Berklund and Detamore, 2010; Cross *et al.*, 2016). Furthermore, it has also been demonstrated that although the tidemark is effective at splitting the multiphasic scaffold and preventing bony invasion to the cartilage phase, it can also lead to the creation of two distinct zones rather than a blended tissue going from cartilage to bone, leading to another potential point of failure (Chen *et al.*, 2023c). Therefore, within the biphasic scaffolds utilised in this project, it was selected at the design phase not to include a tidemark as it was believed that the risk of creating a stress point with poor phase integration within the scaffold, was far greater than the benefits of including a tidemark.

### **3.2.2 Mechanical properties**

Mechanical properties of the scaffold are fundamental to its regenerative capacity; its mechanical properties need to be great enough to resist articulation and manipulation during implantation, but not so great that they do not represent native tissue. The selection to blend two material types for the bone phase enables the scaffold to possess improved characteristics for osteochondral tissue regeneration, as each material can compensate and complement the limitations seen within the other material. Silk scaffolds have previously been shown to have extremely good biocompatibility, outperforming other scaffold materials such as collagen and polylactic acid when comparing the *in vivo* foreign body response of these materials (Foschi *et al.*, 2001; Altman *et al.*, 2003; Zhang *et al.*, 2014).

However, they have also been shown to have weak mechanical properties, making them difficult and undesirable in load-bearing applications. Therefore, as this study has demonstrated, the utilisation of a synthetic 3D printed lattice infilled with silk means the scaffold's mechanical properties are able to be

improved. The addition of the 3D printed lattice increases the scaffold's long-term survival and regenerative capacity. The ultimate compressive strength of the bone phase within the biphasic scaffold (1.465 MPa) sits just below that of native cancellous bone (2–12 MPa), this ultimate compressive strength appears to be high enough to allow the scaffold to survive implantation as well as joint loading (Li *et al.*, 2015a). The seamlessly integrated silk layer further enables the scaffold to represent native tissue, as together with the bone phase the biphasic scaffold was able to show stratified mechanical properties which more closely represent native osteochondral tissue. Native osteochondral tissue has been shown to have a gradient of compressive moduli, ranging from a relatively low 0.079 MPa in the superficial layer of articular cartilage to a 5.7 GPa in the subchondral bone, which is mimicked by the biphasic scaffold (Castro, Hacking and Zhang, 2012). Although the biphasic scaffold's mechanical properties sit slightly below that of native tissue, they are still high enough to theoretically survive implantation. The scaffolds also show a low enough compressive modulus to prevent stress shielding of highly mechanosensitive cells such as chondrocytes and osteoblasts (Guilak, Butler and Goldstein, 2001; Hu and Athanasiou, 2006; Huey, Hu and Athanasiou, 2012; Salinas, Hu and Athanasiou, 2018).

Rather than implanted scaffolds experiencing overloading forces, it is much more likely that they will experience low intensity repeated fatigue loading during normal articulation (Vikingsson *et al.*, 2015). Fatigue loading of an osteochondral scaffold refers to the application of cyclic mechanical stresses to the scaffold to simulate the repetitive loading that occurs *in vivo*. By determining the fatigue hysteresis loop of osteochondral scaffolds, information on the energy absorption characteristics of the scaffold material under cyclic loading was obtained. Energy absorption is an important factor to consider in the design of osteochondral scaffolds, as it directly affects the ability of the scaffold to withstand repetitive mechanical stresses and promote tissue regeneration. The hysteresis loop represents the energy lost during each cycle of loading and unloading, as the scaffold material undergoes deformation and recovers its original shape

(Abramowitch and Easley, 2016). The area enclosed by the hysteresis loop represents the total energy absorbed by the scaffold material over one complete cycle. A larger loop area indicates that more energy is being absorbed by the material, which can be beneficial in applications where high impact loads are expected (Teruna, Majid and Budiono, 2015; Allen *et al.*, 2020). However, excessive energy absorption can also lead to material failure or fatigue damage over time (Klemenc *et al.*, 2019). This is shown by the plastic deformation of the scaffold, leading to a permanent reduction in its height. Therefore, it is important to optimize the energy absorption characteristics of the scaffold material to ensure a balance between load-bearing capacity and durability.

It has previously been shown that cartilage is loaded at approximately 1Hz during normal walking, and the cartilage has a strain no greater than 6% (Eckstein *et al.*, 2005; Vikingsson *et al.*, 2015; Eckstein *et al.*, 2000). As demonstrated, all three scaffolds are able to survive repeated loading far in excess of the strain seen within normal articular cartilage of 6% with no major failure being seen on any of the scaffolds. 3D printed control scaffolds showed the greatest propensity to resist fatigue loading showing very little change in the scaffold's height ( $2.4 \pm 0.5\%$ ), with silk control scaffolds showing the least propensity to resist fatigue loading with the greatest reduction ( $33.9 \pm 1.5\%$ ). Biphasic scaffolds showed a blend of fatigue behaviour of the two scaffolds ( $18.5 \pm 2.5\%$ ). However, 3D printed scaffolds also showed no energy absorption capabilities, showing complete elastic behaviour during loading and unloading. This was compared to biphasic scaffolds and silk control scaffolds, which showed an ability to absorb energy during their repeated loading and unloading cycles, inferring that the scaffolds showed some viscoelastic properties. At cycle one, silk scaffolds showed the greatest capacity to absorb energy. However, after 1000 cycles, silk scaffolds showed a reduction in energy absorption of 0.54 mJ. This is compared to the energy absorption reduction within biphasic scaffolds of 0.268 mJ. This indicates once again that the silk control scaffolds have a lower fatigue resistance than the biphasic scaffolds. The goal of fatigue testing within this study was to provide a worst-case scenario

for loading of a scaffold post implantation. However, *in vivo*, it is unlikely the scaffold will experience consistent loading and unloading within a fatigue environment without rest periods. Allen *et al.*, 2020 demonstrated that, when working with the foam inners for running shoes, foam had a propensity to recover some of its energy absorbing characteristics over time if given adequate rest periods. Thus, it can be inferred that the foam-like materials used within this project may see a return of their energy absorbing characteristics if given adequate rest periods.

This data demonstrates that theoretically, the biphasic scaffolds within this study can survive low intensity repeated loading post implantation. The biphasic scaffolds' hysteresis properties also indicate that post implantation the scaffold will be able to distribute loads exerted on the vulnerable cartilage phase into underlying subchondral bone by absorbing and redistributing energy within the scaffold structure (Malekipour *et al.*, 2013; Lawless *et al.*, 2017; Mountcastle *et al.*, 2019; Gao *et al.*, 2019; Weizel *et al.*, 2020).

### **3.2.3 Swelling and degradation**

Two fundamental properties of a porous sponge-like biomaterial are the scaffold swelling capacity and degradability. The ability of sponge-like scaffolds to swell and retain a certain amount of water/liquid within their structure is essential for their regenerative capacity and potential cellular interactions (Madhally and Matthew, 1999; Eckstein *et al.*, 2000; Vikingsson *et al.*, 2015; Offeddu *et al.*, 2016). A scaffold's failure to rehydrate from the dried form can fundamentally reduce its effectiveness in regards to tissue engineering and its ability to regenerate natural tissue. Failure of rehydration can lead to collapse of scaffold pores, leading to a reduction in porosity (Costa *et al.*, 2017), which will affect cell penetration and reduce nutrient and waste exchange through the scaffold's interconnected pore network. Furthermore, a lack of an aqueous environment can

lead to a reduction in cell adhesion to the scaffold surface, . The swelling capacity of the scaffolds investigated in this study differed based on the material composition, with the biphasic scaffolds showing a lower capacity than the silk control scaffolds. This difference in swelling capacity was assigned to the 3D printed components of the biphasic scaffolds limiting swelling capacity in the presence of liquid, as well as its large contribution to the scaffolds' initial mass. It was also found that passive diffusion of the liquid into the scaffold was unable to fully rehydrate scaffolds from the dried state and a negative pressure rehydration step is required to completely rehydrate scaffolds. This was done by first placing scaffolds into liquid before lowering the relative atmospheric pressure surrounding the scaffold; the air bubbles enclosed within the scaffold's pores were removed, and the pores were then filled with the liquid in which the scaffold was submerged. This leads to complete scaffold rehydration and removal of any air remaining in the scaffold's pores (as long as they are connected to the surface). The negative pressure rehydration step utilised within this study demonstrates an easy and effective way to induce scaffold rehydration within a relatively short timeframe and should enable an increased potential cell infiltration as well as an increased regenerative capacity.

It is fundamental to understand the scaffold's degradability as it is essential to synchronise scaffold degradation with tissue formation (Bitar and Zakhem, 2014). The scaffold as a temporary matrix is removed and replaced with new tissue over time. To understand the degradation of the silk component of the scaffolds over time, an accelerated selective degradation model was used. This consisted of using protease XIV which is a cocktail of proteolytic enzymes with bacterial origin. Despite its bacterial origin, this technique well mimics the degradation environment found within synovial joints, and is an extremely useful analytical tool and has been extensively used on silk scaffolds previously (Li, Ogiso and Minoura, 2003; Rnjak-Kovacina *et al.*, 2015b; Baptista *et al.*, 2020). Within this study, the biphasic scaffold showed dramatically less degradation compared to the silk control scaffolds. The silk control scaffolds showed similar degradation

profiles to other studies that investigated silk only scaffolds (Rnjak-Kovacina *et al.*, 2015b). The 3D printed component of the biphasic scaffolds showed a greater resistance to degradation than the silk infill material, as confirmed by visual inspection, showing complete degradation of the infilling silk material within the biphasic scaffold after 20 days. There appeared to be no protective effect of the 3D printed scaffold to the infilling silk material. The infilling silk material showed a similar degradation rate to silk control scaffolds. The advantage of selective degradation of the silk component over the 3D printed component is that when implanted *in vivo*, the scaffold will be able to degrade to allow for the introduction of native tissue whilst still maintaining its mechanical stability; this will support regeneration and prevent damage to the newly formed tissue while in an immature state, with the 3D printed components degrading later due to its greater stability associated with synthetic structure (Montaudo, Puglisi and Samperi, 1993; Capito and Spector, 2003). A limitation of utilising a proteolytic model for degradation is that it hasn't been a good method to study the degradation of the 3D synthetic thermoplastic phases simultaneously with that of the silk. Due to the synthetic nature of the thermoplastic 3D printed scaffold, degradation will occur most likely via hydrolysis rather than proteolytic degradation (Deschamps *et al.*, 2004).

### **3.2.4 Summary**

Biphasic scaffolds were successfully created by casting silk fibroin from *Bombyx mori* over a 3D printed PEGT/PBT lattice. This biphasic scaffold showed adequate and equivalent porosity to silk control scaffolds to allow for cell infiltration. EDX data indicated no elemental contaminants remained from the scaffold creation process. The biphasic scaffold showed adequate and equivalent beta sheet formation to the silk control scaffolds. Biphasic scaffolds showed a reduction in swelling capacity compared to silk control scaffolds, however, with a swelling capacity still theoretically great enough to allow for appropriate nutrient

exchange. Both silk control scaffolds and biphasic scaffolds required a negative pressure rehydration step for appropriate rehydration. Biphasic scaffolds showed improved *in vitro* degradation characteristics theoretically allowing for timely degradation *in vivo*. Biphasic scaffolds showed improved mechanical properties compared to silk control scaffolds, as well as improved fatigue resistance.

# **Chapter 4 Osteochondral tissue engineering *in vitro* using human bone marrow stromal cells and biphasic 3D printed silk reinforced scaffolds**

This chapter is designed to cover cell interactions with the created biphasic scaffolds under various conditions and compare these back to the silk control scaffolds.

## 4.1 Results

### 4.1.1 Scaffold sterility

To evaluate whether the autoclave step to encourage  $\beta$ -sheet formation in the silk scaffolds could also effectively sterilize scaffolds, sterility testing was undertaken. Thioglycollate medium is a growth medium with an oxygen gradient which allows for testing for the presence of aerobic and anaerobic bacteria. Sterility testing (Figure 33) showed that at no time point (0d, 3d, 7d, 14d) were there any infections of any scaffold, represented by no turbidity within the media, demonstrating their sterility against aerobic or anaerobic bacterial growth. This was compared to positive controls which showed extensive bacterial growth and corresponding turbidity.

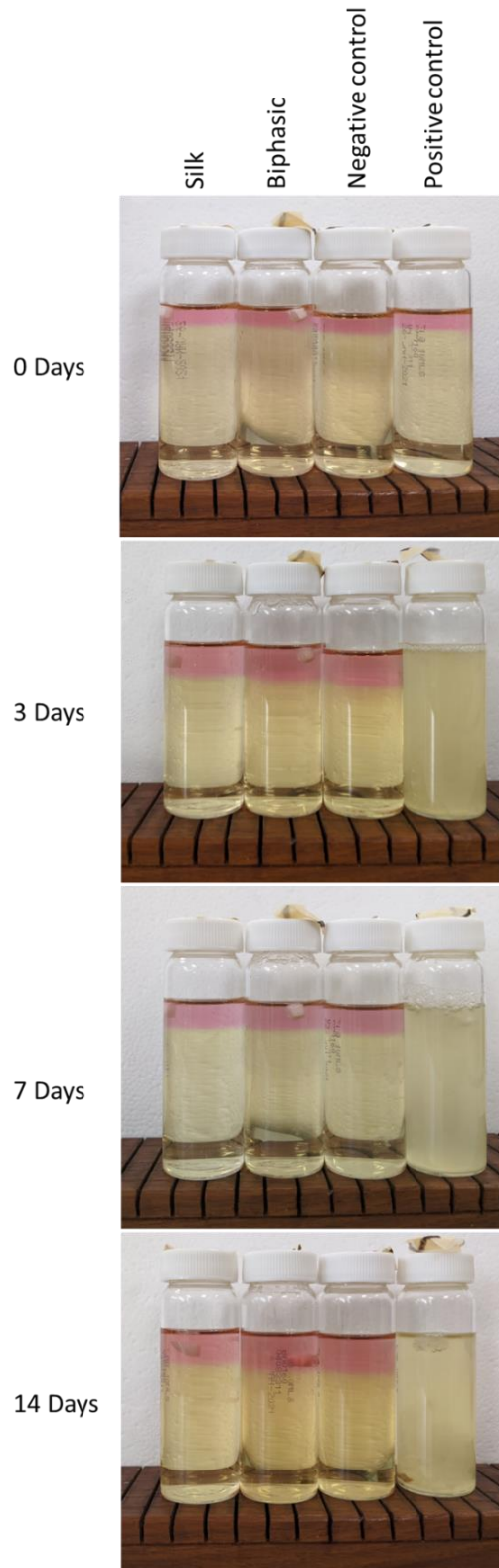


**Figure 33 Scaffold sterility testing**

Sterility testing was undertaken in thioglycolate media. Pink zone represents oxidised aerobic zone, and straw-coloured zone represents low oxygen anaerobic zone (n=4 per group). Positive controls were created via opening tubes to the air and leaving on the bench side at room temperature for 10 minutes. At day zero, no infection is seen in any group. By day 3, large amount of turbidity can be seen in the positive control with no infection being seen in any other group. This continues all the way to day 14 where still only the positive control shows an infection.

## 4.1.2 Scaffold cytotoxicity

### 4.1.2.1 Contact cytotoxicity

To understand the potential of the scaffolds to support cell growth, proliferation and migration, initially, the scaffolds were confirmed to have no contact cytotoxicity before further detailed analysis was undertaken. A contact cytotoxicity assay was undertaken as per ISO 10993-5:2009. All scaffold types showed no signs of contact cytotoxicity after microscopic analysis, with no cytotoxic zone being seen as per Figure 34 A,B, with cells growing up to and in contact with both scaffolds; the scaffolds were graded as grade 0 as per the ISO standard. Both scaffolds showed “*no detectable zone around or under specimen*”. Cells in all groups showed normal cell morphology, with good membrane integrity, with no cell detachment or lysis.

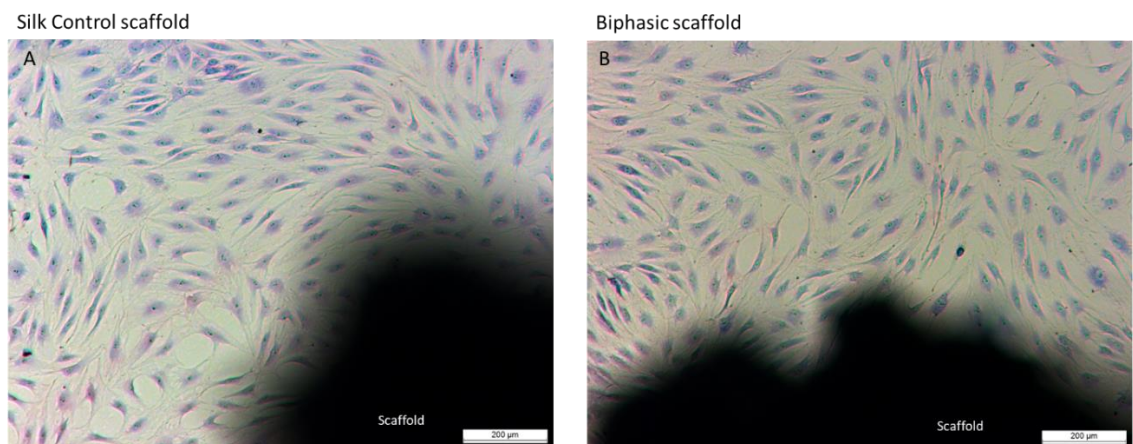


**Figure 34 Scaffold contact cytotoxicity**

Investigation of contact cytotoxicity, as per ISO10993-5:2009(E) of hBMSCs cultured in the presence of silk control (A) and biphasic scaffolds (B) (n=4 per group) for 96 hours, stained with Giemsa solution, and imaged on a Leica DM16000 B inverted microscope.

#### 4.1.2.2 Indirect cytotoxicity

Although the scaffolds showed no signs of contact cytotoxicity, it was still important to understand after long-term submersion in fluid whether any toxic degradation products are released over time. This will dramatically impact the success of the scaffold during long-term *in vitro* culture, as well as post implantation *in vivo*. To evaluate any potential cytotoxic chemical products produced during scaffold degradation *in vitro*, indirect cytotoxicity assays were undertaken as per ISO 10993-5:2009. 10,000 hBMSCs were seeded within a 96 well plate and were incubated for 48 h in conditioned media that had been preincubated undisturbed in the presence of silk control scaffolds or biphasic scaffolds for 72 hours, 1 week, 2 weeks, 3 weeks, 4 weeks or 8 weeks. Following this the cytotoxic reaction of the cell monolayer to the scaffold aliquots was evaluated cell viability was measured as seen in Figure 35. A slight decrease in cell viability over the 48h was seen with the increasing age of the conditioned media (72 hours, 1 week, 2 weeks, 3 weeks, 4 weeks or 8 weeks). However, this was non-significantly different from the unconditioned media ( $p>0.05$ ). There was also no significant difference between either group or age of scaffold incubated media. All conditioned media and unincubated controls showed significantly greater viability than the negative control (media containing 10% DMSO).

To understand whether the scaffold degradation products had a long term effect on cell growth, a 96 well plate was seeded with a 1000 hBMSCs per well and incubated in the presence of media aliquots that had been preincubated undisturbed in the presence of silk control scaffolds or biphasic scaffolds for 72 hours, 1 week, 2 weeks, 3 weeks, 4 weeks or 8 weeks. Cell monolayers within 96 well plates were incubated in the presence of this conditioned media for six days. Wells were visually confirmed to have not reached confluence. No significant difference ( $p>0.05$ ) in cell growth was seen between the conditioned media at all ages after six days of culture (Figure 36). All test samples showed no significant

difference ( $p < 0.05$ ) in cell growth compared to positive control groups (unincubated media)

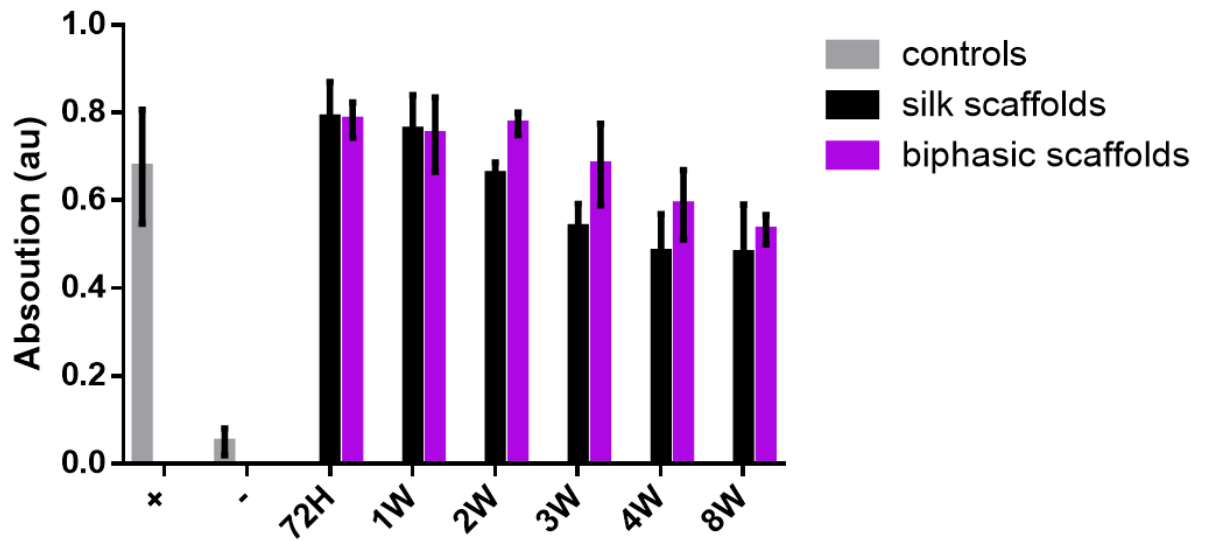


**Figure 35 Indirect cytotoxicity**

Indirect cytotoxicity of silk control and biphasic scaffolds as determined by XTT assays was undertaken. hBMSCs at 10,000 cells/well were subjected to 48 hours incubation in media that had been preincubated with scaffolds for 72 hours, 1 week, 2 weeks, 3 weeks, 4 weeks or 8 weeks ( $n=4$  per group). Positive controls consisted of plain media and negative controls consisted of media containing 40% DMSO. All samples showed significantly greater absorbance than negative controls ( $p < 0.05$ ), and no significant difference between any other group ( $p > 0.05$ ). Data represent mean  $\pm$  SD.

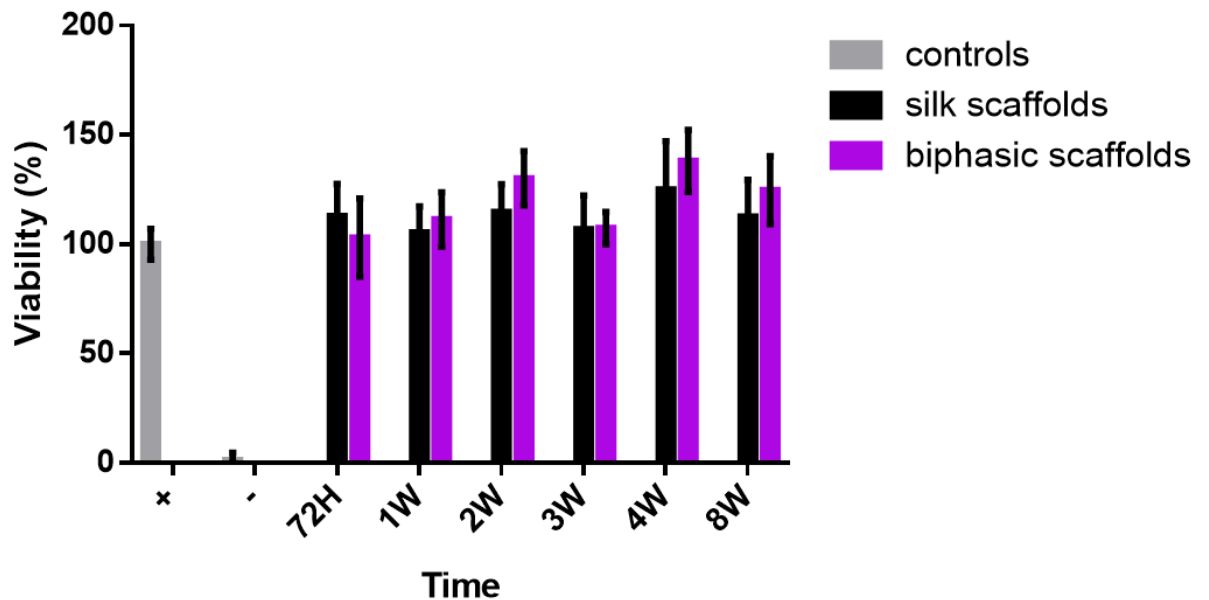


**Figure 36 Indirect cell growth retardation**

Indirect cell proliferation testing of silk control and biphasic scaffolds determined by XTT assays was undertaken. hBMSCs (1000 per well) were subjected to 6 days incubation in media that had been preincubated with scaffolds for 72 hours, 1 week, 2 weeks, 3 weeks, 4 weeks or 8 weeks (n=4 per group). Positive controls consisted of plain media and negative controls consisted of media containing 40% DMSO. All samples showed significantly greater absorbance than negative controls ( $p < 0.05$ ), and no significant difference between any other group ( $p > 0.05$ ). Data represent mean  $\pm$  SD.

### 4.1.3 Scaffold seeding optimisation

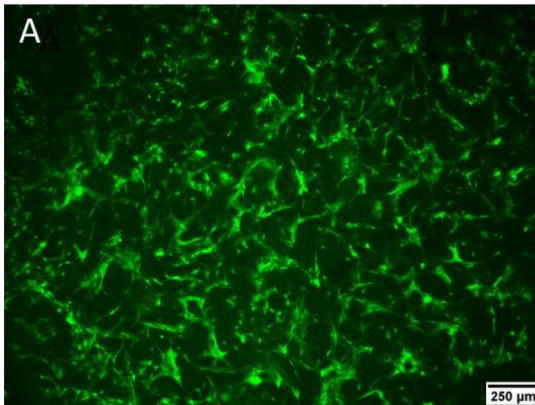
To optimise seeding density, initially, scaffolds were seeded with a range of seeding densities (100000, 250000, 500000, 1000000 cell per scaffold). These were then stained with cell tracker green and visualised under a fluorescent microscope. This data was then utilised to select the optimal seeding density. Each future experiment is based on the density of cells seen in the individual experiments requirements. For experiments 4.1.6 and 4.1.7, 100000 cells were selected to be utilized, as this density was believed to allow for the visualization of cells on the scaffold surface without forming a dense monolayer for experiment 4.1.6, and allowing for available scaffold surface area for cell proliferation to be investigated in experiment 4.1.7. For experiments 4.1.9, 4.1.10 and 4.1.11, 500000 cells were selected to be utilized. This density was believed to be high

enough to promote rapid scaffold colonization and allow for cellular differentiation into osteogenic and chondrogenic lineages, without being excessively high to deplete the limited stock of cells. Experiments 4.1.4, 4.1.5 and 4.1.8 also utilized 500,000 cells to maintain consistent seeding density with the differentiation experiments (4.1.9, 4.1.10 and 4.1.11).

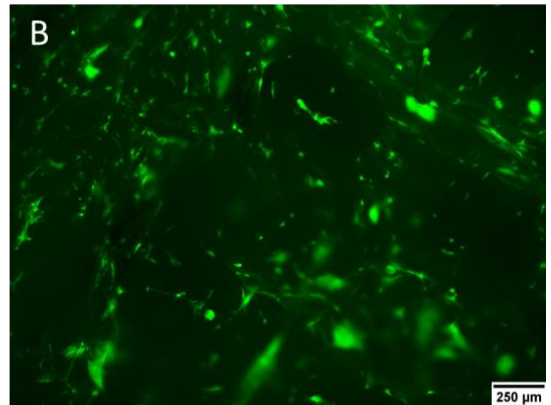
#### **4.1.4 The effect of surface modification on the attachment and growth of hBMSCs on biphasic scaffolds**

Cell adhesion behaviour on the scaffolds was investigated to confirm that they could allow for cell adhesion and support cell growth. To help increase the potential of cell adhesion, all scaffolds (silk control and biphasic) were preincubated at 4°C overnight in basal media in the presence or absence of 20% FBS. After 24 hours of static seeding, fluorescence microscopy images showed that the hBMSCs pre-labelled with CellTracker™ Green can attach and adhere onto all the scaffold groups (Figure 37). There were no obvious differences between the 20% FBS pre-treatment groups (Figure 37 A,B) compared with that of the same scaffold without FBS pre-treatment (Figure 37 C,D). Any potential differences seen in cell adhesion between silk control scaffolds and biphasic scaffolds was assigned to the limitation of utilising a fluorescent microscope with porous materials due to its single focal plane. All groups showing excellent cell adhesion to the surface of the scaffolds and cells possessing normal morphology, with cell processes being visible. It was decided for all future experiments that scaffolds would be preincubated at 4°C overnight with 10% FBS. This level was selected to help remove variability from when the preincubation media was exchanged to the culture media, as 10% FBS is the level found within the culture media.

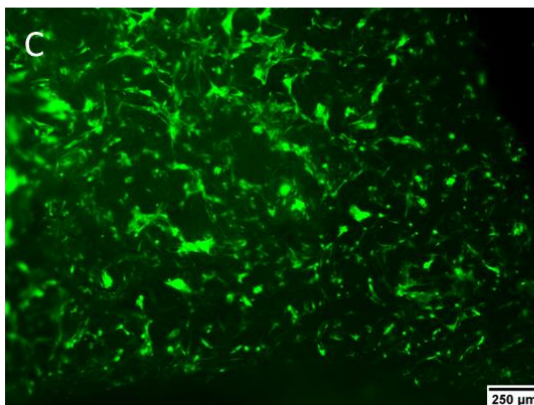
0% FBS Silk Control



0% FBS Biphasic scaffold



20% FBS Silk Control



20% FBS Biphasic scaffold

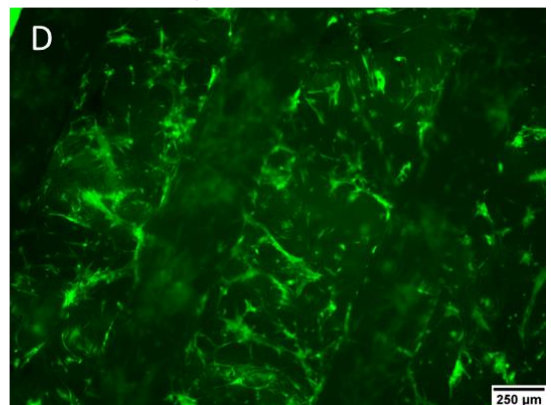


**Figure 37 Impact of FBS scaffold preincubation on cell adhesion**

Cell adhesion behaviour of hBMSCs labelled with CellTracker™ Green CMFDA Dye after 24 hours between silk control scaffolds and biphasic scaffolds in the presence or absence of an overnight (4°C) incubation period with 20% FBS. (A) Silk control scaffolds incubated in 0% FBS, (B), biphasic scaffolds incubated in 0% FBS, (C) Silk control scaffolds incubated in 20% FBS, (D), biphasic scaffolds incubated in 20% FBS (n=4 per group).

### 4.1.5 Dynamic versus static seeding

It was important to identify the correct scaffold seeding technique, as the method selected can dramatically affect scaffold regenerative capacity as well as the cells' ability to migrate and distribute throughout the scaffold. To evaluate different approaches to cell seeding, dynamic and static seeding were compared (Figure 38). Prior to seeding in the two condition types, hBMSCs were pre-labelled with CellTracker™ Green. It was shown in both the static and dynamic seeding

conditions that the biphasic scaffolds and the silk control scaffolds could support cell attachment to the scaffolds with no differences in cell attachment behaviour being noted. The static seeding group demonstrated a relatively dense homogeneous layer of cells on the scaffold surface, with no cell attachment being seen on any of the scaffold's other faces (side and bottom) (Figure 38 A-D). This was compared to the dynamic seeding group where an even distribution of cell attachment was seen across all six of its faces; however, this was at a lower density than the single face seen within the static seeding group (Figure 38 E-H). This highlighted the potential utilisation of static seeding to direct cell types across different areas of the scaffold, i.e., chondrogenic cells to the cartilage phase and osteogenic cells to the bone phase. Therefore, static seeding was the chosen seeding type for all future experimentation.

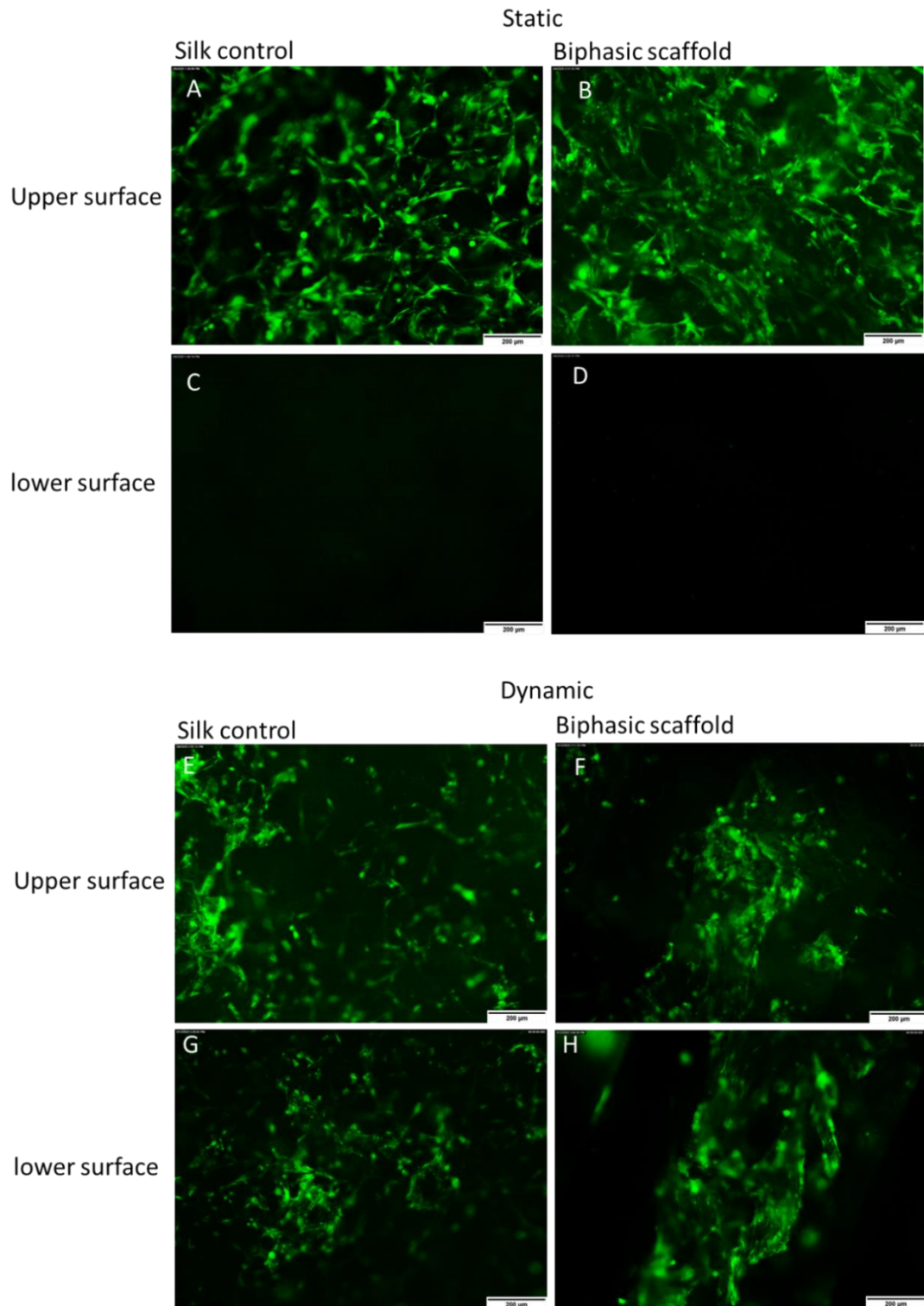


**Figure 38 . A comparison of cell distribution after dynamic or static seeding**

A comparison of cell adhesion behaviour of hBMSCs labelled with CellTracker™ Green CMFDA after 24 hours of static and dynamic seeding. Images were taken on the top and bottom of the same scaffold on the two scaffold types- silk control and biphasic. (A) upper face of Silk control scaffolds statically seeded, (B) upper face of biphasic scaffolds statically seeded, (C) lower face of Silk control scaffolds statically seeded, (D) lower face of biphasic scaffolds statically seeded, (E) upper face of Silk control scaffolds, dynamic seeded, (F) upper face of biphasic scaffolds dynamic seeded, (G) lower face of Silk control scaffolds dynamic seeded, (H) lower face of biphasic scaffolds dynamic seeded (n=4 per group).

## 4.1.6 Cell migration and morphological shape

To better understand cell morphology as well as the ability for cells to adhere to pore surfaces, visualisation of cell adhesion was undertaken. Cells were labelled with phalloidin to identify actin fibres (green fluorescence) and with a nuclear stain DAPI (blue fluorescence). Typical images of each scaffold are shown in Figure 39. hBMSCs were shown to be growing robustly on all three scaffold types (silk control Figure 39 A, biphasic (cartilage phase) Figure 39 B and biphasic (bone phase) Figure 39 C) with good stretching and a spread and elongated morphology suggesting excellent cell adhesion. Cells were also shown to be able to effectively conform to the inner surface of scaffold pores. No clumping or balling of cells was seen. There were no obvious differences in cell adhesion morphology between scaffold types (silk control scaffolds, biphasic scaffolds (bone phase and cartilage phase)). Absorption of the DAPI to the silk component of the scaffolds was seen and was represented by a strong blue fluorescence which was not present in the absence of the dye.

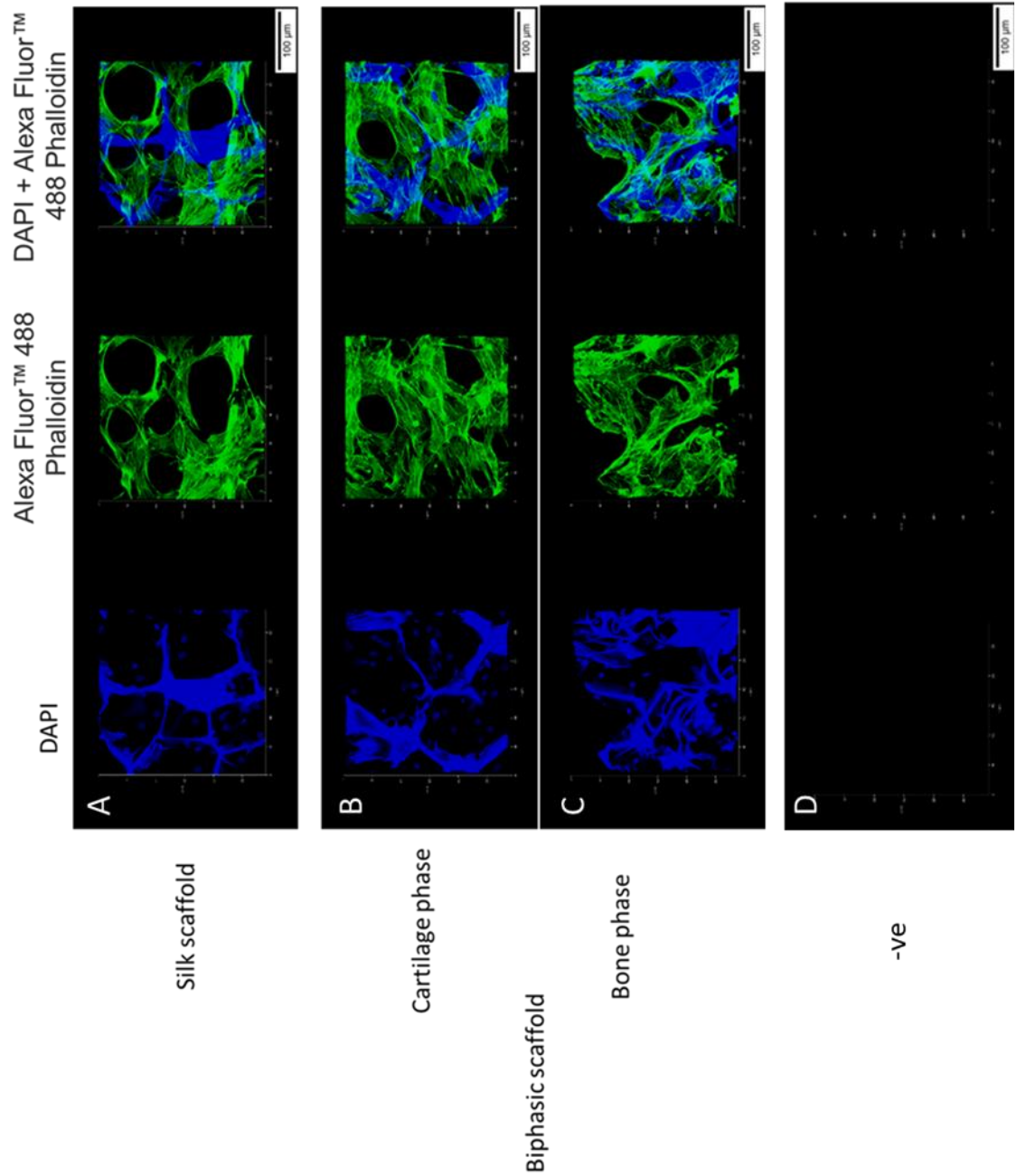


**Figure 39 Cell cytoskeleton scaffold interaction**

Confocal microscopy of hBMSCs on different scaffolds after 2 days (50,000 cells per scaffold). (A) Silk control scaffolds, (B) cartilage phase, (C) Bone phase of biphasic scaffolds (D) unseeded and unstained control silk scaffold (n=4 per group). Blue colouring (DAPI) represents cell nuclei and silk scaffolds. Green colouring (Alexa Fluor™ 488 phalloidin) represents actin within the cell cytoskeleton.

### 4.1.7 Cell metabolic activity and cell death rate

It is important to understand the cells' interaction with the scaffold and how it affects cell metabolic activity- it is important that over time cells are able to maintain or increase their metabolic activity. The interactions between relative cell metabolic activity and scaffold type were investigated by an Alamar blue assay, by seeding of 100,000 hBMSCs onto silk control scaffolds, the cartilage phase of the biphasic scaffolds and the bone phase of the biphasic scaffolds (Figure 40). All scaffold types showed an increase in cell metabolic activity over 16 days. On day one, silk control scaffolds showed a relative fluorescence of  $196.1 \pm 42.5$ , the cartilage phase of the biphasic scaffolds showed a relative fluorescence of  $172.1 \pm 25.2$ , and the bone phase of the biphasic scaffolds showed a relative fluorescence of  $112.4 \pm 24.1$ . All scaffolds showed a significant increase ( $p < 0.001$ ) over the 16 days from the day one results, with the silk control scaffold showing  $555.2 \pm 55.0$ , the cartilage phase of the biphasic scaffold showing  $488.2 \pm 72.4$ , and the bone phase of the biphasic scaffold showing  $488.6 \pm 62.4$ . At no time point did any scaffold show significantly different ( $p > 0.05$ ) metabolic activity compared with any of the other scaffold types.

To evaluate relative cellular toxicity, an LDH assay was undertaken, consisting of seeding 100,000 hBMSCs onto the silk control scaffolds, the cartilage phase of the biphasic scaffolds and the bone phase of the biphasic scaffolds, and then measuring released LDH in the cell culture media. LDH levels decreased over the first eight days before plateauing and seeing no further decreases (Figure 41). LDH levels on day 2 in the silk control scaffolds showed a relative absorbance of  $0.390 \pm 0.047$ , the cartilage phase of the biphasic scaffolds showed  $0.393 \pm 0.062$ , and the bone phase of the biphasic scaffolds showed  $0.335 \pm 0.049$ . All scaffolds showed a significant decrease ( $p < 0.05$ ) in LDH activity after 8 days, with silk scaffolds showing a relative activity of  $0.095 \pm 0.052$ , the cartilage phase of the biphasic scaffolds showing a relative activity of  $0.031 \pm 0.078$ , and the bone phase of the biphasic scaffolds showing a relative activity of  $0.039 \pm 0.093$ . After eight

days, no significant further ( $p > 0.05$ ) changes in LDH activity were seen. At no time point did any scaffold show significantly different ( $p > 0.05$ ) LDH activity compared with any of the other scaffold types. The decreasing LDH activity was assigned to reduced cell apoptosis over time as cells settled and began to proliferate onto the seeded scaffolds. It was further confirmed that the reducing LDH activity was not due to complete cell death, as the Alamar blue assay showed increasing metabolic activity over the same time period. Data for both Alamar blue and LDH activity is displayed as a relative absorption data.

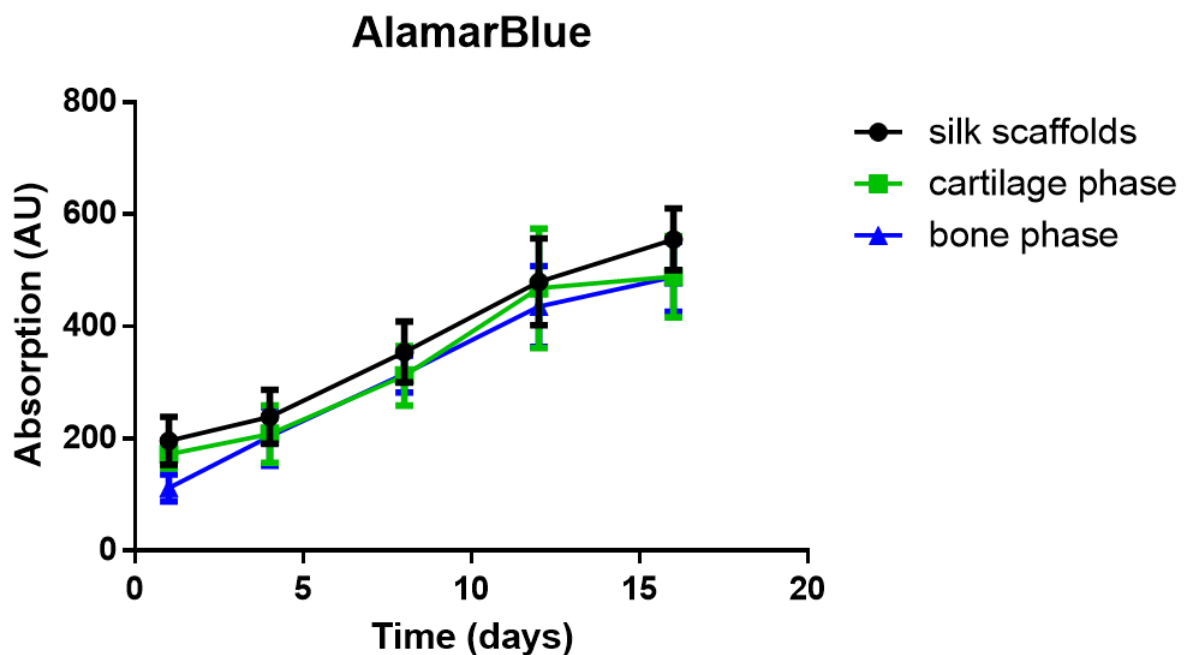


**Figure 40 Cell metabolic activity on scaffolds as determined by alamarBlue**

initially scaffolds were seeded with 100,000 hBMSCs and changes in metabolic activity were evaluated over a 16 day time period of the silk control scaffolds (black circle), cartilage phase of the biphasic scaffolds (green square) and bone phase of biphasic scaffolds (blue triangle) ( $n=4$  per group) were evaluated via alamarBlue assay. No significant difference between any scaffold at any time point was seen ( $P > 0.05$ ). However, all scaffolds showed a significant increase in metabolic activity over the 16-day time period ( $p < 0.001$ ). Data represent mean  $\pm$  SD.

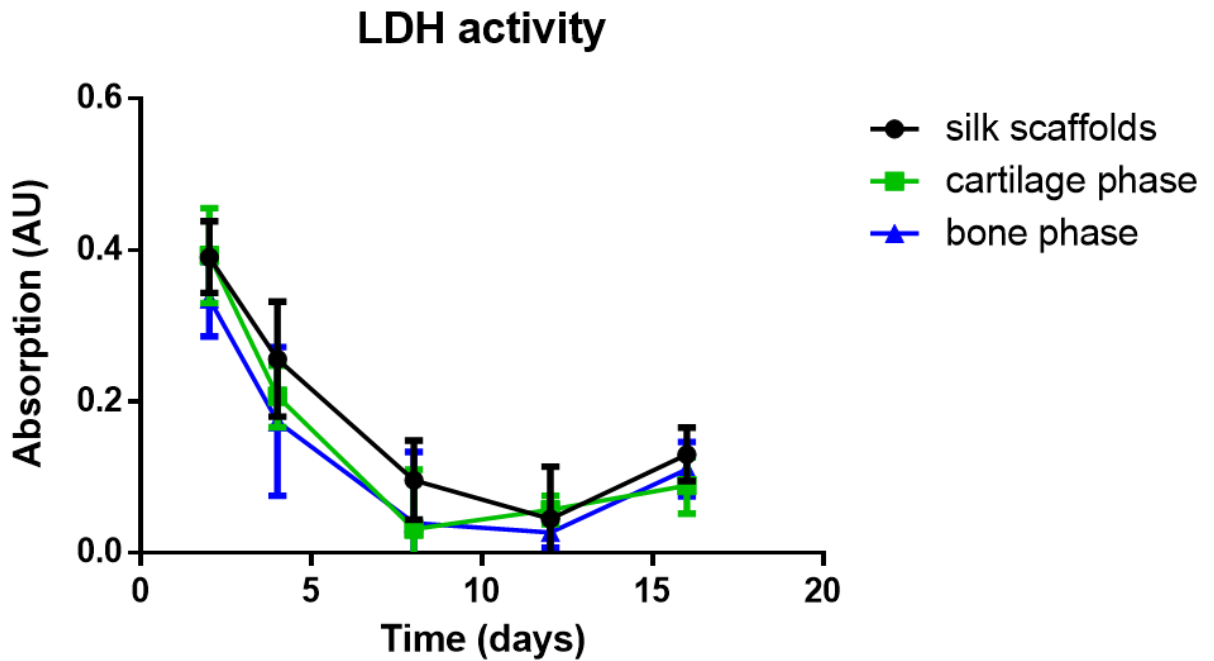


**Figure 41 Released LDH activity**

LDH activity within culture media was measured over a 16 day time period. scaffolds were initially seeded with 100,000 hBMSCs. silk control scaffolds (black circle), cartilage phase of biphasic scaffolds (green square) and bone phase of biphasic scaffolds (blue triangle) (n=4 per group). No significant difference between any scaffold at any time point was seen ( $P>0.05$ ). All scaffolds showed a significant decrease ( $p<0.05$ ) in LDH activity after 8 days, followed by no further significant changes ( $P>0.05$ ). Data represent mean  $\pm$  SD.

#### 4.1.8 Scaffold seeding technique

To further investigate and confirm whether cells can be directed to different locations via the utilisation of static seeding orientation (as indicated in the static versus dynamic seeding experiments), multicoloured cell tracking was undertaken. This was undertaken to two individual populations of hBMSCs, pre-labelled with cell tracker green or red. Following this, scaffolds (silk control and biphasic) were placed in the bottom of screw-top Eppendorfs, and cells labelled with cell tracker green were placed onto the upward facing surface of the scaffold and left for 12 hours. Following this, scaffolds were inverted and placed in new Eppendorfs. Cells labelled with cell tracker red were then placed on the upward facing side of the scaffold and left for a further 12 hours. Scaffolds were then inspected under a

confocal microscope, which demonstrated effective directing of cell types to the desired surface with no undesirable red labelled cells being seen on the surface seeded with green labelled cells (Figure 42 A, B) and vice versa (Figure 42 C, B). This lack of cross seeding was seen in both silk control scaffolds and biphasic scaffolds. These results indicated that this static seeding method is an effective way to direct different populations of cells to different scaffold surfaces. The silk component of both scaffolds was labelled red by excreted cell tracker red from the seeded cells. However, there was no impact on the experimental results as labelled cells are clearly present around the stained scaffold component.

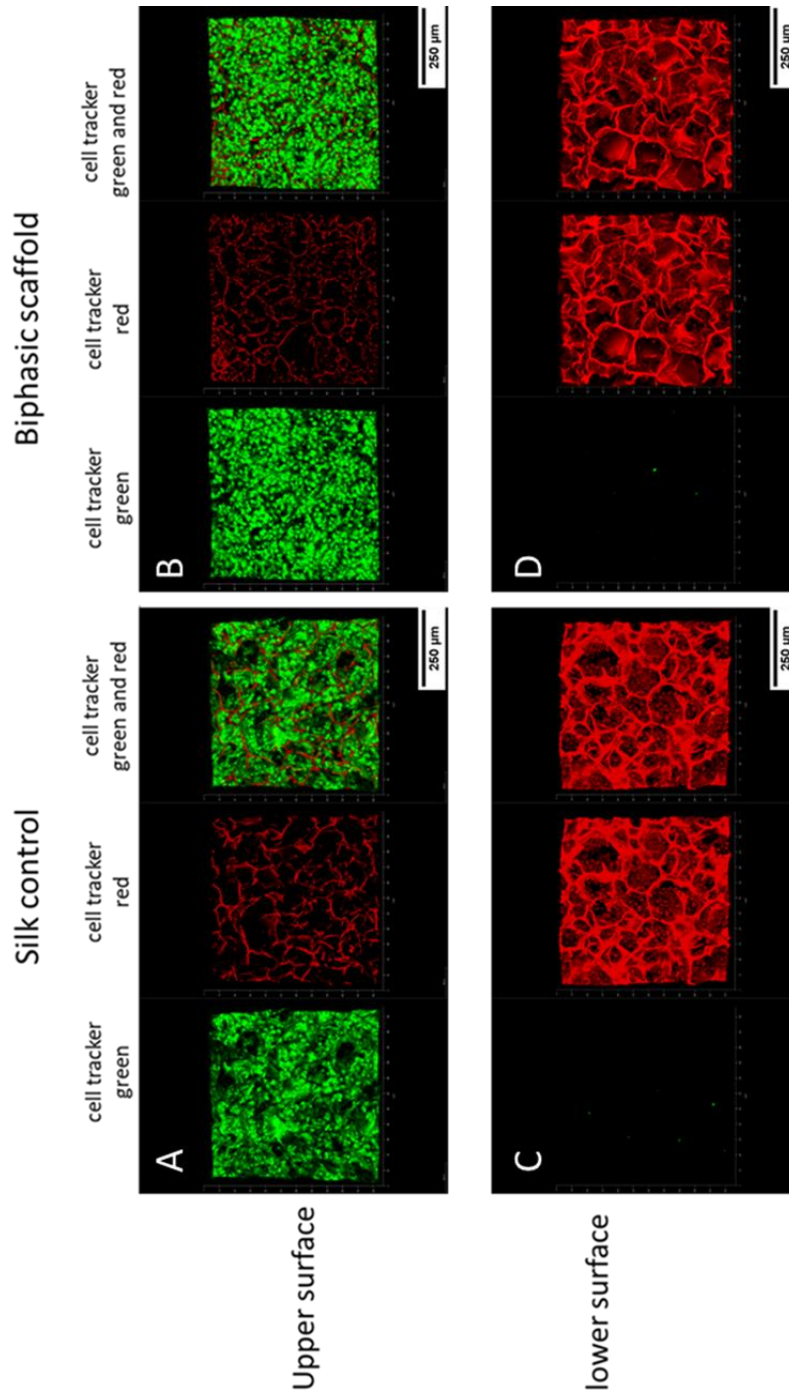


**Figure 42, valuation of impact of scaffold orientation during static seeding**

two separate groups of hBMSCs were labelled with cell tracker green and red and statically seeded onto biphasic and silk scaffolds in opposite orientations 12 hours apart. Cells labelled with cell tracker green (500,000 cells) were seeded on to the cartilage phase of the biphasic scaffolds and the top of silk scaffolds. Scaffolds were then rotated after 12 hours and seeded with 500,000 cells on the opposite face (bone phase for biphasic scaffolds, lower face for silk scaffolds) with cells labelled with cell tracker red. Cells were found to be localised to the face seeded upwards during their respective seeding period, with no mixing of red and green labelled cells. (A) top of silk scaffolds, (B) cartilage phase of the biphasic scaffolds, (C) bottom of silk scaffolds, (D) bone phase of biphasic scaffolds (n=4 per group).

## **4.1.9 Culturing of hBMSCs on scaffolds under chondrogenic conditions**

### **4.1.9.1 Evaluation of cell migration and morphology via H and E staining under Chondrogenic conditions**

To understand the longer-term response of cells under chondrogenic conditions, and whether negative pressure rehydration is indeed necessary within scaffolds, silk control scaffolds and the cartilage phase of biphasic scaffolds were seeded with hBMSCs and placed under chondrogenic conditions for three weeks. Following this, scaffolds were embedded, sectioned and stained with H&E to identify cell nuclei and cytoplasm respectively. All scaffolds under these conditions, including scaffolds that had not undergone negative pressure rehydration, showed successful cell adhesion to the scaffold surface. However, the silk control and cartilage phase scaffolds that had not undergone negative pressure rehydration showed extremely poor cell infiltration, with cells remaining on the surface (Figure 43 A, B). However, after negative pressure rehydration of the scaffolds, there was satisfactory cell penetration within chondrogenic conditions during the three-week culture period which showed a thick cell layer along the seeded surface, with large quantities of extracellular matrix production; the cells were also able to penetrate the majority of the cartilage phase during the three-week culture period (Figure 43 C,D). Cell morphology and density was similar between the cartilage phase of biphasic scaffolds and silk scaffolds.

However, there were some cells present within the bone phase and non-seeded face of both scaffolds (Figure 43 G,H). Rather than this being due to cells penetrating fully through the scaffold, this was identified to be due to undesirable seeding of the cells from the culture dish, since at the time of culture there were no available low adhesion culture dishes (coronavirus related supply chain issues). It was believed to be this rather than cells penetrating through the whole scaffold due to the lack of presence of cells within the centre of the scaffold.

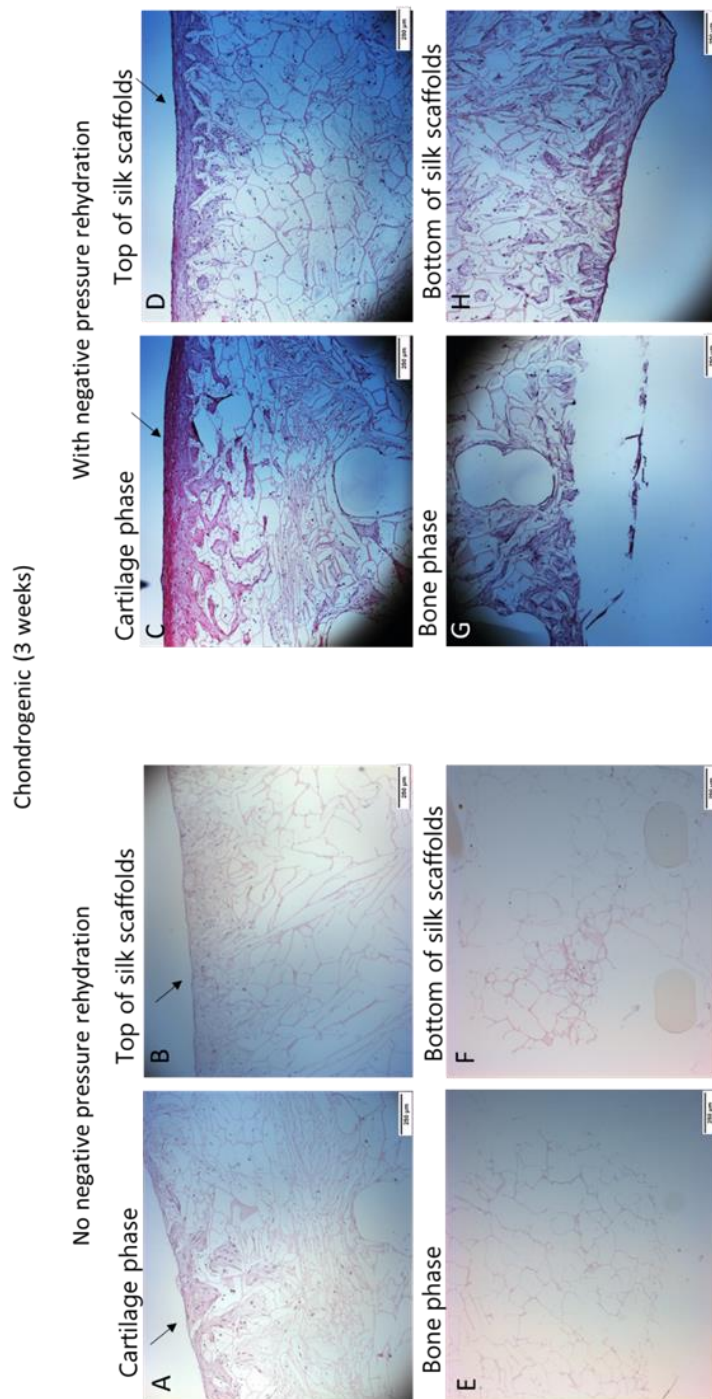


**Figure 43 H&E staining of biphasic and silk control scaffolds under chondrogenic conditions**  
 Representative images at five times magnification of H&E staining of silk (n=4) and biphasic scaffolds (n=4) following three weeks of chondrogenic culture in the presence or absence of a negative pressure rehydration step. Arrow indicates seeded face of scaffold (500,000 hBMSC per scaffold). (A) cartilage phase of the biphasic scaffolds that have not undergone negative pressure rehydration. (B) top of silk control scaffolds that have not undergone negative pressure rehydration. (C) cartilage phase of biphasic scaffolds that have undergone negative pressure rehydration. (D) top of silk control scaffolds that have undergone negative pressure rehydration. (E) bone phase of the biphasic scaffolds that have not undergone negative pressure rehydration. (F) bottom of silk control scaffolds that have not undergone negative pressure rehydration. (G) bone phase of the biphasic scaffolds that have undergone negative pressure rehydration. (H) bottom of silk control scaffolds that have undergone negative pressure rehydration.

#### **4.1.9.2 Long term viability in chondrogenic conditions of cells on scaffolds**

To investigate long-term viability of cells on the scaffold surface of the silk control scaffolds and the cartilage phase of the biphasic scaffolds, and to confirm no long-term contact cytotoxicity was present, live cell imaging was undertaken. This was with the aim to evaluate cell survival as well as cell morphology on the scaffold surface. This was evaluated by seeding and culturing of hBMSCs on the silk scaffold and cartilage phases of the biphasic scaffolds, followed by visualisation with cell tracker green labelling. The confocal laser scanning micrographs revealed a high proportion of viable green cells in both scaffold types and chondrogenic conditions (Figure 44); no observable differences were seen in viability in both groups at both the 24-hour (Figure 44 A,B) and the 3-week time points (Figure 44 C,D) in chondrogenic conditions, although a higher density of cells was seen at the 3 week time point for both scaffolds compared to the 24 hour time point. Within all scaffold types and culture conditions, cells appear to have an even distribution over the seeded surface. These findings demonstrate that the scaffolds have low cytotoxicity due to the high number of viable cells, further reinforcing the hypothesis that the poor cell infiltration seen in Figure 43 A,B resulted from incomplete rehydration rather than toxicity of the scaffolds. Dead staining with EthD-1 could not be undertaken due to preferential binding of the stain to the silk component of scaffolds, masking the presence or absence of dead cells. However, due to the extremely high prevalence and density of living cells, the scaffolds were confirmed to be non-toxic.

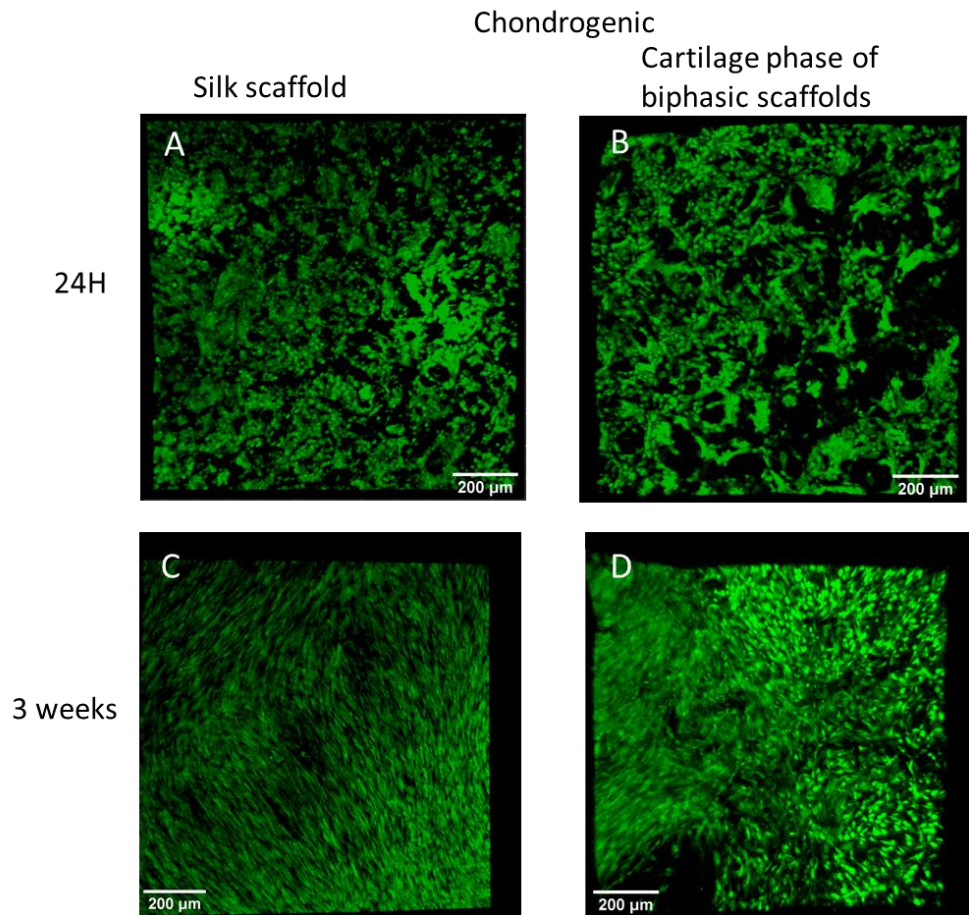


**Figure 44 Live cell staining of hBMSCs on biphasic and silk control scaffolds under chondrogenic conditions**

Representative images of the comparison of cell viability of hBMSCs labelled with CellTracker™ Green CMFDA after 24 hours of chondrogenic culture on (A) silk control scaffolds (n=4) and (B) the cartilage phase of the biphasic scaffolds (B) (n=4); and after three weeks of chondrogenic culture (C) silk control scaffolds (n=4) and (D) the cartilage phase of the biphasic scaffolds (B) (n=4). Seeding density of each scaffold was 500,000 hBMSCs.

#### **4.1.9.3 Collagen and GAG deposition by hBMSCs within scaffolds under chondrogenic conditions.**

To better understand the impact of chondrogenic culture and seeding on silk control scaffolds and biphasic scaffolds, staining was undertaken. The Picrosirius red/Alcian blue staining assessed the expression of collagens and GAGs of hBMSCs within both the biphasic scaffolds (Figure 45 C,D) and silk control scaffolds (Figure 45 A,B). This showed intense collagen staining (red) and GAG staining (blue) on the scaffolds' surface with a large amount of extracellular matrix production. The beginnings of the formation of a cartilage-like surface was observed. No obvious differences were seen between the cartilage phase of the biphasic scaffolds and silk control scaffolds. Cells within both scaffolds demonstrated typical chondrocyte morphology with cells being seen to have formed dense extracellular matrix with lacunae formation, with no contact seen between cells as within native articular cartilage. Furthermore, the beginnings of cartilage stratification can be seen, with cells presenting a more flattened morphology at the surface of scaffolds, as seen within the superficial zone of native cartilage. Cells took on a more rounded or oval-shape deeper into the scaffold, more closely resembling chondrocytes seen within the mid zone of articular cartilage.

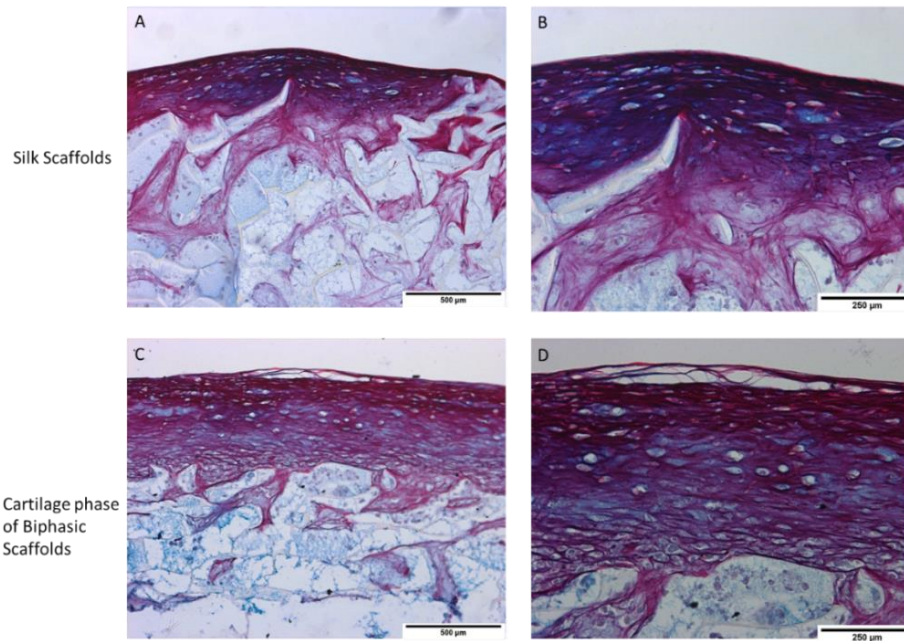


**Figure 45 Picosirius red/Alcian blue staining of biphasic and silk control scaffolds under chondrogenic conditions**

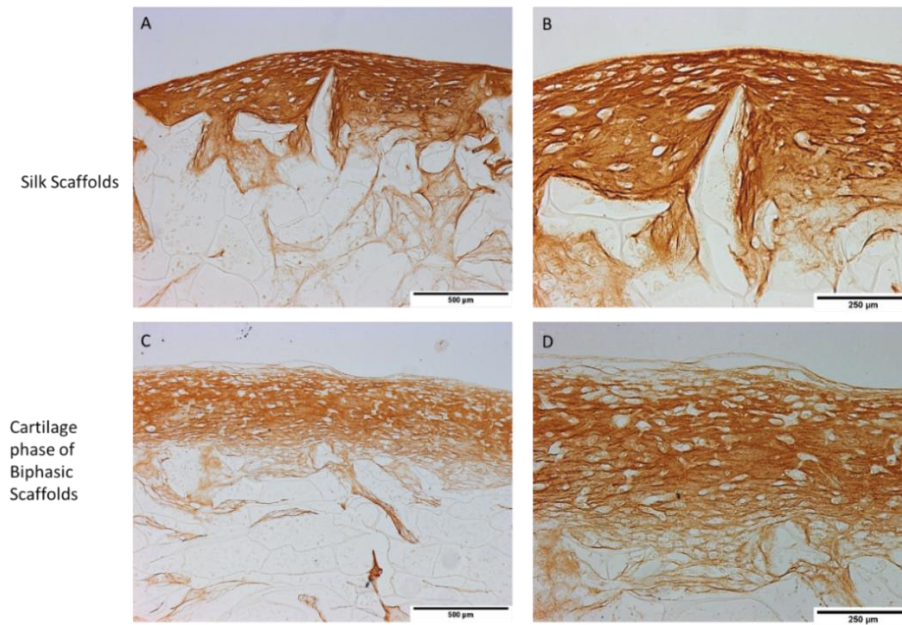
Representative images of picosirius red/Alcian blue staining of silk control scaffolds and the cartilage phase of the biphasic scaffolds after three weeks of chondrogenic culture with seeded hBMSCs (seeding density 500,000 cells per scaffold) (n=4). Collagen is stained with Picosirius red and is represented by a red colour. GAGs are stained with Alcian blue and is represented in blue. (A). Silk control scaffolds at 10x magnification. (B) Silk control scaffolds at 20x magnification (C). Cartilage phase of biphasic scaffold at 10x magnification. (D) Cartilage phase of biphasic scaffold at 20x magnification.

#### **4.1.9.4 Collagen Type I and II deposition by hBMSCs within scaffolds under chondrogenic conditions.**

To further differentiate the type of collagen deposition seen by the Picosirius red staining and to better understand the exact collagen types deposited by cells within the scaffolds under chondrogenic conditions, immunohistochemistry was undertaken. This staining demonstrated the presence of Type I collagen shown by brown staining in both the biphasic (Figure 46 C,D) and silk scaffolds (Figure 46 A,B) with no obvious difference between both scaffold types. As well as this, Type II collagen deposition was also shown by brown staining in both the biphasic (Figure 46 G,H) and silk scaffolds (Figure 46 E,F), with no obvious difference between both scaffold types. It was selected to utilise Type I collagen staining as a negative

marker for cartilage formation and a positive marker for bone and fibrocartilage or fibrous tissue formation. As a mix of both Type I and Type II collagen (as seen in figure 46) would indicate the formation of fibrous cartilage rather than the more desirable hyaline.

Immunohistochemistry for Collagen 1



Immunohistochemistry for Collagen 2

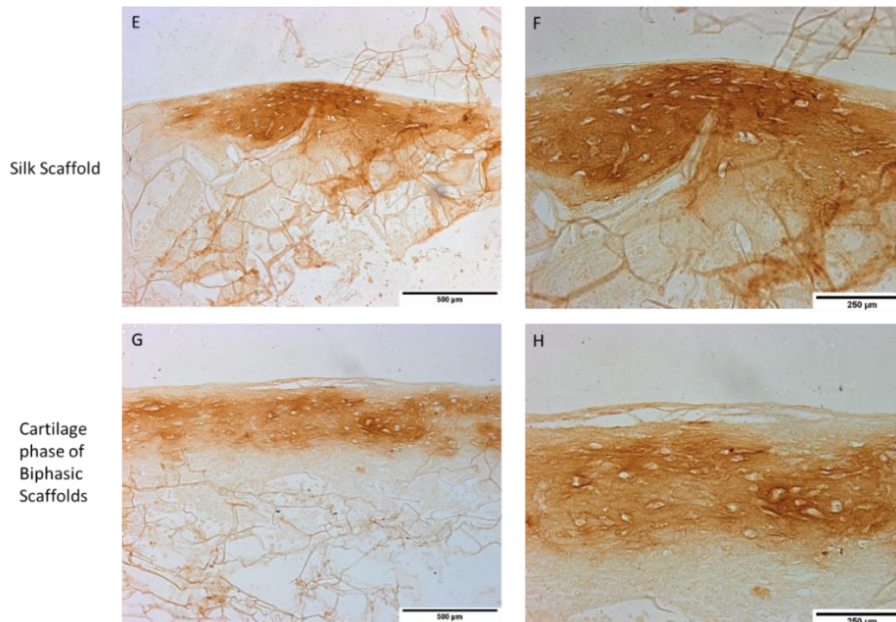


**Figure 46 ICH staining for Type I and Type II collagen of biphasic and silk control scaffolds under chondrogenic conditions**

Representative images of collagen Type I and Type II staining by immunohistochemistry of silk control scaffolds and the cartilage phase of biphasic scaffolds after three weeks of chondrogenic culture with seeded hBMSCs (seeding density 500,000 hBMSC per scaffold) (n=4 per group). Positive staining is represented by a brown coloration. (A) Silk control scaffolds at 10x magnification stained for Type I collagen. (B) Silk control scaffolds at 20x magnification stained for Type I collagen. (C) Cartilage phase of biphasic scaffolds at 10x magnification stained for Type I collagen. (D) Cartilage phase of biphasic scaffolds at 20x magnification stained for Type I collagen. (E) Silk control scaffolds at 10x magnification stained for Type II collagen. (F) Silk control scaffolds at 20x magnification stained for Type II collagen. (G) Cartilage phase of the biphasic scaffolds at 10x magnification stained for Type II collagen. (H) Cartilage phase of biphasic scaffolds at 20x magnification stained for Type II collagen.

#### 4.1.9.5 Proteoglycan deposition by hBMSCs within scaffolds under chondrogenic conditions.

Safranin-O staining was used to assess the expression of proteoglycan of hBMSCs within the cartilage phase of the biphasic scaffolds and silk control scaffolds after three weeks of culture. Both biphasic scaffolds (Figure 47 C,D) and silk control scaffolds (Figure 47 A,B) showed moderate proteoglycan staining on the scaffold surface with a large amount of extracellular matrix production. The beginnings of a formation of a cartilage-like surface was observed. No obvious differences were seen between the cartilage phase of the biphasic scaffolds and silk control scaffolds. Cartilage-like lacunae formation was also seen in both scaffold types similar to that seen in the Alcian blue and Picosirius red staining (Figure 46).

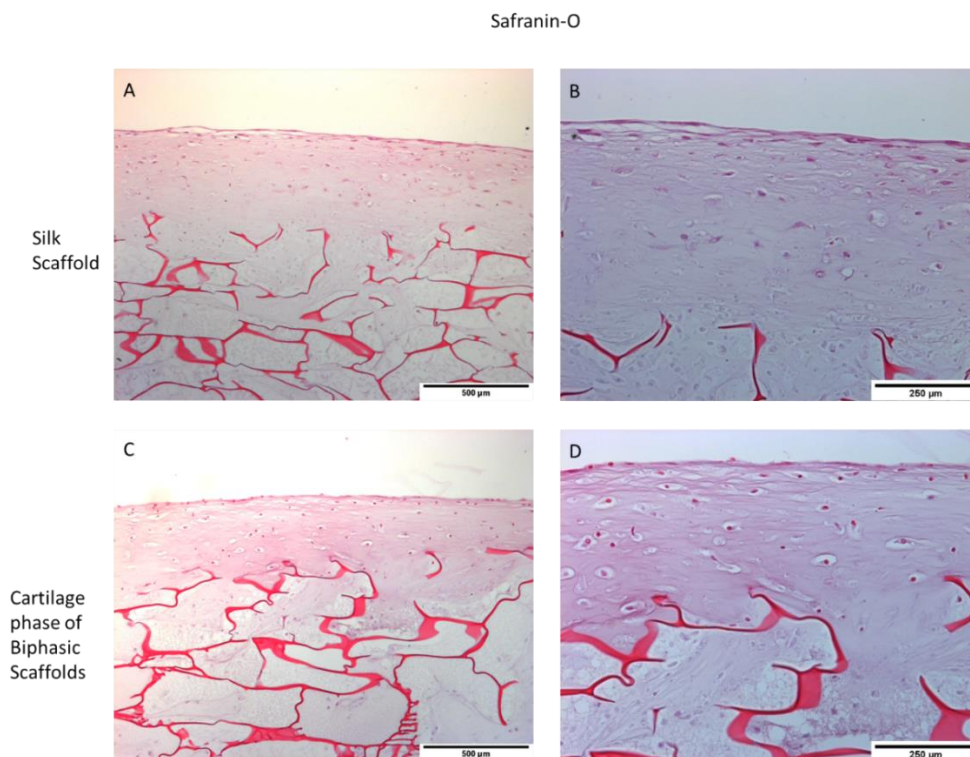


**Figure 47 Safranin-O staining of biphasic and silk control scaffolds under chondrogenic conditions** Representative images of Safranin-O staining of silk control scaffolds and the cartilage phase of biphasic scaffolds after three weeks of chondrogenic culture, with seeded hBMSCs (seeding density 500,000 hBMSC) (n=4 per group). Proteoglycans are stained in pink with Safranin-O. (A) Silk control scaffolds at 10x magnification. (B) Silk control scaffolds at 20x magnification. (C) Cartilage phase of biphasic scaffolds at 10x magnification. (D) Cartilage phase of biphasic scaffolds at 20x magnification.

## **4.1.10 Culturing of hBMSCs on scaffolds under osteogenic conditions**

### **4.1.10.1 Evaluation of cell migration and morphology via H&E staining under osteogenic conditions**

To understand the long-term response of cells under osteogenic conditions, scaffolds were seeded with hBMSCs and placed under osteogenic conditions for six weeks. Following this, cells were embedded, sectioned and stained with H&E to identify cell nuclei and cytoplasm respectively. H&E staining of the seeded bone phase of the biphasic scaffolds and the silk control scaffolds was carried out under osteogenic conditions (Figure 48 C, D, G, H), also incorporating a negative pressure rehydration step (Figure 48 A, B, E, F). This experiment showed similar results to those seen under chondrogenic conditions (Figure 43); when a negative pressure rehydration step is not included, cells showed very little migration into the scaffold, even after six weeks of osteogenic culture. However, similarly to the results seen in chondrogenic culture, once the scaffold had undergone a negative pressure rehydration step to improve hydration, the scaffolds showed excellent cell migration throughout the entire bone phase and into the initial stages of the cartilage phase. The cells seen in the cartilage phase were believed to be due to cells penetrating through the scaffold, rather than undesirable seeding, as seen in chondrogenic culture- this is due to no cells being seen on the surface of the cartilage phase, rather a continuation of cells throughout the entire bone phase and into the cartilage phase. No difference in density or migration was seen between biphasic scaffolds and silk control scaffolds under osteogenic conditions when scaffolds had been exposed to a negative pressure rehydration step.

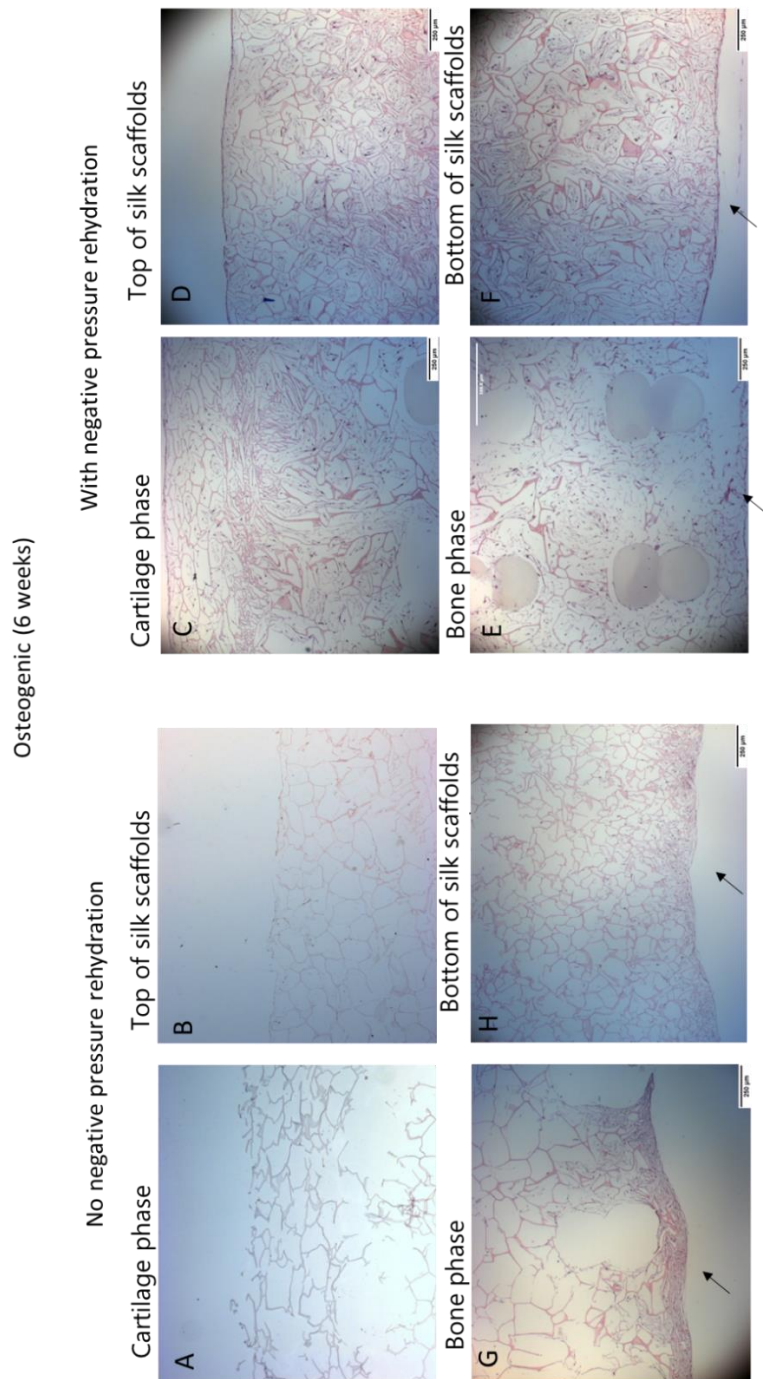


**Figure 48 H&E staining of biphasic and silk control scaffolds under osteogenic conditions**  
 Representative images at five times magnification of H&E staining of silk (n=4) and biphasic scaffolds (n=4) following 6 weeks of osteogenic culture in the presence or absence of a negative pressure rehydration step. Arrow indicates seeded face of scaffold (seeding density 500,000 hBMSC). (A) cartilage phase of the biphasic scaffolds that have not undergone negative pressure rehydration. (B) top of silk control scaffolds that have not undergone negative pressure rehydration. (C) cartilage phase of biphasic scaffolds that have undergone negative pressure rehydration. (D) top of silk control scaffolds that have undergone negative pressure rehydration. (E) bone phase of the biphasic scaffolds that have not undergone negative pressure rehydration. (F) bottom of silk control scaffolds that have not undergone negative pressure rehydration. (G) bone phase of the biphasic scaffolds that have undergone negative pressure rehydration. (H) bottom of silk control scaffolds that have undergone negative pressure rehydration

#### **4.1.10.2 Long term viability of cells on scaffolds under osteogenic conditions**

To evaluate cell long-term survival on the bone phase of the biphasic scaffolds compared to the silk control scaffolds under osteogenic conditions, cells were labelled with cell tracker green and were evaluated under the same conditions as in Chondrogenic culture but with a longer culture time of six weeks and under osteogenic conditions. The confocal laser scanning micrographs revealed a high proportion of viable green cells in both scaffold types (n=4) under osteogenic conditions (Figure 49). No observable differences were seen in viability in both groups at both the 24 hour (Figure 49 A,B) and the 6-week time (Figure 49 C,D) points in osteogenic conditions; although a higher density of cells was seen at the 6-week time point for both scaffolds compared to the 24 hour time point. Within all scaffold types and culture conditions, cells appear to have an even distribution over the seeded surface with a spindle like morphology. However, in the 6-week culture group of the biphasic scaffolds, hBMSCs appear to show greater affinity to the silk component of the scaffold, with fewer being visibly attached to the 3D printed component. This was thought to be due to the porous nature of the silk component compared with the nonporous 3D printed component, allowing for a greater density of cells to grow and be visualised under the Z-stack. These findings demonstrate that the scaffolds have low cytotoxicity due to the high number of viable cells, further reinforcing the hypothesis that the poor cell infiltration seen in Figure 43 and Figure 48 was resultant from incomplete rehydration rather than toxicity of the scaffolds. As with the chondrogenic live cell imaging, dead staining with EthD-1 could not be undertaken due to preferential binding of the stain to the silk component of scaffolds masking the presence or absence of dead cells.

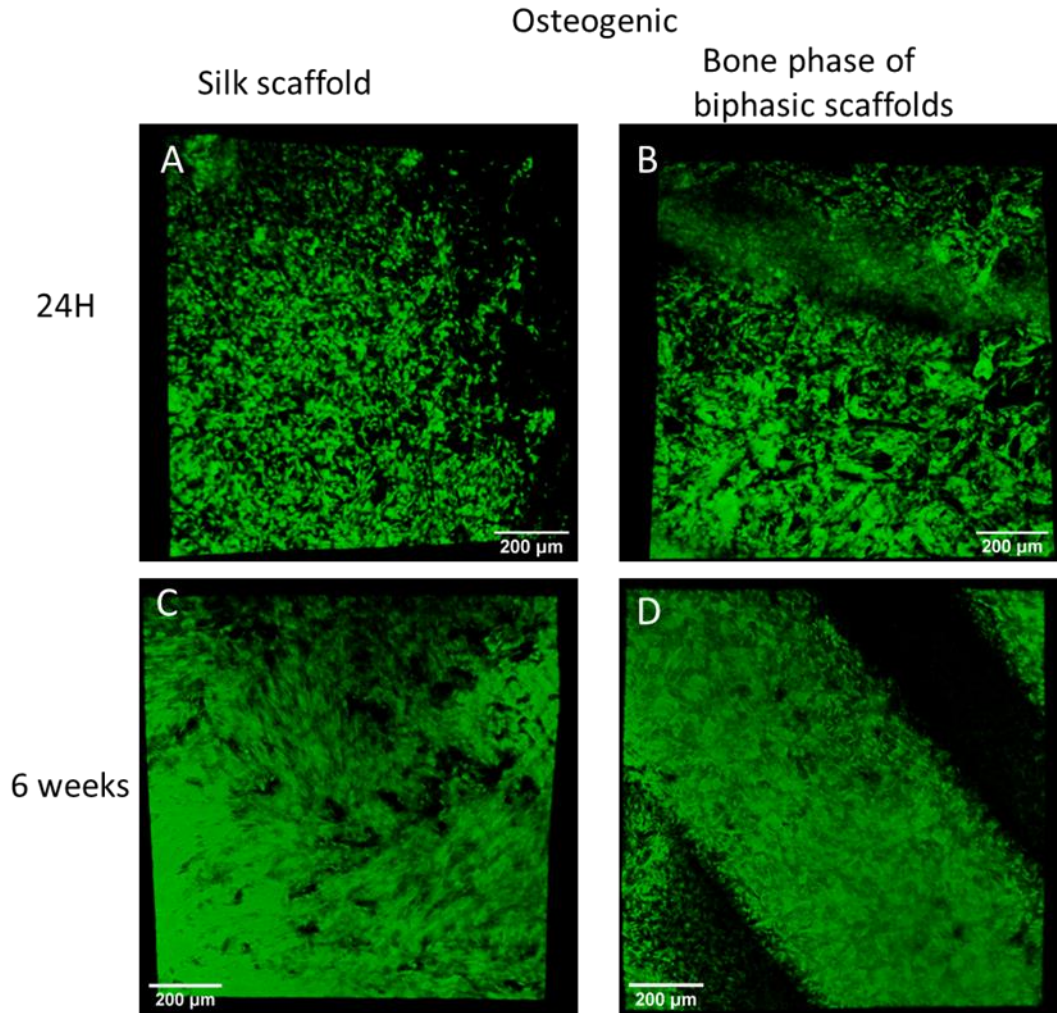


**Figure 49 live cell staining of hBMSCs on biphasic and silk control scaffolds under osteogenic conditions**

representative images of the comparison of cell viability of hBMSCs labelled with CellTracker™ Green CMFDA after 24 hours of osteogenic culture on (A) silk control scaffolds (n=4) . (B) cartilage phase of Biphasic scaffolds (B) (n=4) and after 6 weeks of osteogenic culture on (C) silk control scaffolds (n=4). (D) cartilage phase of Biphasic scaffolds (B) (n=4). Seeding density of each scaffold was 500,000 hBMSCs per scaffold.

#### 4.1.10.3 Collagen and GAG of hBMSCs within deposition within scaffolds under osteogenic conditions.

To better understand the impact of osteogenic culture and seeding on the silk control scaffolds and the biphasic scaffolds, staining was undertaken. This was done by utilising Picrosirius red/Alcian blue staining to assess the expression of collagens and GAGs respectively of hBMSCs within the bone phase of biphasic scaffolds (Figure 50 C,D) and silk control scaffolds (Figure 50 A,B) after 6 weeks of culture. Both the biphasic scaffolds and silk control scaffolds showed collagen staining (red) and GAG staining (blue) on the scaffold interior with a large amount of extracellular matrix production.

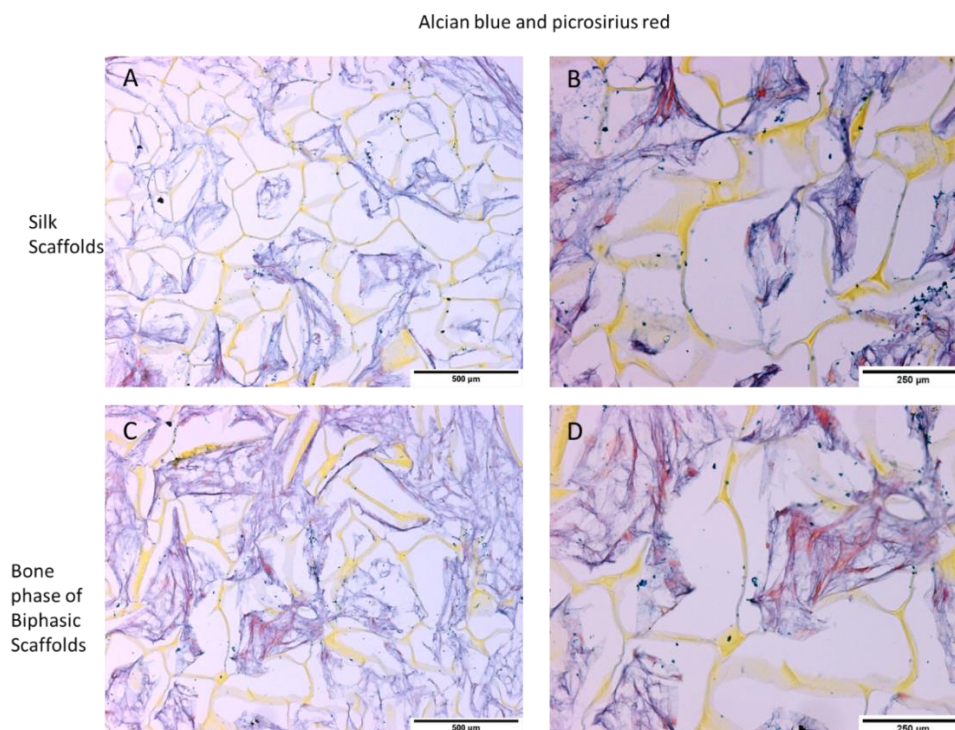


**Figure 50 Picrosirius red/Alcian blue staining of biphasic and silk control scaffolds under osteogenic conditions**

Representative images of picrosirius red/Alcian blue staining of silk control scaffolds and the bone phase of biphasic scaffolds after 6 weeks of osteogenic culture with seeded hBMSCs (seeding density 500,000 cells per scaffold) (n=4 per group). Collagen is stained with Picrosirius red and is represented by a red colour. GAGs are stained with Alcian blue and is represented in blue. (A) Silk control scaffolds at 10x magnification. (B) Silk control scaffolds at 20x magnification. (C) The bone phase of the biphasic scaffolds at 10x magnification. (D) The bone phase of the biphasic scaffolds at 20x magnification.

#### **4.1.10.4 Collagen Type I and II deposition of hBMSCs within scaffolds under osteogenic conditions.**

To further differentiate the type of collagen deposition seen by the Picrosirius red staining and to better understand the exact collagen types deposited by cells within the scaffolds under osteogenic conditions, immunohistochemistry was undertaken. This staining demonstrated the presence of only Type I collagen deposition shown by brown staining in both the biphasic (Figure 51 C,D) and silk control scaffolds (Figure 51 A,D) , with no obvious difference between both scaffold types. No Type II collagen staining was seen in either the biphasic (Figure 51 G,H) or silk control scaffolds (Figure 51 E,F) under osteogenic conditions, indicating the deposition of the correct collagen type for bone. As previously mentioned, Type I collagen staining functioned as a negative marker for cartilage formation and a positive marker for bone and fibrocartilage or fibrous tissue formation, and Type II collagen staining functioned as a positive marker for cartilage formation.

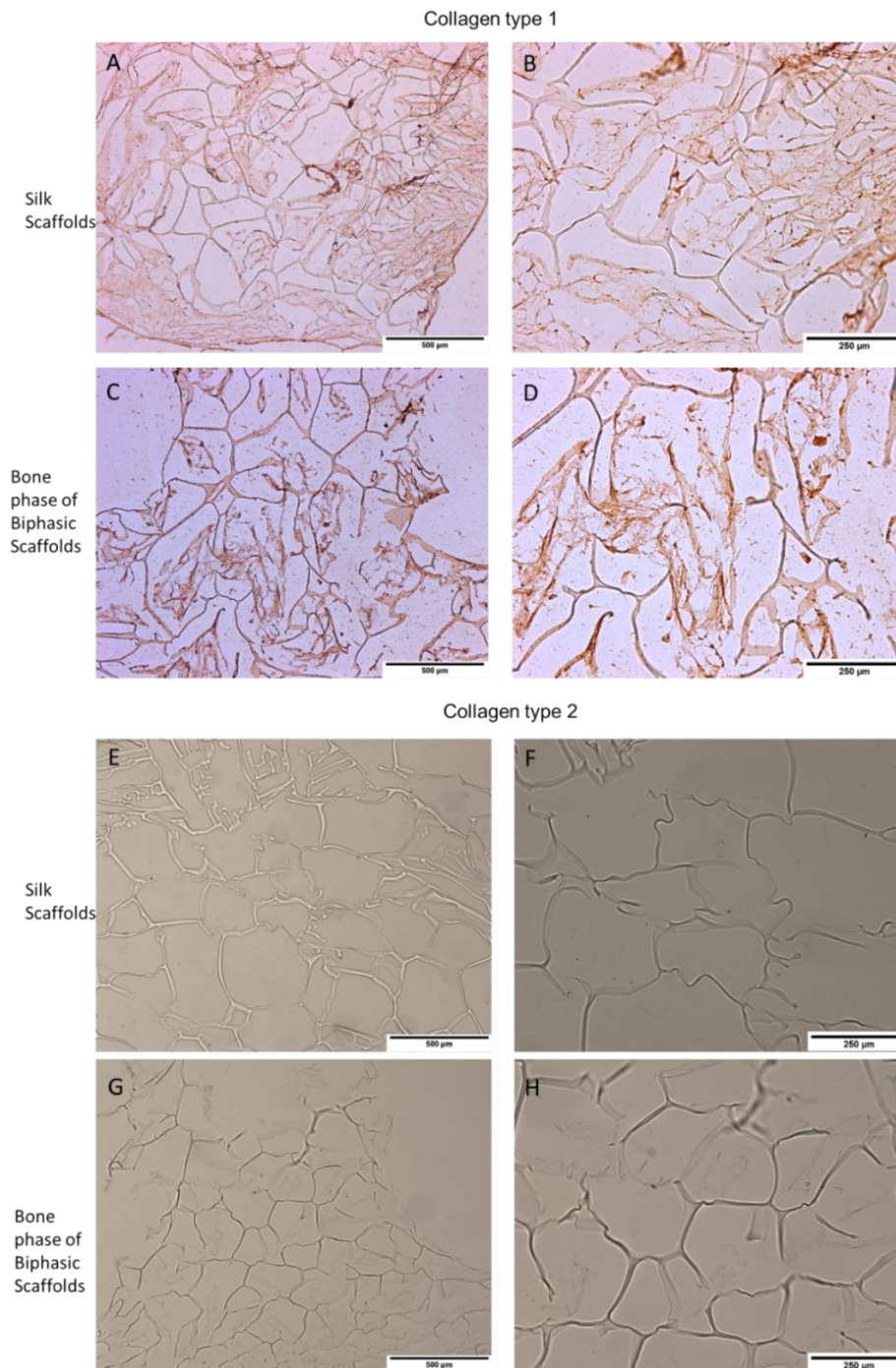


**Figure 51 IHC staining of Type I and Type II collagen of biphasic and silk control scaffolds under osteogenic conditions**

Representative images of collagen Type I and Type II staining by immunohistochemistry of silk control scaffolds and the bone phase of biphasic scaffolds after 6 weeks of osteogenic culture with seeded hBMSCs (seeding density 500,000 cells per scaffold) (n=4 per group). Positive staining is represented by a brown coloration. (A). Silk control scaffolds at 10x magnification stained for Type I collagen. (B) Silk control scaffolds at 20x magnification stained for Type I collagen. (C) The bone phase of the biphasic scaffolds at 10x magnification stained for Type I collagen. (D) The bone phase of the biphasic scaffolds at 20x magnification stained for Type I collagen. (E) Silk control scaffolds at 10x magnification stained for Type II collagen. (F) Silk control scaffolds at 20x magnification stained for Type II collagen. (G) The bone phase of the biphasic scaffolds at 10x magnification stained for Type II collagen. (H) The bone phase of the biphasic scaffolds at 20x magnification stained for Type II collagen.

#### 4.1.10.5 Mineral nodule deposition of hBMSCs within scaffolds under osteogenic conditions.

To evaluate calcium deposition, Von Kossa staining was utilised. This indicated small amounts of mineral nodule formation within both the bone phase of the biphasic scaffolds (Figure 52 C,D) and within the silk control scaffolds (Figure 52 A,B), with there being no clear difference between the two groups. A slightly larger density of mineral nodules was observed towards the seeded face of scaffolds.

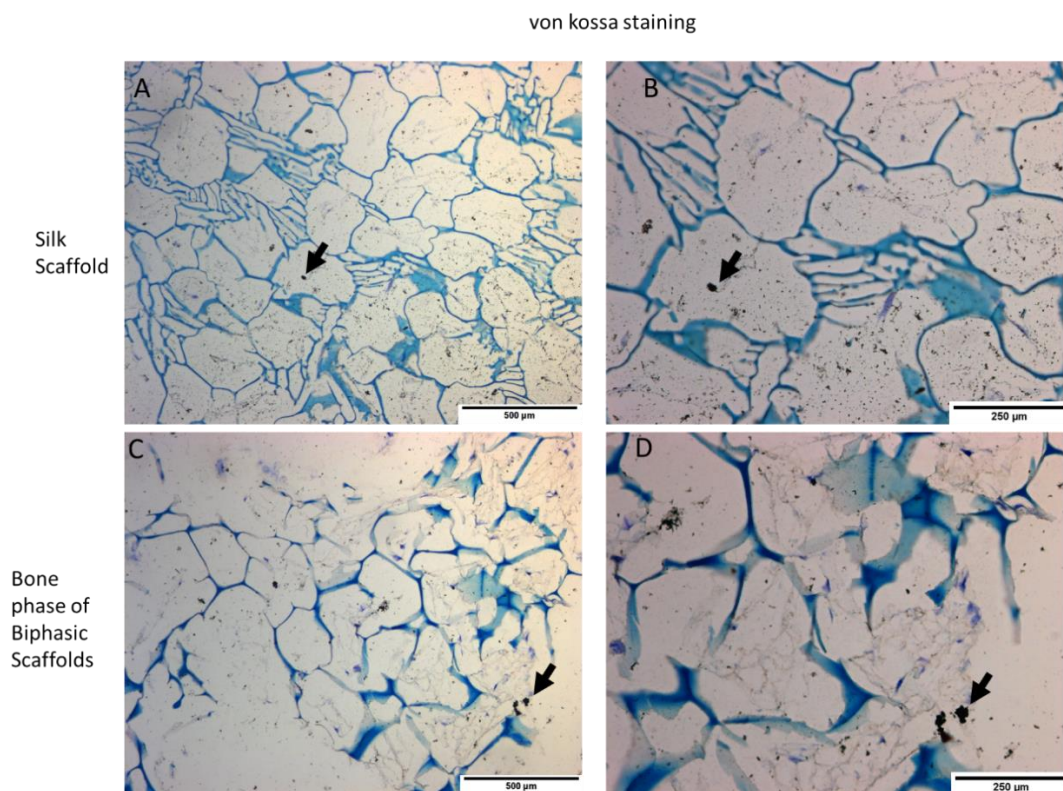


**Figure 52 Von Kossa staining of biphasic and silk control scaffolds under osteogenic conditions**  
Representative images of mineral nodule formation by Von Kossa staining of silk control scaffolds and the bone phase of biphasic scaffolds after 6 weeks of osteogenic culture with seeded hBMSCs (seeding density 500,000 cells per scaffold) (n=4 per group). Mineral nodules are indicated with black arrows. (A) Silk control scaffolds at 10x magnification. (B) Silk control scaffolds at 20x magnification. (C) The bone phase of the biphasic scaffolds at 10x magnification. (D) The bone phase of the biphasic scaffolds at 20x magnification.

#### **4.1.11 Culturing of hBMSCs on scaffolds under osteochondral conditions**

To investigate the potential of biphasic scaffolds to be used for osteochondral interventions, osteochondral culture was undertaken. This consisted of seeding the bone phase of the biphasic scaffolds and the bottom face of the silk control scaffolds with 500,000 hBMSCs, and then culturing them under osteogenic conditions for six weeks. Following this, the cartilage phase of the biphasic scaffolds and the top face of the silk control scaffolds were seeded with either 500,000 hBMSCs or 500,000 hBMSCs that had been pre-cultured in chondrogenic media for two weeks. Both scaffolds were then cultured for three weeks in chondrogenic media before embedding and sectioning.

##### **4.1.11.1 Evaluation of cell migration and morphology via H&E staining within osteochondral conditions**

H&E staining of osteochondral constructs showed excellent pore filling with a continuous, uninterrupted distribution of cells from the cartilage phase to the bone phase in the biphasic scaffolds and throughout the entirety of the silk control scaffolds (Figure 53 B,D,F,H,J,L). No obvious differences were seen in pore filling or cell distribution between scaffolds containing chondrogenic pre-cultured hBMSCs (Figure 53 B,C,F,H,J,L) and non-pre-cultured cells (Figure 53 A,C,E,G,I,K).

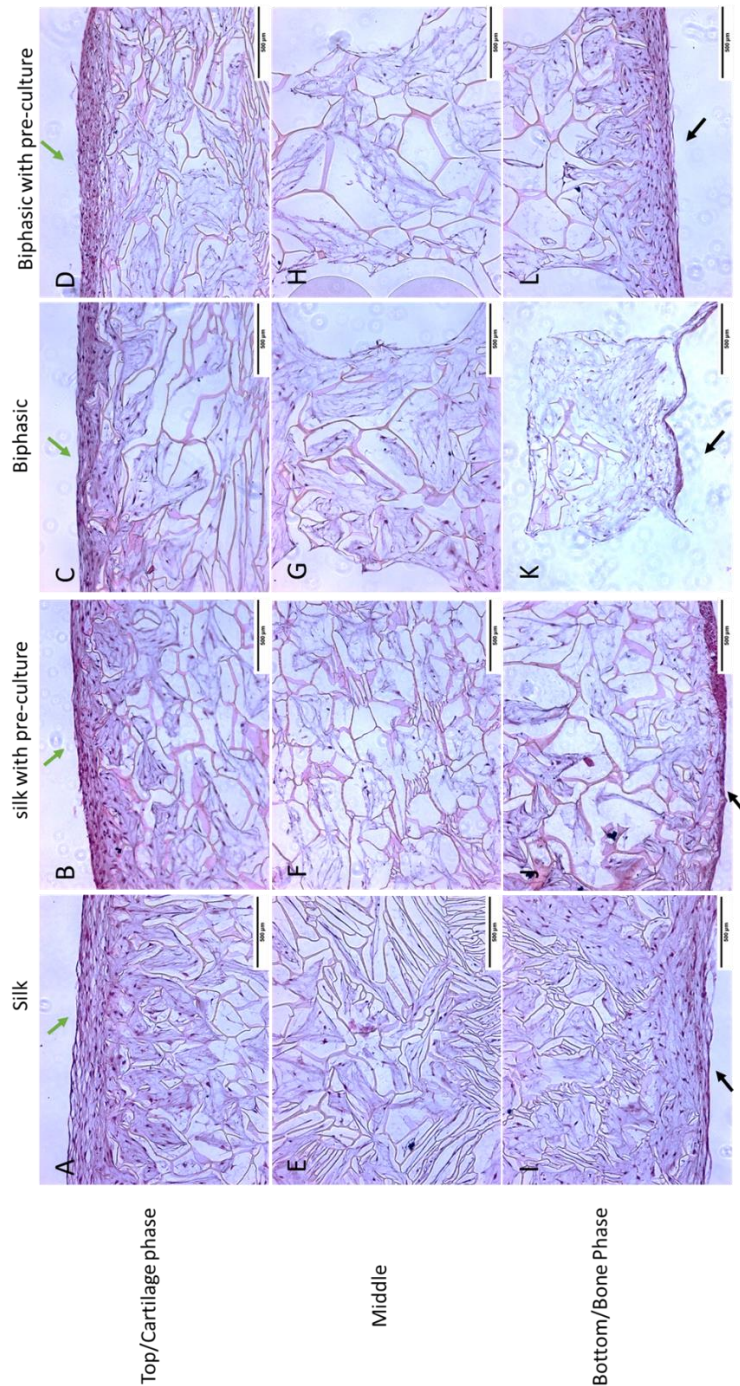


**Figure 53 H&E staining of biphasic and silk control scaffolds under osteochondral conditions**

Representative images at 10 times magnification of H&E staining of silk (n=4) and biphasic scaffolds (n=4), with (n=4) and without (n=4) chondrogenic pre-culture, following 9 weeks of osteochondral culture. Black arrow indicates seeded face of scaffold (seeding density 500,000 hBMSC per scaffold), green arrow represents secondary seeded face of scaffold (seeding density 500,000 hBMSC per scaffold). (A) top of silk scaffold. (B) top of silk scaffold that has undergone chondrogenic pre-culture of cells. (C) the cartilage phase of the biphasic scaffold. (D) the cartilage phase of the biphasic scaffold that has undergone chondrogenic pre-culture of cells. (E) middle of silk scaffold. (F) middle of silk scaffold that has undergone chondrogenic pre-culture of cells. (G) middle of the biphasic scaffold. (H) middle of the biphasic scaffold that has undergone chondrogenic pre-culture of cells. (I) bottom of silk scaffold. (J) bottom of silk scaffold that has undergone chondrogenic pre-culture of cells. (K) bone phase of the biphasic scaffold. (L) bone phase of the biphasic scaffold that has undergone chondrogenic pre-culture of cells.

#### **4.1.11.2 Collagen and GAG deposition within scaffolds under osteochondral conditions.**

Picrosirius red/Alcian blue staining was performed to assess the expression of collagens and GAGs respectively of hBMSCs. No obvious difference in staining was seen between the biphasic scaffolds and silk control scaffolds, as well as the chondrogenic pre-culture group for both the biphasic scaffolds and silk control scaffolds (Figure 54). All groups showed extensive GAG and collagen staining, with higher densities being seen in the chondrogenic phase of the biphasic scaffolds (Figure 54 I,J) and the top of silk scaffolds (Figure 54 A,B), with once again there being no obvious impact of chondrogenic pre-culture on collagen and GAGs of the biphasic (Figure 54 K,L) or silk scaffolds (Figure 54 C,D). However, all groups showed considerably reduced extracellular matrix deposition in the cartilage phase of the biphasic scaffolds and the top of the silk scaffolds compared to that seen within chondrogenic culture alone (Figure 45), along with a considerable reduction in lacunae formation.

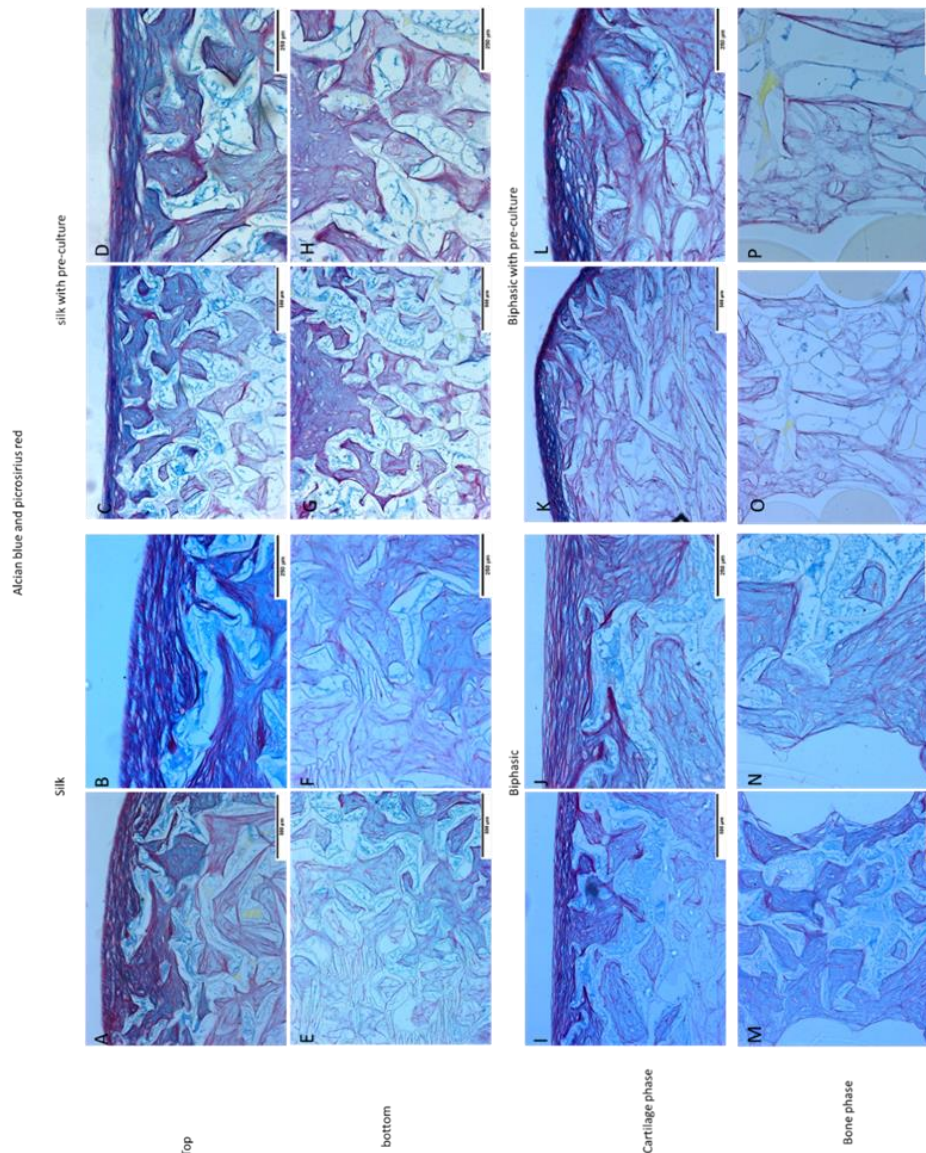


**Figure 54 Picrosirius red/Alcian blue staining of biphasic and silk control scaffolds under osteochondral conditions**

Representative images of picrosirius red/Alcian blue staining of silk control scaffolds and biphasic scaffolds after 9 weeks of osteochondral culture with seeded hBMSCs (n=4 per group). Collagen is stained with Picrosirius red and is represented by a red colour. GAGs are stained with Alcian blue and is represented in blue. (A) Top of silk control scaffolds at 10x magnification. (B) Top of silk control scaffolds at 20x magnification. (C) Top of silk control scaffolds with chondrogenic pre-culture of hBMSCs at 10x magnification. (D) Top of silk control scaffolds with chondrogenic pre-culture of hBMSCs at 20x magnification. (E) The cartilage phase of the biphasic scaffolds at 10x magnification. (F) The cartilage phase of the biphasic scaffolds at 20x magnification. (G) The cartilage phase of the biphasic scaffolds with chondrogenic pre-culture of hBMSCs at 10x magnification. (H) The cartilage phase of the biphasic scaffolds with chondrogenic pre-culture of hBMSCs at 20x magnification. (I) Bottom of silk control scaffolds at 10x magnification. (J) Bottom of silk control scaffolds at 20x magnification. (K) Bottom of silk control scaffolds with chondrogenic pre-culture of hBMSCs at 10x magnification. (L) Bottom of silk control scaffolds with chondrogenic pre-culture of hBMSCs at 20x magnification. (M) The bone phase of the biphasic scaffolds at 10x magnification. (N) The bone phase of the biphasic scaffolds at 20x magnification. (O) The bone phase of the biphasic scaffolds with chondrogenic pre-culture of hBMSCs at 10x magnification. (P) The bone phase of the biphasic scaffolds with chondrogenic pre-culture of hBMSCs at 20x magnification.

#### **4.1.11.3 Collagen Type I and II deposition of hBMSCs within scaffolds under osteochondral conditions.**

Immunohistochemistry was used to identify the type of collagen seen within the scaffolds. This showed extensive Type I collagen deposition in both the bone phase (Figure 55 M,N) and the cartilage phase (Figure 55 I,J) of the biphasic scaffold, as well as within the top (Figure 55 A,B) and bottom of the silk control scaffolds (Figure 55 E,F). There was no impact of pre-culture on Type I collagen deposition within the biphasic (Figure 55 K,L,O,P) or silk scaffolds (Figure 55 C,D,G,H). No Type II collagen deposition was seen in any group (Figure 56), which demonstrated that osteochondral culture had changed the phenotype of collagen expression seen in the cartilage phase from the mix of Type I and Type II to Type I only expression (Figure 55). There was a shift from the formation of cartilage like tissue as seen under chondrogenic culture alone to the formation of fibrous tissue under osteochondral culture. As previously mentioned, Collagen Type I staining functioned as a negative marker for cartilage formation and a positive marker for bone and fibrocartilage or fibrous tissue formation, and Type II collagen staining functioned as a positive marker for cartilage formation.

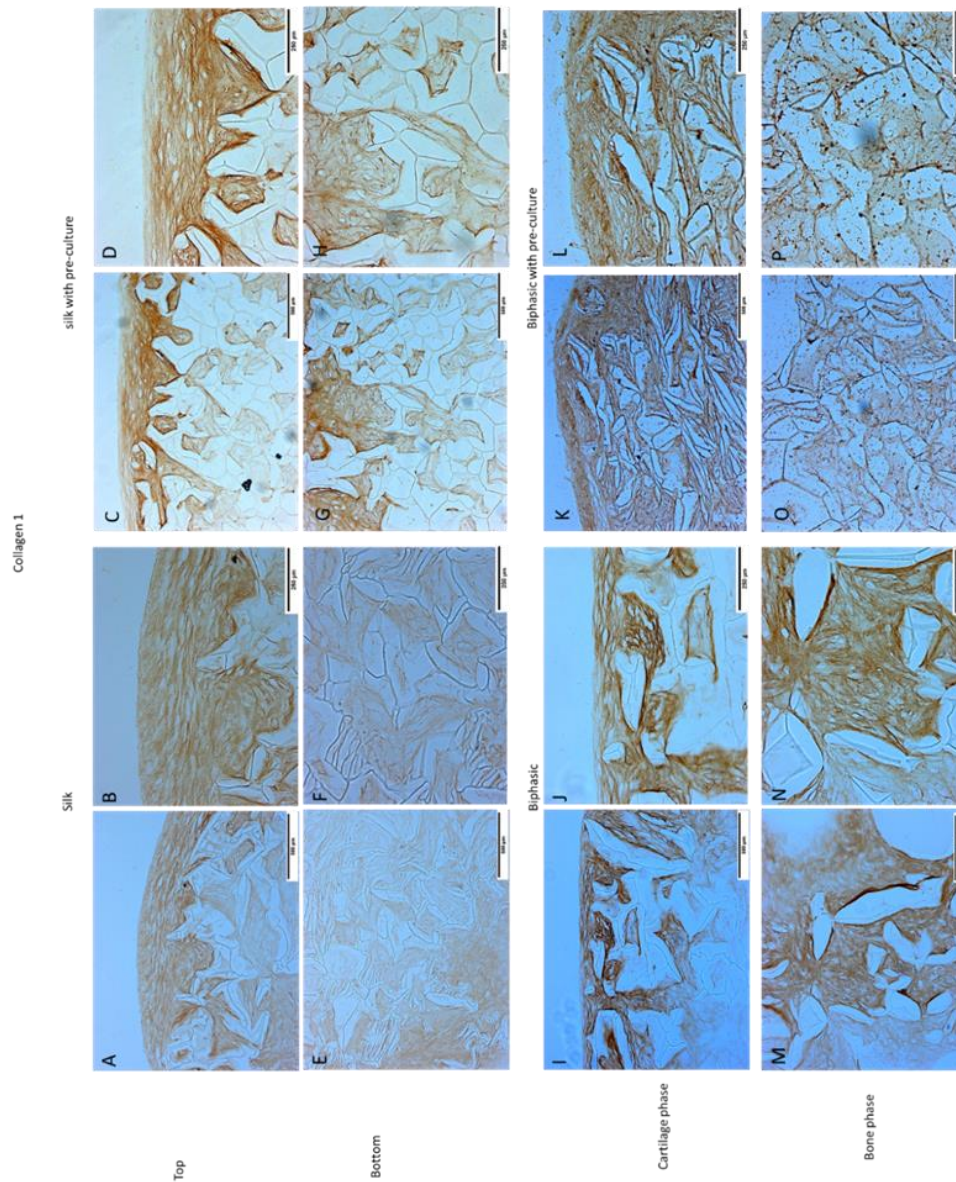


**Figure 55 IHC staining for Type I collagen of biphasic and silk control scaffolds under osteochondral conditions**

Representative images of collagen Type I staining by immunohistochemistry of silk control scaffolds and the bone phase of the biphasic scaffolds after 9 weeks of osteochondral culture with seeded hBMSCs (n=4 per group). Positive staining is represented by a brown coloration. (A) Top of silk control scaffolds at 10x magnification. (B) Top of silk control scaffolds at 20x magnification. (C) Top of silk control scaffolds with chondrogenic pre-culture of hBMSCs at 10x magnification. (D) Top of silk control scaffolds with chondrogenic pre-culture of hBMSCs at 20x magnification. (E) The cartilage phase of the biphasic scaffolds at 10x magnification. (F) The cartilage phase of the biphasic scaffolds at 20x magnification. (G) The cartilage phase of the biphasic scaffolds with chondrogenic pre-culture of hBMSCs at 10x magnification. (H) The cartilage phase of the biphasic scaffolds with chondrogenic pre-culture of hBMSCs at 20x magnification. (I) Bottom of silk control scaffolds at 10x magnification. (J) Bottom of silk control scaffolds at 20x magnification. (K) Bottom of silk control scaffolds with chondrogenic pre-culture of hBMSCs at 10x magnification. (L) Bottom of silk control scaffolds with chondrogenic pre-culture of hBMSCs at 20x magnification. (M) The bone phase of the biphasic scaffolds at 10x magnification. (N) The bone phase of the biphasic scaffolds at 20x magnification. (O) The bone phase of the biphasic scaffolds with chondrogenic pre-culture of hBMSCs at 10x magnification. (P) The bone phase of the biphasic scaffolds with chondrogenic pre-culture of hBMSCs at 20x magnification.

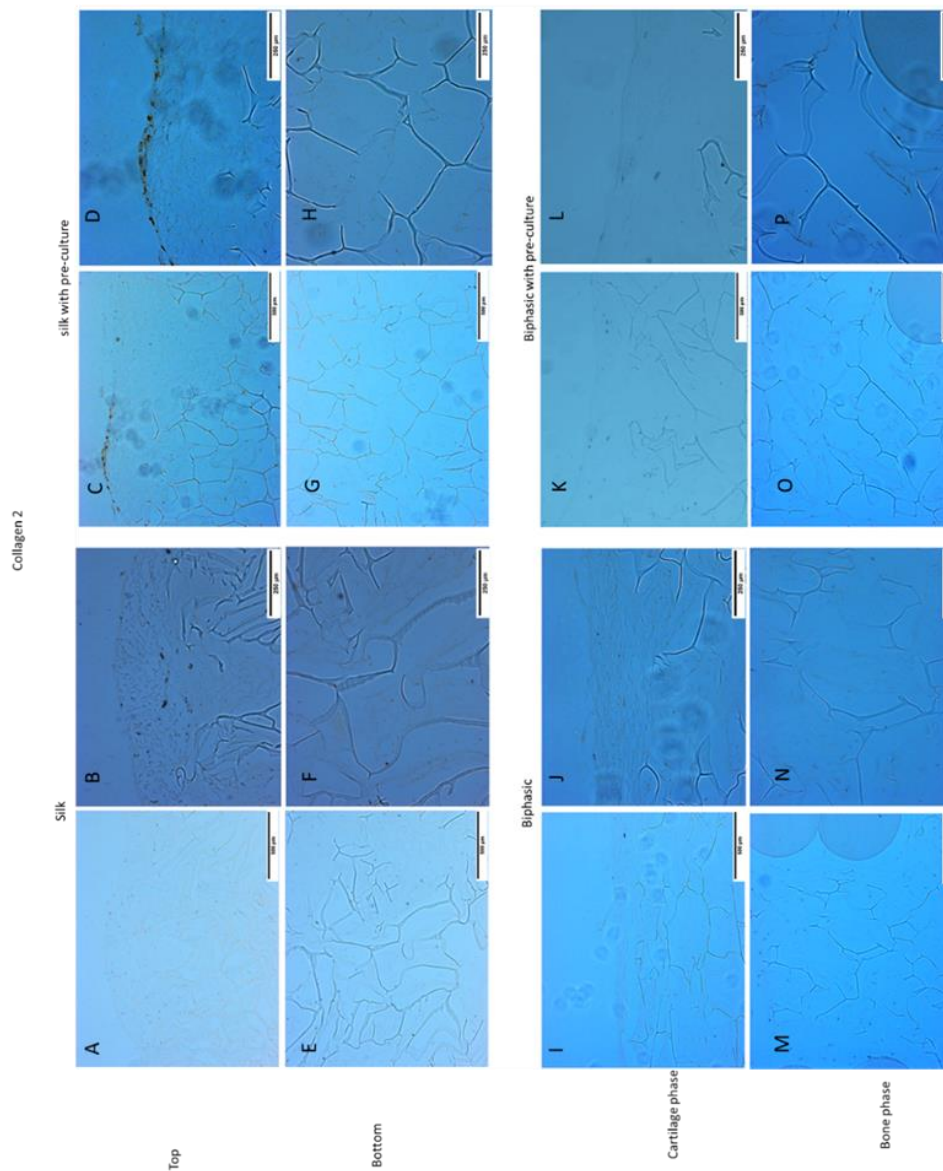


**Figure 56 IHC staining for type II collagen of biphasic and silk control scaffolds under osteochondral conditions**

Representative images of collagen type II staining by immunohistochemistry of silk control scaffolds and the bone phase of biphasic scaffolds after 9 weeks of osteochondral culture, with seeded hBMSCs (n=4 per group). Positive staining is represented by a brown coloration. (A) Top of silk control scaffolds at 10x magnification. (B) Top of silk control scaffolds at 20x magnification. (C) Top of silk control scaffolds with chondrogenic pre-culture of hBMSCs at 10x magnification. (D) Top of silk control scaffolds with chondrogenic pre-culture of hBMSCs at 20x magnification. (E) The cartilage phase of the biphasic scaffolds at 10x magnification. (F) The cartilage phase of the biphasic scaffolds at 20x magnification. (G) The cartilage phase of the biphasic scaffolds with chondrogenic pre-culture of hBMSCs at 10x magnification. (H) The cartilage phase of the biphasic scaffolds with chondrogenic pre-culture of hBMSCs at 20x magnification. (I) Bottom of silk control scaffolds at 10x magnification. (J) Bottom of silk control scaffolds at 20x magnification. (K) Bottom of silk control scaffolds with chondrogenic pre-culture of hBMSCs at 10x magnification. (L) Bottom of silk control scaffolds with chondrogenic pre-culture of hBMSCs at 20x magnification. (M) The bone phase of the biphasic scaffolds at 10x magnification. (N) The bone phase of the biphasic scaffolds at 20x magnification. (O) The bone phase of the biphasic scaffolds with chondrogenic pre-culture of hBMSCs at 10x magnification. (P) The bone phase of the biphasic scaffolds with chondrogenic pre-culture of hBMSCs at 20x magnification.

#### **4.1.11.4 Proteoglycan deposition of hBMSCs within scaffolds under osteochondral conditions.**

Safranin-O staining was used to assess the expression of proteoglycans by hBMSCs. Moderate proteoglycan staining was seen in all groups (Figure 57), with no obvious differences being seen between any groups, similar to Alcian blue and picosirius red staining (Figure 54). A higher proportion of proteoglycans was seen in the cartilage phase of the biphasic scaffolds (Figure 57 I,J) and the top of the silk scaffolds (Figure 57 A,B), compared to the bottom of the silk scaffolds (Figure 57 E,F) and the bone phase of the biphasic scaffolds (Figure 57 M,N), as demonstrated by a reduction in Safranin-O staining. Chondrogenic pre-culture also appeared to have no impact on the proteoglycans expression in biphasic (Figure 57 K,L,O,P) and silk scaffolds (Figure 57 C,D,G,H). A reduction in extracellular matrix production in the cartilage phase was seen compared to chondrogenic culture alone (Figure 47). All groups showed considerably reduced lacunae formation in comparison to during chondrogenic culture alone, with a reduction in cartilage-like tissue formation.

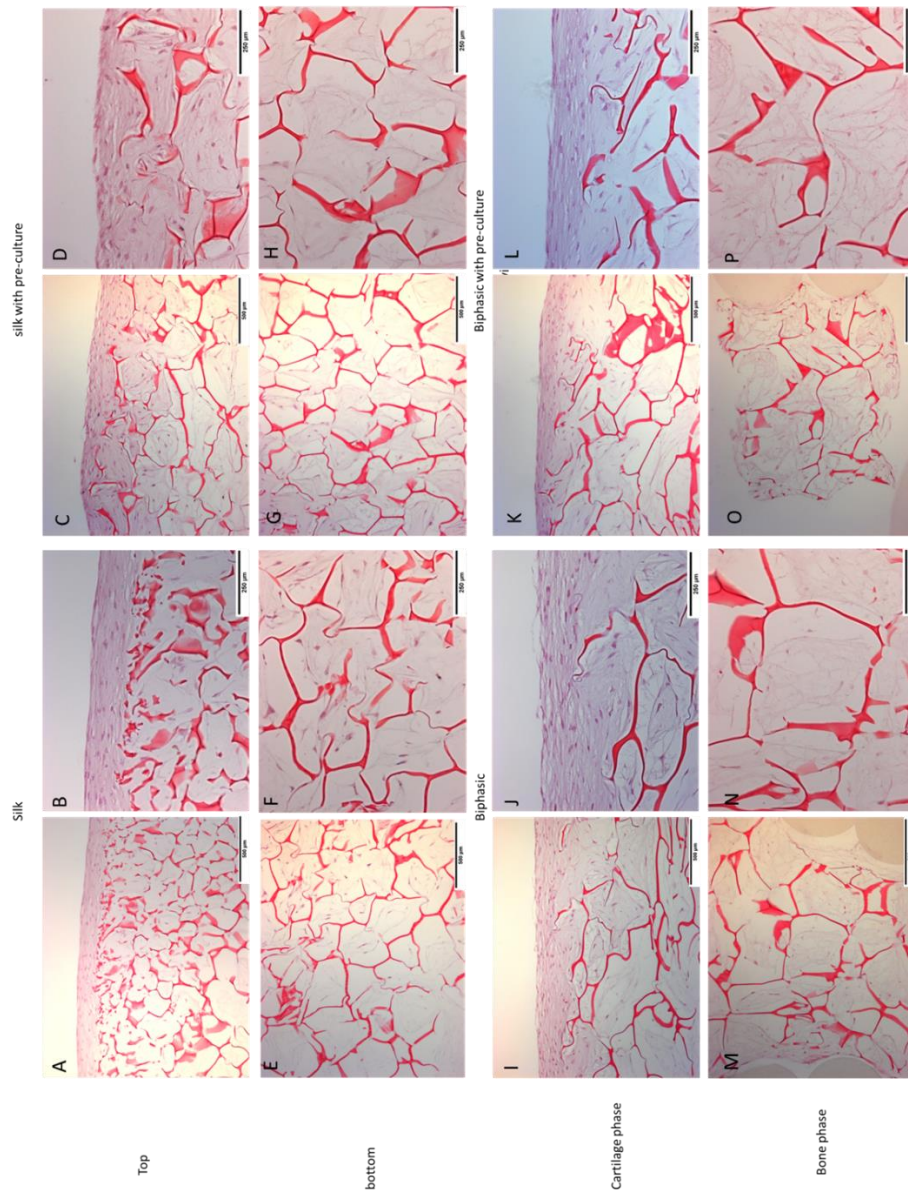


**Figure 57 Safranin-O staining of biphasic and silk control scaffolds under osteochondral conditions**

Representative images of Safranin-O staining of silk control scaffolds and the cartilage phase of biphasic scaffolds after 9 weeks of osteochondral culture, with seeded hBMSCs (n=4 per group). Proteoglycans stained in pink with Safranin-O. (A) Top of silk control scaffolds at 10x magnification. (B) Top of silk control scaffolds at 20x magnification. (C) Top of silk control scaffolds with chondrogenic pre-culture of hBMSCs at 10x magnification. (D) Top of silk control scaffolds with chondrogenic pre-culture of hBMSCs at 20x magnification. (E) The cartilage phase of the biphasic scaffolds at 10x magnification. (F) The cartilage phase of the biphasic scaffolds at 20x magnification. (G) The cartilage phase of the biphasic scaffolds with chondrogenic pre-culture of hBMSCs at 10x magnification. (H) The cartilage phase of the biphasic scaffolds with chondrogenic pre-culture of hBMSCs at 20x magnification. (I) Bottom of silk control scaffolds at 10x magnification. (J) Bottom of silk control scaffolds at 20x magnification. (K) Bottom of silk control scaffolds with chondrogenic pre-culture of hBMSCs at 10x magnification. (L) Bottom of silk control scaffolds with chondrogenic pre-culture of hBMSCs at 20x magnification. (M) The bone phase of the biphasic scaffolds at 10x magnification. (N) The bone phase of the biphasic scaffolds at 20x magnification. (O) The bone phase of the biphasic scaffolds with chondrogenic pre-culture of hBMSCs at 10x magnification. (P) The bone phase of the biphasic scaffolds with chondrogenic pre-culture of hBMSCs at 20x magnification.

#### **4.1.11.5 Mineral nodule deposition of hBMSCs within scaffolds under osteochondral conditions.**

To evaluate calcium deposition, Von Kossa staining was utilised. This indicated small amounts of mineral nodule formation on the bottom side of the silk control scaffolds (Figure 58 E,F) and the bone phase of the biphasic scaffolds (Figure 58 M,N). There was no clear difference in distribution of mineral nodules between groups and chondrogenic pre-culture appeared to have no impact on mineral deposition within biphasic (Figure 58 Q,P) and silk scaffolds (Figure 58 G,H). It was noted that there was slightly larger amounts of mineral nodule formation closer to the osteogenic seeded surface. No obvious mineral nodule formation was seen within the cartilage phase of the biphasic scaffolds (Figure 58 A-D) and the top of the silk control scaffolds (Figure 58 I-L).

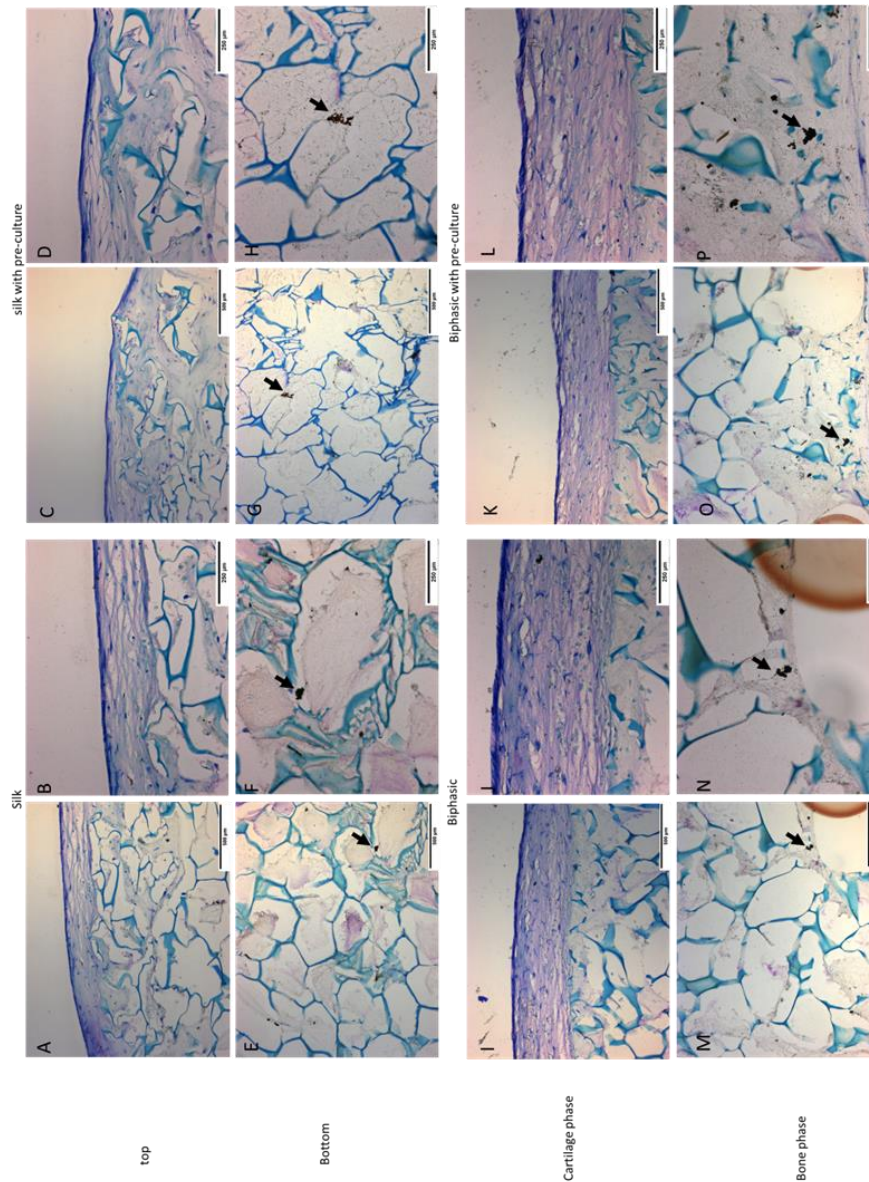


**Figure 58 Von Kossa staining of biphasic and silk control scaffolds under osteochondral conditions**

Representative images of Mineral nodule formation by Von Kossa staining of silk control scaffolds and the bone phase of biphasic scaffolds after 9 weeks of osteochondral culture, with seeded hBMSCs (n=4 per group). Mineral nodule is indicated with black arrows. (A) Top of silk control scaffolds at 10x magnification. (B) Top of silk control scaffolds at 20x magnification. (C) Top of silk control scaffolds with chondrogenic pre-culture of hBMSCs at 10x magnification. (D) Top of silk control scaffolds with chondrogenic pre-culture of hBMSCs at 20x magnification. (E) The cartilage phase of the biphasic scaffolds at 10x magnification. (F) The cartilage phase of the biphasic scaffolds at 20x magnification. (G) The cartilage phase of the biphasic scaffolds with chondrogenic pre-culture of hBMSCs at 10x magnification. (H) The cartilage phase of the biphasic scaffolds with chondrogenic pre-culture of hBMSCs at 20x magnification. (I) Bottom of silk control scaffolds at 10x magnification. (J) Bottom of silk control scaffolds at 20x magnification. (K) Bottom of silk control scaffolds with chondrogenic pre-culture of hBMSCs at 10x magnification. (L) Bottom of silk control scaffolds with chondrogenic pre-culture of hBMSCs at 20x magnification. (M) The bone phase of the biphasic scaffolds at 10x magnification. (N) The bone phase of the biphasic scaffolds at 20x magnification. (O) The bone phase of the biphasic scaffolds with chondrogenic pre-culture of hBMSCs at 10x magnification. (P) The bone phase of the biphasic scaffolds with chondrogenic pre-culture of hBMSCs at 20x magnification.

## 4.1 Discussion

### 4.1.1 Scaffold sterilisation

The large number of potential sources of infection during surgical operations offers great concern, ranging from the operating room, surgical equipment or contaminated medical devices. It has been estimated within epidemiological studies that between 2% and 5% of all implant-related surgeries have post-operative infections (Darouiche, 2004; Johnson and García, 2015; Anastasiou *et al.*, 2019). This introduces a dramatic risk to patient survival, which has been highlighted by a case where unsterilized allografts were used and disease transmission had occurred, giving rise to sepsis of the knee. Post-operative. Infections also lead to increased health-related costs in the form of prolonged hospitalisation and revision surgeries (Kainer *et al.*, 2004; Knetsch and Koole, 2011; Holmes *et al.*, 2014).

The autoclave step used in the creation of the scaffolds clearly showed successful sterilisation in both the silk control scaffolds and the biphasic scaffolds, with no infection being seen even after 14 days of testing. As well as this, no infection of cell cultures was seen throughout any of the other culture experiments. These results concur with the findings of (Rnjak-Kovacina *et al.*, 2015a) which also used autoclaving as a step to sterilise silk scaffolds. This indicates that utilisation of an autoclave step to induce beta sheet formation within the scaffolds is also able to successfully sterilise biphasic scaffolds, eliminating the risk of patient-based infection from this source, as long as the scaffolds are properly handled post sterilisation.

## 4.1.2 Cytotoxicity

First and foremost, it is fundamental to understand whether a newly developed biomaterial is safe for use within living organisms (Liu *et al.*, 2018; Podgórski, Wojasiński and Ciach, 2022). Whether it is a brand-new material or a unique combination of pre-existing materials, it is critical to understand the biocompatibility of the biomaterial and whether it possesses any cytotoxic properties. A scaffold can induce cytotoxicity from a variety of sources, for example from the scaffold itself, or from degradation products released from the scaffold (Forman *et al.*, 1999; O'Brien, 2011; Liu *et al.*, 2018; Iqbal *et al.*, 2022; Chraniuk *et al.*, 2022); although some degradation products may lead to retardation of cell growth rather than cytotoxicity. Interestingly, toxicity can also arise from the lowering or raising of local pH (Echeverria Molina, Malollari and Komvopoulos, 2021). It is therefore important to undertake a diverse range of experiments to determine potential sources of cytotoxicity or cell growth retardation before a scaffold can be thought of as biocompatible (Podgórski, Wojasiński and Ciach, 2022).

A wide range of cytotoxicity tests were undertaken because, as highlighted by Podgórski, Wojasiński and Ciach, 2022, when working with biological scaffolds the porous nature and material of the scaffold can impact the findings, leading to false negative or positive results. Therefore, to demonstrate *in vitro* biocompatibility contact cytotoxicity, indirect cytotoxicity, analysis of metabolic activity, LDH activity, and live cell staining (under chondrogenic and osteogenic conditions) were undertaken. All toxicity tests showed that all scaffold types were non-toxic, with no significant difference being seen between biphasic scaffolds and silk scaffolds. At no time point during any experiment was a change in the phenol red colour of media seen, which would have indicated a lowering of local pH due to scaffold degradation. No contact or indirect cytotoxicity was detected. Scaffolds also demonstrated their ability to support increased metabolic activity, and thus inferring a proliferation of cells over time. Although LDH activity showed an

initially high LDH level corresponding with initial seeding, this then settled over time and plateaued at a low level. A positive control demonstrating a 100% death rate was not included. Therefore, the LDH activity was only compared relative to the scaffold types, thus presenting a study limitation.

Live cell imaging demonstrated that under both osteogenic and chondrogenic conditions under long-term culture, cells were able to form dense monolayers on the scaffold surface as well as cell penetration into the scaffold. Unfortunately, no dead staining could be utilised as all dead staining preferentially bound to the scaffolds, staining them a bright red under confocal examination, making it impossible to see dead cells on the scaffold. Other dead staining was also selected not to be used such as propidium iodide as this stain has the same mechanism of labelling as EthD-1, therefore it was decided not to attempt to use another kind of dead staining due to the extremely high probability that it would also bond to the silk component. Furthermore, it is prevalent in the literature that only live staining can be conducted when utilising silk scaffolds (Rnjak-Kovacina *et al.*, 2015b; Rnjak-Kovacina *et al.*, 2015a; Lu *et al.*, 2017).

Even with these results indicating a high level of *in vitro* biocompatibility of the materials, further testing is still required. *In vivo* tests on animals are necessary before entering a human clinical trial, and even throughout a product's life cycle it is important to continue evaluating for potential cytotoxicity and proper reporting of negative effects needs to be undertaken. Furthermore, this *in vitro* data cannot show any inflammatory and immune response that may be seen *in vivo*, further reinforcing the need for animal testing and continuous screening post human implantation.

### 4.1.3 Cell adhesion

The ability for cells to adhere to scaffolds is fundamental for a wide array of cellular processes and the overall regenerative capacity of a scaffold. When cells attach to the scaffold, they form anchoring points and begin to spread out and interact with the scaffold surface (Revach, Grosheva and Geiger, 2020). This process triggers the activation of signalling pathways that can stimulate survival, migration, integration, cell proliferation, and differentiation (Collins *et al.*, 2017). These processes are necessary for the formation of new tissue and scaffold remodelling. Without the ability to attach to the scaffold, cells would not be able to grow and differentiate in a controlled and organized manner. They would also be more likely to undergo apoptosis or detach and migrate away from the scaffold, which could impair tissue regeneration (Reddig and Juliano, 2005).

Previous attempts to utilise a synthetic 3D printed lattice for tissue regeneration have been successful (Ji and Guvendiren, 2019; Egan, 2019). However, these studies have also demonstrated an issue with the lattice structure; due to the large pore size seen within the lattice structure, cells often struggle to migrate between the filament's large gaps, retarding the migration of cells. The larger pore size also demonstrates the problem of reduced cell adhesion due to the lower availability of specific area for ligand binding (O'Brien *et al.*, 2005; Murphy, Haugh and O'Brien, 2010).

Therefore, within this study we investigated the potential of a novel infill material to increase surface area for ligand binding while simultaneously reducing the lattice pore size to increase cell migratory potential whilst maintaining scaffold porosity. Results indicate that hBMSCs show equivalent adherence and proliferation on silk control scaffolds as well as biphasic scaffolds. This demonstrates that the use of a silk infill is an effective technique to improve cell adherence and migratory potential for scaffolds incorporating 3D printed components. Furthermore, the behaviour of the infill silk material also showed

similar characteristics to other freeze-dried silk scaffolds utilised for tissue regeneration (Rnjak-Kovacina *et al.*, 2015b; Sang *et al.*, 2018).

The use of FBS for scaffold surface modification is a technique used to improve the biocompatibility and functionality of scaffolds in tissue engineering applications (Yang *et al.*, 2001). FBS is a nutrient-rich fluid that contains growth factors, cytokines, and other bioactive molecules that can enhance cell adhesion, proliferation, and differentiation (Liau *et al.*, 2021). The process of FBS surface modification typically involves incubating the scaffold in a solution of FBS for a specified period of time, allowing the FBS molecules to adsorb onto the scaffold surface and create a protein layer (Tallawi *et al.*, 2015; Sönmezer *et al.*, 2021). This layer can then facilitate cell attachment and growth, making the scaffold more suitable for tissue engineering applications (Luo, Humayun and Mills, 2020). There are several benefits to using FBS surface modification. First, FBS is a readily available and cost-effective source of bioactive molecules that can improve scaffold biological properties. Additionally, FBS has been extensively studied and characterized, making it a well-understood material in the field of tissue engineering (Courtenay *et al.*, 2017; Luo, Humayun and Mills, 2020). However, there are also some limitations to using FBS surface modification. For example, FBS can contain variable levels of growth factors and other bioactive molecules, depending on the source and processing method leading to batch variation (Vetsch *et al.*, 2015). Additionally, FBS surface modification may not be suitable for all tissue engineering applications, as the presence of FBS may interfere with certain cell signalling pathways or induce unwanted immune responses. Within this study, evaluation of cell adhesion indicated that, for both the silk control scaffolds and the biphasic scaffolds, pre-treatment with FBS prior to cell seeding was not necessary for cell adhesion and furthermore, no enhancement of cell adhesion was seen over scaffolds not preincubated in FBS. This indicated that silk alone contains appropriate binding ligands to allow for cell adhesion to its surface, which is beneficial, as this leads to a corresponding reduction in requirements in

scaffold processing and reduces requirement for additional animal derived products.

#### **4.1.4 Cell seeding strategies**

Cellular seeding is an extremely critical step in the creation of a functional scaffold, with the cellularity of the scaffold being able to dramatically increase the success of an intervention (Zhou *et al.*, 2006; Yassin *et al.*, 2015). The selection of the correct technique to do this can majorly impact a scaffold's ability to provide uniform tissue regeneration (Kurzyk *et al.*, 2019). Therefore, a variety of different seeding methods have been utilised within the literature; these can be broadly split into two approaches: dynamic and static. Dynamic seeding normally involves placing of the scaffold in a cell suspension and using agitation to move the fluid around the scaffold. This can be done by utilisation of perfusion bioreactors, spinner flasks, orbitals shakers and centrifugation (Vunjak-Novakovic *et al.*, 1998; Zhao and Ma, 2005). This compares to static seeding, which involves placing the scaffolds into a cell solution or pipetting cells onto one surface of the scaffold; however, it should be noted that injecting cells into scaffolds has also been utilised (Hofmann *et al.*, 2003; Wan *et al.*, 2005).

In this study, it was shown that cells could attach to the surface of the biphasic scaffold, with no differences seen when compared to the silk controls in both static and dynamic seeding. The static seeding group showed a relatively dense homogeneous layer of cells on the scaffold surface, but this was only seen on one side, with the other sides presenting no cell attachment. On the other hand, the dynamic seeding group saw an even distribution of cells across all six of its sides, but at a lower density than the single side within the static seeding group. The reason for this difference in density can easily be explained by the fact that the same seeding density of cells was used for both groups (dynamic and static), therefore, in the static seeding group this cell number was focused onto a single

side, whereas the dynamic group was spread over all six. This distribution difference is similar to that found within the literature (Burg *et al.*, 2000). It has also been previously demonstrated that an increased uniformity of cell distribution across the whole scaffold at the point of seeding increases the scaffold's long-term cellularity and more even distribution of cells throughout the entire scaffold, thus leading to improved regenerative capacity of the scaffold as a whole *in vivo* and *in vitro* (Kim *et al.*, 1998; Thevenot *et al.*, 2008). However, in the case of biphasic scaffolds, a unique problem arises when utilising dynamic seeding, as often certain cell types need to be focused to different phases (chondrocytes to the cartilage phase, osteoblasts to the bone phase). A few studies have tried to subvert this problem using complex dynamic seeding techniques (Chang *et al.*, 2004); however, within this study static seeding could be used to deploy cells into different phases within the scaffold, thus effectively seeding different cells to different phases. This was confirmed by cell tracker green and cell tracker red cell tracking which showed no mixing of cells between phases during seeding. This highlights the success of this easy and versatile method to meet the unique seeding requirements of biphasic scaffolds due to their usage within tissues that require regeneration of distinctly different tissue types within the same scaffold. Furthermore, this indicates that this seeding method can be deployed in a wide range of different tissues that require regeneration within distinct regions like that seen in a bone-tendon interface (Enthesis) (Baawad *et al.*, 2022).

#### **4.1.5 Long-term *in vitro* term cell culture**

Overall, long-term cell culture is essential for the development of functional osteochondral scaffolds that can repair damaged or diseased bone and cartilage tissue. It allows for the optimization of scaffold design, tissue regeneration, preclinical testing, and biomaterial evaluation, which are critical steps in the development of safe and effective therapies for musculoskeletal disorders. As

previously mentioned, the cellularity of the scaffold for tissue regeneration is fundamental to its ability to regenerate tissue (Zhou et al., 2006; Yassin et al., 2015). The requirement for cells to be able to uniformly penetrate and colonise an entire scaffold over time to allow for its eventual degradation and replacement with newly formed natural tissue is essential to its function (Kurzyk et al., 2019). Due to funding limitations in conjunction with limited specimen availability, it was selected to not include basal media controls for comparison during long term cell culture. This is recognised as a study limitation as this group would be required to definitively demonstrate that silk has no innate differentiation capacity in regards to osteogenic and chondrogenic differentiation of BMSCs and rather, the cellular differentiation seen within this study was due to the osteogenic and chondrogenic induction media. Although it is likely that the differentiation observed was due to the culture media utilized rather than the scaffold material composition, as similar cellular behaviour was observed in the multilineage differentiation experiments compared to that observed in the osteogenic and chondrogenic culture of biphasic scaffolds and silk control scaffolds.

To further confirm that the negative pressure rehydration step was required for appropriate cell penetration, it was selected to compare scaffolds that have undergone negative pressure rehydration to scaffolds that have not. Scaffolds that had not been exposed to this negative pressure rehydration step showed poor penetration of hBMSCs into the biphasic scaffolds and the silk control scaffolds under osteogenic and chondrogenic conditions, with cells barely able to penetrate into the scaffolds surface. This is compared to scaffolds that had been rehydrated by negative pressure, which showed extensive cell penetration into the majority of the scaffold. These findings further reinforce the rehydration results seen within Chapter 4 and highlight a potential problem with utilising silk scaffolds with an approximate thickness of 3 mm or greater, in the fact that poor rehydration is seen. This also potentially shows a problem with using the scaffolds in environments or methods that do not incorporate a negative pressure rehydration or equivalent step to mechanically support an increase in scaffold

rehydration. A simple diffusion alone is unable to rehydrate the scaffolds, even with the addition of rocking, shaking or rotating the scaffolds during rehydration. Therefore, due to the extremely wide availability of desiccators or vacuum pumps within the biological lab setting, it is recommended for porous scaffolds to incorporate a negative pressure rehydration step, even if it is believed that the scaffold has been fully rehydrated by passive diffusion.

#### **4.1.6 Scaffold capability for cartilage regeneration *in vitro***

To understand the potential of biphasic scaffolds to be utilised for osteochondral tissue regeneration, initially, the scaffolds' potential to regenerate only cartilage tissue was evaluated. An osteochondral scaffold's ability to regenerate cartilage tissue is fundamental to its role and usage. Thus, it is essential to understand and evaluate the potential for cartilage regeneration on and within the scaffold *in vitro* as this will give an analogue and indication for its potential for use *in vivo*, as well as its long-term regenerative capacity.

To evaluate the effectiveness of the cartilage phase of the biphasic scaffolds to regenerate cartilage, *in vitro* experimentation was undertaken by seeding constructs with hBMSCs for three weeks under chondrogenic conditions. Following this culture period, scaffolds were histologically evaluated for their ability to support growth and differentiation of seeded cells. Three weeks of chondrogenic culture was selected as due to its prevalence and wide use within the literature as a standard endpoint for chondrogenesis. At this point, the cells have had sufficient time to differentiate into chondrocytes and produce a significant amount of ECM (Zha *et al.*, 2021). The results of chondrogenic culture of hBMSCs seeded on the biphasic scaffolds showed the ability of isolated hBMSCs to differentiate down a chondrocytic phenotype within the biphasic scaffolds with no histological differences to the silk control scaffolds over a three-week time

period. Cells were localised to the cartilage phase of the biphasic scaffolds and the upper region of the silk control scaffolds. Robust, continuous cartilage-like tissue can be observed along the entire length of the scaffold. Within this newly formed tissue there was extensive GAG and Type II collagen production and deposition, as well as cells within constructs showing a chondrocyte morphology being rounded and found within lacunae. However, Type I collagen deposition was also seen. The presence of both Type I and Type II collagen in a cartilage scaffold can indicate that the newly formed tissue is a mix of fibrocartilage and the more desirable hyaline (Armiento, Alini and Stoddart, 2019). Type II collagen is the main structural protein found in healthy cartilage tissue. Its presence in a cartilage scaffold indicates that the scaffold has successfully supported the growth of new cartilage tissue that closely resembles native tissue. Type I collagen, on the other hand, is the main structural protein found in other connective tissues, such as bone, skin, and tendon (Naomi, Ridzuan and Bahari, 2021). Its presence in a cartilage scaffold can indicate that the newly formed tissue may have a fibrous or fibrocartilage-like composition, which may not be as effective at providing the mechanical resilience and proper functionality as native cartilage tissue (Buchanan, 2022).

The distribution of Type II collagen and proteoglycans seen within *in vitro* culture presented within this project showed similar findings in cartilage quality and structure to that seen within Gu et al., 2022. Within this study, the authors utilised primary goat chondrocytes within a silk scaffold for cartilage regeneration over a 14 day culture period. Although, interestingly, within this project a greater quantity of cartilage like tissue formation was seen as represented by a thicker amount of cartilage tissue seen under histological analysis. There was also a greater quantity of lacunae seen. This difference was assigned to the longer culture period seen within this project of 21 days. Furthermore, the mix of type I and type II collagen seen within biphasic scaffolds demonstrated similar findings to those seen by Saha et al., 2013. In this study, silk scaffolds seeded with hBMSC were placed in an *in vivo* model of osteochondral defects. This model consisted of

placing the scaffold in the patellar groove of the knee joints of male Wistar rats for 8 weeks. With the immunohistochemistry showing silk scaffolds showed type one and type II collagen deposition.

These findings show that the cartilage phase of the biphasic scaffolds can support the differentiation of hBMSCs to differentiate down a chondrogenic lineage, allowing for extensive extracellular matrix deposition and the generation of cartilage like tissue, although a mix of Type I and Type II collagen deposition is seen. Furthermore, these results indicate the potential of the cartilage phase to be able to regenerate cartilage as part of an osteochondral unit for osteochondral tissue regeneration.

#### **4.1.7 Scaffold capability for subchondral bone regeneration *in vitro***

To provide further understanding to the potential for the biphasic scaffolds to be utilised for osteochondral tissue regeneration, the potential for the biphasic scaffolds to support bone tissue formation was evaluated. It is important for an osteochondral scaffold to support adequate bone regeneration as the subchondral bone plays a fundamental role in supporting the overlying cartilage, providing stability and support during joint loading and articulation (Yu *et al.*, 2023; Yildirim *et al.*, 2023). If the scaffold only regenerates cartilage and not bone, the joint may still be prone to damage and deterioration over time, leading to the need for additional surgeries or treatments. Furthermore, in order for the scaffold to be effective, it needs to integrate seamlessly with the surrounding bone tissue (Niu *et al.*, 2023). Without proper bone regeneration, the scaffold may not be able to fuse properly with the existing bone, leading to instability and potential failure when implanted *in vivo*.

To evaluate the effectiveness of the bone phase of the biphasic scaffolds to regenerate subchondral bone, *in vitro* experimentation was undertaken by seeding constructs with hBMSCs for six weeks under osteogenic conditions. Following this culture period, the scaffolds were histologically evaluated for their ability to support growth and differentiation of seeded cells. Six weeks of osteogenic culture was selected as upon review of the literature this culture period appears to be an adequate amount of time to allow for osteogenic differentiation without being so long to make the experiments unfeasible in length due to time constraints (Lozito *et al.*, 2013; Persson *et al.*, 2018; Breathwaite *et al.*, 2020; Oliveros Anerillas *et al.*, 2021; Man *et al.*, 2022a). The results of osteogenic culture of hBMSCs seeded on the biphasic scaffolds showed the ability of isolated hBMSCs to differentiate down an osteoblastic phenotype within the bone phase of the biphasic scaffolds, with no histological differences to the silk control scaffolds over a 6-week time period. These showed extensive Type I collagen deposition and low levels of mineral deposition within the scaffolds. The regions which demonstrated the greatest amount of mineral deposition corresponded to the regions closer to the seeded edge of the scaffold. Furthermore, these regions showed an increased amount of extracellular matrix deposition, inferring that the cells within this region have a more mature osteogenic phenotype. The presence of the 3-D printed component in the bone phase seem to have no impact on cell's ability to migrate through the scaffold as well as their ability to proliferate and colonise scaffolds with a comparable depth of penetration of cells between the bone phase of biphasic scaffolds and silk control scaffolds. The level of mineral nodule deposition seen within the scaffolds seem comparable to other bone scaffolds seen within the literature that utilise silk alone in *in vitro* culture (Woloszyk *et al.*, 2014; Man *et al.*, 2022b).

These findings show that the bone phase of the biphasic scaffolds can support the differentiation of hBMSCs to differentiate down an osteogenic lineage, allowing for extensive extracellular matrix deposition and the generation of initial bone like tissue. Furthermore, these results indicate the potential of the bone phase to be

able to regenerate subchondral bone as part of an osteochondral unit for osteochondral tissue regeneration.

#### **4.1.8 Scaffold capability for osteochondral tissue regeneration *in vitro***

Ultimately, it is important that an osteochondral scaffold is able to functionally regenerate both bone and cartilage. Due to the nature of the biphasic scaffold's use within this study, there is a requirement for it to regenerate both bone and cartilage simultaneously within one scaffold, to provide a seamless osteochondral unit to be utilised during *in vivo* implantation for joint regeneration.

The split culture technique utilised within this study to attempt to create complete osteochondral units consisted of six weeks of osteogenic culture with only the bone phase of the scaffolds seeded, followed by three weeks of chondrogenic culture with the addition of new hBMSCs to the cartilage phase. The time periods selected (three weeks and six weeks of chondrogenic and osteogenic culture, respectively) were chosen to match up with the culture period selected when chondrogenic and osteogenic culture was undertaken separately, as this had previously shown to provide relatively successful regeneration of these tissue types individually. Furthermore, it was selected to initially begin with osteogenic culture as it was theorised differentiated osteoblasts would have a more stable phenotype than chondrocytes, and thus be more likely to maintain their phenotype when the culture media was exchanged in the second phase of seeding. To evaluate further whether hBMSCs would be driven towards the chondrogenic lineage, a pre-culture group was utilised which consisted of two weeks of chondrogenic culture prior to seeding. This was hoped to help lock in hBMSCs to a chondrogenic phenotype before experiencing split culture, hopefully reducing the likelihood of dedifferentiation/inappropriate osteogenic differentiation of the cells seeded to the cartilage phase. It was selected not to undertake pre-culture of hBMSCs under osteogenic conditions as the first 6 weeks

of osteochondral culture are conducted only under osteogenic conditions, which was previously shown to be successful.

The results of osteochondral culture of hBMSCs seeded on the biphasic scaffolds and the silk control scaffolds showed a dominance of a fibrous tissues morphology, with extensive Type I collagen deposition, low levels of mineral deposition and a dramatic suppression of any cartilage-like tissue formation in the scaffold. Unlike chondrogenic culture, no Type II collagen deposition was seen at all during osteochondral culture in the cartilage phase of the biphasic scaffolds or the silk control scaffolds. As well as this, a reduction in proteoglycan and GAG deposition was seen. Furthermore, hBMSCs in the cartilage phase presented far fewer cells possessing a chondrocyte-like phenotype, with very few lacunae formations being seen. No mineralisation of the cartilage phase is seen in the biphasic scaffolds or on the top of the silk control scaffolds. This data shows that, even in the presence of chondrogenic media, the six weeks of osteogenic culture before the seeding of the cartilage phase is able to completely suppress cartilage formation, even when hBMSCs have spent two weeks in pre-culture in chondrogenic media to direct them down the chondrogenic lineage. This suppression of chondrogenesis in the presence of osteoblasts is supported by the results of Chen *et al.*, 2012, which found in a 2D–3D interface coculture model cartilage related protein expression such as Type II collagen and aggrecan were downregulated significantly, and a significant increase in Type I collagen expression was seen. Furthermore, Mukundan, Nirmal and Nair, 2022 also had a similar finding in which their osteochondral constructs utilising primary chondrocytes in their cartilage and BMSCs in their bone phase failed to create a phenotypically stable layer of cartilage tissue and rather in their opinion saw the formation of bone like tissue formation throughout their osteochondral scaffold. These results reinforce the idea that the reason that osteochondral culture failed within the biphasic scaffolds was due to cellular signalling and communication between the osteogenic differentiated cells seen within the bone phase and the chondrogenic differentiated cells in the cartilage phase, leading to the suppression

of chondrogenesis, and thus a failure to regenerate osteochondral tissue. This would also explain why osteogenic and chondrogenic differentiation was successful alone, as this cross talk between cell populations would not have been present. It is still unclear what the exact mechanism of action is in cell-cell communication that leads to the suppression of chondrogenesis and the development of fibrous tissue seen within this study. Some studies have suggested that the presence of osteogenic differentiated cells leads to the formation of hypertrophic chondrocytes in coculture via cell-cell communication, thus resulting in the upregulation of collagen 1 and the downregulation of GAGs (Jiang, Nicoll and Lu, 2005; Chen *et al.*, 2012; Zhang *et al.*, 2018b; Wolff and Hartmann, 2019). To confirm whether hypertrophic chondrocytes were indeed forming in the cartilage phase of the biphasic scaffold, immunohistochemical staining for Sox 9 and collagen X would have to be undertaken, as Sox 9 is not expressed in hypertrophic chondrocytes and collagen X deposition is a hallmark of hypertrophic chondrocyte presence (Shen, 2005; Diederichs *et al.*, 2016; Lefebvre and Dvir-Ginzberg, 2017; Yi *et al.*, 2018; He *et al.*, 2018). To evaluate the effectiveness of the pre-incubation on driving hBMSCs down the chondrogenic lineage and to investigate potential reasons for its failure to improve osteochondral tissue regeneration, characterization of cell chondrogenic lineage commitment could be undertaken on the pre-cultured cells. This would indicate whether this pre-incubation had any effect on chondrogenic lineage commitment and give an indication whether pre-culture failed due to an inability to initially direct chondrogenic lineage commitment, or whether the cell-cell interactions seen within the biphasic scaffolds were able to override any lineage commitment induced by pre-culture.

The limited success in osteochondral tissue regeneration seen within this project could be related to the relatively simple osteochondral culture strategy. It was hoped that the presence of the chondrogenic pre-culture for two weeks would be enough to drive hBMSCs down a chondrogenic lineage, thus allowing for a simple and scalable process for creating osteochondral constructs. However, as

previously discussed, the presence of differentiated hBMSCs down osteogenic lineages within the bone phase of biphasic scaffolds was able to overpower the presence of pure chondrogenic media. Thus, in future experimentation, osteochondral scaffolds may need to be subjected to more complex osteochondral culture methods such as those seen within Tuerlings *et al.*, 2022 which created a microfluidic chip (Figure 59) for the organ on a chip model of osteoarthritis. Within this study, a functional osteochondral unit was able to be created before subjecting it to a disease state. Theoretically, the same microfluidic strategy could be utilised to create osteochondral constructs for implantation rather than disease modelling.

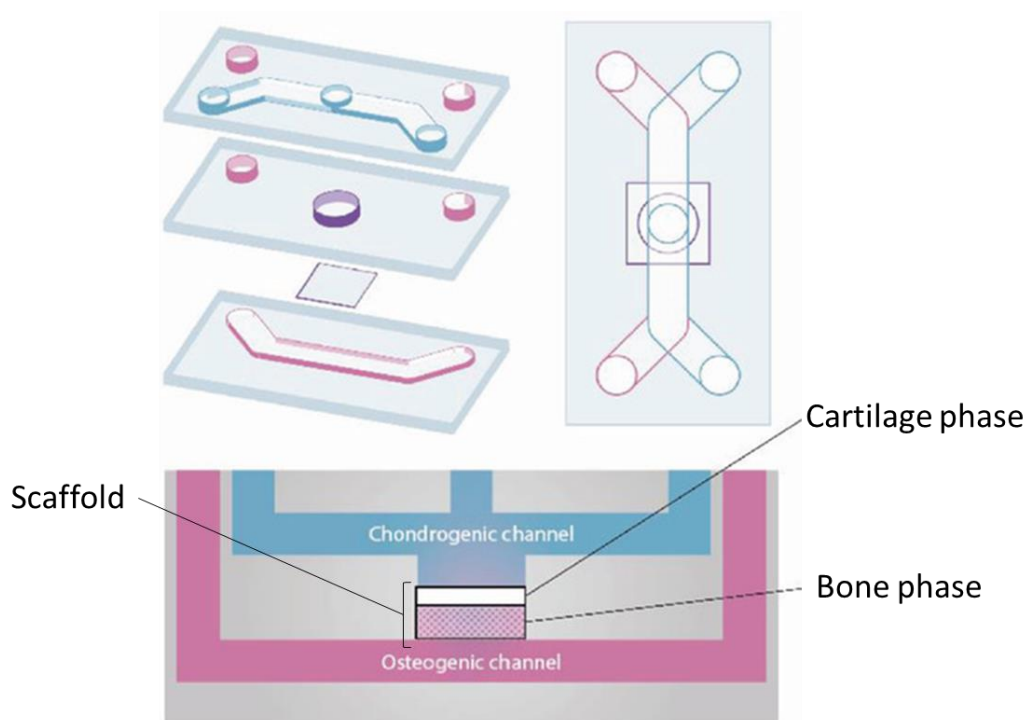


**Figure 59 Microfluidic culture device for osteochondral tissue on a chip model**

Schematic image of the design for an osteochondral unit-on-a-chip model system (pink: osteogenic channel, blue: chondrogenic channel, purple: co-culture compartment). Reprinted from Tuerlings, M., Boone, I., Eslami Amirabadi, H., Vis, M., Suchiman, E., van der Linden, E., Hofmann, S., Nelissen, R., den Toonder, J., Ramos, Y. and Meulenbelt, I. (2022) 'Capturing Essential Physiological Aspects of Interacting Cartilage and Bone Tissue with Osteoarthritis Pathophysiology: A Human Osteochondral Unit-on-a-Chip Model', *Advanced Materials Technologies*, 7(8), pp. 2101310. With permission of the Journal of Advanced Materials Technologies.

Rather than take a complex microfluidic strategy for osteochondral culture, alternative simpler strategies could be undertaken such as those shown within Fu *et al.*, 2022, where three individual and separate scaffolds were created; one for cartilage regeneration, one for regeneration of transitional tissue between cartilage and bone, and one for bone tissue regeneration. By culturing scaffolds separately, they were able to create established generated tissues before combining them to make the full osteochondral complex. Within this study, a similar strategy could be undertaken as both phases have been individually shown to adequately support the growth and differentiation of the desired tissue types. It is only when a combined approach is taken that the scaffold fails in its function. Thus, by separately seeding the cartilage phase and the bone phase, and then recombining them prior to implantation, a functional osteochondral unit could be created. However, by undertaking this strategy, there runs the risk of creating two distinct tissue types (cartilage and bone) rather than creating a gradient from bone to cartilage, which more closely mimics native tissue (Grayson *et al.*, 2008; Niu *et al.*, 2023). Furthermore, additional strategies could be undertaken to add molecular cues to the scaffold itself, helping to give the scaffold chondrogenic and osteogenic differentiation capacity in its own right. This strategy was undertaken by Yang *et al.*, 2017, who showed that the presence of TGF- $\beta$ 3 improved chondrogenic regeneration of their cartilage constructs. Other factors such as IGF have also previously demonstrated to show effectiveness when blended with cartilage constructs to improve cartilage relevant ECM deposition and chondrogenesis (Schmidt, Chen and Lynch, 2006; An *et al.*, 2010; Gugjoo *et al.*, 2017; Liebesny *et al.*, 2019). Furthermore, growth factors have been incorporated into scaffold design to improve osteogenic capacity with the use BMP2 seeing a wide prevalence of use (Saha *et al.*, 2013; Di Luca *et al.*, 2017; Ruan *et al.*, 2018; Bi *et al.*, 2023).

### 4.1.9 Summary

Biphasic scaffolds were shown to be sterile and biocompatible, allowing for cell attachment, proliferation and migration. Static seeding was shown to be able to be effectively used to differentially direct cells to regions of the biphasic scaffolds, i.e. particular cells to the cartilage and bone phases. Scaffolds were also shown to separately be able to support chondrogenic differentiation and osteogenic differentiation, showing cartilage and bone like tissue formation *in vitro*, respectively. However, a failure to form osteochondral tissue was seen during the nine-week coculture experiments, with a preferential formation of a bone-like tissue and suppression of cartilage like tissue features and chondrogenesis of hBMSCs.

# Chapter 5 General discussion

This chapter is designed to provide a general discussion combining findings and concepts previously discussed in Chapters 3 and 4 in relation to each other.

### 5.1.1 Project overview

The aim of this project was to regenerate osteochondral tissue *in vitro* utilising a novel biphasic 3D printed silk reinforced scaffold.

The development of osteochondral scaffolds has been driven by the need to address the limitations of traditional treatments for joint injuries and diseases, such as joint replacement. Osteochondral scaffolds offer the potential to provide a less invasive and more effective means of restoring joint function and improving patient outcomes.

Within this project, a unique biphasic scaffold was successfully fabricated. The scaffold consisted of a PEGT/PBT 3D printed lattice which was infilled with a 5% silk solution, the silk solution was then continued to create a seamless silk top layer on the top of the scaffold. The PEGT/PBT 3D printed lattice infilled with silk made up the bone phase of the scaffold and the seamless silk top layer made up the cartilage phase.

The scaffold was designed such that the 3D printed PEGT/PBT lattice would provide rigidity to the scaffold, helping it to create a mechanically stable bone phase. The silk component provided a secondary cell friendly environment to the 3D printed component of the bone phase whilst also simultaneously giving rise to a more compliant silk only cartilage phase. This, theoretically, gives rise to both a mechanically stable and cell friendly scaffold for osteochondral tissue regeneration.

## 5.1.2 Pore size and its impact on cellular differentiation

Evaluation of scaffold pore size indicated that the silk control scaffolds had a mean pore size of  $103 \pm 13 \mu\text{m}$ , the biphasic scaffolds had a mean pore size of  $117 \pm 15 \mu\text{m}$  in the cartilage phase and a mean pore size of  $124 \pm 24 \mu\text{m}$  in the bone phase. This was theorised to be large enough to allow for cell infiltration as well as chondrogenic differentiation (Kuboki, Jin and Takita, 2001; Kim *et al.*, 2010; Wang *et al.*, 2021). However, there were concerns that the porosity may be too small to allow for direct osteogenesis and rather bone formation would have to occur by osteochondral ossification (Tsuruga *et al.*, 1997; Kuboki, Jin and Takita, 2001; Götz *et al.*, 2004; Karageorgiou and Kaplan, 2005). *In vitro* culture of the scaffolds showed that the pore size was adequate to allow for chondrogenic differentiation of hBMSCs with mostly appropriate extracellular matrix deposition for cartilage regeneration. Osteogenic differentiation of hBMSCs was also seen, with cells depositing the appropriate extracellular matrix for subchondral bone regeneration. Mineral deposition was also seen, although this was not extensive. The level of osteogenic differentiation relieved any concerns that the pore size seen within the bone phase of the biphasic scaffolds would be too small to allow for osteogenic differentiation; however, it does remain to be seen whether a larger pore size would lead to increased osteogenic differentiation, and thus improved regenerative capacity of the scaffold.

The silk component of the bone phase of the biphasic scaffold was able to functionally reduce the pore size of the 3D printed component and dramatically increase scaffold surface area in this phase, compared to that found within the literature for other 3D printed lattices (Hu and Athanasiou, 2006; Ji and Guvendiren, 2019; Egan *et al.*, 2019; Buenzli *et al.*, 2020). This led to a dramatic increase in cell migration, as well as cell pore infilling ability compared to that seen within the literature of conventional 3D printed lattices.

### 5.1.3 Biocompatibility

Cells can be influenced by the materials that make up a biological scaffold in a multitude of different ways, ranging from the influence of direct contact between cells to how the products of scaffold degradation interact with cells (Zhang *et al.*, 2018a; Iqbal *et al.*, 2022). When biological scaffolds undergo degradation, waste products are generated as part of this process. These degradation products can have an impact on cell viability and cellular responses within the scaffold microenvironment. Biomaterial scaffolds can degrade through various mechanisms, such as enzymatic degradation, hydrolysis, or cellular-mediated degradation (Li, Ogiso and Minoura, 2003; Deschamps *et al.*, 2004). The specific mechanisms by which scaffold degradation products influence cell viability and cellular responses are diverse and complex, with degradation products being able to interact with cell surface receptors, activate intracellular signalling pathways, and modulate gene expression (Polo-Corrales, Latorre-Esteves and Ramirez-Vick, 2014). They can also directly affect the physicochemical properties of the microenvironment, such as pH, oxygen tension, and nutrient availability, thereby influencing cell behaviour (Zhang *et al.*, 2016). Scaffold degradation products can impact cell viability, either positively or negatively. Some scaffold degradation products such as  $\beta$ -tricalcium phosphate ( $\beta$ -TCP) have been shown to increase cell viability (Yi *et al.*, 2016), whereas others such as the degradation products of PLGA and PLLA have been shown a decrease to cellular viability. This is because the degradation of these products leads to the production of lactate, which causes the lowering of local pH (Zhang *et al.*, 2016). This lowered pH has been demonstrated to inhibit chondrocyte proliferation and matrix synthesis.

Elemental analysis via EDX of the biphasic scaffolds indicated only the presence of nitrogen, carbon, and oxygen, with no contaminants introduced as part of the scaffold fabrication process. This indicated that, along with the pre-existing research into utilisation of silk scaffolds and PEGT/PBT thermoplastic scaffolds and the impact on cellular behaviour of the degradation products, there was a high

likelihood that the scaffold would show adequate biocompatibility (Altman *et al.*, 2003; Mutreja *et al.*, 2015; Schuurman *et al.*, 2016; Mekhileri *et al.*, 2018; Chen *et al.*, 2023b; Sapudom *et al.*, 2023). However, this still needed to be investigated *in vitro* as to the best of our knowledge, these two materials (silk and PEGT/PBT) had not been combined and utilised together in a biological setting. All cytotoxicity and biocompatibility testing showed no indication of any cellular toxicity of the scaffold, rather the scaffold provided an excellent environment for cell attachment, proliferation and differentiation, although the material selected did not encourage differentiation in its own right. Furthermore, with all degradation products released over the eight week indirect cytotoxicity test, they were shown to have no influence on cells' viability or growth rate.

#### **5.1.4 Rehydration and cell penetration**

Analysis of swelling behaviour of the scaffolds indicated that negative pressure rehydration was required to fully rehydrate the scaffolds- that is to ensure removal of all air from all open pores and replace it with fluid. This was indicated by examination of swelling potential over time. These results were reinforced by *in vitro* findings that scaffolds that had not been rehydrated using negative pressure did not allow for cell penetration into the core of the scaffold. This was hypothesised to be due to the presence of impassable air bubbles in the core of the scaffolds, retarding cell migration. These air bubbles are removed by negative pressure rehydration, and cells are then able to functionally pass through. This was furthermore reinforced by the fact that scaffolds transition to floating within liquid to sinking after the negative pressure rehydration.

### 5.1.5 Mechanical properties and handling

The main advantage of the 3D printed component within the biphasic scaffolds over the silk control scaffolds was the resistance to mechanical loading, as the 3D printed component provided rigidity to the scaffold. This increased rigidity and corresponding mechanical properties should theoretically allow for scaffold survival post-implantation. Furthermore, this rigidity led to noticeably easier handling of the biphasic scaffold with tweezers and other utensils compared to the silk control scaffolds.

However, the bulk mechanical properties of scaffolds and their survivability post implantation are not the only factors to bear in mind when considering a scaffold's mechanical properties. It has been extensively shown that scaffold stiffness can dramatically impact the differentiation or capacity of hBMSCs (Discher, Janmey and Wang, 2005; Vining and Mooney, 2017; Gavazzo *et al.*, 2021). Stiffer substrates have shown to direct hBMSCs down osteogenic lineage where softer substrates are more conducive of adipogenic differentiation; the optimal stiffness for chondrogenic differentiation seems to lie in between. This variation is thought to be due to differential activation of signalling pathways and gene expression patterns depending on the substrate stiffness. It has been shown that stiffer substrates lead to the increased formation of focal adhesions that tether the cell to the extracellular matrix (Gavazzo *et al.*, 2021). Formation of these focal adhesions cause signalling pathway activation and thus a cellular response to surface stiffness (Huvneers and Danen, 2009; Vining and Mooney, 2017; Gavazzo *et al.*, 2021).

Optimal substrate stiffness for osteogenic differentiation appears to vary widely between studies with an optimal stiffness appearing to lie between 40-100 kPa (Kong *et al.*, 2005; Engler *et al.*, 2006; Rowlands, George and Cooper-White, 2008; Shih *et al.*, 2011; Witkowska-Zimny *et al.*, 2013; Yang *et al.*, 2017b; Datko Williams *et al.*, 2018; Sun *et al.*, 2018; Yang *et al.*, 2020; Gavazzo *et al.*, 2021). This stiffness

appears to sit many orders of magnitude less than the stiffness seen within the bone phase of the biphasic scaffolds within this project (12,560 KPa). However, due to the nuances of the scaffold, cells seeded on to the bone phase of the biphasic scaffolds are unlikely to register a stiffness of this magnitude, as the majority of the surface area available for cell binding is actually made of the silk infill material. Thus, it is more likely for the cells to register and experience a stiffness much more similar to that found within the silk control scaffolds (113 KPa); this still sits slightly higher than the optimal range seen within the literature, but not by such a dramatic margin. This indicates further versatility of the combination of a 3D printed lattice infilled with silk: the 3D printed component is able to give the bulk compressive modulus and resistance to compressive loading that can protect newly forming tissue, whilst still providing optimal substrate stiffness for osteogenic differentiation and subsequent bone regeneration.

The optimal substrate stiffness for chondrogenic differentiation of hBMSCs is not as well-defined as it is for osteogenic differentiation. However, some studies have suggested that an intermediate range of substrate stiffness, typically in the range of 10-50 kPa, may be optimal for promoting chondrogenic differentiation of hBMSCs. (Ahmed *et al.*, 2015; Wang and Yang, 2017; Olivares-Navarrete *et al.*, 2017; Zhan, 2020; Zhou *et al.*, 2022; Volz *et al.*, 2022). The stiffness of the cartilage phase of the biphasic scaffolds created with this project sits considerably higher than this optimal stiffness at a level of 152 KPa. However, the impact of growth factors and signalling molecules on the differentiation capacity of hBMSCs towards chondrogenic differentiation appeared to have a greater impact than substrate stiffness (Zhou *et al.*, 2022). Therefore, it is still more likely that the failure to create osteochondral tissue in this project was due to cell interactions and signalling between the different phases rather than a lack of appropriate substrate stiffness. This was further supported by the ability of the biphasic scaffold to produce cartilage-like tissue when seeded with hBMSCs only under chondrogenic conditions.

## 5.1.6 Osteochondral culture

Biphasic scaffolds demonstrated that blending of both a rigid 3D printed lattice infilled with silk material provides an excellent cell supportive environment whilst maintaining structural rigidity. Although the created biphasic scaffolds within this project showed an excellent ability to support cell migration, cell proliferation and scaffold colonisation, they lacked an ability to support and drive cell differentiation in their own right. When combined with media supplemented for osteogenic and chondrogenic differentiation, they supported the differentiation of these hBMSCs down these lineages, respectively. However, when the scaffolds were placed in a more complex osteochondral environment the scaffold failed to regenerate osteochondral tissue, and rather saw dominance of a bone-like phenotype that overpowered any chondrogenic differentiation. These results indicate that this biphasic scaffold's use within osteochondral tissue engineering requires further refinement of its capacity to support differentiation of seeded cells. As previously discussed, this could come from a number of adaptations to the scaffold, such as the addition of more complex culture methods utilising microfluidics or even splitting the scaffold into two distinct scaffolds (a silk scaffold for cartilage regeneration and a 3D printed silk reinforced scaffold for bone regeneration) that could be cultured separately and combined at a later point. Another adaptation that could be undertaken based on the proven platform shown within this project is the addition of growth factors and other bioactive molecules to the scaffold. Adding biological cues to the already demonstrated biocompatible cell supportive biphasic scaffolds created within this project could give the scaffold capacity to cause cartilage and bone differentiation in its own right, potentially without the requirements of supplemented media, microfluidics or scaffolds splitting.

### **5.1.7 Study limitations**

Due to funding limitations in conjunction with low specimen availability, a number of experiments could not be undertaken, which led to a few notable study limitations. Basal controls were not included during long-term cell culture. This is recognized as a study limitation as this group would be required to definitively demonstrate that silk has no innate differentiation capacity in regards to osteogenic and chondrogenic differentiation of BMSCs, and rather, the cellular differentiation seen within this study was due to the osteogenic and chondrogenic induction media. This is recognized as a study limitation as this group would be required to definitively demonstrate that silk has no innate differentiation capacity in regards to osteogenic and chondrogenic differentiation of BMSCs and rather, the cellular differentiation seen within this study was due to the osteogenic and chondrogenic induction media. The method conducted to investigate scaffold degradation only investigated the mechanism of proteolytic degradation. This allowed for the analysis of silk degradation over time but fails to properly investigate the degradation of the thermoplastic component of the scaffolds. Mercury intrusion porosimetry could not be undertaken due to equipment and funding availability; thus, in-depth analysis of scaffold porosity and interconnectivity could not be undertaken. Due to limited donor tissue availability BMSCs were obtained from elderly patients (>72 years old). Thus, the cell population may be less relevant than seen within young trauma patients in which the biphasic scaffold is designed to treat.

# Chapter 6 Conclusions and Future Work

This section is designed to provide a conclusion to the overall findings of the project as well as to discuss potential future directions for the osteochondral scaffold designed and created within this project.

### **6.1.1 Conclusion**

Within this study, a novel biphasic scaffold was created. The use of 3D printing within this novel scaffold provides a solid framework and increases its versatility, providing a mechanically robust structure that can theoretically survive the forces seen during joint articulation, as well as improving the degradation profile. The silk infilling not only provides the secondary porous structure to the 3D printed scaffold for the bone phase, but also a superficial layer for the cartilage phase. Silk within both phases improves the scaffold's biocompatibility and cell adhesion characteristics, increasing the scaffold's surface area. This unique biphasic scaffold has the potential to fill a niche within osteochondral tissue regeneration, especially with the possibility for its use within personalised medicine, with the 3D printed structure easily being adapted to different individuals. However, although the scaffold provides an excellent biocompatibility environment for cell growth, proliferation and migration, it lacks biological cues to direct osteochondral tissue formation. Thus, when placed within osteochondral culture *in vitro*, a failure to create osteochondral tissue is seen, and a dominant bone-like tissue regeneration is seen instead.

### **6.1.2 Future work**

Future experimentation on this work should focus on initially gaining a better understanding on why tissue regeneration in chondrogenic and osteogenic conditions was successful, but under osteochondral conditions a complete failure to make cartilage-like tissue was seen. This could consist of a more in-depth look into cartilage and bone specific markers via immunohistochemistry, such as SOX9 and Collagen X. SOX9 could demonstrate presence or absence of chondrogenesis, as well as helping to identify chondrocytes as it is permanently expressed within the cell type (Diederichs *et al.*, 2016; Lefebvre and Dvir-Ginzberg, 2017; Yi *et al.*, 2018). Collagen X would help to identify whether the tissue seen in the cartilage phase of biphasic scaffolds under osteochondral conditions is indeed a specific

fibrous tissue as suspected, or tissue created by hypertrophic chondrocytes undergoing osteochondral ossification (Shen, 2005; He *et al.*, 2018). This would also work well in conjunction with the SOX9 staining as hypertrophic chondrocytes do not express SOX9 (Lui *et al.*, 2019). In conjunction with this, bone specific markers such as RUNX2 could be investigated to glean further information on the stage and amount of osteogenic differentiation within osteogenic culture and osteochondral culture. RUNX2 is a critical factor in differentiation and maturation of osteoblasts (Kawane *et al.*, 2018; Xin, Zhao and Wang, 2022). After further testing to help identify the failure mechanism of scaffolds under osteochondral culture, it would be important to investigate improving the scaffold's capacity to drive cells down both the cartilage and bone lineages to better create osteochondral tissue. To investigate this, initially, biphasic scaffolds would have to be cultured within basal media to confirm whether they possess any innate differentiation or capacity. Once this is undertaken, research into adapting the biphasic scaffold to improve its differentiation or capacity can be conducted. This can be done by adapting both the physical characteristics of the scaffold, as well as its chemical makeup. Recent work by Joukhdar *et al.*, 2023 has developed an easy method to create graded porosity within silk scaffolds. Thus, if applied to this work, a larger porosity could be caused in the bone phase and a smaller pore size in the cartilage phase; thus, potentially increasing osteogenesis and chondrogenesis, respectively. Furthermore, growth factors can be incorporated into the scaffold design to provide chemical cues to drive both chondrogenesis and osteogenesis within the biphasic scaffold. This is shown in Yang *et al.*, 2017, where TGF- $\beta$ 3 was incorporated into scaffolds to improve chondrogenesis, and in Saha *et al.*, 2013 where BMP-2 was incorporated to improve osteogenesis. Throughout experimentation with biphasic scaffolds, a preferential binding of positive dyes (DAPI and Ethidium Homodimer-1) to the silk structure has indicated it has a negative charge, thus, the utilisation of positively charged growth factors may be an easy way to absorb these molecules to the scaffold surface, thus improving its osteochondral regenerative capacity; although this will need to be confirmed via streaming zeta potential. Furthermore, ceramic components, such

as hydroxyapatite, could be incorporated into the thermoplastic (Bernardo *et al.*, 2022) As shown by Castro, O'Brien and Zhang, 2015 where the incorporation of ceramic components dramatically increased osteogenesis within the scaffolds. Furthermore, more complex culturing techniques could be utilised *in vitro* (Tuerlings *et al.*, 2022), such as the utilisation of microfluidics to provide specialised growth media to each phase of the biphasic scaffold during osteochondral culture.

After improvement of the scaffolds osteochondral regenerative capacity *in vitro*, *in vivo* experimentation can be undertaken to further investigate biphasic scaffold biocompatibility, as well as the effectiveness of treatment of OCD. The ideal animal model should sit is closely as possible to that seen within patients in the clinic, having similar biology and cartilage physiology to that seen within humans (Ahern *et al.*, 2009; Li *et al.*, 2015c). Initial *in vivo* testing should utilise small animal models for OCD regeneration, including rats and rabbits (da Silva Morais, Oliveira and Reis, 2018). Following successful small animal model *in vivo* testing, larger models can be utilised to reinforce data before clinical translation. Large animal models for OCD repair include dogs, pigs, sheep, goats, and horses (Dias, Viegas and Carvalho, 2018), although there is a wide range of animal models to consider for OCD regeneration it is also important to bear in mind. Each has their own unique advantages and disadvantages. The most appropriate small animal model for use with the scaffold created within this project is the rat OCD model. Rat OCD models present several advantages, with rats being relatively inexpensive and easy to handle and house with most academic settings having facilities to work with this model (McCoy, 2015). The reasoning for the selection of the rat OCD model over the rabbit is that although the rabbit model shows a larger joint making implantation easier and slightly more relevant to the human joint, the unusual gait of rabbits means that the forces applied to the implanted scaffold may be less clinically relevant than rats when compared to humans (Gushue, Houck and Lerner, 2005). Additionally, rabbits have a higher cost to purchase and house compared to rats. Overall, the rat model strikes a balance between

experimental feasibility and anatomical relevance for studying osteochondral tissue regeneration. It is also important to note when selecting which model to undertake that large animal models are still required for preclinical translation for both rat and rabbit models. (Meng *et al.*, 2020) .In regard to large animal models, a minipig model appears to be the most appropriate utilization with the biphasic scaffold designed within this study. The minipig joint size and weight requirements are close to that of humans, and the bone apposition rate and trabecular thickness also closely resemble those of humans (van der Staay *et al.*, 2009; Søndergaard, Dagnæs-Hansen and Herskin, 2011). The cartilage thickness seen within the minipig presents the second thickest option at 1.5mm, only being outperformed by the horse model (1.75mm) among the available models, but both still sit below that of native human cartilage (2.35mm)(Frisbie, Cross and McIlwraith, 2006; Koch and Betts, 2007; Chu, Szczodry and Bruno, 2009; Fisher *et al.*, 2014; Meng *et al.*, 2020). The reasoning for not selecting the goat or sheep model for OCD is that the cartilage thickness in these animals is considerably lower, at approximately 1.1mm and 0.45mm respectively (Moran *et al.*, 2016; Helgeland *et al.*, 2018; González Vázquez *et al.*, 2021). Although horses have cartilage that sits closest to human cartilage, their longer time to reach maturity (2-4 years compared to the minipig's 18 months) and their extreme cost and difficulty to handle, as well as the requirement of specialist facilities, make the minipig a much more appealing option (Christensen *et al.*, 2015; McCarrel *et al.*, 2016; Dias, Viegas and Carvalho, 2018).

# References

- Abbasi, N., Hamlet, S., Love, R. M. and Nguyen, N.-T. (2020) 'Porous scaffolds for bone regeneration', *Journal of Science: Advanced Materials and Devices*, 5(1), pp. 1-9.
- Abdul Halim, N. A., Hussein, M. Z. and Kandar, M. K. (2021) 'Nanomaterials-Upconverted Hydroxyapatite for Bone Tissue Engineering and a Platform for Drug Delivery', *Int J Nanomedicine*, 16, pp. 6477-6496.
- Abramowitch, S. and Easley, D. (2016) 'Chapter Four - Introduction to Classical Mechanics', in Hoyte, L. and Damaser, M. (eds.) *Biomechanics of the Female Pelvic Floor*: Academic Press, pp. 89-107.
- Acharya, C., Adesida, A., Zajac, P., Mumme, M., Riesle, J., Martin, I. and Barbero, A. (2012) 'Enhanced chondrocyte proliferation and mesenchymal stromal cells chondrogenesis in coculture pellets mediate improved cartilage formation', *Journal of Cellular Physiology*, 227(1), pp. 88-97.
- Ahern, B. J., Parvizi, J., Boston, R. and Schaer, T. P. (2009) 'Preclinical animal models in single site cartilage defect testing: a systematic review', *Osteoarthritis and Cartilage*, 17(6), pp. 705-713.
- Ahmed, M., Ramos, T. A. d. S., Damanik, F., Quang Le, B., Wieringa, P., Bennink, M., van Blitterswijk, C., de Boer, J. and Moroni, L. (2015) 'A combinatorial approach towards the design of nanofibrous scaffolds for chondrogenesis', *Scientific Reports*, 5(1), pp. 14804.
- Akkiraju, H. and Nohe, A. (2015) 'Role of Chondrocytes in Cartilage Formation, Progression of Osteoarthritis and Cartilage Regeneration', *Journal of developmental biology*, 3(4), pp. 177-192.
- Alcaide-Ruggiero, L., Molina-Hernández, V., Granados, M. M. and Domínguez, J. M. (2021) 'Main and Minor Types of Collagens in the Articular Cartilage: The Role of Collagens in Repair Tissue Evaluation in Chondral Defects', *International Journal of Molecular Sciences*, 22(24). DOI: 10.3390/ijms222413329.
- Allen, T., Pagan, M., Martin, R. and Duncan, O. (2020) 'Effect of Rest Periods on Mechanical Ageing of Running Shoes', *Proceedings*, 49(1). DOI: 10.3390/proceedings2020049138.
- Altman, G. H., Diaz, F., Jakuba, C., Calabro, T., Horan, R. L., Chen, J., Lu, H., Richmond, J. and Kaplan, D. L. (2003) 'Silk-based biomaterials', *Biomaterials*, 24(3), pp. 401-16.
- Altman, R. D., Kates, J., Chun, L. E., Dean, D. D. and Eyre, D. (1992) 'Preliminary observations of chondral abrasion in a canine model', *Ann Rheum Dis*, 51(9), pp. 1056-62.
- Amenabar, T., Piriz, J., Mella, C., Hetaimish, B. M. and O'Donnell, J. (2015) 'Reliability of 3 Different Arthroscopic Classifications for Chondral Damage of the Acetabulum', *Arthroscopy*, 31(8), pp. 1492-6.
- An, C., Cheng, Y., Yuan, Q. and Li, J. (2010) 'IGF-1 and BMP-2 Induces Differentiation of Adipose-Derived Mesenchymal Stem Cells into Chondrocytes-Like Cells', *Annals of Biomedical Engineering*, 38(4), pp. 1647-1654.
- Anastasiou, A. D., Nerantzaki, M., Gounari, E., Duggal, M. S., Giannoudis, P. V., Jha, A. and Bikiaris, D. (2019) 'Antibacterial properties and regenerative potential of Sr<sup>2+</sup> and Ce<sup>3+</sup> doped fluorapatites; a potential solution for peri-implantitis', *Scientific Reports*, 9(1), pp. 14469.

- Anderson, D. D., Chubinskaya, S., Guilak, F., Martin, J. A., Oegema, T. R., Olson, S. A. and Buckwalter, J. A. (2011) 'Post-traumatic osteoarthritis: improved understanding and opportunities for early intervention', *J Orthop Res*, 29(6), pp. 802-9.
- Aramwit, P., Kanokpanont, S., De-Eknamkul, W. and Srichana, T. (2009) 'Monitoring of inflammatory mediators induced by silk sericin', *Journal of bioscience and bioengineering*, 107(5), pp. 556-561.
- Archer, C. W. and Francis-West, P. (2003) 'The chondrocyte', *International Journal of Biochemistry and Cell Biology*, 35(4), pp. 401-404.
- Armiento, A. R., Alini, M. and Stoddart, M. J. (2019) 'Articular fibrocartilage - Why does hyaline cartilage fail to repair?', *Advanced Drug Delivery Reviews*, 146, pp. 289-305.
- Armiento, A. R., Stoddart, M. J., Alini, M. and Eglin, D. (2018) 'Biomaterials for articular cartilage tissue engineering: Learning from biology', *Acta Biomater*, 65, pp. 1-20.
- Asik, M., Ciftci, F., Sen, C., Erdil, M. and Atalar, A. (2008) 'The microfracture technique for the treatment of full-thickness articular cartilage lesions of the knee: midterm results', *Arthroscopy*, 24(11), pp. 1214-20.
- Asnaghi, M. A., Duhr, R., Quasnichka, H., Hollander, A. P., Kafienah, W., Martin, I. and Wendt, D. (2018) 'Chondrogenic differentiation of human chondrocytes cultured in the absence of ascorbic acid', *Journal of Tissue Engineering and Regenerative Medicine*, 12(6), pp. 1402-1411.
- Baawad, A., Jacho, D., Hamil, T., Yildirim-Ayan, E. and Kim, D.-S. (2022) 'Polysaccharide-Based Composite Scaffolds for Osteochondral and Enthesis Regeneration', *Tissue Engineering Part B: Reviews*.
- Babensee, J. E., Anderson, J. M., McIntire, L. V. and Mikos, A. G. (1998) 'Host response to tissue engineered devices', *Advanced Drug Delivery Reviews*, 33(1-2), pp. 111-139.
- Bachtiar, E. W., Amir, L. R., Suhardi, P. and Abas, B. (2016) 'Scaffold degradation during bone tissue reconstruction in Macaca nemestrina mandible', *Interv Med Appl Sci*, 8(2), pp. 77-81.
- Baker, B. M. and Chen, C. S. (2012) 'Deconstructing the third dimension – how 3D culture microenvironments alter cellular cues', *Journal of Cell Science*, 125(13), pp. 3015-3024.
- Bal, B. S., Rahaman, M. N., Jayabalan, P., Kuroki, K., Cockrell, M. K., Yao, J. Q. and Cook, J. L. (2010) 'In vivo outcomes of tissue-engineered osteochondral grafts', *J Biomed Mater Res B Appl Biomater*, 93(1), pp. 164-74.
- Baptista, M., Joukhdar, H., Alcalá-Orozco, C. R., Lau, K., Jiang, S., Cui, X., He, S., Tang, F., Heu, C., Woodfield, T. B. F., Lim, K. S. and Rnjak-Kovacina, J. (2020) 'Silk fibroin photo-lyogels containing microchannels as a biomaterial platform for in situ tissue engineering', *Biomater Sci*, 8(24), pp. 7093-7105.
- Barié, A., Kruck, P., Sorbi, R., Rehnitz, C., Oberle, D., Walker, T., Zeifang, F. and Moradi, B. (2020) 'Prospective Long-term Follow-up of Autologous Chondrocyte Implantation With Periosteum Versus Matrix-Associated Autologous Chondrocyte Implantation: A Randomized Clinical Trial', *The American Journal of Sports Medicine*, 48(9), pp. 2230-2241.
- Barone, D. T. J., Raquez, J. M. and Dubois, P. (2011) 'Bone-guided regeneration: from inert biomaterials to bioactive polymer (nano)composites', *Polymers for Advanced Technologies*, 22(5), pp. 463-475.
- Barry, F., Boynton, R. E., Liu, B. and Murphy, J. M. (2001) 'Chondrogenic differentiation of mesenchymal stem cells from bone marrow:

- differentiation-dependent gene expression of matrix components', *Exp Cell Res*, 268(2), pp. 189-200.
- Barui, S., Chatterjee, S., Mandal, S., Kumar, A. and Basu, B. (2017) 'Microstructure and compression properties of 3D powder printed Ti-6Al-4V scaffolds with designed porosity: Experimental and computational analysis', *Mater Sci Eng C Mater Biol Appl*, 70(Pt 1), pp. 812-823.
- Baumbach, K., Petersen, J. P., Ueblacker, P., Schröder, J., Göpfert, C., Stork, A., Rueger, J. M., Amling, M. and Meenen, N. M. (2008) 'The fate of osteochondral grafts after autologous osteochondral transplantation: a one-year follow-up study in a minipig model', *Arch Orthop Trauma Surg*, 128(11), pp. 1255-63.
- Becerra, J., Andrades, J. A., Guerado, E., Zamora-Navas, P., Lopez-Puertas, J. M. and Reddi, A. H. (2010) 'Articular cartilage: structure and regeneration', *Tissue Eng Part B Rev*, 16(6), pp. 617-27.
- Benmassaoud, M. M., Gultian, K. A., DiCerbo, M. and Vega, S. L. (2020) 'Hydrogel screening approaches for bone and cartilage tissue regeneration', *Ann N Y Acad Sci*, 1460(1), pp. 25-42.
- Bennike, T., Ayturk, U., Haslauer, C. M., Froehlich, J. W., Proffen, B. L., Barnaby, O., Birkelund, S., Murray, M. M., Warman, M. L., Stensballe, A. and Steen, H. (2014) 'A Normative Study of the Synovial Fluid Proteome from Healthy Porcine Knee Joints', *Journal of Proteome Research*, 13(10), pp. 4377-4387.
- Benz, K., Breit, S., Lukoschek, M., Mau, H. and Richter, W. (2002) 'Molecular analysis of expansion, differentiation, and growth factor treatment of human chondrocytes identifies differentiation markers and growth-related genes', *Biochemical and Biophysical Research Communications*, 293(1), pp. 284-292.
- Bernardo, M. P., da Silva, B. C. R., Hamouda, A. E. I., de Toledo, M. A. S., Schalla, C., Rütten, S., Goetzke, R., Mattoso, L. H. C., Zenke, M. and Sechi, A. (2022) 'PLA/Hydroxyapatite scaffolds exhibit in vitro immunological inertness and promote robust osteogenic differentiation of human mesenchymal stem cells without osteogenic stimuli', *Scientific Reports*, 12(1), pp. 2333.
- Bernhard, J. C. and Vunjak-Novakovic, G. (2016) 'Should we use cells, biomaterials, or tissue engineering for cartilage regeneration?', *Stem Cell Res Ther*, 7(1), pp. 56.
- Bhosale, A. M. and Richardson, J. B. (2008) 'Articular cartilage: structure, injuries and review of management', *Br Med Bull*, 87, pp. 77-95.
- Bi, Z., Shi, X., Liao, S., Li, X., Sun, C. and Liu, J. (2023) 'Strategies of immobilizing BMP-2 with 3D-printed scaffolds to improve osteogenesis', *Regenerative Medicine*, 18(5), pp. 425-441.
- Bitar, K. N. and Zakhem, E. (2014) 'Design strategies of biodegradable scaffolds for tissue regeneration', *Biomed Eng Comput Biol*, 6, pp. 13-20.
- Bohndorf, K. (1996) 'Injuries at the articulating surfaces of bone (chondral, osteochondral, subchondral fractures and osteochondrosis dissecans)', *Eur J Radiol*, 22(1), pp. 22-9.
- Breathwaite, E., Weaver, J., Odanga, J., dela Pena-Ponce, M. and Lee, J. B. (2020) '3D Bioprinted Osteogenic Tissue Models for In Vitro Drug Screening', *Molecules*, 25(15). DOI: 10.3390/molecules25153442.
- Brittberg, M., Lindahl, A., Nilsson, A., Ohlsson, C., Isaksson, O. and Peterson, L. (1994) 'Treatment of deep cartilage defects in the knee with autologous chondrocyte transplantation', *N Engl J Med*, 331(14), pp. 889-95.

- Brittberg, M. and Winalski, C. S. (2003) 'Evaluation of cartilage injuries and repair', *J Bone Joint Surg Am*, 85-A Suppl 2, pp. 58-69.
- Brown, T. D., Johnston, R. C., Saltzman, C. L., Marsh, J. L. and Buckwalter, J. A. (2006) 'Posttraumatic osteoarthritis: a first estimate of incidence, prevalence, and burden of disease', *J Orthop Trauma*, 20(10), pp. 739-44.
- Buchanan, J. L. (2022) 'Types of Fibrocartilage', *Clinics in Podiatric Medicine and Surgery*, 39(3), pp. 357-361.
- Buckwalter, J. A. and Mankin, H. J. (1998) 'Articular cartilage: tissue design and chondrocyte-matrix interactions', *Instr Course Lect*, 47, pp. 477-86.
- Buckwalter, J. A., Martin, J. A., Olmstead, M., Athanasiou, K. A., Rosenwasser, M. P. and Mow, V. C. (2003) 'Osteochondral repair of primate knee femoral and patellar articular surfaces: implications for preventing post-traumatic osteoarthritis', *Iowa Orthop J*, 23, pp. 66-74.
- Buckwalter, J. A., Mow, V. C. and Ratcliffe, A. (1994) 'Restoration of Injured or Degenerated Articular Cartilage', *J Am Acad Orthop Surg*, 2(4), pp. 192-201.
- Buenzli, P. R., Lanaro, M., Wong, C. S., McLaughlin, M. P., Allenby, M. C., Woodruff, M. A. and Simpson, M. J. (2020) 'Cell proliferation and migration explain pore bridging dynamics in 3D printed scaffolds of different pore size', *Acta Biomaterialia*, 114, pp. 285-295.
- Buffington, S. L., Paul, J. E., Ali, M. M., Macios, M. M., Mather, P. T. and Henderson, J. H. (2019) 'Enzymatically triggered shape memory polymers', *Acta Biomaterialia*, 84, pp. 88-97.
- Burg, K. J. L., Holder Jr, W. D., Culberson, C. R., Beiler, R. J., Greene, K. G., Loeb sack, A. B., Roland, W. D., Eiselt, P., Mooney, D. J. and Halberstadt, C. R. (2000) 'Comparative study of seeding methods for three-dimensional polymeric scaffolds', *Journal of Biomedical Materials Research*, 51(4), pp. 642-649.
- Cameron, M. L., Briggs, K. K. and Steadman, J. R. (2003) 'Reproducibility and reliability of the outerbridge classification for grading chondral lesions of the knee arthroscopically', *Am J Sports Med*, 31(1), pp. 83-6.
- Camp, C. L., Stuart, M. J. and Krych, A. J. (2013) 'Current Concepts of Articular Cartilage Restoration Techniques in the Knee', *Sports Health*, 6(3), pp. 265-273.
- Cao, Y. and Wang, B. (2009) 'Biodegradation of silk biomaterials', *Int J Mol Sci*, 10(4), pp. 1514-24.
- Capito, R. M. and Spector, M. (2003) 'Scaffold-based articular cartilage repair', *IEEE Eng Med Biol Mag*, 22(5), pp. 42-50.
- Cassiede, P., Dennis, J. E., Ma, F. and Caplan, A. I. (1996) 'Osteochondrogenic potential of marrow mesenchymal progenitor cells exposed to TGF-beta 1 or PDGF-BB as assayed in vivo and in vitro', *J Bone Miner Res*, 11(9), pp. 1264-73.
- Castro, N. J., Hacking, S. A. and Zhang, L. G. (2012) 'Recent progress in interfacial tissue engineering approaches for osteochondral defects', *Ann Biomed Eng*, 40(8), pp. 1628-40.
- Castro, N. J., O'Brien, J. and Zhang, L. G. (2015) 'Integrating biologically inspired nanomaterials and table-top stereolithography for 3D printed biomimetic osteochondral scaffolds', *Nanoscale*, 7(33), pp. 14010-14022.
- Cengiz, I. F., Pereira, H., Espregueira-Mendes, J., Kwon, I. K., Reis, R. L. and Oliveira, J. M. (2019) 'Suturable regenerated silk fibroin scaffold reinforced with 3D-printed polycaprolactone mesh: biomechanical performance and subcutaneous implantation', *Journal of Materials Science: Materials in Medicine*, 30(6), pp. 63.

- Cengiz, I. F., Pereira, H., Espregueira-Mendes, J., Oliveira, J. M. and Reis, R. L. (2017) 'Treatments of Meniscus Lesions of the Knee: Current Concepts and Future Perspectives', *Regenerative Engineering and Translational Medicine*, 3(1), pp. 32-50.
- Chahal, J., Gross, A. E., Gross, C., Mall, N., Dwyer, T., Chahal, A., Whelan, D. B. and Cole, B. J. (2013) 'Outcomes of osteochondral allograft transplantation in the knee', *Arthroscopy*, 29(3), pp. 575-88.
- Chang, C. H., Lin, F. H., Lin, C. C., Chou, C. H. and Liu, H. C. (2004) 'Cartilage tissue engineering on the surface of a novel gelatin-calcium-phosphate biphasic scaffold in a double-chamber bioreactor', *J Biomed Mater Res B Appl Biomater*, 71(2), pp. 313-21.
- Chang, L. R., K, O. C. and Martin, A. (2020) 'Anatomy, Cartilage', *StatPearls*. Treasure Island (FL): StatPearls Publishing
- Copyright © 2020, StatPearls Publishing LLC.
- Chen, C., Huang, B., Liu, Y., Liu, F. and Lee, I.-S. (2023a) 'Functional engineering strategies of 3D printed implants for hard tissue replacement', *Regenerative Biomaterials*, 10, pp. rbac094.
- Chen, H., Sun, J., Hoemann, C. D., Lascau-Coman, V., Ouyang, W., McKee, M. D., Shive, M. S. and Buschmann, M. D. (2009) 'Drilling and microfracture lead to different bone structure and necrosis during bone-marrow stimulation for cartilage repair', *Journal of orthopaedic research : official publication of the Orthopaedic Research Society*, 27(11), pp. 1432-1438.
- Chen, K., Li, Y., Li, Y., Pan, W. and Tan, G. (2023b) 'Silk Fibroin Combined with Electrospinning as a Promising Strategy for Tissue Regeneration', *Macromolecular Bioscience*, 23(2), pp. 2200380.
- Chen, K., Teh, T. K. H., Ravi, S., Toh, S. L. and Goh, J. C. H. (2012) 'Osteochondral Interface Generation by Rabbit Bone Marrow Stromal Cells and Osteoblasts Coculture', *Tissue Engineering Part A*, 18(17-18), pp. 1902-1911.
- Chen, L., Wei, L., Su, X., Qin, L., Xu, Z., Huang, X., Chen, H. and Hu, N. (2023c) 'Preparation and Characterization of Biomimetic Functional Scaffold with Gradient Structure for Osteochondral Defect Repair', *Bioengineering*, 10(2). DOI: 10.3390/bioengineering10020213.
- Chen, T., Hilton, M. J., Brown, E. B., Zuscik, M. J. and Awad, H. A. (2013) 'Engineering superficial zone features in tissue engineered cartilage', *Biotechnol Bioeng*, 110(5), pp. 1476-86.
- Cheng, A., Schwartz, Z., Kahn, A., Li, X., Shao, Z., Sun, M., Ao, Y., Boyan, B. D. and Chen, H. (2018) 'Advances in Porous Scaffold Design for Bone and Cartilage Tissue Engineering and Regeneration', *Tissue Engineering Part B: Reviews*, 25(1), pp. 14-29.
- Chimutengwende-Gordon, M., Donaldson, J. and Bentley, G. (2020) 'Current solutions for the treatment of chronic articular cartilage defects in the knee', *EFORT Open Rev*, 5(3), pp. 156-163.
- Choi, J. H., Kim, D. K., Song, J. E., Oliveira, J. M., Reis, R. L. and Khang, G. (2018) 'Silk Fibroin-Based Scaffold for Bone Tissue Engineering', *Adv Exp Med Biol*, 1077, pp. 371-387.
- Chraniuk, M., Panasiuk, M., Hovhannisyan, L., Żołądowska, S., Nidzworski, D., Ciołek, L., Woźniak, A., Kubiś, A., Karska, N., Jaegermann, Z., Rodziejewicz-Motowidło, S., Biernat, M. and Gromadzka, B. (2022) 'Assessment of the Toxicity of Biocompatible Materials Supporting Bone Regeneration: Impact of the Type of Assay and Used Controls', *Toxics*, 10(1), pp. 20.

- Christensen, B. B., Foldager, C. B., Olesen, M. L., Vingtoft, L., Rölfing, J. H. D., Ringgaard, S. and Lind, M. (2015) 'Experimental articular cartilage repair in the Göttingen minipig: the influence of multiple defects per knee', *Journal of Experimental Orthopaedics*, 2(1), pp. 13.
- Chu, C. R. (2001) 'Chondral and osteochondral injuries: Mechanisms of injury and repair responses', *Operative Techniques in Orthopaedics*, 11(2), pp. 70-75.
- Chu, C. R., Szczodry, M. and Bruno, S. (2009) 'Animal Models for Cartilage Regeneration and Repair', *Tissue Engineering Part B: Reviews*, 16(1), pp. 105-115.
- Cicotte, K. N., Reed, J. A., Nguyen, P. A. H., De Lora, J. A., Hedberg-Dirk, E. L. and Canavan, H. E. (2017) 'Optimization of electrospun poly(N-isopropyl acrylamide) mats for the rapid reversible adhesion of mammalian cells', *Biointerphases*, 12(2), pp. 02C417.
- Collins, K. L., Gates, E. M., Gilchrist, C. L. and Hoffman, B. D. (2017) 'Chapter 1 - Bio-Instructive Cues in Scaffolds for Musculoskeletal Tissue Engineering and Regenerative Medicine', in Brown, J.L., Kumbar, S.G. and Banik, B.L. (eds.) *Bio-Instructive Scaffolds for Musculoskeletal Tissue Engineering and Regenerative Medicine*: Academic Press, pp. 3-35.
- Colombini, A., Libonati, F., Lopa, S., Peretti, G. M., Moretti, M. and de Girolamo, L. (2023) 'Autologous chondrocyte implantation provides good long-term clinical results in the treatment of knee osteoarthritis: a systematic review', *Knee Surgery, Sports Traumatology, Arthroscopy*, 31(6), pp. 2338-2348.
- Costa, A., Naranjo, J. D., Londono, R. and Badylak, S. F. (2017) 'Biologic Scaffolds', *Cold Spring Harbor Perspectives in Medicine*, 7(9).
- Courtenay, J. C., Johns, M. A., Galembeck, F., Deneke, C., Lanzoni, E. M., Costa, C. A., Scott, J. L. and Sharma, R. I. (2017) 'Surface modified cellulose scaffolds for tissue engineering', *Cellulose*, 24(1), pp. 253-267.
- Craig, C. L. (1997) 'Evolution of arthropod silks', *Annu Rev Entomol*, 42, pp. 231-67.
- Cross, L. M., Thakur, A., Jalili, N. A., Detamore, M. and Gaharwar, A. K. (2016) 'Nanoengineered biomaterials for repair and regeneration of orthopedic tissue interfaces', *Acta Biomaterialia*, 42, pp. 2-17.
- da Silva Morais, A., Oliveira, J. M. and Reis, R. L. (2018) 'Small Animal Models', in Oliveira, J.M., Pina, S., Reis, R.L. and San Roman, J. (eds.) *Osteochondral Tissue Engineering: Challenges, Current Strategies, and Technological Advances*. Cham: Springer International Publishing, pp. 423-439.
- Dahlin, R. L., Kasper, F. K. and Mikos, A. G. (2011) 'Polymeric nanofibers in tissue engineering', *Tissue Eng Part B Rev*, 17(5), pp. 349-64.
- Dai, Z., Ronholm, J., Tian, Y., Sethi, B. and Cao, X. (2016) 'Sterilization techniques for biodegradable scaffolds in tissue engineering applications', *Journal of Tissue Engineering*, 7, pp. 2041731416648810.
- Darouiche, R. O. (2004) 'Treatment of Infections Associated with Surgical Implants', *New England Journal of Medicine*, 350(14), pp. 1422-1429.
- Datko Williams, L., Farley, A., Cupelli, M., Alapati, S., Kennedy, M. S. and Dean, D. (2018) 'Effects of substrate stiffness on dental pulp stromal cells in culture', *Journal of Biomedical Materials Research Part A*, 106(7), pp. 1789-1797.
- Davies, L. C., Blain, E. J., Gilbert, S. J., Caterson, B. and Duance, V. C. (2008) 'The Potential of IGF-1 and TGF $\beta$ 1 for Promoting "Adult" Articular Cartilage Repair: An In Vitro Study', *Tissue Engineering Part A*, 14(7), pp. 1251-1261.
- de Terris, T., Andreau, O., Peyre, P., Adamski, F., Koutiri, I., Gorny, C. and Dupuy, C. (2019) 'Optimization and comparison of porosity rate measurement

- methods of Selective Laser Melted metallic parts', *Additive Manufacturing*, 28, pp. 802-813.
- Dell'accio, F. and Vincent, T. L. (2010) 'Joint surface defects: clinical course and cellular response in spontaneous and experimental lesions', *Eur Cell Mater*, 20, pp. 210-7.
- Deng, C., Chang, J. and Wu, C. (2019) 'Bioactive scaffolds for osteochondral regeneration', *J Orthop Translat*, 17, pp. 15-25.
- Derfoul, A., Perkins, G. L., Hall, D. J. and Tuan, R. S. (2006) 'Glucocorticoids Promote Chondrogenic Differentiation of Adult Human Mesenchymal Stem Cells by Enhancing Expression of Cartilage Extracellular Matrix Genes', *Stem Cells*, 24(6), pp. 1487-1495.
- Deschamps, A. A., van Apeldoorn, A. A., Hayen, H., de Bruijn, J. D., Karst, U., Grijpma, D. W. and Feijen, J. (2004) 'In vivo and in vitro degradation of poly(ether ester) block copolymers based on poly(ethylene glycol) and poly(butylene terephthalate)', *Biomaterials*, 25(2), pp. 247-258.
- Di Luca, A., Klein-Gunnewiek, M., Vancso, J. G., van Blitterswijk, C. A., Benetti, E. M. and Moroni, L. (2017) 'Covalent Binding of Bone Morphogenetic Protein-2 and Transforming Growth Factor- $\beta$ 3 to 3D Plotted Scaffolds for Osteochondral Tissue Regeneration', *Biotechnology Journal*, 12(12), pp. 1700072.
- Dias, I. R., Viegas, C. A. and Carvalho, P. P. (2018) 'Large Animal Models for Osteochondral Regeneration', in Oliveira, J.M., Pina, S., Reis, R.L. and San Roman, J. (eds.) *Osteochondral Tissue Engineering: Challenges, Current Strategies, and Technological Advances*. Cham: Springer International Publishing, pp. 441-501.
- Diederichs, S., Gabler, J., Autenrieth, J., Kynast, K. L., Merle, C., Walles, H., Utikal, J. and Richter, W. (2016) 'Differential Regulation of SOX9 Protein During Chondrogenesis of Induced Pluripotent Stem Cells Versus Mesenchymal Stromal Cells: A Shortcoming for Cartilage Formation', *Stem Cells and Development*, 25(8), pp. 598-609.
- Discher, D. E., Janmey, P. and Wang, Y.-I. (2005) 'Tissue Cells Feel and Respond to the Stiffness of Their Substrate', *Science*, 310(5751), pp. 1139-1143.
- Do, A. V., Khorsand, B., Geary, S. M. and Salem, A. K. (2015) '3D Printing of Scaffolds for Tissue Regeneration Applications', *Adv Healthc Mater*, 4(12), pp. 1742-62.
- Dormer, N. H., Berkland, C. J. and Detamore, M. S. (2010) 'Emerging Techniques in Stratified Designs and Continuous Gradients for Tissue Engineering of Interfaces', *Annals of Biomedical Engineering*, 38(6), pp. 2121-2141.
- Du, Y., Liu, H., Yang, Q., Wang, S., Wang, J., Ma, J., Noh, I., Mikos, A. G. and Zhang, S. (2017) 'Selective laser sintering scaffold with hierarchical architecture and gradient composition for osteochondral repair in rabbits', *Biomaterials*, 137, pp. 37-48.
- Echeverria Molina, M. I., Malollari, K. G. and Komvopoulos, K. (2021) 'Design Challenges in Polymeric Scaffolds for Tissue Engineering', *Frontiers in Bioengineering and Biotechnology*, 9.
- Eckstein, F., Lemberger, B., Gratzke, C., Hudelmaier, M., Glaser, C., Englmeier, K. H. and Reiser, M. (2005) 'In vivo cartilage deformation after different types of activity and its dependence on physical training status', *Ann Rheum Dis*, 64(2), pp. 291-5.

- Eckstein, F., Lemberger, B., Stammberger, T., Englmeier, K. H. and Reiser, M. (2000) 'Patellar cartilage deformation in vivo after static versus dynamic loading', *J Biomech*, 33(7), pp. 819-25.
- Egan, P., Wang, X., Greutert, H., Shea, K., Wuertz-Kozak, K. and Ferguson, S. (2019) 'Mechanical and Biological Characterization of 3D Printed Lattices', *3D Printing and Additive Manufacturing*, 6(2), pp. 73-81.
- Egan, P. F. (2019) 'Integrated Design Approaches for 3D Printed Tissue Scaffolds: Review and Outlook', *Materials (Basel)*, 12(15).
- Engler, A. J., Sen, S., Sweeney, H. L. and Discher, D. E. (2006) 'Matrix Elasticity Directs Stem Cell Lineage Specification', *Cell*, 126(4), pp. 677-689.
- Enochson, L., Brittberg, M. and Lindahl, A. (2012) 'Optimization of a Chondrogenic Medium Through the Use of Factorial Design of Experiments', *BioResearch Open Access*, 1(6), pp. 306-313.
- Fahmy, M. D., Shah, B., Razavi, M., Jazayeri, H., Fahimipour, F., White, J., Masri, R. and Tayebi, L. (2017) *Smart Biomaterials for Tissue Engineering of Cartilage*. Royal Society of Chemistry.
- Fakirov, S. and Gogeva, T. (1990a) 'Poly(ether/ester)s based on poly(butylene terephthalate) and poly(ethylene glycol), 1. Poly(ether/ester)s with various polyether: polyester ratios', *Die Makromolekulare Chemie*, 191(3), pp. 603-614.
- Fakirov, S. and Gogeva, T. (1990b) 'Poly(ether/ester)s based on poly(butylene terephthalate) and poly(ethylene glycol), 2. Effect of polyether segment length', *Die Makromolekulare Chemie*, 191(3), pp. 615-624.
- Filippi, M., Born, G., Chaaban, M. and Scherberich, A. (2020) 'Natural Polymeric Scaffolds in Bone Regeneration', *Frontiers in Bioengineering and Biotechnology*, 8.
- Fisher, M. B., Belkin, N. S., Milby, A. H., Henning, E. A., Bostrom, M., Kim, M., Pfeifer, C., Meloni, G., Dodge, G. R., Burdick, J. A., Schaer, T. P., Steinberg, D. R. and Mauck, R. L. (2014) 'Cartilage Repair and Subchondral Bone Remodeling in Response to Focal Lesions in a Mini-Pig Model: Implications for Tissue Engineering', *Tissue Engineering Part A*, 21(3-4), pp. 850-860.
- Fleming, B. C., Hulstyn, M. J., Oksendahl, H. L. and Fadale, P. D. (2005) 'Ligament Injury, Reconstruction and Osteoarthritis', *Current opinion in orthopaedics*, 16(5), pp. 354.
- Forman, S., Ká's, J., Fini, F., Steinberg, M. and Ruml, T. (1999) 'The effect of different solvents on the ATP/ADP content and growth properties of HeLa cells', *Journal of Biochemical and Molecular Toxicology*, 13(1), pp. 11-15.
- Formica, F. A., Öztürk, E., Hess, S. C., Stark, W. J., Maniura-Weber, K., Rottmar, M. and Zenobi-Wong, M. (2016) 'A Bioinspired Ultraporous Nanofiber-Hydrogel Mimic of the Cartilage Extracellular Matrix', *Adv Healthc Mater*, 5(24), pp. 3129-3138.
- Foschi, D., Corsi, F., Cellerino, P., Rizzi, A., Morandi, E. and Trabucchi, E. (2001) 'Angiogenic effects of suture biomaterials: An experimental study in rats', *European Surgical Research*, 33(1), pp. 16-20.
- Francis, S. L., Di Bella, C., Wallace, G. G. and Choong, P. F. M. (2018) 'Cartilage Tissue Engineering Using Stem Cells and Bioprinting Technology-Barriers to Clinical Translation', *Front Surg*, 5, pp. 70.
- Frenkel, S. and Di Cesare, P. (2004) 'Scaffolds for Articular Cartilage Repair', *Annals of Biomedical Engineering*, 32(1), pp. 26-34.
- Frisbie, D. D., Cross, M. W. and McIlwraith, C. W. (2006) 'A comparative study of articular cartilage thickness in the stifle of animal species used in human

- pre-clinical studies compared to articular cartilage thickness in the human knee', *Vet Comp Orthop Traumatol*, 19(03), pp. 142-146.
- Fu, L., Zhao, W., Zhang, L., Gao, C., Zhang, X., Yang, X. and Cai, Q. (2022) 'Mimicking osteochondral interface using pre-differentiated BMSCs/fibrous mesh complexes to promote tissue regeneration', *Journal of Biomaterials Science, Polymer Edition*, 33(16), pp. 2081-2103.
- Fukui, T., Kitamura, N., Kurokawa, T., Yokota, M., Kondo, E., Gong, J. P. and Yasuda, K. (2014) 'Intra-articular administration of hyaluronic acid increases the volume of the hyaline cartilage regenerated in a large osteochondral defect by implantation of a double-network gel', *J Mater Sci Mater Med*, 25(4), pp. 1173-82.
- Furukawa, T., Eyre, D. R., Koide, S. and Glimcher, M. J. (1980) 'Biochemical studies on repair cartilage resurfacing experimental defects in the rabbit knee', *J Bone Joint Surg Am*, 62(1), pp. 79-89.
- Gademan, M. G., Hofstede, S. N., Vliet Vlieland, T. P., Nelissen, R. G. and Marangvan de Mheen, P. J. (2016) 'Indication criteria for total hip or knee arthroplasty in osteoarthritis: a state-of-the-science overview', *BMC Musculoskelet Disord*, 17(1), pp. 463.
- Gao, J., Dennis, J. E., Solchaga, L. A., Awadallah, A. S., Goldberg, V. M. and Caplan, A. I. (2001) 'Tissue-engineered fabrication of an osteochondral composite graft using rat bone marrow-derived mesenchymal stem cells', *Tissue Eng*, 7(4), pp. 363-71.
- Gao, L.-L., Lin, X.-L., Liu, D.-D., Chen, L., Zhang, C.-Q. and Gao, H. (2019) 'Depth-dependent ratcheting strains of young and adult articular cartilages by experiments and predictions', *BioMedical Engineering OnLine*, 18(1), pp. 85.
- Gartsman, G. M. and Taverna, E. (1997) 'The incidence of glenohumeral joint abnormalities associated with full-thickness, reparable rotator cuff tears', *Arthroscopy*, 13(4), pp. 450-5.
- Gavazzo, P., Viti, F., Donnelly, H., Oliva, M. A. G., Salmeron-Sanchez, M., Dalby, M. J. and Vassalli, M. (2021) 'Biophysical phenotyping of mesenchymal stem cells along the osteogenic differentiation pathway', *Cell Biology and Toxicology*, 37(6), pp. 915-933.
- Ge, Z., Li, C., Heng, B. C., Cao, G. and Yang, Z. (2012) 'Functional biomaterials for cartilage regeneration', *J Biomed Mater Res A*, 100(9), pp. 2526-36.
- Geiger, M., Li, R. H. and Friess, W. (2003) 'Collagen sponges for bone regeneration with rhBMP-2', *Advanced Drug Delivery Reviews*, 55(12), pp. 1613-1629.
- Getgood, A., Brooks, R., Fortier, L. and Rushton, N. (2009) 'Articular cartilage tissue engineering: today's research, tomorrow's practice?', *J Bone Joint Surg Br*, 91(5), pp. 565-76.
- Gomoll, A. H. and Minas, T. (2014) 'The quality of healing: articular cartilage', *Wound Repair Regen*, 22 Suppl 1, pp. 30-8.
- González Vázquez, A. G., Blokpoel Ferreras, L. A., Bennett, K. E., Casey, S. M., Brama, P. A. J. and O'Brien, F. J. (2021) 'Systematic Comparison of Biomaterials-Based Strategies for Osteochondral and Chondral Repair in Large Animal Models', *Advanced Healthcare Materials*, 10(20), pp. 2100878.
- Gorbachova, T., Melenevsky, Y., Cohen, M. and Cerniglia, B. W. (2018) 'Osteochondral Lesions of the Knee: Differentiating the Most Common Entities at MRI', *Radiographics*, 38(5), pp. 1478-1495.

- Gratz, K. R., Wong, B. L., Bae, W. C. and Sah, R. L. (2009) 'The effects of focal articular defects on cartilage contact mechanics', *J Orthop Res*, 27(5), pp. 584-92.
- Grayson, W. L., Chao, P.-H. G., Marolt, D., Kaplan, D. L. and Vunjak-Novakovic, G. (2008) 'Engineering custom-designed osteochondral tissue grafts', *Trends in Biotechnology*, 26(4), pp. 181-189.
- Grenier, S., Bhargava, M. M. and Torzilli, P. A. (2014) 'An in vitro model for the pathological degradation of articular cartilage in osteoarthritis', *J Biomech*, 47(3), pp. 645-52.
- Grote, J. J. (1990) 'Reconstruction of the middle ear with hydroxylapatite implants: long-term results', *Ann Otol Rhinol Laryngol Suppl*, 144, pp. 12-6.
- Gu, M., Fan, S., Zhou, G., Ma, K., Yao, X. and Zhang, Y. (2022) 'Effects of dynamic mechanical stimulations on the regeneration of in vitro and in vivo cartilage tissue based on silk fibroin scaffold', *Composites Part B: Engineering*, 235, pp. 109764.
- Gugjoo, M. B., Amarpal, Abdelbaset-Ismael, A., Aithal, H. P., Kinjavdekar, P., Pawde, A. M., Kumar, G. S. and Sharma, G. T. (2017) 'Mesenchymal stem cells with IGF-1 and TGF-  $\beta$ 1 in laminin gel for osteochondral defects in rabbits', *Biomedicine & Pharmacotherapy*, 93, pp. 1165-1174.
- Guilak, F., Butler, D. L. and Goldstein, S. A. (2001) 'Functional tissue engineering: the role of biomechanics in articular cartilage repair', *Clin Orthop Relat Res*, (391 Suppl), pp. S295-305.
- Guo, Z., Iku, S., Mu, L., Wang, Y., Shima, T., Seki, Y., Li, Q. and Kuboki, Y. (2013) 'Implantation with new three-dimensional porous titanium web for treatment of parietal bone defect in rabbit', *Artif Organs*, 37(7), pp. 623-8.
- Gushue, D. L., Houck, J. and Lerner, A. L. (2005) 'Rabbit knee joint biomechanics: Motion analysis and modeling of forces during hopping', *Journal of Orthopaedic Research*, 23(4), pp. 735-742.
- Götz, H. E., Müller, M., Emmel, A., Holzwarth, U., Erben, R. G. and Stangl, R. (2004) 'Effect of surface finish on the osseointegration of laser-treated titanium alloy implants', *Biomaterials*, 25(18), pp. 4057-64.
- Günther, T., Rücker, M., Förster, C., Vormann, J. and Stahlmann, R. (1997) 'In vitro evidence for a Donnan distribution of Mg<sup>2+</sup> and Ca<sup>2+</sup> by chondroitin sulphate in cartilage', *Arch Toxicol*, 71(7), pp. 471-5.
- Hangody, L., Kish, G., Modis, L., Szerb, I., Gaspar, L., Dioszegi, Z. and Kendik, Z. (2001) 'Mosaicplasty for the treatment of osteochondritis dissecans of the talus: two to seven year results in 36 patients', *Foot Ankle Int*, 22(7), pp. 552-8.
- Hangody, L., Vásárhelyi, G., Hangody, L. R., Sükösd, Z., Tibay, G., Bartha, L. and Bodó, G. (2008) 'Autologous osteochondral grafting--technique and long-term results', *Injury*, 39 Suppl 1, pp. S32-9.
- Hatano, K., Inoue, H., Kojo, T., Matsunaga, T., Tsujisawa, T., Uchiyama, C. and Uchida, Y. (1999) 'Effect of surface roughness on proliferation and alkaline phosphatase expression of rat calvarial cells cultured on polystyrene', *Bone*, 25(4), pp. 439-445.
- Hayes, D. W., Jr., Brower, R. L. and John, K. J. (2001) 'Articular cartilage. Anatomy, injury, and repair', *Clin Podiatr Med Surg*, 18(1), pp. 35-53.
- He, Y., Manon-Jensen, T., Arendt-Nielsen, L., Pedersen, K. K., Christiansen, T., Samuels, J., Abramson, S., Karsdal, M. K., Mukundan, A. and Bay-Jensen, A. C. (2018) 'A biomarker of hypertrophic chondrocytes, type X collagen,

- completely distinguishes between OA and RA', *Osteoarthritis and Cartilage*, 26, pp. S175-S176.
- Helgeland, E., Shanbhag, S., Pedersen, T. O., Mustafa, K. and Rosén, A. (2018) 'Scaffold-Based Temporomandibular Joint Tissue Regeneration in Experimental Animal Models: A Systematic Review' An abstract of this article was presented as a poster, at The Bergen Stem Cell Consortium (BSCC), Annual meeting, Bergen, Norway, September 3–4, 2017', *Tissue Engineering Part B: Reviews*, 24(4), pp. 300-316.
- Hersel, U., Dahmen, C. and Kessler, H. (2003) 'RGD modified polymers: biomaterials for stimulated cell adhesion and beyond', *Biomaterials*, 24(24), pp. 4385-4415.
- Ho, S. T. and Hutmacher, D. W. (2006) 'A comparison of micro CT with other techniques used in the characterization of scaffolds', *Biomaterials*, 27(8), pp. 1362-1376.
- Hoemann, C., Kandel, R., Roberts, S., Saris, D. B., Creemers, L., Mainil-Varlet, P., Méthot, S., Hollander, A. P. and Buschmann, M. D. (2011) 'International Cartilage Repair Society (ICRS) Recommended Guidelines for Histological Endpoints for Cartilage Repair Studies in Animal Models and Clinical Trials', *Cartilage*, 2(2), pp. 153-72.
- Hofmann, A., Konrad, L., Gotzen, L., Printz, H., Ramaswamy, A. and Hofmann, C. (2003) 'Bioengineered human bone tissue using autogenous osteoblasts cultured on different biomatrices', *Journal of Biomedical Materials Research Part A*, 67A(1), pp. 191-199.
- Holmes, N. E., Turnidge, J. D., Munckhof, W. J., Robinson, J. O., Korman, T. M., O'Sullivan, M. V. N., Anderson, T. L., Roberts, S. A., Warren, S. J. C., Coombs, G. W., Tan, H.-L., Gao, W., Johnson, P. D. R. and Howden, B. P. (2014) 'Genetic and Molecular Predictors of High Vancomycin MIC in Staphylococcus aureus Bacteremia Isolates', *Journal of Clinical Microbiology*, 52(9), pp. 3384-3393.
- Hori, Y., Inoue, S., Hirano, Y. and Tabata, Y. (2004) 'Effect of Culture Substrates and Fibroblast Growth Factor Addition on the Proliferation and Differentiation of Rat Bone Marrow Stromal Cells', *Tissue Engineering*, 10(7-8), pp. 995-1005.
- Hu, J. C. and Athanasiou, K. A. (2006) 'A self-assembling process in articular cartilage tissue engineering', *Tissue Eng*, 12(4), pp. 969-79.
- Hu, X., Shmelev, K., Sun, L., Gil, E. S., Park, S. H., Cebe, P. and Kaplan, D. L. (2011) 'Regulation of silk material structure by temperature-controlled water vapor annealing', *Biomacromolecules*, 12(5), pp. 1686-96.
- Huang, L., Quesada, C., Aliabouzar, M., Fowlkes, J. B., Franceschi, R. T., Liu, Z., Putnam, A. J. and Fabiilli, M. L. (2021) 'Spatially-directed angiogenesis using ultrasound-controlled release of basic fibroblast growth factor from acoustically-responsive scaffolds', *Acta Biomaterialia*, 129, pp. 73-83.
- Huber, M., Trattng, S. and Lintner, F. (2000) 'Anatomy, Biochemistry, and Physiology of Articular Cartilage', *Investigative Radiology*, 35(10), pp. 573-580.
- Huey, D., Hu, J. and Athanasiou, K. (2012) 'Unlike Bone, Cartilage Regeneration Remains Elusive', *Science*, 338(6109), pp. 917-921.
- Hui, W., Rowan, A. D. and Cawston, T. (2001) 'MODULATION OF THE EXPRESSION OF MATRIX METALLOPROTEINASE AND TISSUE INHIBITORS OF METALLOPROTEINASES BY TGF- $\beta$ 1 AND IGF-1 IN PRIMARY HUMAN

- ARTICULAR AND BOVINE NASAL CHONDROCYTES STIMULATED WITH TNF- $\alpha$ ', *Cytokine*, 16(1), pp. 31-35.
- Hunziker, E. B., Lippuner, K., Keel, M. J. B. and Shintani, N. (2014) 'An educational review of cartilage repair: precepts & practice – myths & misconceptions – progress & prospects', *Osteoarthritis and Cartilage*, 23(3), pp. 334-350.
- Hutmacher, D. W. (2000) 'Scaffolds in tissue engineering bone and cartilage', *Biomaterials*, 21(24), pp. 2529-2543.
- Huvneers, S. and Danen, E. H. J. (2009) 'Adhesion signaling – crosstalk between integrins, Src and Rho', *Journal of Cell Science*, 122(8), pp. 1059-1069.
- Inoue, S., Tanaka, K., Arisaka, F., Kimura, S., Ohtomo, K. and Mizuno, S. (2000) 'Silk fibroin of Bombyx mori is secreted, assembling a high molecular mass elementary unit consisting of H-chain, L-chain, and P25, with a 6:6:1 molar ratio', *J Biol Chem*, 275(51), pp. 40517-28.
- Iqbal, N., Braxton, T. M., Anastasiou, A., Raif, E. M., Chung, C. K. Y., Kumar, S., Giannoudis, P. V. and Jha, A. (2022) 'Dicalcium Phosphate Dihydrate Mineral Loaded Freeze-Dried Scaffolds for Potential Synthetic Bone Applications', *Materials*, 15(18), pp. 6245.
- Izadifar, Z., Chen, X. and Kulyk, W. (2012) 'Strategic design and fabrication of engineered scaffolds for articular cartilage repair', *J Funct Biomater*, 3(4), pp. 799-838.
- Jackson, D. W., Lalor, P. A., Aberman, H. M. and Simon, T. M. (2001) 'Spontaneous repair of full-thickness defects of articular cartilage in a goat model. A preliminary study', *J Bone Joint Surg Am*, 83(1), pp. 53-64.
- Jackson, M. and Mantsch, H. H. (1995) 'The use and misuse of FTIR spectroscopy in the determination of protein structure', *Critical Reviews in Biochemistry and Molecular Biology*, (1040-9238 (Print)).
- Jacobs, J. J., Hallab, N. J., Urban, R. M. and Wimmer, M. A. (2006) 'Wear particles', *J Bone Joint Surg Am*, 88 Suppl 2, pp. 99-102.
- Jang, S., Lee, K. and Ju, J. H. (2021) 'Recent Updates of Diagnosis, Pathophysiology, and Treatment on Osteoarthritis of the Knee', *International Journal of Molecular Sciences*, 22(5), pp. 2619.
- Jansen, K. A., Atherton, P. and Ballestrom, C. (2017) 'Mechanotransduction at the cell-matrix interface', *Seminars in Cell & Developmental Biology*, 71, pp. 75-83.
- Jeffrey, J. E., Thomson, L. A. and Aspden, R. M. (1997) 'Matrix loss and synthesis following a single impact load on articular cartilage in vitro', *BBA - General Subjects*, 1334(2), pp. 223-232.
- Ji, S. and Guvendiren, M. (2019) '3D Printed Wavy Scaffolds Enhance Mesenchymal Stem Cell Osteogenesis', *Micromachines (Basel)*, 11(1).
- Jia, L., Zhang, P., Ci, Z., Zhang, W., Liu, Y., Jiang, H. and Zhou, G. (2021) 'Immune-Inflammatory Responses of an Acellular Cartilage Matrix Biomimetic Scaffold in a Xenotransplantation Goat Model for Cartilage Tissue Engineering', *Frontiers in Bioengineering and Biotechnology*, 9.
- Jiang, J., Nicoll, S. B. and Lu, H. H. (2005) 'Co-culture of osteoblasts and chondrocytes modulates cellular differentiation in vitro', *Biochemical and Biophysical Research Communications*, 338(2), pp. 762-770.
- Jiang, Y. and Tuan, R. S. (2015) 'Origin and function of cartilage stem/progenitor cells in osteoarthritis', *Nat Rev Rheumatol*, 11(4), pp. 206-12.
- Johnson, C. T. and García, A. J. (2015) 'Scaffold-based Anti-infection Strategies in Bone Repair', *Annals of Biomedical Engineering*, 43(3), pp. 515-528.

- Johnstone, B., Hering, T. M., Caplan, A. I., Goldberg, V. M. and Yoo, J. U. (1998) 'In vitro chondrogenesis of bone marrow-derived mesenchymal progenitor cells', *Exp Cell Res*, 238(1), pp. 265-72.
- Jones, C. W., Willers, C., Keogh, A., Smolinski, D., Fick, D., Yates, P. J., Kirk, T. B. and Zheng, M. H. (2008) 'Matrix-induced autologous chondrocyte implantation in sheep: objective assessments including confocal arthroscopy', *J Orthop Res*, 26(3), pp. 292-303.
- Jones, J. R., Lee, P. D. and Hench, L. L. (2006) 'Hierarchical porous materials for tissue engineering', *Philos Trans A Math Phys Eng Sci*, 364(1838), pp. 263-81.
- Joukhdar, H., Och, Z., Tran, H., Heu, C., Vasquez, G. M., Sultana, N., Stevens, M., Dokos, S., Lim, K. S., Lord, M. S. and Rnjak-Kovacina, J. (2023) 'Imparting Multi-Scalar Architectural Control into Silk Materials Using a Simple Multi-Functional Ice-Templating Fabrication Platform', *Advanced Materials Technologies*, n/a(n/a), pp. 2201642.
- Kainer, M. A., Linden, J. V., Whaley, D. N., Holmes, H. T., Jarvis, W. R., Jernigan, D. B. and Archibald, L. K. (2004) 'Clostridium infections associated with musculoskeletal-tissue allografts', *New England Journal of Medicine*, 350(25), pp. 2564-2571.
- Kajitani, K., Ochi, M., Uchio, Y., Adachi, N., Kawasaki, K., Katsube, K., Maniwa, S., Furukawa, S. and Kataoka, H. (2004) 'Role of the Periosteal Flap in Chondrocyte Transplantation: An Experimental Study in Rabbits', *Tissue Engineering*, 10(3-4), pp. 331-342.
- Karageorgiou, V. and Kaplan, D. (2005) 'Porosity of 3D biomaterial scaffolds and osteogenesis', *Biomaterials*, 26(27), pp. 5474-91.
- Kawane, T., Qin, X., Jiang, Q., Miyazaki, T., Komori, H., Yoshida, C. A., Matsuura-Kawata, V. K. d. S., Sakane, C., Matsuo, Y., Nagai, K., Maeno, T., Date, Y., Nishimura, R. and Komori, T. (2018) 'Runx2 is required for the proliferation of osteoblast progenitors and induces proliferation by regulating Fgfr2 and Fgfr3', *Scientific Reports*, 8(1), pp. 13551.
- Kellner, K., Schulz, M. B., Göpferich, A. and Blunk, T. (2001) 'Insulin in Tissue Engineering of Cartilage: A Potential Model System for Growth Factor Application', *Journal of Drug Targeting*, 9(6), pp. 439-448.
- Khan, F. and Tanaka, M. (2018) 'Designing Smart Biomaterials for Tissue Engineering', *International Journal of Molecular Sciences*, 19(1). DOI: 10.3390/ijms19010017.
- Kim, B. S., Putnam, A. J., Kulik, T. J. and Mooney, D. J. (1998) 'Optimizing seeding and culture methods to engineer smooth muscle tissue on biodegradable polymer matrices', *Biotechnol Bioeng*, 57(1), pp. 46-54.
- Kim, K., Yeatts, A., Dean, D. and Fisher, J. P. (2010) 'Stereolithographic bone scaffold design parameters: osteogenic differentiation and signal expression', *Tissue Eng Part B Rev*, 16(5), pp. 523-39.
- King, L., March, L. and Anandacoomarasamy, A. (2013) 'Obesity & osteoarthritis', *The Indian Journal of Medical Research*, 138(2), pp. 185-193.
- Kisiday, J. D., Kurz, B., DiMicco, M. A. and Grodzinsky, A. J. (2005) 'Evaluation of Medium Supplemented with Insulin–Transferrin–Selenium for Culture of Primary Bovine Calf Chondrocytes in Three-Dimensional Hydrogel Scaffolds', *Tissue Engineering*, 11(1-2), pp. 141-151.
- Klemenc, J., Šeruga, D., Nagode, A. and Nagode, M. (2019) 'Comprehensive Modelling of the Hysteresis Loops and Strain–Energy Density for Low-Cycle

- Fatigue-Life Predictions of the AZ31 Magnesium Alloy', *Materials*, 12(22). DOI: 10.3390/ma12223692.
- Knetsch, M. L. W. and Koole, L. H. (2011) 'New Strategies in the Development of Antimicrobial Coatings: The Example of Increasing Usage of Silver and Silver Nanoparticles', *Polymers*, 3(1), pp. 340-366.
- Knudson, C. B. and Knudson, W. (2001) 'Cartilage proteoglycans', *Semin Cell Dev Biol*, 12(2), pp. 69-78.
- Koch, T. G. and Betts, D. H. (2007) 'Stem cell therapy for joint problems using the horse as a clinically relevant animal model', *Expert Opinion on Biological Therapy*, 7(11), pp. 1621-1626.
- Koh, J. L., Wirsing, K., Lautenschlager, E. and Zhang, L. O. (2004) 'The effect of graft height mismatch on contact pressure following osteochondral grafting: a biomechanical study', *Am J Sports Med*, 32(2), pp. 317-20.
- Kong, H. J., Polte, T. R., Alsberg, E. and Mooney, D. J. (2005) 'FRET measurements of cell-traction forces and nano-scale clustering of adhesion ligands varied by substrate stiffness', *Proceedings of the National Academy of Sciences*, 102(12), pp. 4300-4305.
- Krishnan, Y. and Grodzinsky, A. J. (2018) 'Cartilage diseases', *Matrix Biol*, 71-72, pp. 51-69.
- Kuboki, Y., Jin, Q. and Takita, H. (2001) 'Geometry of carriers controlling phenotypic expression in BMP-induced osteogenesis and chondrogenesis', *J Bone Joint Surg Am*, 83-A Suppl 1(Pt 2), pp. S105-15.
- Kurzyk, A., Ostrowska, B., Świążkowski, W. and Pojda, Z. (2019) 'Characterization and Optimization of the Seeding Process of Adipose Stem Cells on the Polycaprolactone Scaffolds', *Stem Cells Int*, 2019, pp. 1201927.
- Lamme, E. N., Druেকে, D., Pieper, J., May, P. S., Kaim, P., Jacobsen, F., Steinau, H. U. and Steintraesser, L. (2008) 'Long-term evaluation of porous PEGT/PBT implants for soft tissue augmentation', *J Biomater Appl*, 22(4), pp. 309-35.
- Lawless, B. M., Sadeghi, H., Temple, D. K., Dhaliwal, H., Espino, D. M. and Hukins, D. W. L. (2017) 'Viscoelasticity of articular cartilage: Analysing the effect of induced stress and the restraint of bone in a dynamic environment', *Journal of the Mechanical Behavior of Biomedical Materials*, 75, pp. 293-301.
- Lee, E., Epanomeritakis, I. E., Lu, V. and Khan, W. (2023) 'Bone Marrow-Derived Mesenchymal Stem Cell Implants for the Treatment of Focal Chondral Defects of the Knee in Animal Models: A Systematic Review and Meta-Analysis', *International Journal of Molecular Sciences*, 24(4). DOI: 10.3390/ijms24043227.
- Lee, R. H., Kim, B., Choi, I., Kim, H., Choi, H., Suh, K., Bae, Y. C. and Jung, J. S. (2004) 'Characterization and Expression Analysis of Mesenchymal Stem Cells from Human Bone Marrow and Adipose Tissue', *Cellular Physiology and Biochemistry*, 14(4-6), pp. 311-324.
- Lee, S. H. and Shin, H. (2007) 'Matrices and scaffolds for delivery of bioactive molecules in bone and cartilage tissue engineering', *Adv Drug Deliv Rev*, 59(4-5), pp. 339-59.
- Lefebvre, V. and Dvir-Ginzberg, M. (2017) 'SOX9 and the many facets of its regulation in the chondrocyte lineage', *Connective Tissue Research*, 58(1), pp. 2-14.
- Li, C., Vepari, C., Jin, H.-J., Kim, H. J. and Kaplan, D. L. (2006) 'Electrospun silk-BMP-2 scaffolds for bone tissue engineering', *Biomaterials*, 27(16), pp. 3115-3124.

- Li, G. and Sun, S. (2022) 'Silk Fibroin-Based Biomaterials for Tissue Engineering Applications', *Molecules*, 27(9). DOI: 10.3390/molecules27092757.
- Li, J. J., Kim, K., Roohani-Esfahani, S. I., Guo, J., Kaplan, D. L. and Zreiqat, H. (2015a) 'A biphasic scaffold based on silk and bioactive ceramic with stratified properties for osteochondral tissue regeneration', *J Mater Chem B*, 3(26), pp. 5361-5376.
- Li, L., Qian, Y., Lin, C., Li, H., Jiang, C., Lv, Y., Liu, W., Cai, K., Germershaus, O. and Yang, L. (2015b) 'The effect of silk gland sericin protein incorporation into electrospun polycaprolactone nanofibers on in vitro and in vivo characteristics', *Journal of Materials Chemistry B*, 3(5), pp. 859-870.
- Li, M., Ogiso, M. and Minoura, N. (2003) 'Enzymatic degradation behavior of porous silk fibroin sheets', *Biomaterials*, 24(2), pp. 357-65.
- Li, M., Yin, H., Yan, Z., Li, H., Wu, J., Wang, Y., Wei, F., Tian, G., Ning, C., Li, H., Gao, C., Fu, L., Jiang, S., Chen, M., Sui, X., Liu, S., Chen, Z. and Guo, Q. (2022) 'The immune microenvironment in cartilage injury and repair', *Acta Biomaterialia*, 140, pp. 23-42.
- Li, M. H., Xiao, R., Li, J. B. and Zhu, Q. (2017) 'Regenerative approaches for cartilage repair in the treatment of osteoarthritis', *Osteoarthritis Cartilage*, 25(10), pp. 1577-1587.
- Li, Y., Chen, S.-K., Li, L., Qin, L., Wang, X.-L. and Lai, Y.-X. (2015c) 'Bone defect animal models for testing efficacy of bone substitute biomaterials', *Journal of Orthopaedic Translation*, 3(3), pp. 95-104.
- Li, Y., Zhou, M., Zheng, W., Yang, J. and Jiang, N. (2023) 'Scaffold-based tissue engineering strategies for soft–hard interface regeneration', *Regenerative Biomaterials*, 10, pp. rbac091.
- Liau, L. L., Hassan, M. N., Tang, Y. L., Ng, M. H. and Law, J. X. (2021) 'Feasibility of Human Platelet Lysate as an Alternative to Foetal Bovine Serum for In Vitro Expansion of Chondrocytes', *International Journal of Molecular Sciences*, 22(3). DOI: 10.3390/ijms22031269.
- Liebesny, P. H., Mrosczyk, K., Zlotnick, H., Hung, H.-H., Frank, E., Kurz, B., Zanotto, G., Frisbie, D. and Grodzinsky, A. J. (2019) 'Enzyme Pretreatment plus Locally Delivered HB-IGF-1 Stimulate Integrative Cartilage Repair In Vitro', *Tissue Engineering Part A*, 25(17-18), pp. 1191-1201.
- Lin, H., Cheng, A. W., Alexander, P. G., Beck, A. M. and Tuan, R. S. (2014) 'Cartilage tissue engineering application of injectable gelatin hydrogel with in situ visible-light-activated gelation capability in both air and aqueous solution', *Tissue Eng Part A*, 20(17-18), pp. 2402-11.
- Lin, T. H., Wang, H. C., Cheng, W. H., Hsu, H. C. and Yeh, M. L. (2019) 'Osteochondral Tissue Regeneration Using a Tyramine-Modified Bilayered PLGA Scaffold Combined with Articular Chondrocytes in a Porcine Model', *Int J Mol Sci*, 20(2).
- Liu, X., Rodeheaver, D. P., White, J. C., Wright, A. M., Walker, L. M., Zhang, F. and Shannon, S. (2018) 'A comparison of in vitro cytotoxicity assays in medical device regulatory studies', *Regulatory Toxicology and Pharmacology*, 97, pp. 24-32.
- Liu, Y., Shah, K. M. and Luo, J. (2021) 'Strategies for Articular Cartilage Repair and Regeneration', *Frontiers in Bioengineering and Biotechnology*, 9.
- Loening, A., James, I., Levenston, M. E., Badger, A., Frank, E., Kurz, B., Nuttall, M. E., Hung, H., Blake, S. M., Grodzinsky, A. and Lark, M. (2000) 'Injurious mechanical compression of bovine articular cartilage induces chondrocyte apoptosis', *Archives Of Biochemistry And Biophysics*, 381(2), pp. 205-212.

- Loeser, R. F. (2010) 'Age-related changes in the musculoskeletal system and the development of osteoarthritis', *Clin Geriatr Med*, 26(3), pp. 371-86.
- Longobardi, L., O'Rear, L., Aakula, S., Johnstone, B., Shimer, K., Chytil, A., Horton, W. A., Moses, H. L. and Spagnoli, A. (2006) 'Effect of IGF-I in the Chondrogenesis of Bone Marrow Mesenchymal Stem Cells in the Presence or Absence of TGF- $\beta$  Signaling', *Journal of Bone and Mineral Research*, 21(4), pp. 626-636.
- Lopa, S. and Madry, H. (2014) 'Bioinspired scaffolds for osteochondral regeneration', *Tissue Eng Part A*, 20(15-16), pp. 2052-76.
- Lozito, T. P., Alexander, P. G., Lin, H., Gottardi, R., Cheng, A. W.-M. and Tuan, R. S. (2013) 'Three-dimensional osteochondral microtissue to model pathogenesis of osteoarthritis', *Stem Cell Research & Therapy*, 4(1), pp. S6.
- Lu, L. C., Zhu, X., Valenzuela, R. G., Currier, B. and Yaszemski, M. (2001) 'Biodegradable polymer scaffolds for cartilage tissue engineering', *Clinical Orthopaedics And Related Research*, (391), pp. S251-S270.
- Lu, Y., Zhang, S., Liu, X., Ye, S., Zhou, X., Huang, Q. and Ren, L. (2017) 'Silk/agarose scaffolds with tunable properties via SDS assisted rapid gelation', *RSC Advances*, 7(35), pp. 21740-21748.
- Luckman, S. P., Rees, E. and Kwan, A. P. (2003) 'Partial characterization of cell-type X collagen interactions', *Biochem J*, 372(Pt 2), pp. 485-93.
- Lui, J. C., Yue, S., Lee, A., Kikani, B., Temnycky, A., Barnes, K. M. and Baron, J. (2019) 'Persistent Sox9 expression in hypertrophic chondrocytes suppresses transdifferentiation into osteoblasts', *Bone*, 125, pp. 169-177.
- Luo, Y., Humayun, A. and Mills, D. K. (2020) 'Surface Modification of 3D Printed PLA/Halloysite Composite Scaffolds with Antibacterial and Osteogenic Capabilities', *Applied Sciences*, 10(11). DOI: 10.3390/app10113971.
- Luo, Z., Zhang, Q., Shi, M., Zhang, Y., Tao, W. and Li, M. (2015) 'Effect of Pore Size on the Biodegradation Rate of Silk Fibroin Scaffolds', *Advances in Materials Science and Engineering*, 2015, pp. 315397.
- Lutolf, M. P. and Hubbell, J. A. (2005) 'Synthetic biomaterials as instructive extracellular microenvironments for morphogenesis in tissue engineering', *Nature Biotechnology*, 23(1), pp. 47-55.
- Lutzweiler, G., Ndreu Halili, A. and Engin Vrana, N. (2020) 'The Overview of Porous, Bioactive Scaffolds as Instructive Biomaterials for Tissue Regeneration and Their Clinical Translation', *Pharmaceutics*, 12(7).
- Ma, P. X. and Zhang, R. (2001) 'Microtubular architecture of biodegradable polymer scaffolds', *Journal of Biomedical Materials Research*, 56(4), pp. 469-477.
- MacLeod, A. S. and Mansbridge, J. N. (2015) 'The Innate Immune System in Acute and Chronic Wounds', *Advances in Wound Care*, 5(2), pp. 65-78.
- Madihally, S. V. and Matthew, H. W. T. (1999) 'Porous chitosan scaffolds for tissue engineering', *Biomaterials*, 20(12), pp. 1133-1142.
- Madry, H., Luyten, F. P. and Facchini, A. (2012) 'Biological aspects of early osteoarthritis', *Knee Surg Sports Traumatol Arthrosc*, 20(3), pp. 407-22.
- Madry, H., van Dijk, C. N. and Mueller-Gerbl, M. (2010) 'The basic science of the subchondral bone', *Knee Surgery, Sports Traumatology, Arthroscopy*, 18(4), pp. 419-433.
- Majhy, B., Priyadarshini, P. and Sen, A. K. (2021) 'Effect of surface energy and roughness on cell adhesion and growth – facile surface modification for enhanced cell culture', *RSC Advances*, 11(25), pp. 15467-15476.

- Malekipour, F., Whitton, C., Oetomo, D. and Lee, P. V. S. (2013) 'Shock absorbing ability of articular cartilage and subchondral bone under impact compression', *Journal of the Mechanical Behavior of Biomedical Materials*, 26, pp. 127-135.
- Man, K., Alcala, C., Mekhileri, N. V., Lim, K. S., Jiang, L.-H., Woodfield, T. B. F. and Yang, X. B. (2022a) 'GelMA Hydrogel Reinforced with 3D Printed PEGT/PBT Scaffolds for Supporting Epigenetically-Activated Human Bone Marrow Stromal Cells for Bone Repair', *Journal of Functional Biomaterials*, 13(2). DOI: 10.3390/jfb13020041.
- Man, K., Joukhdar, H., Manz, X. D., Brunet, M. Y., Jiang, L.-H., Rnjak-Kovacina, J. and Yang, X. B. (2022b) 'Bone tissue engineering using 3D silk scaffolds and human dental pulp stromal cells epigenetic reprogrammed with the selective histone deacetylase inhibitor MI192', *Cell and Tissue Research*, 388(3), pp. 565-581.
- Mano, J. F. and Reis, R. L. (2007) 'Osteochondral defects: present situation and tissue engineering approaches', *J Tissue Eng Regen Med*, 1(4), pp. 261-73.
- Mansfield, J. C. and Peter Winlove, C. (2012) 'A multi-modal multiphoton investigation of microstructure in the deep zone and calcified cartilage', *Journal of Anatomy*, 220(4), pp. 405-416.
- Mansour, J. M., Gu, D. W., Chung, C. Y., Heebner, J., Althans, J., Abdalian, S., Schluchter, M. D., Liu, Y. and Welter, J. F. (2014) 'Towards the feasibility of using ultrasound to determine mechanical properties of tissues in a bioreactor', *Ann Biomed Eng*, 42(10), pp. 2190-202.
- Maroudas, A., Wachtel, E., Grushko, G., Katz, E. P. and Weinberg, P. (1991) 'The effect of osmotic and mechanical pressures on water partitioning in articular cartilage', *Biochim Biophys Acta*, 1073(2), pp. 285-94.
- Martin, I., Miot, S., Barbero, A., Jakob, M. and Wendt, D. (2007) 'Osteochondral tissue engineering', *J Biomech*, 40(4), pp. 750-65.
- Martín, A. R., Patel, J. M., Zlotnick, H. M., Carey, J. L. and Mauck, R. L. (2019) 'Emerging therapies for cartilage regeneration in currently excluded 'red knee' populations', *NPJ Regen Med*, 4, pp. 12.
- Mastrogiacomo, M., Muraglia, A., Komlev, V., Peyrin, F., Rustichelli, F., Crovace, A. and Cancedda, R. (2005) 'Tissue engineering of bone: search for a better scaffold', *Orthod Craniofac Res*, 8(4), pp. 277-84.
- McBeath, R., Pirone, D. M., Nelson, C. M., Bhadriraju, K. and Chen, C. S. (2004) 'Cell Shape, Cytoskeletal Tension, and RhoA Regulate Stem Cell Lineage Commitment', *Developmental Cell*, 6(4), pp. 483-495.
- McCarrel, T. M., Pownder, S. L., Gilbert, S., Koff, M. F., Castiglione, E., Saska, R. A., Bradica, G. and Fortier, L. A. (2016) 'Two-Year Evaluation of Osteochondral Repair with a Novel Biphasic Graft Saturated in Bone Marrow in an Equine Model', *CARTILAGE*, 8(4), pp. 406-416.
- McCoy, A. M. (2015) 'Animal Models of Osteoarthritis: Comparisons and Key Considerations', *Veterinary Pathology*, 52(5), pp. 803-818.
- McMahon, L. A., O'Brien, F. J. and Prendergast, P. J. (2008) 'Biomechanics and mechanobiology in osteochondral tissues', *Regen Med*, 3(5), pp. 743-59.
- Meijer, G. J., Radder, A., Dalmeijer, R., de Putter, C. and Van Blitterswijk, C. A. (1995) 'Observations of the bone activity adjacent to unloaded dental implants coated with Polyactive or HA', *J Oral Rehabil*, 22(3), pp. 167-74.
- Mekhileri, N. V., Lim, K. S., Brown, G. C. J., Mutreja, I., Schon, B. S., Hooper, G. J. and Woodfield, T. B. F. (2018) 'Automated 3D bioassembly of micro-tissues

- for biofabrication of hybrid tissue engineered constructs', *Biofabrication*, 10(2), pp. 024103.
- Meng, X., Ziadlou, R., Grad, S., Alini, M., Wen, C., Lai, Y., Qin, L., Zhao, Y. and Wang, X. (2020) 'Animal Models of Osteochondral Defect for Testing Biomaterials', *Biochemistry Research International*, 2020, pp. 9659412.
- Messner, K. and Maletius, W. (1996) 'The long-term prognosis for severe damage to weight-bearing cartilage in the knee: a 14-year clinical and radiographic follow-up in 28 young athletes', *Acta Orthop Scand*, 67(2), pp. 165-8.
- Metsäranta, M., Kujala, U. M., Pelliniemi, L., Osterman, H., Aho, H. and Vuorio, E. (1996) 'Evidence for insufficient chondrocytic differentiation during repair of full-thickness defects of articular cartilage', *Matrix Biol*, 15(1), pp. 39-47.
- Meyers, J., Craig, J. and Odde, David J. (2006) 'Potential for Control of Signaling Pathways via Cell Size and Shape', *Current Biology*, 16(17), pp. 1685-1693.
- Mintz, B. R. and Cooper, J. A., Jr. (2014) 'Hybrid hyaluronic acid hydrogel/poly( $\epsilon$ -caprolactone) scaffold provides mechanically favorable platform for cartilage tissue engineering studies', *J Biomed Mater Res A*, 102(9), pp. 2918-26.
- Miyata, T., Asami, N. and Urugami, T. (1999) 'A reversibly antigen-responsive hydrogel', *Nature*, 399(6738), pp. 766-769.
- Mobasheri, A., Kalamegam, G., Musumeci, G. and Batt, M. E. (2014) 'Chondrocyte and mesenchymal stem cell-based therapies for cartilage repair in osteoarthritis and related orthopaedic conditions', *Maturitas*, 78(3), pp. 188-198.
- Montaudo, G., Puglisi, C. and Samperi, F. (1993) 'Primary thermal degradation mechanisms of PET and PBT', *Polymer Degradation and Stability*, 42(1), pp. 13-28.
- Morales, T. I. (2007) 'Chondrocyte moves: clever strategies?', *Osteoarthritis Cartilage*, 15(8), pp. 861-71.
- Moran, C. J., Ramesh, A., Brama, P. A. J., O'Byrne, J. M., O'Brien, F. J. and Levingstone, T. J. (2016) 'The benefits and limitations of animal models for translational research in cartilage repair', *Journal of Experimental Orthopaedics*, 3(1), pp. 1.
- Mountcastle, S. E., Allen, P., Mellors, B. O. L., Lawless, B. M., Cooke, M. E., Lavecchia, C. E., Fell, N. L. A., Espino, D. M., Jones, S. W. and Cox, S. C. (2019) 'Dynamic viscoelastic characterisation of human osteochondral tissue: understanding the effect of the cartilage-bone interface', *BMC Musculoskeletal Disorders*, 20(1), pp. 575.
- Mseka, T., Bamburg, J. R. and Cramer, L. P. (2007) 'ADF/cofilin family proteins control formation of oriented actin-filament bundles in the cell body to trigger fibroblast polarization', *Journal of Cell Science*, 120(24), pp. 4332-4344.
- Mueller, M. B., Blunk, T., Appel, B., Maschke, A., Goepferich, A., Zellner, J., Englert, C., Prantl, L., Kujat, R., Nerlich, M. and Angele, P. (2013) 'Insulin is essential for in vitro chondrogenesis of mesenchymal progenitor cells and influences chondrogenesis in a dose-dependent manner', *International Orthopaedics*, 37(1), pp. 153-158.
- Mukundan, L. M., Nirmal, R. S. and Nair, P. D. (2022) 'Growth and Regeneration of Osteochondral Cells in Bioactive Niche: A Promising Approach for Osteochondral Tissue Repair', *ACS Applied Bio Materials*, 5(6), pp. 2676-2688.

- Murphy, C. M., Haugh, M. G. and O'Brien, F. J. (2010) 'The effect of mean pore size on cell attachment, proliferation and migration in collagen-glycosaminoglycan scaffolds for bone tissue engineering', *Biomaterials*, 31(3), pp. 461-6.
- Mutreja, I., Woodfield, T. B. F., Sperling, S., Nock, V., Evans, J. J. and Alkaisi, M. M. (2015) 'Positive and negative bioimprinted polymeric substrates: new platforms for cell culture', *Biofabrication*, 7(2), pp. 025002.
- Muzzarelli, R. A. A., El Mehtedi, M., Bottegoni, C. and Gigante, A. (2016) 'Physical properties imparted by genipin to chitosan for tissue regeneration with human stem cells: A review', *International Journal of Biological Macromolecules*, 93, pp. 1366-1381.
- Naomi, R., Ridzuan, P. M. and Bahari, H. (2021) 'Current Insights into Collagen Type I', *Polymers*, 13(16). DOI: 10.3390/polym13162642.
- Niederauer, G. G., A. Slivka, M., Leatherbury, N. C., Korvick, D. L., Hugh Harroff, J. H., Ehler, W. C., Dunn, C. J. and Kieswetter, K. (2000) 'Evaluation of multiphase implants for repair of focal osteochondral defects in goats', *Biomaterials*, 21(24), pp. 2561-2574.
- Niemczyk-Soczynska, B., Zaszczynska, A., Zabielski, K. and Sajkiewicz, P. (2021) 'Hydrogel, Electrospun and Composite Materials for Bone/Cartilage and Neural Tissue Engineering', *Materials (Basel)*, 14(22).
- Niu, X., Li, N., Du, Z. and Li, X. (2023) 'Integrated gradient tissue-engineered osteochondral scaffolds: Challenges, current efforts and future perspectives', *Bioactive Materials*, 20, pp. 574-597.
- Nixon, A. J., Begum, L., Mohammed, H. O., Huibregtse, B., O'Callaghan, M. M. and Matthews, G. L. (2011) 'Autologous chondrocyte implantation drives early chondrogenesis and organized repair in extensive full- and partial-thickness cartilage defects in an equine model', *J Orthop Res*, 29(7), pp. 1121-30.
- Nocera, A. D., Comin, R., Salvatierra, N. A. and Cid, M. P. (2018) 'Development of 3D printed fibrillar collagen scaffold for tissue engineering', *Biomed Microdevices*, 20(2), pp. 26.
- Nooeaid, P., Salih, V., Beier, J. P. and Boccaccini, A. R. (2012) 'Osteochondral tissue engineering: scaffolds, stem cells and applications', *J Cell Mol Med*, 16(10), pp. 2247-70.
- O'Brien, F. J. (2011) 'Biomaterials & scaffolds for tissue engineering', *Materials Today*, 14(3), pp. 88-95.
- O'Brien, F. J., Harley, B. A., Yannas, I. V. and Gibson, L. J. (2005) 'The effect of pore size on cell adhesion in collagen-GAG scaffolds', *Biomaterials*, 26(4), pp. 433-41.
- O'Shea, T. M. and Miao, X. (2008) 'Bilayered scaffolds for osteochondral tissue engineering', *Tissue Eng Part B Rev*, 14(4), pp. 447-64.
- Ode Boni, B. O., Bakadia, B. M., Osi, A. R., Shi, Z., Chen, H., Gauthier, M. and Yang, G. (2022) 'Immune Response to Silk Sericin–Fibroin Composites: Potential Immunogenic Elements and Alternatives for Immunomodulation', *Macromolecular Bioscience*, 22(1), pp. 2100292.
- Offeddu, G. S., Ashworth, J. C., Cameron, R. E. and Oyen, M. L. (2016) 'Structural determinants of hydration, mechanics and fluid flow in freeze-dried collagen scaffolds', *Acta Biomaterialia*, 41, pp. 193-203.
- Oh, C.-d., Lu, Y., Liang, S., Mori-Akiyama, Y., Chen, D., de Crombrughe, B. and Yasuda, H. (2014) 'SOX9 Regulates Multiple Genes in Chondrocytes,

- Including Genes Encoding ECM Proteins, ECM Modification Enzymes, Receptors, and Transporters', *PLOS ONE*, 9(9), pp. e107577.
- Oh, S. H., Kang, S. G., Kim, E. S., Cho, S. H. and Lee, J. H. (2003) 'Fabrication and characterization of hydrophilic poly(lactic-co-glycolic acid)/poly(vinyl alcohol) blend cell scaffolds by melt-molding particulate-leaching method', *Biomaterials*, 24(22), pp. 4011-21.
- Olivares-Navarrete, R., Lee, E. M., Smith, K., Hyzy, S. L., Doroudi, M., Williams, J. K., Gall, K., Boyan, B. D. and Schwartz, Z. (2017) 'Substrate Stiffness Controls Osteoblastic and Chondrocytic Differentiation of Mesenchymal Stem Cells without Exogenous Stimuli', *PLOS ONE*, 12(1), pp. e0170312.
- Oliveros Anerillas, L., Kingham, P. J., Lammi, M. J., Wiberg, M. and Kelk, P. (2021) 'Three-Dimensional Osteogenic Differentiation of Bone Marrow Mesenchymal Stem Cells Promotes Matrix Metalloproteinase 13 (MMP13) Expression in Type I Collagen Hydrogels', *International Journal of Molecular Sciences*, 22(24). DOI: 10.3390/ijms222413594.
- Outerbridge, R. E. (1961) 'The etiology of chondromalacia patellae', *J Bone Joint Surg Br*, 43-b, pp. 752-7.
- Panseri, S., Russo, A., Cunha, C., Bondi, A., Di Martino, A., Patella, S. and Kon, E. (2012) 'Osteochondral tissue engineering approaches for articular cartilage and subchondral bone regeneration', *Knee Surg Sports Traumatol Arthrosc*, 20(6), pp. 1182-91.
- Papadaki, M., Mahmood, T., Gupta, P., Claase, M. B., Grijpma, D. W., Riesle, J., van Blitterswijk, C. A. and Langer, R. (2001) 'The different behaviors of skeletal muscle cells and chondrocytes on PEGT/PBT block copolymers are related to the surface properties of the substrate', *J Biomed Mater Res*, 54(1), pp. 47-58.
- Pape, D., Filardo, G., Kon, E., van Dijk, C. N. and Madry, H. (2010) 'Disease-specific clinical problems associated with the subchondral bone', *Knee Surg Sports Traumatol Arthrosc*, 18(4), pp. 448-62.
- Patil, S. and Tapasvi, S. (2015) 'Osteochondral autografts', *Current Reviews in Musculoskeletal Medicine*, 8(4), pp. 423-428.
- Pelham, R. J. and Wang, Y.-I. (1997) 'Cell locomotion and focal adhesions are regulated by substrate flexibility', *Proceedings of the National Academy of Sciences*, 94(25), pp. 13661-13665.
- Pelttari, K., Winter, A., Steck, E., Goetzke, K., Hennig, T., Ochs, B. G., Aigner, T. and Richter, W. (2006) 'Premature induction of hypertrophy during in vitro chondrogenesis of human mesenchymal stem cells correlates with calcification and vascular invasion after ectopic transplantation in SCID mice', *Arthritis & Rheumatism*, 54(10), pp. 3254-3266.
- Perez, R. A. and Mestres, G. (2016) 'Role of pore size and morphology in musculoskeletal tissue regeneration', *Materials Science and Engineering: C*, 61, pp. 922-939.
- Persson, M., Lehenkari, P. P., Berglin, L., Turunen, S., Finnilä, M. A. J., Risteli, J., Skrifvars, M. and Tuukkanen, J. (2018) 'Osteogenic Differentiation of Human Mesenchymal Stem cells in a 3D Woven Scaffold', *Scientific Reports*, 8(1), pp. 10457.
- Pfaff, M., Aumailley, M., Specks, U., Knolle, J., Zerwes, H. G. and Timpl, R. (1993) 'Integrin and Arg-Gly-Asp dependence of cell adhesion to the native and unfolded triple helix of collagen type VI', *Exp Cell Res*, 206(1), pp. 167-76.

- Phipatanakul, W. P., VandeVord, P. J., Teitge, R. A. and Wooley, P. H. (2004) 'Immune response in patients receiving fresh osteochondral allografts', *Am J Orthop (Belle Mead NJ)*, 33(7), pp. 345-8.
- Plantz, M. A. and Hsu, W. K. (2020) 'Recent Research Advances in Biologic Bone Graft Materials for Spine Surgery', *Current Reviews in Musculoskeletal Medicine*, 13(3), pp. 318-325.
- Podgórski, R., Wojasiński, M. and Ciach, T. (2022) 'Nanofibrous materials affect the reaction of cytotoxicity assays', *Scientific Reports*, 12(1), pp. 9047.
- Polo-Corrales, L., Latorre-Esteves, M. and Ramirez-Vick, J. E. (2014) 'Scaffold Design for Bone Regeneration', *Journal of Nanoscience and Nanotechnology*, 14(1), pp. 15-56.
- Pérez, R. A., Won, J.-E., Knowles, J. C. and Kim, H.-W. (2013) 'Naturally and synthetic smart composite biomaterials for tissue regeneration', *Advanced Drug Delivery Reviews*, 65(4), pp. 471-496.
- Rannou, F., Francois, M., Corvol, M. T. and Berenbaum, F. (2006) 'Cartilage breakdown in rheumatoid arthritis', *Joint Bone Spine*, 73(1), pp. 29-36.
- Reddig, P. J. and Juliano, R. L. (2005) 'Clinging to life: cell to matrix adhesion and cell survival', *Cancer and Metastasis Reviews*, 24(3), pp. 425-439.
- Responde, D. J., Natoli, R. M. and Athanasiou, K. A. (2007) 'Collagens of articular cartilage: structure, function, and importance in tissue engineering', *Crit Rev Biomed Eng*, 35(5), pp. 363-411.
- Revach, O.-Y., Grosheva, I. and Geiger, B. (2020) 'Biomechanical regulation of focal adhesion and invadopodia formation', *Journal of Cell Science*, 133(20), pp. jcs244848.
- Rezwan, K., Chen, Q. Z., Blaker, J. J. and Boccaccini, A. R. (2006) 'Biodegradable and bioactive porous polymer/inorganic composite scaffolds for bone tissue engineering', *Biomaterials*, 27(18), pp. 3413-31.
- Re'em, T., Kaminer-Israeli, Y., Ruvinov, E. and Cohen, S. (2012) 'Chondrogenesis of hMSC in affinity-bound TGF-beta scaffolds', *Biomaterials*, 33(3), pp. 751-761.
- Ring, A., Steinstraesser, L., Muhr, G., Steinau, H. U., Hauser, J. and Langer, S. (2007) 'Improved neovascularization of PEGT/PBT copolymer matrices in response to surface modification by biomimetic coating', *Eur Surg Res*, 39(2), pp. 75-81.
- Risbud, M. V. and Sittinger, M. 2002. Tissue engineering: advances in in vitro cartilage generation. Elsevier Ltd.
- Rnjak-Kovacina, J., DesRochers, T. M., Burke, K. A. and Kaplan, D. L. (2015a) 'The effect of sterilization on silk fibroin biomaterial properties', *Macromol Biosci*, 15(6), pp. 861-74.
- Rnjak-Kovacina, J., Wray, L. S., Burke, K. A., Torregrosa, T., Golinski, J. M., Huang, W. and Kaplan, D. L. (2015b) 'Lyophilized Silk Sponges: A Versatile Biomaterial Platform for Soft Tissue Engineering', *ACS Biomater Sci Eng*, 1(4), pp. 260-270.
- Roughley, P. and Mort, J. (2014) 'The role of aggrecan in normal and osteoarthritic cartilage', *Journal of Experimental Orthopaedics*, 1(1), pp. 1-11.
- Roughley, P. J. and Lee, E. R. (1994) 'Cartilage proteoglycans: structure and potential functions', *Microsc Res Tech*, 28(5), pp. 385-97.
- Rowlands, A. S., George, P. A. and Cooper-White, J. J. (2008) 'Directing osteogenic and myogenic differentiation of MSCs: interplay of stiffness and adhesive ligand presentation', *American Journal of Physiology-Cell Physiology*, 295(4), pp. C1037-C1044.

- Ruan, S., Deng, J., Yan, L. and Huang, W. (2018) 'Evaluation of the effects of the combination of BMP-2-modified BMSCs and PRP on cartilage defects', *Exp Ther Med*, 16(6), pp. 4569-4577.
- Rubin, D. A. (1998) 'Magnetic resonance imaging of chondral and osteochondral injuries', *Top Magn Reson Imaging*, 9(6), pp. 348-59.
- Ruiz Martínez, M. A., Peralta Galisteo, S., Castán, H. and Morales Hernández, M. E. (2020) 'Role of proteoglycans on skin ageing: a review', *International Journal of Cosmetic Science*, 42(6), pp. 529-535.
- Ruskowitz, E. R. and Deforest, C. A. (2018) 'Photoresponsive biomaterials for targeted drug delivery and 4D cell culture', *Nature Reviews Materials*, 3.
- Saha, S., Kundu, B., Kirkham, J., Wood, D., Kundu, S. C. and Yang, X. B. (2013) 'Osteochondral Tissue Engineering In Vivo: A Comparative Study Using Layered Silk Fibroin Scaffolds from Mulberry and Nonmulberry Silkworms', *PLOS ONE*, 8(11), pp. e80004.
- Sakkers, R. J. B., Dalmeyer, R. A. J., de Wijn, J. R. and van Blitterswijk, C. A. (2000) 'Use of bone-bonding hydrogel copolymers in bone: An in vitro and in vivo study of expanding PEO-PBT copolymers in goat femora', *Journal of Biomedical Materials Research*, 49(3), pp. 312-318.
- Salgado, A. J., Coutinho, O. P. and Reis, R. L. (2004) 'Bone Tissue Engineering: State of the Art and Future Trends', *Macromolecular Bioscience*, 4(8), pp. 743-765.
- Salinas, E. Y., Hu, J. C. and Athanasiou, K. (2018) 'A Guide for Using Mechanical Stimulation to Enhance Tissue-Engineered Articular Cartilage Properties', *Tissue Eng Part B Rev*, 24(5), pp. 345-358.
- Sanders, R. K. and Crim, J. R. (2001) 'Osteochondral injuries', *Semin Ultrasound CT MR*, 22(4), pp. 352-70.
- Sandker, M. J., Petit, A., Redout, E. M., Siebelt, M., Müller, B., Bruin, P., Meyboom, R., Vermonden, T., Hennink, W. E. and Weinans, H. (2013) 'In situ forming acyl-capped PCLA-PEG-PCLA triblock copolymer based hydrogels', *Biomaterials*, 34(32), pp. 8002-11.
- Sang, Y., Li, M., Liu, J., Yao, Y., Ding, Z., Wang, L., Xiao, L., Lu, Q., Fu, X. and Kaplan, D. L. (2018) 'Biomimetic Silk Scaffolds with an Amorphous Structure for Soft Tissue Engineering', *ACS Appl Mater Interfaces*, 10(11), pp. 9290-9300.
- Santo, V. E., Gomes, M. E., Mano, J. F. and Reis, R. L. (2012) 'Controlled Release Strategies for Bone, Cartilage, and Osteochondral Engineering—Part I: Recapitulation of Native Tissue Healing and Variables for the Design of Delivery Systems', *Tissue Engineering Part B: Reviews*, 19(4), pp. 308-326.
- Sapudom, J., Kongsema, M., Methachittipan, A., Damrongsakkul, S., Kanokpanont, S., Teo, J. C. M., Khongkow, M., Tonsomboon, K. and Thongnuek, P. (2023) 'Degradation products of crosslinked silk fibroin scaffolds modulate the immune response but not cell toxicity', *Journal of Materials Chemistry B*, 11(16), pp. 3607-3616.
- Sarasam, A. R., Krishnaswamy, R. K. and Madihally, S. V. (2006) 'Blending chitosan with polycaprolactone: effects on physicochemical and antibacterial properties', *Biomacromolecules*, 7(4), pp. 1131-8.
- Schaefer, D., Martin, I., Jundt, G., Seidel, J., Heberer, M., Grodzinsky, A., Bergin, I., Vunjak-Novakovic, G. and Freed, L. E. (2002) 'Tissue-engineered composites for the repair of large osteochondral defects', *Arthritis Rheum*, 46(9), pp. 2524-34.
- Schindler, O. S. (2011) 'Current concepts of articular cartilage repair', *Acta Orthop Belg*, 77(6), pp. 709-26.

- Schmidt, M. B., Chen, E. H. and Lynch, S. E. (2006) 'A review of the effects of insulin-like growth factor and platelet derived growth factor on in vivo cartilage healing and repair', *Osteoarthritis and Cartilage*, 14(5), pp. 403-412.
- Schuurman, W., Harimulyo, E. B., Gawlitta, D., Woodfield, T. B. F., Dhert, W. J. A., van Weeren, P. R. and Malda, J. (2016) 'Three-dimensional assembly of tissue-engineered cartilage constructs results in cartilaginous tissue formation without retainment of zonal characteristics', *Journal of Tissue Engineering and Regenerative Medicine*, 10(4), pp. 315-324.
- Sekiya, I., Colter, D. C. and Prockop, D. J. (2001) 'BMP-6 enhances chondrogenesis in a subpopulation of human marrow stromal cells', *Biochem Biophys Res Commun*, 284(2), pp. 411-8.
- Sekiya, I., Vuoristo, J. T., Larson, B. L. and Prockop, D. J. (2002) 'In vitro cartilage formation by human adult stem cells from bone marrow stroma defines the sequence of cellular and molecular events during chondrogenesis', *Proceedings of the National Academy of Sciences*, 99(7), pp. 4397-4402.
- Seo, S.-J., Mahapatra, C., Singh, R. K., Knowles, J. C. and Kim, H.-W. (2014) 'Strategies for osteochondral repair: Focus on scaffolds', *Journal of Tissue Engineering*, 5, pp. 2041731414541850.
- Shapiro, F., Koide, S. and Glimcher, M. J. (1993) 'Cell origin and differentiation in the repair of full-thickness defects of articular cartilage', *J Bone Joint Surg Am*, 75(4), pp. 532-53.
- Sheikh, F. A., Ju, H. W., Moon, B. M., Lee, O. J., Kim, J. H., Park, H. J., Kim, D. W., Kim, D. K., Jang, J. E., Khang, G. and Park, C. H. (2016) 'Hybrid scaffolds based on PLGA and silk for bone tissue engineering', *J Tissue Eng Regen Med*, 10(3), pp. 209-21.
- Shen, G. (2005) 'The role of type X collagen in facilitating and regulating endochondral ossification of articular cartilage', *Orthodontics & Craniofacial Research*, 8(1), pp. 11-17.
- Shih, Y.-R. V., Tseng, K.-F., Lai, H.-Y., Lin, C.-H. and Lee, O. K. (2011) 'Matrix stiffness regulation of integrin-mediated mechanotransduction during osteogenic differentiation of human mesenchymal stem cells', *Journal of Bone and Mineral Research*, 26(4), pp. 730-738.
- Solchaga, L. A., Penick, K. J. and Welter, J. F. (2011) 'Chondrogenic Differentiation of Bone Marrow-Derived Mesenchymal Stem Cells: Tips and Tricks', in Vemuri, M., Chase, L.G. and Rao, M.S. (eds.) *Mesenchymal Stem Cell Assays and Applications*. Totowa, NJ: Humana Press, pp. 253-278.
- Sophia Fox, A. J., Bedi, A. and Rodeo, S. A. (2009) 'The basic science of articular cartilage: structure, composition, and function', *Sports health*, 1(6), pp. 461.
- Sosio, C., Di Giancamillo, A., Deponti, D., Gervaso, F., Scalera, F., Melato, M., Campagnol, M., Boschetti, F., Nonis, A., Domeneghini, C., Sannino, A. and Peretti, G. M. (2015) 'Osteochondral repair by a novel interconnecting collagen-hydroxyapatite substitute: a large-animal study', *Tissue Eng Part A*, 21(3-4), pp. 704-15.
- Steadman, J. R., Rodkey, W. G., Singleton, S. B. and Briggs, K. K. (1997) 'Microfracture technique for full-thickness chondral defects: Technique and clinical results', *Operative Techniques in Orthopaedics*, 7(4), pp. 300-304.
- Sun, M., Chi, G., Xu, J., Tan, Y., Xu, J., Lv, S., Xu, Z., Xia, Y., Li, L. and Li, Y. (2018) 'Extracellular matrix stiffness controls osteogenic differentiation of

- mesenchymal stem cells mediated by integrin  $\alpha 5$ ', *Stem Cell Research & Therapy*, 9(1), pp. 52.
- Sun, W., Xue, B., Li, Y., Qin, M., Wu, J., Lu, K., Wu, J., Cao, Y., Jiang, Q. and Wang, W. (2016) 'Polymer-Supramolecular Polymer Double-Network Hydrogel', *Advanced Functional Materials*, 26(48), pp. 9044-9052.
- Sun, Z., Guo, S. S. and Fässler, R. (2016) 'Integrin-mediated mechanotransduction', *Journal of Cell Biology*, 215(4), pp. 445-456.
- Sánchez-Télez, D. A., Télez-Jurado, L. and Rodríguez-Lorenzo, L. M. (2017) 'Hydrogels for Cartilage Regeneration, from Polysaccharides to Hybrids', *Polymers (Basel)*, 9(12).
- Sönmez, D., Latifoğlu, F., Toprak, G., Düzler, A. and İsoğlu, İ. A. (2021) 'Pericardial fluid and vascular tissue engineering: A preliminary study', *Bio-Medical Materials and Engineering*, 32, pp. 101-113.
- Søndergaard, L. V., Dagnæs-Hansen, F. and Herskin, M. S. (2011) 'Welfare assessment in porcine biomedical research – Suggestion for an operational tool', *Research in Veterinary Science*, 91(3), pp. e1-e9.
- Tahimic, C. G., Wang, Y. and Bikle, D. (2013) 'Anabolic effects of IGF-1 signaling on the skeleton', *Frontiers in Endocrinology*, 4.
- Tallawi, M., Rosellini, E., Barbani, N., Cascone, M. G., Rai, R., Saint-Pierre, G. and Boccaccini, A. R. (2015) 'Strategies for the chemical and biological functionalization of scaffolds for cardiac tissue engineering: a review', *Journal of The Royal Society Interface*, 12(108), pp. 20150254.
- Tamer, T. M. (2014) 'Hyaluronan and synovial joint: function, distribution and healing', *Interdisciplinary Toxicology*, 6(3), pp. 111-125.
- Tanaka, K., Inoue, S. and Mizuno, S. (1999) 'Hydrophobic interaction of P25, containing Asn-linked oligosaccharide chains, with the H-L complex of silk fibroin produced by *Bombyx mori*', *Insect Biochem Mol Biol*, 29(3), pp. 269-76.
- Tanaka, K., Kajiyama, N., Ishikura, K., Waga, S., Kikuchi, A., Ohtomo, K., Takagi, T. and Mizuno, S. (1999) 'Determination of the site of disulfide linkage between heavy and light chains of silk fibroin produced by *Bombyx mori*', *Biochim Biophys Acta*, 1432(1), pp. 92-103.
- Tanaka, K., Mori, K. and Mizuno, S. (1993) 'Immunological identification of the major disulfide-linked light component of silk fibroin', *J Biochem*, 114(1), pp. 1-4.
- Tangtrongsup, S. and Kisiday, J. D. (2015) 'Effects of Dexamethasone Concentration and Timing of Exposure on Chondrogenesis of Equine Bone Marrow-Derived Mesenchymal Stem Cells', *CARTILAGE*, 7(1), pp. 92-103.
- Temu, T. M., Wu, K.-Y., Gruppuso, P. A. and Phornphutkul, C. (2010) 'The mechanism of ascorbic acid-induced differentiation of ATDC5 chondrogenic cells', *American Journal of Physiology-Endocrinology and Metabolism*, 299(2), pp. E325-E334.
- Teramoto, H., Shirakawa, M. and Tamada, Y. (2020) 'Click Decoration of *Bombyx mori* Silk Fibroin for Cell Adhesion Control', *Molecules*, 25(18).
- Teruna, D. R., Majid, T. A. and Budiono, B. (2015) 'Experimental Study of Hysteretic Steel Damper for Energy Dissipation Capacity', *Advances in Civil Engineering*, 2015, pp. 631726.
- Tetteh, E. S., Bajaj, S. and Ghodadra, N. S. (2012) 'Basic science and surgical treatment options for articular cartilage injuries of the knee', *J Orthop Sports Phys Ther*, 42(3), pp. 243-53.

- Teuschl, A. H., van Griensven, M. and Redl, H. (2013) 'Sericin Removal from Raw Bombyx mori Silk Scaffolds of High Hierarchical Order', *Tissue Engineering Part C: Methods*, 20(5), pp. 431-439.
- Theruvath, A. J., Mahmoud, E. E., Wu, W., Nejadnik, H., Kiru, L., Liang, T., Felt, S. and Daldrup-Link, H. E. (2021) 'Ascorbic Acid and Iron Supplement Treatment Improves Stem Cell-Mediated Cartilage Regeneration in a Minipig Model', *The American Journal of Sports Medicine*, 49(7), pp. 1861-1870.
- Thevenot, P., Nair, A., Dey, J., Yang, J. and Tang, L. (2008) 'Method to Analyze Three-Dimensional Cell Distribution and Infiltration in Degradable Scaffolds', *Tissue Engineering Part C: Methods*, 14(4), pp. 319-331.
- Thompson, R. C., Oegema, T. R., Lewis, J. L. and Wallace, L. (1991) 'Osteoarthrotic changes after acute transarticular load. An animal model', *The Journal of bone and joint surgery. American volume*, 73(7), pp. 990-1001.
- Thurber, A. E., Omenetto, F. G. and Kaplan, D. L. (2015) 'In vivo bioresponses to silk proteins', *Biomaterials*, 71, pp. 145-157.
- Torzilli, P. A., Dethmers, D. A., Rose, D. E. and Schryuer, H. F. (1983) 'Movement of interstitial water through loaded articular cartilage', *J Biomech*, 16(3), pp. 169-79.
- Trofa, D. P., Hong, I. S., Lopez, C. D., Rao, A. J., Yu, Z., Odum, S. M., Moorman, C. T., Piasecki, D. P., Fleischli, J. E. and Saltzman, B. M. (2022) 'Isolated Osteochondral Autograft Versus Allograft Transplantation for the Treatment of Symptomatic Cartilage Lesions of the Knee: A Systematic Review and Meta-analysis', *The American Journal of Sports Medicine*, 51(3), pp. 812-824.
- Tsuruga, E., Takita, H., Itoh, H., Wakisaka, Y. and Kuboki, Y. (1997) 'Pore size of porous hydroxyapatite as the cell-substratum controls BMP-induced osteogenesis', *J Biochem*, 121(2), pp. 317-24.
- Tuan, R. S., Boland, G. and Tuli, R. (2003) 'Adult mesenchymal stem cells and cell-based tissue engineering', *Arthritis research & therapy*, 5(1), pp. 32-45.
- Tuerlings, M., Boone, I., Eslami Amirabadi, H., Vis, M., Suchiman, E., van der Linden, E., Hofmann, S., Nelissen, R., den Toonder, J., Ramos, Y. and Meulenbelt, I. (2022) 'Capturing Essential Physiological Aspects of Interacting Cartilage and Bone Tissue with Osteoarthritis Pathophysiology: A Human Osteochondral Unit-on-a-Chip Model', *Advanced Materials Technologies*, 7(8), pp. 2101310.
- van der Staay, F. J., Pouzet, B., Mahieu, M., Nordquist, R. E. and Schuurman, T. (2009) 'The d-amphetamine-treated Göttingen miniature pig: an animal model for assessing behavioral effects of antipsychotics', *Psychopharmacology*, 206(4), pp. 715-729.
- van Dorp, A. G., Verhoeven, M. C., Koerten, H. K., van Blitterswijk, C. A. and Ponec, M. (1999) 'Bilayered biodegradable poly(ethylene glycol)/poly(butylene terephthalate) copolymer (Polyactive) as substrate for human fibroblasts and keratinocytes', *J Biomed Mater Res*, 47(3), pp. 292-300.
- Vetsch, J. R., Paulsen, S. J., Müller, R. and Hofmann, S. (2015) 'Effect of fetal bovine serum on mineralization in silk fibroin scaffolds', *Acta Biomaterialia*, 13, pp. 277-285.
- Vikingsson, L., Gómez-Tejedor, J. A., Gallego Ferrer, G. and Gómez Ribelles, J. L. (2015) 'An experimental fatigue study of a porous scaffold for the regeneration of articular cartilage', *J Biomech*, 48(7), pp. 1310-7.

- Vining, K. H. and Mooney, D. J. (2017) 'Mechanical forces direct stem cell behaviour in development and regeneration', *Nature Reviews Molecular Cell Biology*, 18(12), pp. 728-742.
- Volz, M., Wyse-Sookoo, K. R., Travascio, F., Huang, C.-Y. and Best, T. M. (2022) 'Mechanobiological Approaches for Stimulating Chondrogenesis of Stem Cells', *Stem Cells and Development*, 31(15-16), pp. 460-487.
- Vunjak-Novakovic, G., Obradovic, B., Martin, I., Bursac, P. M., Langer, R. and Freed, L. E. (1998) 'Dynamic Cell Seeding of Polymer Scaffolds for Cartilage Tissue Engineering', *Biotechnology Progress*, 14(2), pp. 193-202.
- Wall, A. and Board, T. (2014) 'Chemical Basis for the Histological Use of Safranin O in the Study of Articular Cartilage', in Banaszkiwicz, P.A. and Kader, D.F. (eds.) *Classic Papers in Orthopaedics*. London: Springer London, pp. 433-435.
- Wan, Y., Wang, Y., Liu, Z., Qu, X., Han, B., Bei, J. and Wang, S. (2005) 'Adhesion and proliferation of OCT-1 osteoblast-like cells on micro- and nano-scale topography structured poly(L-lactide)', *Biomaterials*, 26(21), pp. 4453-4459.
- Wang, R., Liu, W., Du, M., Yang, C., Li, X. and Yang, P. (2018) 'The differential effect of basic fibroblast growth factor and stromal cell-derived factor-1 pretreatment on bone marrow mesenchymal stem cells osteogenic differentiation potency', *Mol Med Rep*, 17(3), pp. 3715-3721.
- Wang, S., Lu, L., Wang, C., Gao, C. and Wang, X. (2011) 'Polymeric Biomaterials for Tissue Engineering Applications 2011', *International Journal of Polymer Science*, 2011(2011).
- Wang, T. and Yang, F. (2017) 'A comparative study of chondroitin sulfate and heparan sulfate for directing three-dimensional chondrogenesis of mesenchymal stem cells', *Stem Cell Research & Therapy*, 8(1), pp. 284.
- Wang, W. and Yeung, K. W. K. (2017) 'Bone grafts and biomaterials substitutes for bone defect repair: A review', *Bioact Mater*, 2(4), pp. 224-247.
- Wang, Y., Xu, Y., Zhou, G., Liu, Y. and Cao, Y. (2021) 'Biological Evaluation of Acellular Cartilaginous and Dermal Matrixes as Tissue Engineering Scaffolds for Cartilage Regeneration', *Frontiers in Cell and Developmental Biology*, 8.
- Wasyłeczko, M., Sikorska, W. and Chwojnowski, A. (2020) 'Review of Synthetic and Hybrid Scaffolds in Cartilage Tissue Engineering', *Membranes*, 10(11). DOI: 10.3390/membranes10110348.
- Weaver, V. M., Lelièvre, S., Lakins, J. N., Chrenek, M. A., Jones, J. C. R., Giancotti, F., Werb, Z. and Bissell, M. J. (2002) 'β4 integrin-dependent formation of polarized three-dimensional architecture confers resistance to apoptosis in normal and malignant mammary epithelium', *Cancer Cell*, 2(3), pp. 205-216.
- Weizel, A., Distler, T., Schneidereit, D., Friedrich, O., Bräuer, L., Paulsen, F., Detsch, R., Boccaccini, A. R., Budday, S. and Seitz, H. (2020) 'Complex mechanical behavior of human articular cartilage and hydrogels for cartilage repair', *Acta Biomaterialia*, 118, pp. 113-128.
- Wen, C., Xu, L., Xu, X., Wang, D., Liang, Y. and Duan, L. (2021) 'Insulin-like growth factor-1 in articular cartilage repair for osteoarthritis treatment', *Arthritis Research & Therapy*, 23(1), pp. 277.
- Wilkinson, P., Bozo, I. Y., Braxton, T., Just, P., Jones, E., Deev, R. V., Giannoudis, P. V. and Feichtinger, G. A. (2021) 'Systematic Review of the Preclinical Technology Readiness of Orthopedic Gene Therapy and Outlook for Clinical Translation', *Front Bioeng Biotechnol*, 9, pp. 626315.

- Williams, G. M., Klisch, S. M. and Sah, R. L. (2008) 'Bioengineering cartilage growth, maturation, and form', *Pediatr Res*, 63(5), pp. 527-34.
- Winter, A., Breit, S., Parsch, D., Benz, K., Steck, E., Hauner, H., Weber, R. M., Ewerbeck, V. and Richter, W. (2003) 'Cartilage-like gene expression in differentiated human stem cell spheroids: A comparison of bone marrow-derived and adipose tissue-derived stromal cells', *Arthritis & Rheumatism*, 48(2), pp. 418-429.
- Witkowska-Zimny, M., Walenko, K., Wrobel, E., Mrowka, P., Mikulska, A. and Przybylski, J. (2013) 'Effect of substrate stiffness on the osteogenic differentiation of bone marrow stem cells and bone-derived cells', *Cell Biology International*, 37(6), pp. 608-616.
- Wolff, L. I. and Hartmann, C. (2019) 'A Second Career for Chondrocytes—Transformation into Osteoblasts', *Current Osteoporosis Reports*, 17(3), pp. 129-137.
- Woloszyk, A., Holsten Dirksen, S., Bostanci, N., Müller, R., Hofmann, S. and Mitsiadis, T. A. (2014) 'Influence of the Mechanical Environment on the Engineering of Mineralised Tissues Using Human Dental Pulp Stem Cells and Silk Fibroin Scaffolds', *PLOS ONE*, 9(10), pp. e111010.
- Wong, J. Y., Langer, R. and Ingber, D. E. (1994) 'Electrically conducting polymers can noninvasively control the shape and growth of mammalian cells', *Proceedings of the National Academy of Sciences*, 91(8), pp. 3201-3204.
- Wray, L. S., Rnjak-Kovacina, J., Mandal, B. B., Schmidt, D. F., Gil, E. S. and Kaplan, D. L. (2012) 'A silk-based scaffold platform with tunable architecture for engineering critically-sized tissue constructs', *Biomaterials*, 33(36), pp. 9214-24.
- Wu, J. J., Woods, P. E. and Eyre, D. R. (1992) 'Identification of cross-linking sites in bovine cartilage type IX collagen reveals an antiparallel type II-type IX molecular relationship and type IX to type IX bonding', *The Journal of biological chemistry*, 267(32), pp. 23007-23014.
- Wu, Y., Yang, Z., Law, J. B. K., He, A. Y., Abbas, A. A., Denslin, V., Kamarul, T., Hui, J. H. P. and Lee, E. H. (2016) 'The Combined Effect of Substrate Stiffness and Surface Topography on Chondrogenic Differentiation of Mesenchymal Stem Cells', *Tissue Engineering Part A*, 23(1-2), pp. 43-54.
- Xin, Y., Zhao, N. and Wang, Y. (2022) 'Multiple roles of Runt-related transcription factor-2 in tooth eruption: bone formation and resorption', *Archives of Oral Biology*, 141, pp. 105484.
- Xu, J., Wang, W., Ludeman, M., Cheng, K., Hayami, T., Lotz, J. C. and Kapila, S. (2008) 'Chondrogenic differentiation of human mesenchymal stem cells in three-dimensional alginate gels', *Tissue Eng Part A*, 14(5), pp. 667-80.
- Xue, J., Wu, T., Dai, Y. and Xia, Y. (2019) 'Electrospinning and Electrospun Nanofibers: Methods, Materials, and Applications', *Chem Rev*, 119(8), pp. 5298-5415.
- Xynos, I. D., Hukkanen, M. V., Batten, J. J., Buttery, L. D., Hench, L. L. and Polak, J. M. (2000) 'Bioglass 45S5 stimulates osteoblast turnover and enhances bone formation In vitro: implications and applications for bone tissue engineering', *Calcif Tissue Int*, 67(4), pp. 321-9.
- Yan, L. P., Silva-Correia, J., Oliveira, M. B., Vilela, C., Pereira, H., Sousa, R. A., Mano, J. F., Oliveira, A. L., Oliveira, J. M. and Reis, R. L. (2015) 'Bilayered silk/silk-nanoCaP scaffolds for osteochondral tissue engineering: In vitro and in vivo assessment of biological performance', *Acta Biomater*, 12, pp. 227-241.

- Yanagishita, M. (1993) 'Function of proteoglycans in the extracellular matrix', *Acta Pathol Jpn*, 43(6), pp. 283-93.
- Yang, Q., Teng, B.-H., Wang, L.-N., Li, K., Xu, C., Ma, X.-L., Zhang, Y., Kong, D.-L., Wang, L.-Y. and Zhao, Y.-H. (2017a) 'Silk fibroin/cartilage extracellular matrix scaffolds with sequential delivery of TGF- $\beta$ 3 for chondrogenic differentiation of adipose-derived stem cells', *International Journal of Nanomedicine*, Volume 12, pp. 6721-6733.
- Yang, X. B., Roach, H. I., Clarke, N. M., Howdle, S. M., Quirk, R., Shakesheff, K. M. and Oreffo, R. O. (2001) 'Human osteoprogenitor growth and differentiation on synthetic biodegradable structures after surface modification', *Bone*, 29(6), pp. 523-31.
- Yang, Y., Feng, Y., Qu, R., Li, Q., Rong, D., Fan, T., Yang, Y., Sun, B., Bi, Z., Khan, A. U., Deng, T., Dai, J. and Ouyang, J. (2020) 'Synthesis of aligned porous polyethylene glycol/silk fibroin/hydroxyapatite scaffolds for osteoinduction in bone tissue engineering', *Stem Cell Research & Therapy*, 11(1), pp. 522.
- Yang, Y., Wang, K., Gu, X. and Leong, K. W. (2017b) 'Biophysical Regulation of Cell Behavior—Cross Talk between Substrate Stiffness and Nanotopography', *Engineering*, 3(1), pp. 36-54.
- Yassin, M. A., Leknes, K. N., Pedersen, T. O., Xing, Z., Sun, Y., Lie, S. A., Finne-Wistrand, A. and Mustafa, K. (2015) 'Cell seeding density is a critical determinant for copolymer scaffolds-induced bone regeneration', *Journal of Biomedical Materials Research Part A*, 103(11), pp. 3649-3658.
- Yi, J., Xiong, F., Li, B., Chen, H., Yin, Y., Dai, H. and Li, S. (2016) 'Degradation characteristics, cell viability and host tissue responses of PDLLA-based scaffold with PRGD and  $\beta$ -TCP nanoparticles incorporation', *Regenerative Biomaterials*, 3(3), pp. 159-166.
- Yi, S. W., Kim, H. J., Oh, H. J., Shin, H., Lee, J. S., Park, J. S. and Park, K.-H. (2018) 'Gene expression profiling of chondrogenic differentiation by dexamethasone-conjugated polyethyleneimine with SOX trio genes in stem cells', *Stem Cell Research & Therapy*, 9(1), pp. 341.
- Yildirim, N., Amanzhanova, A., Kulzhanova, G., Mukasheva, F. and Eriskin, C. (2023) 'Osteochondral Interface: Regenerative Engineering and Challenges', *ACS Biomaterials Science & Engineering*.
- Yu, L., Cavelier, S., Hannon, B. and Wei, M. (2023) 'Recent development in multizonal scaffolds for osteochondral regeneration', *Bioactive Materials*, 25, pp. 122-159.
- Yun, A., Lee, S. H. and Kim, J. (2013) 'A phase-field model for articular cartilage regeneration in degradable scaffolds', *Bull Math Biol*, 75(12), pp. 2389-409.
- Zha, K., Sun, Z., Yang, Y., Chen, M., Gao, C., Fu, L., Li, H., Sui, X., Guo, Q. and Liu, S. (2021) 'Recent Developed Strategies for Enhancing Chondrogenic Differentiation of MSC: Impact on MSC-Based Therapy for Cartilage Regeneration', *Stem Cells International*, 2021, pp. 8830834.
- Zhan, X. (2020) 'Effect of matrix stiffness and adhesion ligand density on chondrogenic differentiation of mesenchymal stem cells', *Journal of Biomedical Materials Research Part A*, 108(3), pp. 675-683.
- Zhang, K., Fan, Y., Dunne, N. and Li, X. (2018a) 'Effect of microporosity on scaffolds for bone tissue engineering', *Regenerative Biomaterials*, 5(2), pp. 115-124.
- Zhang, L., Yang, G., Johnson, B. N. and Jia, X. (2019) 'Three-dimensional (3D) printed scaffold and material selection for bone repair', *Acta Biomater*, 84, pp. 16-33.

- Zhang, Q., Yu, Y. and Zhao, H. (2016) 'The effect of matrix stiffness on biomechanical properties of chondrocytes', *Acta Biochimica et Biophysica Sinica*, 48(10), pp. 958-965.
- Zhang, W., Zhu, C., Ye, D., Xu, L., Zhang, X., Wu, Q., Kaplan, D. L. and Jiang, X. (2014) 'Porous silk scaffolds for delivery of growth factors and stem cells to enhance bone regeneration', *PLoS One*, 9(7), pp. e102371.
- Zhang, X., Wu, Y., Pan, Z., Sun, H., Wang, J., Yu, D., Zhu, S., Dai, J., Chen, Y., Tian, N., Heng, B. C., Coen, N. D., Xu, H. and Ouyang, H. (2016) 'The effects of lactate and acid on articular chondrocytes function: Implications for polymeric cartilage scaffold design', *Acta Biomaterialia*, 42, pp. 329-340.
- Zhang, Y., Guo, W., Wang, M., Hao, C., Lu, L., Gao, S., Zhang, X., Li, X., Chen, M., Li, P., Jiang, P., Lu, S., Liu, S. and Guo, Q. (2018b) 'Co-culture systems-based strategies for articular cartilage tissue engineering', *Journal of Cellular Physiology*, 233(3), pp. 1940-1951.
- Zhang, Y., Shi, N., He, L., Wang, S., Li, X., Lu, S., Zhang, Q. and Niu, H. (2021) 'Silk Sericin Activates Mild Immune Response and Increases Antibody Production', *Journal of Biomedical Nanotechnology*, 17(12), pp. 2433-2443.
- Zhang, Y. Q. (2002) 'Applications of natural silk protein sericin in biomaterials', *Biotechnol Adv*, 20(2), pp. 91-100.
- Zhao, F. and Ma, T. (2005) 'Perfusion bioreactor system for human mesenchymal stem cell tissue engineering: Dynamic cell seeding and construct development', *Biotechnology and Bioengineering*, 91(4), pp. 482-493.
- Zhao, X., Kim, J., Cezar, C. A., Huebsch, N., Lee, K., Bouhadir, K. and Mooney, D. J. (2011) 'Active scaffolds for on-demand drug and cell delivery', *Proceedings of the National Academy of Sciences*, 108(1), pp. 67-72.
- Zheng Ming, H., Kirk Thomas, B. and Wu Jian, P. (2008) 'Study of the collagen structure in the superficial zone and physiological state of articular cartilage using a 3D confocal imaging technique', *Journal of Orthopaedic Surgery and Research*, 3(1), pp. 29.
- Zhou, C. Z., Confalonieri, F., Medina, N., Zivanovic, Y., Esnault, C., Yang, T., Jacquet, M., Janin, J., Duguet, M., Perasso, R. and Li, Z. G. (2000) 'Fine organization of Bombyx mori fibroin heavy chain gene', *Nucleic Acids Res*, 28(12), pp. 2413-9.
- Zhou, Y., Qiu, J., Wan, L. and Li, J. (2022) 'The effect of matrix stiffness on the chondrogenic differentiation of mesenchymal stem cells', *Journal of Molecular Histology*, 53(5), pp. 805-816.
- Zhou, Y. F., Sae-Lim, V., Chou, A. M., Hutmacher, D. W. and Lim, T. M. (2006) 'Does seeding density affect in vitro mineral nodules formation in novel composite scaffolds?', *Journal of Biomedical Materials Research Part A*, 78A(1), pp. 183-193.
- Zuk, P. A., Zhu, M., Mizuno, H., Huang, J., Futrell, J. W., Katz, A. J., Benhaim, P., Lorenz, H. P. and Hedrick, M. H. (2001) 'Multilineage Cells from Human Adipose Tissue: Implications for Cell-Based Therapies', *Tissue Engineering*, 7(2), pp. 211-228.

# Appendix 1

## Trilineage differentiation assay

Trilineage differentiation assays were conducted for all collected hBMSC used within this thesis. All patient donors showed positive trilineage differentiation for adipogenic, osteogenic and Chondrogenic differentiation representative photos are shown in Figure 60.

After 21 days of incubation in osteogenic media, the hBMSC were shown to exhibit positive calcium staining by alizarin red, as well as positive alkaline phosphatase staining. Compared to their basal controls, which showed very little alizarin red and alkaline phosphatase staining.

After 21 days of culture in Chondrogenic conditions upon silk scaffolds. hBMSC is showed extensive GAG and collagen accumulation with a collagenous capsule on the upper surface and more extensive gag expression within the centre

After 21 days culture in adipogenic media (StemMACS™ AdipoDiff, MACS, 130-091-677 ) hBMSC is showed lipid vesicle formation as determined by positive oil red O staining. Compared to basal controls, which showed no lipid formation indicated by no staining with oil red O

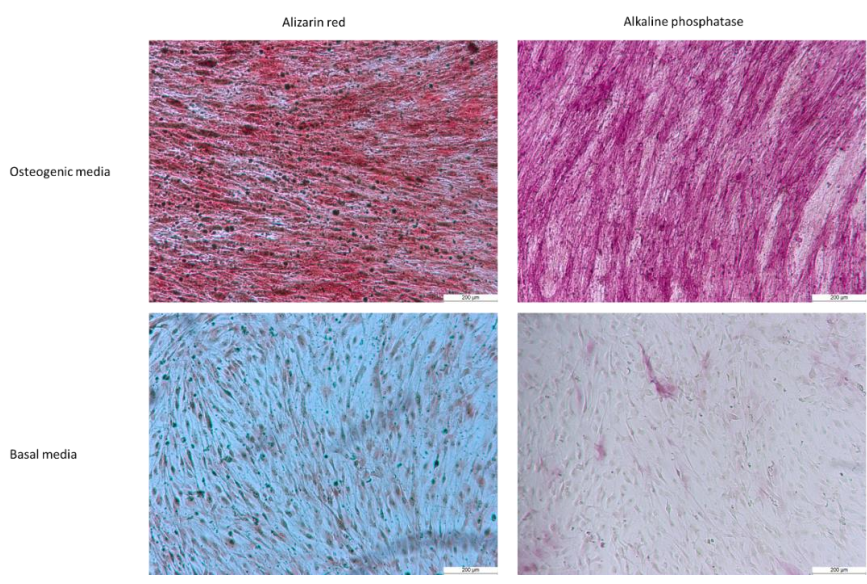
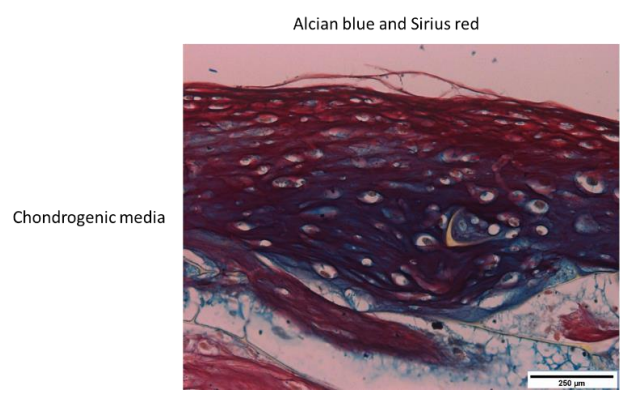
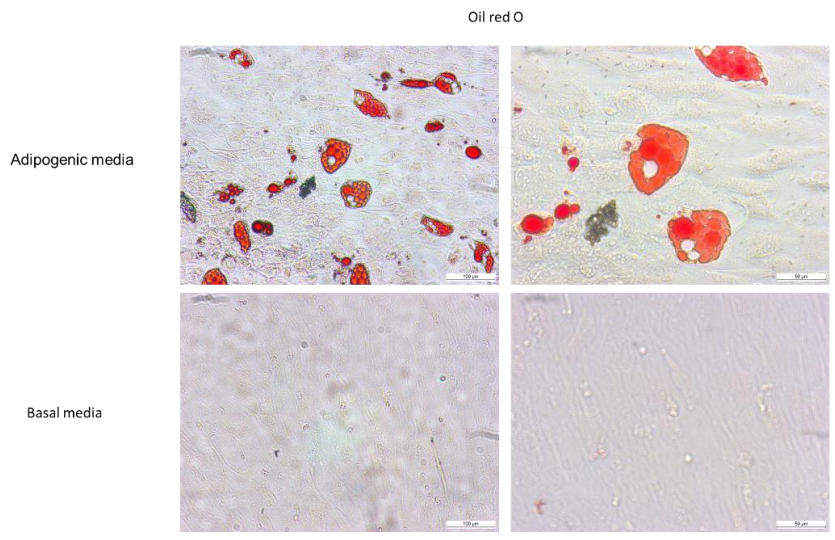


**Figure 60 (appendix) trilineage differentiation assay of isolated hBMSC from routine hip arthroplasty**

Raw FTIR data

Figure 61 demonstrates raw FTIR data utilised to determine the protein's secondary structure (beta sheets, random coils and alpha helices) seen within Figure 21 in the Amide I region (1600–1800  $\text{cm}^{-1}$ )

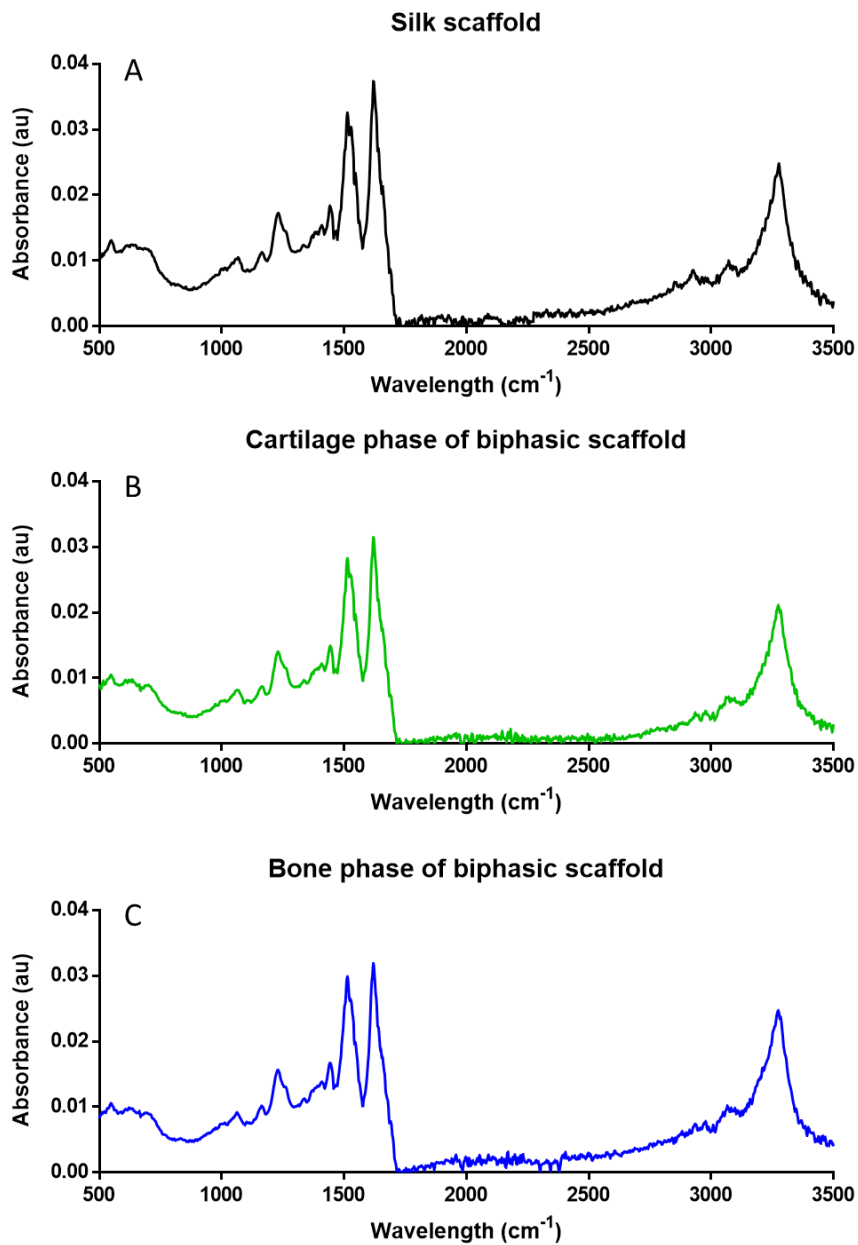


**Figure 61 (appendix) Raw FTIR data utilised to determine protein secondary structure.**

Comparing (A) silk scaffolds (B) the cartilage phase of biphasic scaffolds (D) the bone phase of biphasic scaffolds. Data obtained in the 500  $\text{cm}^{-1}$  to 3500  $\text{cm}^{-1}$  regions at a resolution of 4  $\text{cm}^{-1}$  using the Vertex 70 FTIR spectrometer in attenuated total reflection mode.